

**Bioengineering an Ovarian-specific ECM Hydrogel to Facilitate Intraovarian Follicle
Delivery for Fertility Preservation**

by

Michael Joseph Buckenmeyer

Bachelor of Science, Mechanical Engineering, Fairfield University, 2011

Master of Science, Bioengineering, Syracuse University, 2014

Submitted to the Graduate Faculty of the
Swanson School of Engineering in partial fulfillment
of the requirements for the degree of
Doctor of Philosophy

University of Pittsburgh

2020

UNIVERSITY OF PITTSBURGH

SWANSON SCHOOL OF ENGINEERING

This dissertation was presented

by

Michael Joseph Buckenmeyer

It was defended on

June 19, 2020

and approved by

Lance A. Davidson, Ph.D.,
Professor, Department of Bioengineering

Kyle E. Orwig, Ph.D.,
Professor, Department of Obstetrics, Gynecology and Reproductive Sciences

Aleksandar Rajkovic, M.D., Ph.D.,
Professor, Department of Obstetrics, Gynecology and Reproductive Sciences

Sanjeev G. Shroff, Ph.D.,
Professor, Department of Bioengineering

Dissertation Director:
Bryan N. Brown, Ph.D.,
Associate Professor, Department of Bioengineering

Copyright © by Michael Joseph Buckenmeyer

2020

Bioengineering an Ovarian-specific ECM Hydrogel to Facilitate Intraovarian Follicle Delivery for Fertility Preservation

Michael Joseph Buckenmeyer, PhD

University of Pittsburgh, 2020

The ovarian reserve represents the absolute number of primordial follicles with the potential to release a fertilizable oocyte. A reduction of follicles occurs naturally with aging until the reserve is depleted and induces menopause. However, there is a growing population of post pubertal women who experience aberrant reproductive function prior to the onset of menopause, classified as premature ovarian failure (POF). A subset of POF cases directly result from surgical or chemical procedures used to ameliorate cancer or other ovarian-associated pathologies. The current gold standard used to treat iatrogenic POF is the transplantation of cryopreserved ovarian tissues, which has led to greater than 130 reported live-births to-date. This strategy has shown clinical success, but there remain risks of malignant cell transmission and complications due to surgery. We hypothesized that an ovarian-specific hydrogel could provide a minimally-invasive platform to facilitate the intraovarian delivery, engraftment and survival of isolated immature ovarian follicles.

The first aim of this study was to prepare a hydrogel from ovarian tissues that retained ovarian specificity. Porcine ovaries were decellularized using a series of enzymes and detergents to remove immunogenic components from the tissues. Decellularization significantly reduced dsDNA, while preserving ovarian tissue morphology, extracellular matrix (ECM) proteins and proteoglycans. Additionally, ovarian-specific hormones, such as anti-Müllerian hormone, estradiol and progesterone, were detected within decellularized ovaries. Ovarian ECM (OECM) hydrogels

formed via physical crosslinking when exposed to physiological conditions. Hydrogel viscoelastic and ultrastructural properties were sensitive to changes in ECM concentration, while gelation time remained constant. Successful *in vitro* follicle maturation using OECM hydrogels demonstrated follicle compatibility.

The second aim of this study was to examine the efficacy of an OECM hydrogel as a vehicle to support intraovarian follicle delivery and graft survival within chemotherapy-induced POF (ciPOF) mice. Immature ovarian follicles from young DBA-GFP/nu female mice were enzymatically isolated and microinjected into the ovaries of ciPOF nude mice within the OECM hydrogel. Mating studies resulted in multiple litters containing pups derived from transplanted donor follicles. Transplanted ovarian tissues contained developing donor follicles suggesting hydrogel-facilitated intraovarian microinjection could offer a low-risk, minimally-invasive alternative for fertility preservation.

Table of Contents

Preface.....	xviii
1.0 Introduction.....	1
1.1 Female Reproductive Biology.....	1
1.1.1 Ovarian Development	2
1.1.1.1 Oogenesis.....	7
1.1.1.2 Folliculogenesis	11
1.1.2 Ovarian Anatomy and Physiology.....	13
1.1.2.1 Tissue Organization and Cell Types.....	15
1.1.2.1.1 Ovarian Extracellular Matrix	15
1.1.2.1.2 Ovarian Follicles	16
1.1.2.1.3 Granulosa Cells.....	17
1.1.2.1.4 Theca Cells	17
1.1.2.1.5 Luteal Cells.....	18
1.1.2.1.6 Stromal Cells	18
1.1.2.1.7 Endothelial Cells	19
1.1.2.1.8 Ovarian Surface Epithelial Cells.....	19
1.1.2.2 The Menstrual Cycle.....	20
1.1.2.3 Role of Hormones and Growth Factors	23
1.1.2.3.1 Gonadotropin Releasing Hormone	23
1.1.2.3.2 Follicle Stimulating Hormone.....	24
1.1.2.3.3 Luteinizing Hormone	24

1.1.2.3.4	Ovarian Steroidogenesis.....	25
1.1.2.3.5	Estradiol	27
1.1.2.3.6	Progesterone.....	27
1.1.2.3.7	Other Accessory Molecules.....	28
1.1.2.4	Reproductive Differences in Female Mammalian Species	29
1.2	Female Fertility Preservation	37
1.2.1	Female Infertility.....	38
1.2.2	Premature Ovarian Failure.....	38
1.2.3	Causes of Iatrogenic POF	39
1.2.3.1	Chemotherapy-Induced POF	39
1.2.4	Current Fertility Preservation Techniques	42
1.2.4.1	Cryopreservation.....	43
1.2.4.2	Ovarian Tissue Transplantation	44
1.2.4.3	Biomaterial-Facilitated Approaches.....	45
1.2.4.3.1	In Vitro Follicle Maturation	45
1.2.4.3.2	In Vivo Follicle Maturation	48
1.2.4.3.3	Artificial Ovary	49
1.2.4.4	Ovarian Stem Cells.....	50
2.0	Overview of Decellularized ECM Biomaterials	52
2.1	The Extracellular Matrix.....	53
2.1.1	ECM Components.....	55
2.1.2	Role of the ECM.....	56
2.2	Decellularization.....	57

2.2.1 Methods.....	57
2.2.1.1 Physical Treatments	58
2.2.1.2 Chemical Treatments	59
2.2.2 Enzymatic Treatments.....	60
2.2.3 dECM Derivatives.....	61
2.2.4 Current Decellularization Approaches for Fertility Preservation	62
2.2.5 Regulatory Pathways for dECM Clinical Translation	64
2.2.6 Future Considerations for dECM Biomaterial Development.....	65
3.0 Biomaterial-Assisted Follicle Microinjection as an Alternative Therapy for Fertility Preservation	68
3.1 Introduction	68
3.1.1 Rationale	68
3.1.2 Innovation	69
3.1.3 Central Hypothesis and Specific Aims	71
4.0 Aim 1: Development of an Ovarian-Specific Extracellular Matrix Hydrogel	72
4.1 Introduction	72
4.2 Objectives	74
4.3 Methods	74
4.3.1 Ovarian Tissue Decellularization.....	74
4.3.2 Detergent Assay	75
4.3.3 Functional Assessment of Macrophages	76
4.3.3.1 Isolation of Bone Marrow-Derived Macrophages.....	76
4.3.3.2 Macrophage Treatment	77

4.3.3.3 Indirect Immunolabeling for Arginase and iNOS Expression	77
4.3.3.4 Phagocytosis Assay	78
4.3.3.5 Nitric Oxide Assay	78
4.3.4 Characterization of Decellularized Tissues	79
4.3.4.1 Hematoxylin & Eosin (H&E) Staining	80
4.3.4.2 Periodic Acid Schiff (PAS) Staining	80
4.3.4.3 Hydroxyproline (HYP) and Sulfated Glycosaminoglycans (sGAG) Assays	81
4.3.4.4 Immunohistochemistry	82
4.3.5 Ovarian ECM Digestion and Hydrogel Formation	83
4.3.6 Hydrogel Characterization.....	83
4.3.7 Whole Ovary Culture	84
4.3.8 In Vitro Follicle Culture	85
4.3.9 Statistical Analysis	86
4.4 Results and Discussion	87
4.4.1 Biomaterial Selection and Tissue Processing.....	87
4.4.2 Ovarian Tissue Specificity Present Post-Decellularization	91
4.4.3 Ovarian Hydrogel Properties Modified with Changes in ECM Concentration	95
4.4.4 In Vitro Applications	97
4.4.4.1 Whole Ovary Culture.....	97
4.4.4.2 In Vitro Follicle Maturation	100
4.5 Conclusion	106

5.0 Aim 2: Ovarian ECM Hydrogel-Facilitated Intraovarian Follicle Microinjection	108
5.1 Introduction	108
5.2 Objectives	110
5.3 Methods	111
5.3.1 Chemotherapy-Induced POF Model.....	111
5.3.2 Weigert’s Hematoxylin Picric Methyl Blue Staining.....	111
5.3.3 Ovarian Follicle Classification and Quantification.....	112
5.3.4 Enzymatic Follicle Isolation	112
5.3.5 Ovarian Tissue Decellularization.....	113
5.3.6 Ovarian ECM Digestion and Hydrogel Formation	114
5.3.7 Fluorescent-Labeling of Ovarian ECM Hydrogels.....	115
5.3.8 In Vivo Follicle Microinjection	115
5.3.9 Mating Study	116
5.3.10 Immunofluorescence Staining and Imaging of Microinjected Ovaries	117
5.3.11 Ovarian Single-Cell Isolation, Antibody Staining, and Flow Cytometry .	118
5.3.12 Statistical Analysis	120
5.4 Results and Discussion	120
5.4.1 Alkylating Agents Significantly Reduce Endogenous Follicle Population..	120
5.4.2 Enzymatic Follicle Isolation and Microinjection Provides an Efficient Transplant Procedure.....	123
5.4.3 Microinjected Follicles Give Rise to Multiple Generations of GFP Pups... 	126
5.4.4 Intraovarian Microinjection Supports Follicle Longevity Post-Transplant 	129

5.5 Conclusion	131
6.0 Discussion.....	133
7.0 Concluding Remarks	139
7.1 Study Summary	139
7.2 Limitations	140
7.3 Future Directions.....	142
Appendix A Decellularization Processing.....	144
Appendix B Decellularization Mass Conservation	148
Appendix C Ovarian Hydrogel Cytocompatibility	153
Appendix D Detergent Concentration During Decellularization	155
Appendix E DNA Fragmentation Post-Decellularization	156
Appendix F Ovarian Tissue Immunohistochemistry.....	157
Appendix G Effect of Ovarian Tissue Processing on Hormones and Growth Factors	158
Appendix H Ovarian Hydrogel Optimization.....	159
Appendix I Ovarian Hydrogel Mechanical Characterization	160
Appendix J <i>In Vitro</i> Newborn Mouse Ovary Culture	163
Appendix K <i>In Vitro</i> Mouse Follicle Cultures.....	168
Appendix L Ovarian Follicle Stage Determination	175
Appendix M Follicle Quantification Post-Chemotherapy	176
Appendix N Statistical Differences Comparing Chemotherapy Dose	177
Appendix O Transgenic GFP Mouse Ovary	179
Appendix P Fluorescently Labeled Ovarian ECM Hydrogel.....	180
Appendix Q Breeding Strategy and Outcomes Following Follicle Microinjection.....	181

Appendix R Control Non-Injected ciPOF Ovaries	184
Appendix S Two-Photon Imaging	185
Appendix T Ovarian Flow Cytometry	187
Bibliography	191

List of Tables

Table 1 Differences in Reproductive Cycle of Mammals	34
Table 2 Summary of Notable Pre-Clinical Fertility Preservation Studies	134
Appendix Table 1 Mass Conservation of Initial Decellularization Protocol	144
Appendix Table 2 Effects of Decellularization on Tissue Mass	148
Appendix Table 3 Whole Ovary Culture Medium	163
Appendix Table 4 In Vitro Follicle Culture Media.....	174
Appendix Table 5 Follicle Counts Post-Chemotherapy	176
Appendix Table 6 Dose-Dependent Statistical Differences in Follicle Counts	177
Appendix Table 7 Breeding Strategy for Follicle Recipients.....	181
Appendix Table 8 Breeding Outcomes of ciPOF Female Mice	181
Appendix Table 9 Outbreeding Strategy of GFP Progeny	182
Appendix Table 10 Inbreeding Strategy of GFP Progeny	182
Appendix Table 11 Second Generation Breeding Outcomes.....	183
Appendix Table 12 Ovarian Flow Panel.....	187

List of Figures

Figure 1 Ovarian Development.....	5
Figure 2 Sexual Differentiation and Gonadal Development	6
Figure 3 Process of Meiosis	9
Figure 4 Cross-Section of The Human Ovary.....	14
Figure 5 Ovarian Surface Epithelium and Ovulation	20
Figure 6 The Menstrual Cycle and Hormone Regulation.....	22
Figure 7 Steroidogenesis in the Ovary	26
Figure 8 Human vs. Pig Reproductive Anatomy	32
Figure 9 Human vs Mouse Reproductive Anatomy.....	33
Figure 10 Porcine Estrous Cycle	35
Figure 11 Rodent Estrous Cycle	36
Figure 12 Iatrogenic Premature Ovarian Failure and Fertility Preservation	41
Figure 13 Fertility Preservation Options for Female Cancer Patients	43
Figure 14 Hydrogel-facilitated Follicle Encapsulation for 3D Culture	47
Figure 15 Extracellular Matrix Composition.....	54
Figure 16 Central Hypothesis	71
Figure 17 Ovarian Tissue Processing.....	88
Figure 18 Histological and Ultrastructural Evaluation of Native and Decellularized Ovarian Tissues	90
Figure 19 DNA and ECM Component Quantification.....	90
Figure 20 Characterization of Ovarian-specific ECM Proteins	92

Figure 21 Quantification of Ovarian-specific Hormones after Decellularization.....	94
Figure 22 Ovarian ECM Hydrogel Formation and Ultrastructure	95
Figure 23 OEMC Hydrogel Fiber Network Analysis	96
Figure 24 OEMC Hydrogel Viscoelastic Properties and Gelation Kinetics.....	97
Figure 25 In Vitro Culture of Newborn Mouse Ovaries	99
Figure 26 Mechanical Follicle Isolation and Encapsulation in OEMC Hydrogels.....	103
Figure 27 IVM OEMC Follicle Morphology	104
Figure 28 IVM OEMC Follicle Diameter	104
Figure 29 Cumulus Oocyte Complex (COC) and MII Oocyte	105
Figure 30 Two-cell Embryo Produced After IVF	105
Figure 31 Effects of Chemotherapy Dosing on Ovarian Tissues.....	122
Figure 32 Endogenous Follicle Populations Post-Chemotherapy	122
Figure 33 Follicle Isolation and Quantification	124
Figure 34 Intraovarian Follicle Microinjection	125
Figure 35 Microinjected Follicles Give Rise to Multiple GFP Litters	128
Figure 36 Genotyping of GFP Pups and Littermates	129
Figure 37 Survival of GFP+ Cells Post-Transplantation	130
Appendix Figure 1 Porcine Ovaries for Batch Decellularization.....	145
Appendix Figure 2 Batch of Diced Porcine Ovaries	145
Appendix Figure 3 Tissues in Flasks Before and After Decellularization.....	146
Appendix Figure 4 Decellularized Porcine Ovaries.....	147
Appendix Figure 5 Macrophage iNOS Expression.....	153
Appendix Figure 6 Macrophage Arginase Expression.....	153

Appendix Figure 7 Macrophage Phagocytosis	154
Appendix Figure 8 Macrophage Nitric Oxide Production.....	154
Appendix Figure 9 Effects of Washes on Detergent Concentrations.....	155
Appendix Figure 10 Agarose Gel Electrophoresis.....	156
Appendix Figure 11 IHC Ovarian ECM Proteins	157
Appendix Figure 12 Retention of Ovarian-specific Hormones and Growth Factors.....	158
Appendix Figure 13 Effects of Pepsin on Gelation Kinetics	159
Appendix Figure 14 Ultrasound Elastography	160
Appendix Figure 15 Ultrasound Elastography Experimental Setup	161
Appendix Figure 16 OEMC Soluble/Insoluble Fraction.....	162
Appendix Figure 17 Protein Gel Soluble vs Insoluble Fraction	162
Appendix Figure 18 OEMC Hydrogel Optimization for Whole Ovary Culture	164
Appendix Figure 19 Initial Results of Whole Ovary Culture.....	165
Appendix Figure 20 Follicle Quantification Using Volocity Software.....	166
Appendix Figure 21 Viscoelastic Properties of OEMC Hydrogel for Ovary Culture.....	167
Appendix Figure 22 Mechanical Follicle Isolation for IVM.....	168
Appendix Figure 23 IVM Trial 1 – Isolated Follicles	168
Appendix Figure 24 OEMC-IVM Trial 1 - Single Follicle – Day 1.....	169
Appendix Figure 25 OEMC-IVM Trial 1 – Single Follicle – Day 6.....	169
Appendix Figure 26 OEMC-IVM Trial 1 – Grouped Follicles - Day 1	170
Appendix Figure 27 OEMC-IVM Trial 1 – Grouped Follicles – Day 6.....	170
Appendix Figure 28 OEMC-IVM Trial 1 – Follicle Diameter	171
Appendix Figure 29 OEMC Hydrogel Droplets	172

Appendix Figure 30 Alginate Microspheres.....	172
Appendix Figure 31 New OEM-IVM Trial 2 – Follicle Morphology.....	173
Appendix Figure 32 New OEM-IVM Trial 2 – Follicle Diameter.....	173
Appendix Figure 33 Morphological Characterization of Follicle Stage.....	175
Appendix Figure 34 Tissue Cleared GFP Mouse Ovary.....	179
Appendix Figure 35 TRITC-labeled Ovarian Hydrogel.....	180
Appendix Figure 36 Immunofluorescence of Control ciPOF Ovaries.....	184
Appendix Figure 37 Two-Photon Filter Cube Design.....	185
Appendix Figure 38 Two-Photon Excitation and Emission Wavelengths/Filters.....	186
Appendix Figure 39 Ovarian Flow Gating Strategy.....	187
Appendix Figure 40 Proliferative Cells (Ki67+ Cells).....	188
Appendix Figure 41 Percentage of Apoptotic Cells (Caspase3+ Cells).....	189
Appendix Figure 42 Percentage of Macrophage Populations (CD206+ and CD86+ Cells).....	190
Appendix Figure 43 Percentage of Oocytes (NOBOX+ and Zp3+ cells).....	190

Preface

The following dissertation is the result of years of research aiming to advance the field of female reproductive tissue engineering. Throughout this process, there were many setbacks and failures that ultimately led to the first successful application of intraovarian follicle microinjection for fertility preservation. This procedure produced multiple generations of healthy offspring from chemotherapy-treated mice with severely reduced follicle populations. The development of this novel strategy has the potential to aid in restoring reproductive function and fertility in women suffering from iatrogenic premature ovarian failure.

This work could not have been completed without the guidance and support of several people. First, I would like to thank my Ph.D. advisor and committee chair, Dr. Bryan N. Brown, for giving me the opportunity to join his laboratory at the University of Pittsburgh. Throughout my doctoral studies, Dr. Brown allowed me the scientific freedom to develop as an independent researcher. He gave me autonomy to explore and test my hypotheses that led to some very interesting findings. I am grateful for his unequivocal support and mentorship that was critical for the completion of this graduate program and preparation for a career in biomedical research.

Additionally, I would like to thank my other committee members, Dr. Kyle Orwig, Dr. Sanjeev Shroff, Dr. Aleksandar Rajkovic and Dr. Lance Davidson, for their feedback and guidance to clearly define the aims and experimental design of this study. They are all outstanding scientists and I was very lucky to have them as part of my committee. Specifically, collaborations with Dr. Orwig and Dr. Rajkovic at the Magee-Womens Research Institute were instrumental in my understanding of reproductive biology and allowed me to test our ovarian extracellular matrix (OECM) hydrogel to determine its effects on ovarian tissues and cells. A large portion of my thesis

work was developing and testing our OECM hydrogel to deliver and support follicle integration into chemotherapy treated female mice. Dr. Orwig was incredibly generous and offered his lab's line of transgenic female mice to be used as follicle donors, as well as nude mice as recipients/breeders to perform our in vivo studies. I am greatly appreciative for his expertise and significant contribution of intellectual input, time and resources to design and complete this work. I would like to especially acknowledge Dr. Meena Sukhwani for her assistance with several critical aspects of the in vivo studies including chemotherapy treatments, follicle microinjection surgeries, and animal breeding. I would also like to thank Sarah Steimer for her help with the breeding strategy and animal breeding. I would also like to thank Dr. Yi Sheng for his guidance using IVF and providing his knowledge for genotyping the transgenic progeny. A smaller portion of my thesis work was dedicated to using the OECM for whole ovary cultures in Dr. Rajkovic's lab. I am grateful for Dr. Rajkovic's time, resources and sharing his knowledge of ovarian follicle development. He provided great input for the design of experiments to determine the effects of our OECM hydrogel for whole ovary culture and to assess ovary maintenance and development. I would also like to acknowledge the post-docs, Dr. Yonghyun Shin and Dr. Yu Ren, from the Rajkovic lab who taught me various techniques including ovarian tissue isolation and culture.

I would like to acknowledge the Department of Bioengineering of the Swanson School of Engineering at the University of Pittsburgh for providing both academic and financial support during my time in the program. I would like to especially thank Dr. Shroff for always being supportive and offering his assistance when needed. I would like to acknowledge The McGowan Institute of Regenerative Medicine, where the majority of this work was completed. I am grateful for their outstanding resources and programs that have provided both great research exposure and experience sharing my own data with the scientific community. I will always be thankful for this

collaborative community of researchers who have provided their resources and time. I would like to thank Dr. Antonio D'Amore, who provided software and assisted with the hydrogel fiber network analysis. I would like to acknowledge the Center for Biologic Imaging (CBI) for their assistance performing scanning electron microscopy (SEM) and whole organ imaging. I would especially like to thank Jonathan Franks (SEM), Dr. Alan Watson (tissue clearing and 3D imaging) and Gregory Gibson (multi-photon imaging) for making themselves available to obtain images used for this study.

The entire Brown laboratory has been like a family to me for the past several years. I would like to thank all the past and present members, including assistant professors, post-doctoral students, graduate students, lab technicians and executive assistants: Clint Skillen, Dr. Daniel Hachim Diaz, Dr. Samuel LoPresti, Dr. Travis Prest, Dr. Elizabeth Stahl, Dr. Aimon Iftikhar, Alexis Nolfi, Martin Haschak, Dr. Arta Kelmendi-Doko, Dr. Branimir Popovic, Tyler Meder, Dr. Mangesh Kulkarni, Marrisa Therriault, Marissa Behun, Nancy Briones, Elaine Becker, Joseph Kennedy, and Deepa Mani. I will never forget the memories that we have made together. I sincerely appreciate all your assistance, sharing of knowledge, ideas and feedback to help me grow throughout this process. In addition, I would like to acknowledge all the undergraduate students that directly contributed to development of this work: Rebecca Miller, Brandon Burger, Dipali Shah, Ziyu Xian, Arvind Venkatraman, Srujan Dadi, and Zachary Case.

This work is dedicated to my family and friends. I would not be here without their daily support. To my parents, Philip and Gail, thank you for always pushing me to do my very best and keeping me moving forward even when times have been tough. Thank you for teaching me what hard work means and for sacrificing your own career goals to help your children achieve theirs. To my sisters, Erin and Lynn, thank you for always cheering me on and being my biggest fans. To

my in-laws, thank you for bringing me into your family with open arms. I am so thankful to have your love and support. I love you guys!

To my wife, Cara, I could not have done this without you. Thank you for being patient, positive and providing the encouragement I needed along the way. Your love and sacrifice for our children and I will always be cherished. All my accomplishments are made possible because of you. To my sons, Gallus and Theodore, thank you for always making me smile, laugh and keeping me on my toes. You both continue to inspire and amaze me. I am so lucky to be your dad, and I cannot wait to see what the future holds for you. I love you all!

Finally, my pursuit of a doctoral degree in Bioengineering stems from my goal to improve the quality of life for people battling debilitating disease. My wife and sister have had Type I Diabetes since they were adolescents, and although methods of maintenance for the disease have improved, the physical and emotional toll it takes is devastating. Their affliction with this disease continues to motivate me to build my scientific knowledge to help develop a cure for diabetes and other autoimmune illnesses. I know that this experience has prepared me for the next step of my research career and will allow me to improve the lives of people in need.

1.0 Introduction

The focus of this dissertation is to develop novel methods with the potential to restore fertility for female patients diagnosed with iatrogenic premature ovarian failure (POF). To accomplish this goal, it is important to understand normal female reproductive biology and how invasive mechanical or cytotoxic chemical treatments can impair the ovarian microenvironment. Therefore, the following section will provide an overview of female reproductive biology, causes and consequences of POF and current strategies for fertility preservation.

1.1 Female Reproductive Biology

Female reproductive biology is the study of the cells and tissues that make up the female reproductive system. The major organs of this system include the ovaries, fallopian tubes, uterus, and vagina, which work in concert to support fertility (1). The ovaries provide a permissible environment for the development of the female gametes, or oocytes (2). During embryonic development, primordial germ cells (PGCs) aggregate within the cortex of the ovary and acquire a single layer of granulosa cells forming primordial follicles (3, 4). This population of primordial follicles represents the ovarian reserve, which is an indicator of potential conception for women of reproductive age (5-8). Upon puberty, the hypothalamus and pituitary increase gonadotropin levels (9, 10). In response to gonadotropin production, a small number of primordial follicles are recruited and activated into a growing pool (11). This activation is accompanied by granulosa and theca cell proliferation, which amplifies the secretion of sex steroids that stimulate the growth and

maturation of the recruited follicles (12). Ovarian steroid production actively contributes to an essential feedback loop known as the hypothalamus-pituitary-gonadal (HPG) axis (10, 13-15). The HPG axis establishes the female sexual cycle, which repeats each month to support the release of a single mature oocyte and prepares the uterus for embryo implantation and pregnancy (13).

The following sub-sections of Section 1.1 provide more details on selected subject matter within female reproductive biology that are relevant to the present study. The primary focus will be on the following topics: (1) the development and composition of the ovary, (2) ovarian cell types and function, (3) reproductive differences between mammals and (4) normal ovarian aging.

1.1.1 Ovarian Development

During early embryonic development, undifferentiated sexual organs begin their assembly within the gonadal ridge, which develops from proliferating gonadal ridge epithelial-like (GREL) cells from the coelomic epithelium of the mesonephros (Figure 1) (16, 17). Around five weeks post-coitum, bipotential gonads begin to form out of the expanding gonadal ridge. Meanwhile, primordial germ cells (PGCs), which are the precursor cells to gametes (oocyte and sperm), migrate from the embryonic yolk sac along the gut to the gonadal ridge. During migration, PGCs proliferate substantially, which increases their population from about 100 in the yolk sac to 1,700 upon arrival at the gonadal ridge (18). A breakdown of the basal lamina lying beneath the coelomic epithelium during gonadal ridge formation facilitates the invasion of mesenchymal and stromal cells of the mesonephros into the developing gonads (16).

Once the PGCs enter the gonadal ridge, they undergo sexual differentiation upon which they exclusively develop into either oogonia or spermatogonia. Sex determination is predicated upon the composition of the chromosomes present within the growing embryo (19). Humans are

made up of diploid cells, which contain two sets of chromosomes (23 pairs). Of the 23 pairs, one pair is composed of the genes that determine the sex of the embryo. Male and female gametes are haploid germ cells, which contain one set of chromosomes. Male sperm carry the 22 autosomal chromosomes and either an x or y sex chromosome. Similarly, female oocytes contain the 22 autosomal chromosomes, but only provide an x sex chromosome. Upon fertilization, genetic recombination of the haploid germ cells yields a diploid embryo with 44 autosomal chromosomes and two sex-determining chromosomes: XY (male) or XX (female) (20). The sex of developing human embryos is indicated by the presence of the sexual determining region of the Y (SRY) gene (21). Without the SRY gene, the ovary forms in response to the upregulated expression of the female gonad-specific WNT4/ β -catenin signaling, which inhibits the male gonad-specific SOX9/FGF pathway (Figure 2) (22).

At the conclusion of female sex determination, around 9 weeks post-coitum, PGCs begin to differentiate into oogonia, which are distinguished by their increased rate of mitosis (23). This increase in cell division directly contributes to the formation of oogonial nests (23). Simultaneously, the gonadal ridge undergoes significant expansion, as the migration of mesonephric cells, including stroma and blood vessels, begin to occupy and surround the rapidly dividing germ cell nests, forming the ovigerous cords. The appearance of the sex cords signals the beginning of a compartmentalization of the ovary, as the stromal cells are preferentially separated from the GREL cells and oogonia by a basal lamina (16, 24, 25). The ovary is subsequently divided into two main regions, which are composed of an outer cortex and an inner medulla. The cortex primarily contains proliferating oogonia while the medulla is comprised of connective tissue, large blood and lymphatic vessels (26). Around 11 weeks, oogonia, residing along the interface of the cortex and medulla, enter meiosis I (27). As this process continues, oogonia and oocytes within

the germ cell nests undergo apoptosis, which dramatically reduces the total number of germ cells available for maturation (5). The oocytes that remain acquire a peripheral layer of pre-granulosa cells surrounded by a basal lamina forming the primordial follicles (16). The total number of primordial follicles make up the ovarian reserve, which is an indicator of fertility potential.

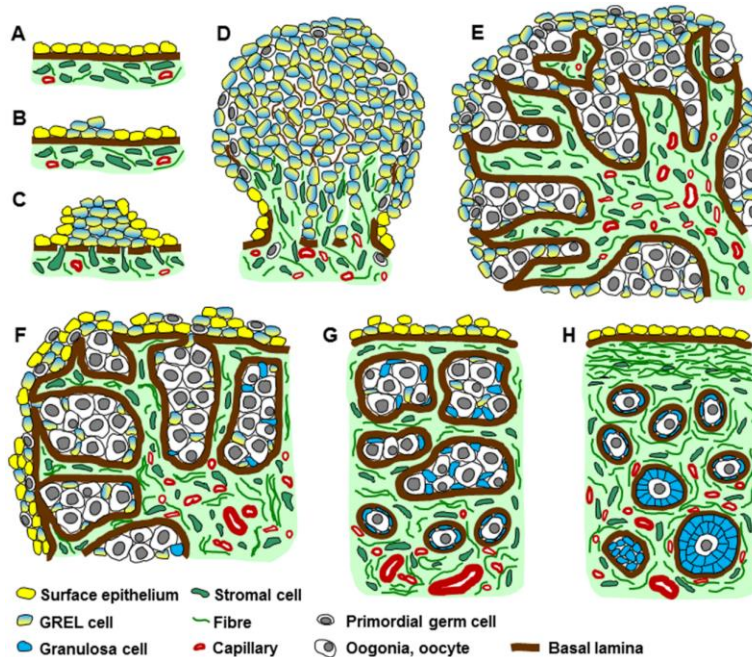


Figure 1 Ovarian Development

(A) The development of the ovary commences at the mesonephric surface epithelium (yellow cells) in the location of the future gonadal ridge. (B) Some mesonephric surface epithelial cells change phenotype into GREL cells (yellow-blue cells). (C) The GREL cells proliferate and the basal lamina underlying the mesonephric surface epithelium breaks down allowing stromal cells (green) to penetrate into the gonadal ridge. (D) GREL cells continue to proliferate and PGCs (grey) migrate into the ridge between the GREL cells. Mesonephric stroma including vasculature (red) continues to penetrate and expand in the ovary. (E) Oogonia proliferate and stroma penetrates further towards the ovarian surface enclosing oogonia and GREL cells into oovigerous cords. (F) Compartmentalization of oogonia occurs surrounded by the basal lamina, which is also formed below GREL cells at the surface. The cortex is characterised by alternating areas of oovigerous cords and stroma, whereas the medulla is formed by stromal cells, vasculature and tubules originating from the mesonephros (rete ovarii). (G) Oovigerous cords are partitioned into smaller cords and eventually into follicles. These contain GREL cells that form granulosa cells (blue cells) and oogonia that form oocytes. The first primordial follicles appear in the inner cortex-medulla region, surrounded by a basal lamina. A now fully intact basal lamina underlies multiple layers of surface epithelial cells. (H) At the final stage the surface epithelium becomes mostly single-layered and a tunica albuginea, densely packed with fibres, develops from the stroma below the surface epithelial basal lamina.

[Figure and text reproduced from (16). Open-access - Creative Commons Attribution License.]

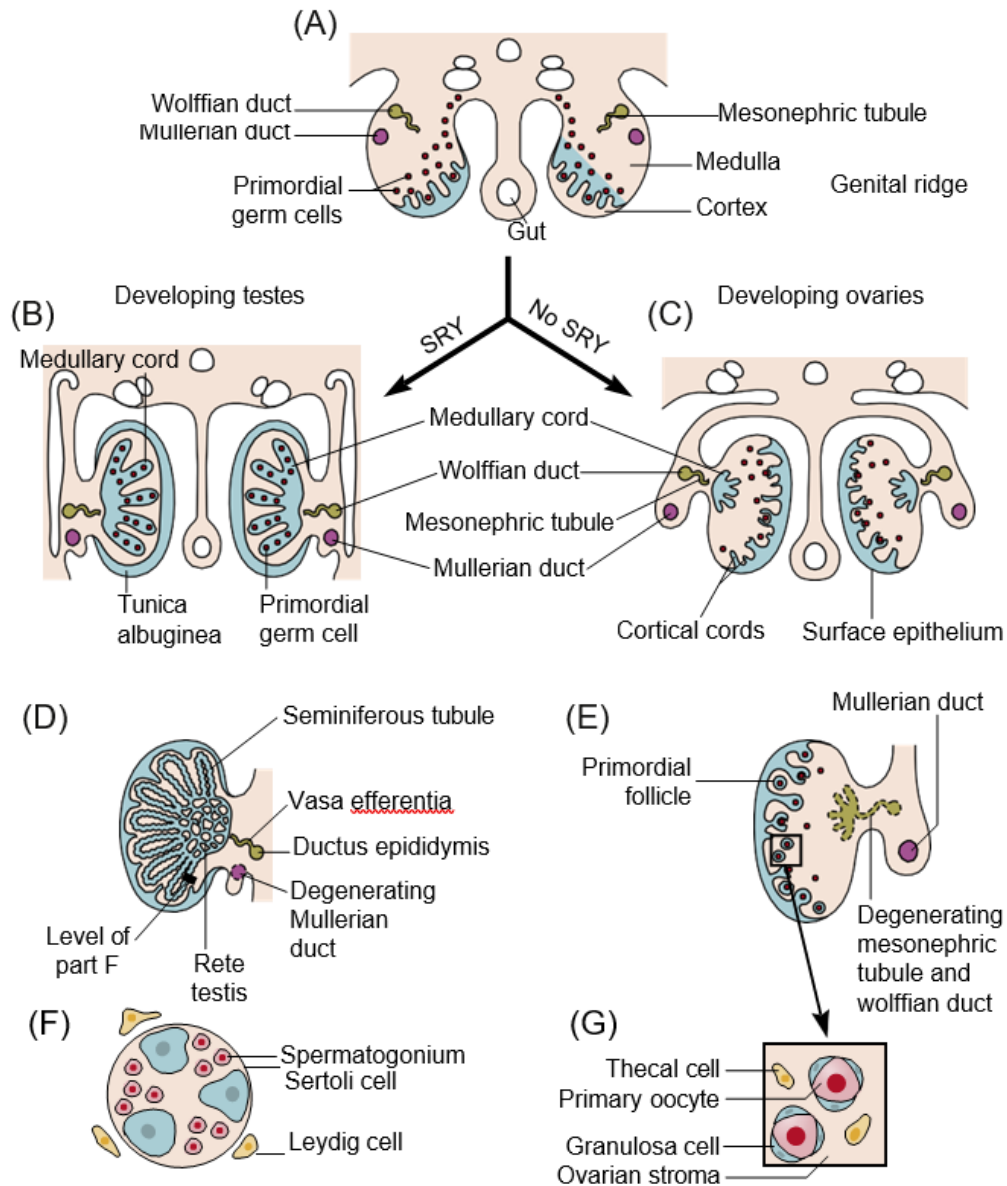


Figure 2 Sexual Differentiation and Gonadal Development

Diagram illustrating differentiation of indifferent gonads into testes or ovaries: (A) Bipotential gonads from a six-week-old embryo; (B) At seven weeks, showing testes developing under the influence of SRY; (C) At 12 weeks, showing ovaries developing in the absence of SRY; (D) Testis at 20 weeks, showing the rete testis and seminiferous tubules derived from medullary cords; (E) Ovary at 20 weeks, showing primordial follicles; (F) Section of a seminiferous tubule from a 20-week fetus; and (G) Section from the ovarian cortex of a 20-week fetus, showing two primordial follicles.

[Figure and text reproduced from (18). License obtained from Elsevier- No. 4797171375381]

1.1.1.1 Oogenesis

To produce genetically distinct progeny, gametes must only contain half of the chromosomes prior to their fusion at fertilization, with half of the genes coming from the male and half from the female. Oogenesis begins during the early stages of embryonic development with the differentiation of PGCs to oogonia after female sex determination (28, 29). Oogonia undergo rapid mitotic proliferation and form germ cell nests or clusters from 2-7 months in utero (23). Oogonia give rise to individual primordial follicles that contain a primary oocyte arrested in prophase I of meiosis (30).

Meiosis is the process that forms haploid daughter cells or sex cells within the female and male gametes (Figure 3) (31). Like mitosis, meiosis undergoes DNA replication and cell division; however, a major difference is that mitosis converts one diploid cell ($2N$) to two exact replicate diploid cells, which contain the same genetic signature (32). Conversely, meiosis converts a single diploid germ cell into four unique haploid (N) gametes (33). One mature ovum in females and one sperm in males, that fuse during fertilization, give rise to a single genetically distinct diploid cell or embryo, which contains half of the genes from the mother and the other half from the father.

Meiosis begins identically to mitosis through the entrance into the first stage of the cell cycle or G1, where the cells start to prepare for replication and division (34). During G1, the cells begin to produce more organelles and proteins to support the functions of an additional cell. After G1, the cells enter the S1 or synthesis phase, where the DNA will undergo replication to double the genetic material (34). After DNA replication in S1, the cell enters the G2 phase. In G2, the cell prepares for division by producing more cytoplasm to grow the total volume of the cell (34). These first three stages together are called interphase. Interphase repeats for all germ cells prior to meiotic division. After interphase, germ cells undergo two cycles of meiotic division, referred to as meiosis

I and meiosis II (31). During each cycle of meiosis, the cells undergo prophase, metaphase, anaphase and telophase. In meiosis I, prophase I starts by breaking down the nuclear envelope and condensing the chromatin into chromosomes that are identified by the presence of a centromere. Maternal and paternal chromosomes approach one another and form homologous pairs, which undergo phenomenon known as crossing over. Crossing over is a process in which a small segment of the maternal and paternal alleles, that code for the same genomic region, swap places and attach to the opposing chromosome (28). This event is one of many that helps to diversify the genes present within the resulting embryo. After forming homologous pairs and randomly crossing over, the cells move into metaphase I. In metaphase I, the chromosomes are centered at the midline of the cell (32). This is facilitated by microtubules that extend from the centrosomes that have relocated to the opposite or polar ends of the cell. Microtubules adhere to the kinetochores on the opposing ends of the centromere of each chromosome (31). During anaphase I, microtubules begin to separate the homologous pairs toward the opposite poles. Once the chromosomes have arrived at their respective poles, the cell enters telophase I, where the cell undergoes cytokinesis and each of the separated chromosomes are surrounded by their own nuclear envelope (35). Normally, cytokinesis divides the cells equally, but this is not the case for oocytes. The first meiotic division of oocytes yields one larger oocyte and a smaller polar body (36). Meiosis II resumes with prophase II, where the chromatin condenses into chromosomes and the nuclear envelope degrades the two haploid cells that resulted from the first meiotic division (31). Metaphase II aligns the chromosomes at the middle of the cells and anaphase II begins to separate the sister chromatids, pulling them towards their respective poles. Finally, in telophase II the two haploid cells from the first meiotic division split into two preparing a total of four genetically distinct haploid gametes(31).

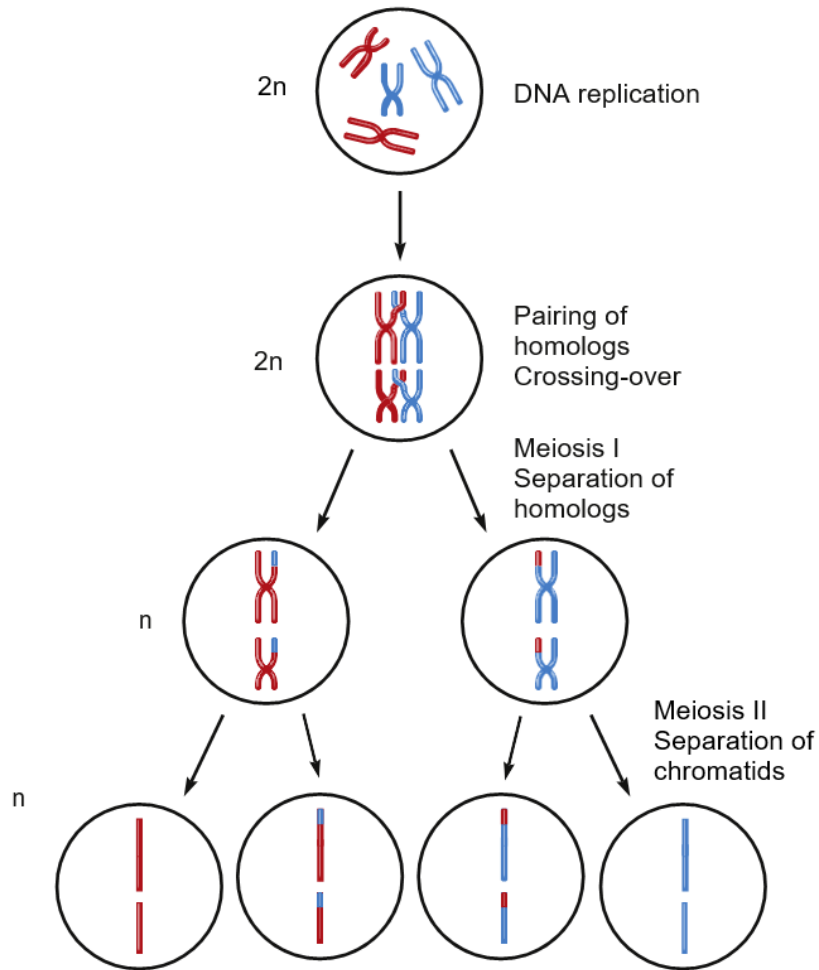


Figure 3 Process of Meiosis

Meiosis is a unique form of nuclear division that results in haploid gametes. In preparation for the first meiotic division, homologous chromosomes come together in synapsis, forming a tetrad of two replicated chromosomes, each with two sister chromatids. As the tetrads line up on the metaphase plate, those from maternal and paternal origin orient (assort) randomly. Crossing-over may occur, in which a piece of a chromatid is physically exchanged with a homologous chromatid, forming new allele combinations. In the meiosis I division, homologs separate, and thus each secondary oocyte is haploid, though each chromosome has two sister chromatids. The meiosis II division separates sister chromatids. Crossing-over and random assortment create new combinations of maternal and paternal genes, resulting in gametes that are genetically unique.

[Figure and text reproduced from (1). License obtained from Elsevier - No. 4842610641195]

In oogenesis, meiosis begins during embryonic development with the formation of oocytes from oogonia in the gonadal ridge (37, 38). Primordial follicles, containing primary oocytes that are arrested in prophase I of the first meiotic division, remain in this developmental phase until puberty (39). Upon activation of primordial follicles, oocytes enlarge to accommodate the maturation of the cytoplasm, but they remain meiotically static until the formation of an antrum appears within the follicle (36). During this pre-antral stage, oocytes undergo dramatic changes which facilitate successful downstream meiotic division and fertilization. For example, the oocyte cytoplasm acquires maternal effect genes, such as zygotic arrest-1 (Zar1) and NOD-like receptor family pyrin domain containing 5 (Nlrp5), which aid in embryonic development (40, 41). Additionally, the stage-dependent positioning and function of organelles can impact the effectiveness of oocyte maturation. Specifically, mitochondria supply the oocyte with adenosine triphosphate (ATP) and preferentially relocate around the poles to become more accessible during meiosis (42-44). Similarly, the endoplasmic reticulum acts as a catalyst upon fertilization by releasing calcium that inhibits polyspermy and concludes oocyte maturation (45, 46). Regulation of oocyte growth is dependent upon the relationship between the oocyte and the surrounding granulosa cells of the follicle compartment. Growth differentiation factor 9 (GDF9) and bone morphogenic factor 15 (BMP15) are produced by the oocyte to induce granulosa cell proliferation and modulate oocyte hypertrophy during meiotic quiescence (47, 48).

Oocytes resume meiosis in response to rising levels of luteinizing hormone (LH), which is augmented by an upregulation of LH receptors presented by granulosa cells (49). This interaction sets off a signaling cascade that effectively removes intraoocyte cyclic adenosine monophosphate (cAMP). The presence of cAMP inhibits oocytes from continuing meiotic cell division and regulates follicle growth (36). The pre-ovulatory LH surge causes cumulus cells to detach from

the oocyte and reduces the translocation of cAMP to the oocyte (50). In addition, residual oocyte cAMP is enzymatically degraded by phosphodiesterase (PDE), which is induced by mitogen-activated protein kinase (MAPK) expression from cumulus cells(51, 52). The loss of cAMP reduces protein kinase A (PKA), which phosphorylates and inhibits the phosphatase, cell division cycle 25 (CDC25) (53). Once CDC25 is activated, it dephosphorylates and activates cyclin-dependent kinase 1 (CDK1), which together with cyclin B (CYB) forms a protein complex known as maturation promoting factor (MPF) that directly facilitates the resumption of meiosis (54-56). This event transforms the oocytes from a germinal vesicle (GV) stage, identified by an intact nuclear membrane to germinal vesicle breakdown (GVBD) stage, classified by an absence of the nuclear membrane. Upon ovulation, meiosis is once again interrupted and arrests at metaphase II (MII) by the degradation of CYB and inactivation of CDK1 (57, 58). At this step of maturation, the MII, or secondary oocyte, has completed the first meiotic division and extrudes a polar body, which will degenerate. Oogenesis concludes after the sperm fertilizes the MII oocyte, resuming meiosis II, as the haploid cells form a genetically distinct embryo.

1.1.1.2 Folliculogenesis

Oogenesis is made possible through the maturation of the ovarian follicles, which synergistically secrete hormones that regulate primary oocyte growth and trigger secondary oocyte ovulation. Folliculogenesis, like oogenesis, undergoes a series of developmental stages, which occurs cyclically for each follicle throughout the female reproductive lifespan (59). Primordial follicles are the initial stage of development that make up the ovarian reserve, or the finite number of oocytes with the potential for maturation and fertilization (5, 7, 8). At this stage, the follicles are tightly clustered within the ovarian cortex and are composed of a central primary oocyte surrounded by a single layer of squamous granulosa cells (3).

In humans, there are approximately one million primordial follicles that make up the ovarian reserve at birth; however, most of these follicles will undergo atresia, which reduces the absolute follicle number by 70% at puberty (7, 60). This drastic reduction has been attributed to a stringent selection process that prematurely removes imperfect follicles, containing genetic errors, poor cytoplasmic composition or low granulosa cell numbers (61, 62). Further, DNA damage incurred by primordial follicles can be recognized by the transactivation domain of tumor protein p63 (TAp63), which can trigger premeditated cell death through the p53 upregulated modulator of apoptosis (PUMA) (63-65). The remaining primordial follicles that make up the reserve are recruited to the growing pool by environmental stimuli. For example, granulosa cell production of growth factors, such as KIT ligand, can be induced through mechanistic target of rapamycin complex 1 (mTORC1) signaling, directly initiating the phosphatidylinositol 3-kinase (PI3K) pathway upon KIT ligand binding of KIT at the oocyte membrane (66, 67). Alternatively, follicle activation can be inhibited by anti-Mullerian hormone (AMH) and activin produced by small pre-antral follicles (68, 69).

Recruited primordial follicles undergo distinct morphological changes as their surrounding granulosa cells begin their transition from a flattened to cuboidal appearance (12). The formation of a full layer of cuboidal granulosa cells surrounding the oocyte represents primary follicles (70). Additionally, the oocytes of primary follicles begin to display a zona pellucida, which is a rich extracellular matrix glycoprotein that facilitate fertilization (70). The proliferation of granulosa cells continues toward the development of secondary follicles, represented by multiple layers of granulosa cells as well as the presence of a theca cell layer. Within pre-antral follicles, the central oocyte is meiotically static; however, it does increase in size to accommodate the maturation of the cytoplasm (70). The transition from pre-antral to antral follicles is distinguished by the

presence of antral fluid surrounding the oocyte. The antral follicles are the final stage development prior to ovulation, when the meiotically competent, MII oocyte is released for fertilization. Upon ovulation, the granulosa cells will differentiate into luteal cells to form a structure known as the corpus luteum (71). The corpus luteum secretes progesterone to maintain pregnancy after successful embryo implantation into the uterine wall.

1.1.2 Ovarian Anatomy and Physiology

The ovary is the female reproductive organ that is responsible for both the maintenance and maturation of oocytes (1). At puberty, the ovary has fully matured and contains active, hormone-producing follicles. Granulosa and theca cells surround oocytes to compose the ovarian follicles, which are the functional subunit of the ovary. The somatic cells are intimately connected with the oocyte and operate as part of a dynamic feedback loop to regulate follicle growth and maturation (72). The predominant cell type within the ovary are stromal cells, which actively remodel the ovarian microenvironment to support the proliferation and migration of follicles throughout reproductive development (73). Transient corpora lutea form a glandular structure from differentiated granulosa cells to facilitate the production of progesterone to sustain pregnancy after ovulation (74). Endocrine function is promoted by an extensive vasculature network that provides the ovary with direct access to essential nutrients from the blood (75). It is essential that each of these components are highly coordinated to maintain normal reproductive function.

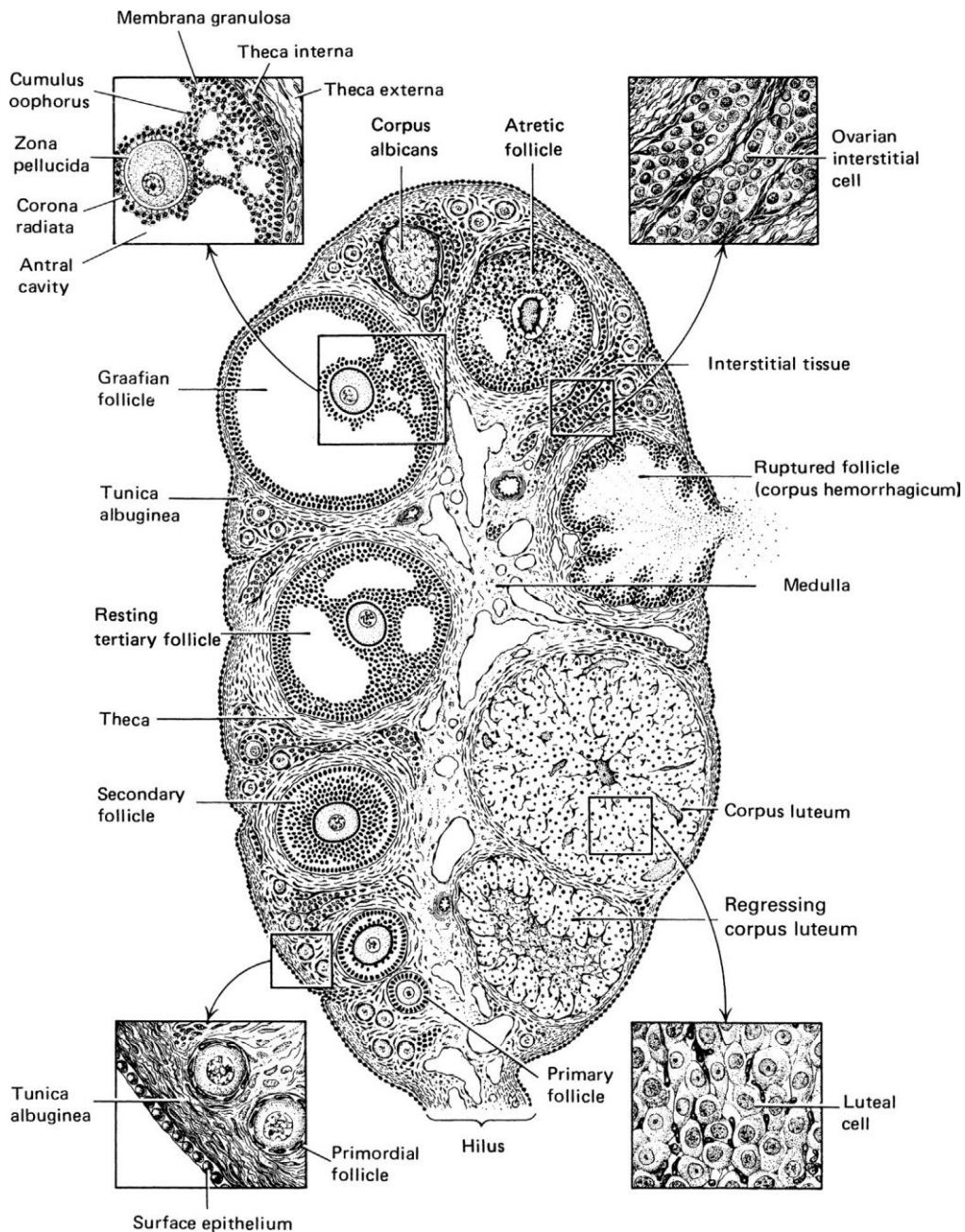


Figure 4 Cross-Section of The Human Ovary

The ovary is a female reproductive organ composed of an outer cortex and inner medulla. The cortex contains primordial follicles, which undergo cyclic activation to support the ovulation of a mature oocyte, whereas the medulla is primarily made up of large blood vessels and lymphatics. Growing follicles and corpora lutea produce hormones to regulate endocrine function and maintain pregnancy.

[Figure reproduced from (1). License obtained from Elsevier - No. 4842610641195]

1.1.2.1 Tissue Organization and Cell Types

The ovary is made up of two main regions: the peripheral cortex and the central medulla (Figure 4) (76). The mechanically rigid cortex is primarily comprised of immature primordial and small growing follicles, whereas the more compliant medulla is home to the bulk of mesenchymal tissue with large blood and lymphatic vessels (75, 77). A diverse extracellular matrix (ECM) is interspersed throughout the stroma, interstitial tissues and follicle compartments. The ECM undergoes rapid changes during folliculogenesis to provide a permissible environment for follicle maturation. The parenchyma is composed of somatic cells, granulosa and theca cells, which surround the oocyte, and form the functional unit of the ovary, known as the ovarian follicle (76). The cells and tissues of the ovary are highly responsive and regulated by the hypothalamus-pituitary signals (13). Active production of hormones and growth factors by ovarian cells ensure tight control over changes within the ovarian microenvironment and sustain endocrine function.

1.1.2.1.1 Ovarian Extracellular Matrix

The ovarian ECM plays a critical role in the maintenance of ovarian follicles. Ovarian ECM is synthesized during the early stages of embryonic gonadal development (78). The first expression of ECM deposition is observed within the genital ridge during the formation of a basement membrane, which surrounds the germ cells nests. The basement membrane is primarily composed of laminin, collagens, fibronectin and proteoglycans (78). Primitive ovarian ECM undergoes significant remodeling by matrix metalloproteinases (MMPs), which actively degrade ECM components (78, 79). MMPs are also active throughout folliculogenesis to accommodate the exponential growth of follicles and release of MII oocytes upon maturation (79).

Throughout the initial stages of ovarian development, ECM production is primarily mediated by three cell types: somatic cells, stromal cells and germ cells (78). Each of these cells express a distinct transcriptional profile of ECM-specific genes that are present during sexual differentiation of mouse gonads (78). However, stromal cells are the most active participant in ECM synthesis, as they account for about 94% of the total ECM genes detected within the immature XX gonads (78). The genes expressed by the stroma are well represented across each major type of ECM, including, collagens, glycoproteins, proteoglycans and matricellular proteins (78). Somatic cells and germ cells only contribute to the expression of 11 and 7 ECM-associated genes respectively, which primarily code for non-collagen ECM components (78).

The ovarian ECM plays a critical role in folliculogenesis, acting as a structural framework for the cells and sequestering essential hormones and growth factors that facilitate cell signaling and proliferation(80, 81). Ovarian-specific ECM components primarily consist of collagen I, collagen IV, laminin and fibronectin and are well conserved across species(82-86). Localization of these specific ECM components varies throughout the ovary and changes depending on the stage of follicle development.

1.1.2.1.2 Ovarian Follicles

The ovarian follicles are the functional subunit of the ovary that produces hormones to regulate oocyte maturation (70). Follicle assembly begins with primordial germ cell migration infiltrating the gonadal ridge and differentiating into oogonia (87). Oogonia cell cysts breakdown to form oocytes that arrested in prophase I of meiosis (88). GREL cells differentiate into pre-granulosa cells that encapsulate the oocyte to form primordial follicles (16). This population of primordial follicles make up the ovarian reserve, which is an indicator of potential fertility (7, 8).

Primordial follicles are activated into the growing pool and acquire numerous layers of granulosa cells that play an essential role in oocyte maintenance (12, 89). Secondary follicles continue granulosa cell proliferation and recruit theca cells to facilitate the production of sex steroids, estradiol and progesterone (59, 90). A single dominant follicle, characterized by a pocket of accumulated antral fluid surrounding a meiotically competent oocyte arrested in metaphase II, will be selected for ovulation (91). Upon ovulation, granulosa cells will differentiate to form a corpus luteum, which is a transient endocrine gland that produces high levels of progesterone to sustain pregnancy (71).

1.1.2.1.3 Granulosa Cells

Granulosa cells are the most abundant cell type within growing ovarian follicles. These cells derive from the GREL cells that are sequestered inside of the ovigerous cords adjacent to the proliferating oogonia (92). Squamous pre-granulosa cells form a loose layer around immature oocytes forming primordial follicles (93). Once the primordial follicles are activated from the resting stage, granulosa cells rapidly proliferate to support the oocyte. Multiple layers of granulosa cells accumulate as they transition from secondary to antral follicles. Granulosa cells directly surrounding the oocyte of antral follicles differentiate into cumulus cells, which expand prior to ovulation (70).

1.1.2.1.4 Theca Cells

Theca cells form the outermost layer of ovarian follicles and produce androgens, which are subsequently converted into estrogens by the granulosa cells(70). These somatic cells are derived

from two distinct populations of theca progenitor cells (94). The predominant theca progenitor population is derived from the fetal ovary and expresses Wilms' tumor 1 (Wt1), which is required for gonad development (95, 96). The other theca progenitor cells originate in the mesonephros and differentiate into glioma-associated oncogene homolog 1 (Gli1) positive cells regulated by growth differentiation factor 9 (GDF9) and hedgehog (Hh) signaling, coordinated through the oocyte and granulosa cells (94).

1.1.2.1.5 Luteal Cells

Luteal cells are the primary cell type of the corpus luteum, which is formed from follicles that have released a mature oocyte (74). Prior to ovulation, granulosa cells begin to differentiate into luteal cells through the acquisition of LH receptors (1). Unlike granulosa or theca cells, luteal cells have all the enzymes needed to directly convert cholesterol into progesterone and estradiol. During the luteal phase of the menstrual cycle, luteal cells are transiently expressed to produce progesterone and estradiol to aid in the preparation of the uterus for pregnancy and will degenerate in the absence of a fertilized oocyte (1). However, if fertilization and pregnancy occur, the menstrual cycle is delayed, and the luteal cells continue to produce high levels of progesterone to sustain pregnancy.

1.1.2.1.6 Stromal Cells

Stromal cells are one of the most prevalent cell types within ovarian tissue. They are primarily responsible for maintaining tissue homeostasis through the production and remodeling of the extracellular matrix(78). These cells are also capable of producing essential growth factors

such as bone morphogenic proteins (BMPs) to support follicle development. Specifically, the release of BMP-4 and BMP-7 has been shown to play a role in the transition from primordial to primary follicles(97, 98). Stromal cells may also differentiate into theca cells, transitioning from a mesenchymal to parenchymal cell type through the acquisition of Gli1 or Wt1.

1.1.2.1.7 Endothelial Cells

Endothelial cells present within the ovary are critical for providing functional blood vessels to the ovarian follicles and corpus luteum (75, 99). Ovarian mediated endocrine function is also highly dependent upon the secretion of steroids into the blood vessels. The ovarian vasculature is primarily found within the stroma; however, as follicles mature, endothelial cells embed themselves within the theca compartment surrounding the granulosa cells (75). Endothelial cells are most prevalent within the developing corpus luteum. Specifically, the peripheral vasculature of the ovarian follicles is transformed into the highly vascularized gland, primarily composed of steroid-producing luteal cells (1).

1.1.2.1.8 Ovarian Surface Epithelial Cells

Ovarian surface epithelial (OSE) cells are derived from the GREL progenitors, which also give rise to granulosa cells, during embryonic development (16). OSE cells make up the outermost layer of the ovary and play a critical role in facilitating ovulatory rupture and repair (Figure 5) (100). More recently, characterization of OSE cells generated data suggesting that they may retain inherent plasticity or stemness, which may play a role in ovarian tissue homeostasis as well as ovarian cancer (101). As ovulatory follicles approach the ovarian surface, proteolytic enzymes

degrade OSE cells as well as the basal lamina and follicular wall components allowing the follicle to rupture, releasing an oocyte (102). After the oocyte has been released, OSE cells proliferate and migrate toward the ruptured surface and facilitate the remodeling of the ovary (103, 104).

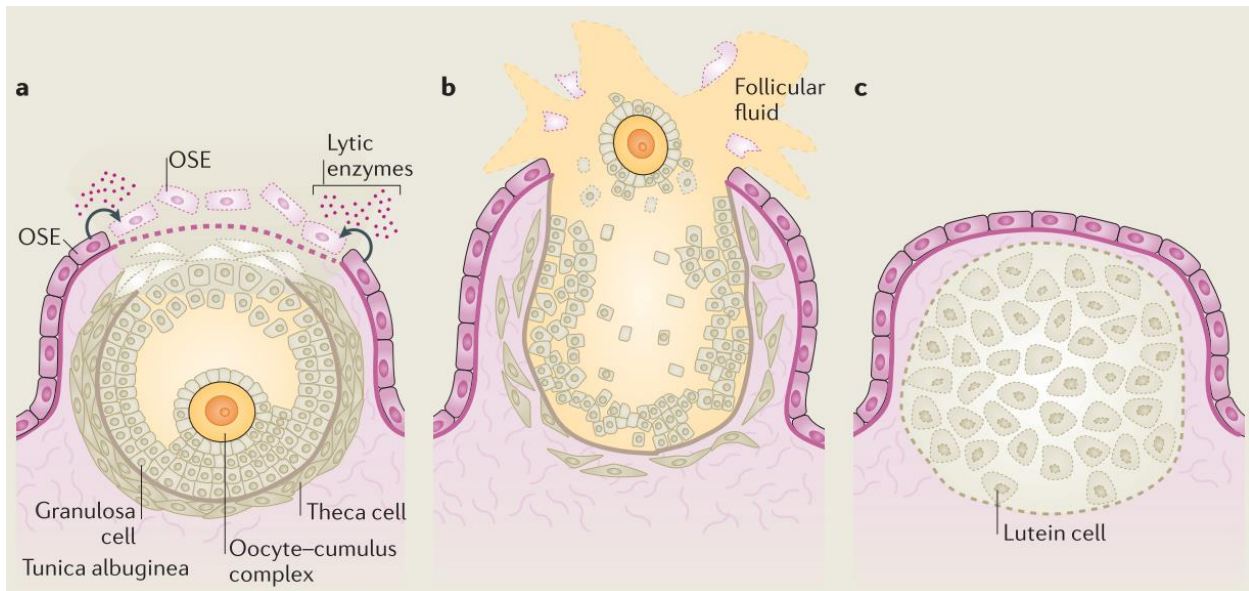


Figure 5 Ovarian Surface Epithelium and Ovulation

Cyclic ovarian surface epithelium (OSE) rupture and repair can be broadly divided into three phases: (a) an ovulatory phase; (b) a rupture phase; and (c) a repair phase.

[Figure and text reproduced from (101). License obtained from Springer Nature – No. 4842620174150]

1.1.2.2 The Menstrual Cycle

The menstrual cycle is a highly regulated process by which the female reproductive tissues prepare to establish pregnancy (Figure 6) (14). This process reoccurs monthly in reproductive aged women until their ovarian reserve is exhausted and initiates menopause. The first stage of the cycle is the menstrual phase, which can last from one to seven days. During the menstrual phase, low estradiol and progesterone levels, reduced from a degenerating corpus luteum, trigger the ischemic death of endometrial lining, which begins to shed (105). The uterine lining is evacuated along with

blood and mucus. This tissue slowly redevelops as the menstrual cycle progresses and fully matures in time for potential embryo implantation.

The second stage of the menstrual cycle, known as the follicular phase, coincides with the start of the menstrual phase and occurs from one to fourteen days (106). The follicular phase is responsive to gonadotropin secretion from the pituitary gland, specifically follicle stimulating hormone (FSH) and luteinizing hormone (LH). These hormones are regulated by the hypothalamus, which directly produces gonadotropin-releasing hormone (GnRH) (15). The rising FSH levels initiate the cyclic recruitment of a cohort of small antral follicles that are selected to grow (93). The granulosa cells of the follicles produce increased levels of estradiol, which influences the production of *de novo* endometrial tissue in preparation of embryo implantation (105). Within a few days after estradiol levels peak, a rapid increase of LH stimulates the resumption of meiosis and triggers the ovulation of a metaphase II oocyte (93).

The final stage of the menstrual cycle is referred to as the luteal phase, which occurs from days fourteen to twenty-eight, and is characterized by the formation of a corpus luteal gland and the maturation of the endometrial tissue lining the uterus (9). Within the ovary, granulosa cells from the ovulated follicle differentiate into luteal cells, forming a corpus luteum that secretes estradiol and progesterone (105). These ovarian hormones work together to inhibit the production of gonadotropins. If fertilization of the oocyte occurs, the corpus luteum will continue hormone production; however, if the egg is not fertilized, the corpus luteum will degenerate and trigger the recurrence of the menstrual cycle (105).

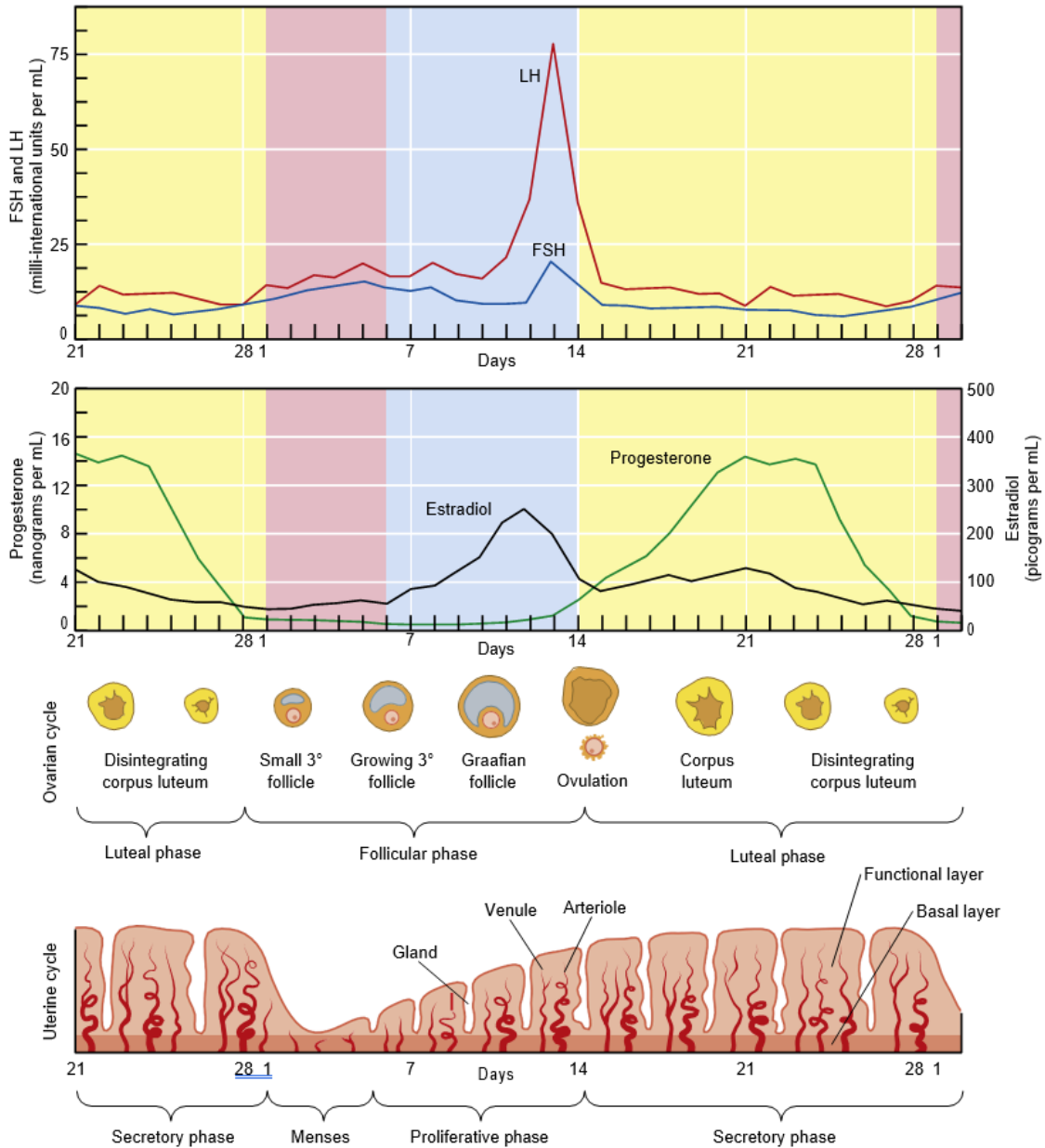


Figure 6 The Menstrual Cycle and Hormone Regulation

Average blood levels of hormones during a 28-day menstrual cycle, along with changes in the ovaries and uterine endometrium. Note that an estradiol peak precedes the LH surge. The ratio of estradiol to progesterone is high during the follicular phase and lower during the luteal phase.

The ovaries also secrete small amounts of another estrogen (estrone), androgens, and 17-hydroxyprogesterone (not shown). Levels of progesterone are in nanograms (one thousandth of a milligram) and of estradiol in picograms (one thousandth of a nanogram). Levels of FSH and LH are in milli-international units (one thousandth of an international unit). An international unit is an amount of a hormone that produces a given biological response in a target tissue. Although average FSH and LH blood amounts are shown, the levels of these hormones and GnRH exhibit hourly pulses.

[Figure and text reproduced from (105). License obtained from Elsevier – No. 4842611244985]

1.1.2.3 Role of Hormones and Growth Factors

A critical function of the ovary is the production and regulation of reproductive hormones. The ovary is part of an intricate feedback loop known as the hypothalamus-pituitary-gonadal (HPG) axis (13). The hypothalamus releases gonadotropin releasing hormone (GnRH), which then stimulates the gonadotropes of the anterior pituitary gland to produce gonadotropins, follicle stimulating hormone (FSH) and luteinizing hormone (LH). These gonadotropins directly mediate the production of estradiol and progesterone from the somatic cells of the ovarian follicles. The presence of the ovarian hormones can provide feedback to control the secretion of FSH and LH. In addition, ovarian accessory molecules can assist with the regulation of the menstrual cycle.

1.1.2.3.1 Gonadotropin Releasing Hormone

Gonadotropin releasing hormone (GnRH) is produced within the hypothalamus and initiates the HPG axis through the stimulation of gonadotrope cells of the anterior pituitary gland (15, 107). GnRH expression varies over time, with limited production in infants and upregulated to normal levels around puberty (108, 109). Once active, GnRH binding to GnRH receptor (GnRHR) takes place in the pituitary and releases follicle stimulating hormone (FSH) and luteinizing hormone (LH), which can regulate the production of ovarian hormones that are critical for follicle maturation, ovulation and pregnancy. GnRHR is also present within the ovarian tissues; however, binding within the ovary can influence cell proliferation (15). GnRH pulses can be modulated by fluctuating estradiol concentrations, with average levels of estradiol producing an inhibitory effect, whereas high levels of estradiol stimulate GnRH production (105). This feedback loop has major implications in the production of FSH and LH throughout the menstrual cycle.

1.1.2.3.2 Follicle Stimulating Hormone

Follicle stimulating hormone (FSH) is one of two hormones secreted by the gonadotropes of the anterior pituitary gland (105). The presence of FSH can trigger the proliferation of granulosa cells and follicular growth. This is made possible through the FSH receptor (FSHR) found on granulosa cells of growing follicles (110). Further, FSH-FSHR binding upregulates aromatase activity, which facilitates the conversion of testosterone to estradiol. As a result of these qualities, the level of FSHR on granulosa cells has been suggested as a differentiating factor in the selection of the dominant follicle (111). FSH can be inhibited due to high estrogen levels further dampening the growth of competing antral follicles and triggering atresia.

1.1.2.3.3 Luteinizing Hormone

Luteinizing hormone (LH) is also produced in response to GnRH pulses from the hypothalamus, which stimulates the pituitary to secrete LH (15). Upon activation, LH can bind to LH receptors (LHR) found on theca cells and can trigger the synthesis of androstenedione, as follicles transition from preantral to antral stage (112). As dominant follicles prepare for ovulation, the granulosa cells start to display LHR to facilitate the production of enzymes to directly produce progesterone (1). Toward the end of the follicular phase, there is a surge of LH production, where high levels of LH promote oocytes to resume meiotic maturation and leads to ovulation. The luteal cells, which differentiate from follicular granulosa cells, make up the highly vascularized corpus luteum (113). Since luteal cells express LHR, LH is necessary to facilitate the synthesis of progesterone and estradiol within the corpus luteum.

1.1.2.3.4 Ovarian Steroidogenesis

Steroidogenesis is the process by which hormones are synthesized (Figure 7) (114). In the ovary, steroid hormones are critical for maintaining reproductive homeostasis. In preparation for steroidogenesis, cholesterol is collected from the blood and taken up by either theca or luteal cells. Cholesterol is a necessary component for all steroid hormone production within the ovary. Further, steroidogenesis is catalyzed by enzymes, which are primarily from the cytochrome P450 (CYP) family (115). To initiate steroidogenesis, enzymes convert cholesterol into pregnenolone, which is a precursor steroid hormone that can follow two distinct pathways. Within ovarian follicles, pregnenolone is converted into 17-hydroxypregnenolone, then into dehydroepiandrosterone (DHEA) and finally, androstenedione (1). Within corpora lutea, pregnenolone is directly converted into progesterone, then into 17-hydroxyprogesterone and finally, androstenedione (1). In both pathways, androstenedione can then be converted into either estrone or testosterone, both of which can give rise to estradiol (1). For follicles to synthesize estradiol, the theca and granulosa cells must work together since neither of the cells alone have the enzymes needed for estradiol synthesis. This phenomenon is known as the two-cell model, where theca cells convert cholesterol to androstenedione and granulosa cells synthesize estradiol, which can then diffuse back into the theca cells and into the blood (112). However, the luteal cells of the corpus luteum can directly synthesize both progesterone and estradiol.

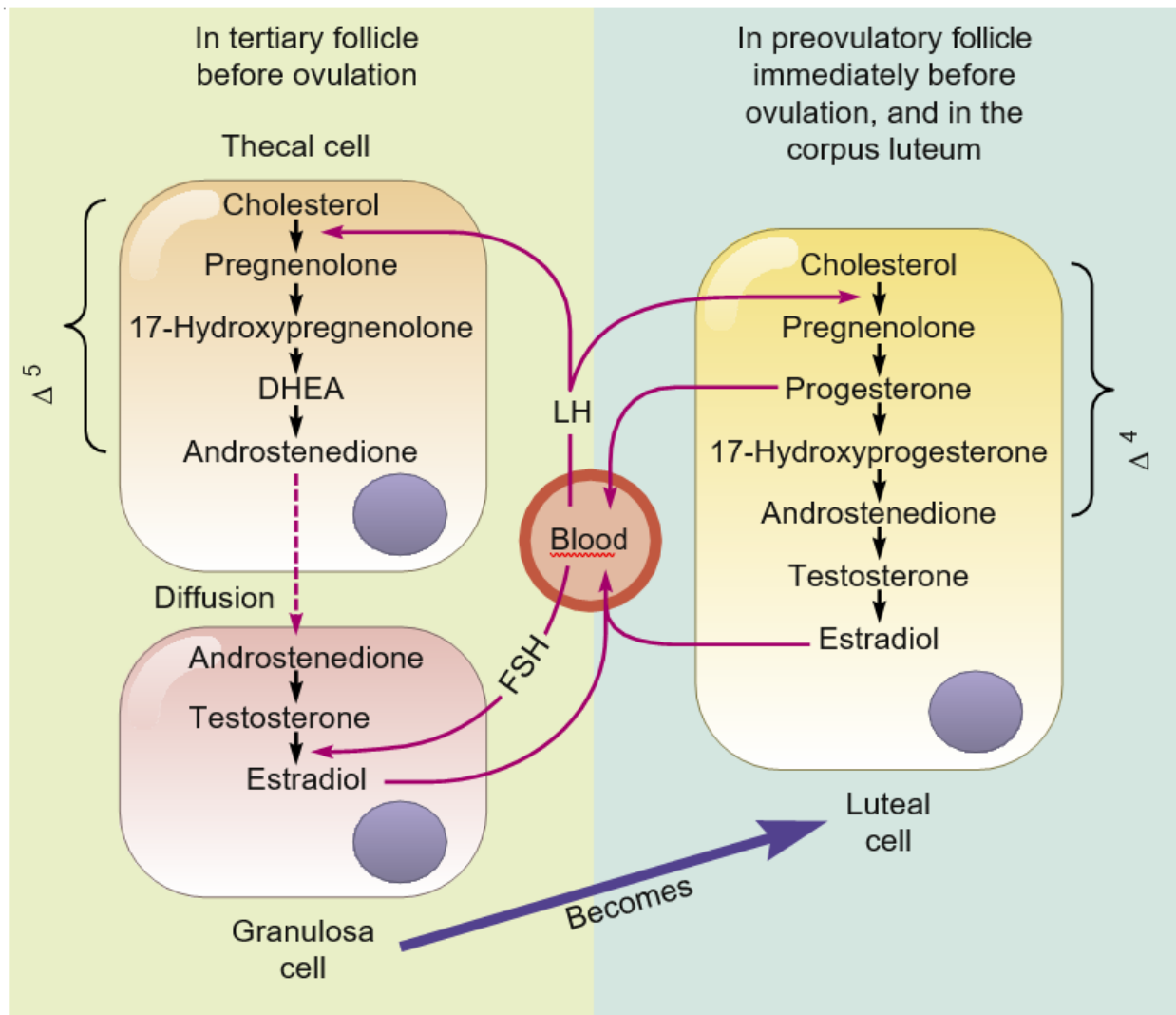


Figure 7 Steroidogenesis in the Ovary

Steroidogenesis in the tertiary and preovulatory follicle and in the corpus luteum after ovulation. Note that the tertiary follicle follows the Δ^5 pathway, producing mostly estradiol in the blood. In contrast, the preovulatory follicle (i.e. a Graafian follicle after the LH surge but before ovulation) and the corpus luteum produce a large amount of progesterone and some estradiol, and thus follow the Δ^4 pathway of steroidogenesis.

[Figure and text reproduced from (1). License obtained from Elsevier - No. 4842610641195]

1.1.2.3.5 Estradiol

Estradiol, also known as 17β -estradiol, is a steroid hormone produced by granulosa cells of growing follicles as well as the luteal cells of the corpus luteum (1). The presence of estradiol promotes the thickening of the uterine lining at the conclusion of the menstrual phase as well as the maturation of the uterus prior to embryo implantation (105). Estradiol levels rise primarily during the follicular phase and peak just before the LH surge, which triggers ovulation. Oocyte release from the dominant follicle during ovulation is facilitated by estradiol, which can lead to the production of collagenase that assists in the breakdown of the connective tissues within the follicle. Another critical function of estradiol is the regulation of the HPG axis through negative and positive feedback. Specifically, intermediate levels of estradiol can elicit negative feedback to GnRH and dampens the production of LH and FSH (15). However, high levels of estradiol can stimulate GnRH, which leads to a spike in the gonadotropins. Although these fluctuations in estradiol concentrations are known to influence GnRH pulse frequency and amplitude, GnRH-specific neurons lack estrogen receptors. Therefore, estradiol must signal through intermediary neurotransmitters that can directly mediate GnRH production. Estradiol-receptive kisspeptin-producing neurons, that directly synapse with GnRH neurons, are believed to facilitate this response(116).

1.1.2.3.6 Progesterone

Progesterone is a steroid hormone from the progestin family that is synthesized by the theca cells of growing follicles and luteal cells of corpus luteum (1). Progesterone plays a significant role in the regulation of reproductive function, specifically targeting the mammary glands and the

uterus to maintain pregnancy (105). During the luteal phase, the luteal cells are activated by LH to synthesize progesterone, which diffuses into the blood vessels embedded within the corpus luteum. A reduction of progesterone concentration in the blood triggers the end of the luteal phase and the endometrial tissue rapidly degenerates (105). Like estradiol, progesterone can also regulate the HPG axis through negative feedback of GnRH production and subsequent loss of gonadotropin secretion.

1.1.2.3.7 Other Accessory Molecules

A significant portion of reproductive function is regulated by GnRH, FSH, LH, estradiol and progesterone; however, there are also several other accessory molecules that can influence ovarian function. Several of these molecules belong to the transforming growth factor β (TGF- β) superfamily, which includes anti-Müllerian hormone (AMH), inhibins, activins, bone morphogenic proteins (BMPs), and growth differentiation factors (GDFs)(4, 72, 117, 118). Anti-Müllerian hormone (AMH), which is a glycoprotein produced by the granulosa cells of small growing follicles, can inhibit the premature recruitment of primordial follicles(68, 119, 120). Inhibin and activin can form dimers, which specifically impact the production of FSH. Inhibin, as the name suggests, inhibits FSH production, whereas activin acts in opposition to inhibin and stimulates FSH secretion (105). Similar to activin, follistatin can bind directly to inhibin and reverse FSH inhibition (105). A number of BMPs have been suggested to play a role in within the ovary, including BMP2, 4, 6, 7 and 15 (121). BMP2 is a regulator of primordial follicle activation and FSH production (121-124). BMP4 is expressed by both granulosa and theca cells and acts as an inhibitor to progesterone synthesis (125-127). Oocytes and granulosa cells express BMP6, which can regulate proliferation and FSHR expression to induce steroidogenesis (125, 128-131).

Theca cells primarily produce BMP7 and has been shown to contribute toward the proliferation of granulosa cells as well as mediate steroid production (125, 126, 132, 133). Like BMP6, BMP15 is also expressed by the oocytes and is upregulated gradually throughout the early stages of follicle development (134-137). A significant presence of BMP15 has been suggested to improve fertility outcomes (128, 138). GDF3 and GDF9 are also present within the oocytes at early primordial follicle stages; however, GDF3 promotes, while GDF9 inhibits the expression of LHR (139, 140). Another key molecule in ovarian physiology is insulin-like growth factor 1 (IGF-1), which can trigger both the proliferation and differentiation of granulosa cells as well as promote gonadotropin function (141). Finally, one of the most critical hormones for ovarian endocrine function is vascular endothelial growth factor (VEGF), which assists in the formation of blood vessels within large antral follicles and corpus luteum (142).

1.1.2.4 Reproductive Differences in Female Mammalian Species

In this study, we were interested in testing a novel method for supporting the delivery and engraftment of ovarian follicles that would lead to a potential therapy for human patients. However, different mammalian species were used to evaluate our approach. We prepared an ovarian ECM hydrogel from porcine ovaries due to tissue volume and availability. We used mice for all follicle transplants, mating and histological assessment. Although there are many reproductive similarities between these mammalian species, there are definitive differences. This raises significant questions regarding how this technology would translate to human patients in the clinic. To compare these differences, the reproductive characteristics in the context of humans, pigs and mice will be examined.

The female mammalian reproductive anatomy of humans, pigs and mice is similar, as all these species include ovaries, fallopian tubes, uterus and vagina; however, they vary slightly in

organization and location (Figure 8 and Figure 9). One of the primary differences, in contrast to the human uterus, is that pigs and mice have a bilateral uterus or uterine horns (143). The uterine horns of pigs are much larger than the human uterus, whereas the mouse uterine horns are significantly smaller. The porcine cervix is also anatomically distinct from the human, as it contains pulvini cervicales, which are undulating mucosa layers that span the total length of the cervix (143). Unlike the separate orifices for the urethra and vagina in humans, pigs share a urogenital opening. Another anatomical difference in pigs and mice is the presence of the ovarian bursa, which is a sack surrounding the ovary and is lacking in humans (101). The ovarian ligament in humans and mice are anatomically dissimilar, where the fimbriae of the fallopian tube is directly in contact with the ovary in humans, the ovarian ligament is placed in a way that brings the ovary close to the fimbria of the fallopian tubes (101).

Female mammalian species also differ in their reproductive cycles (Figure 10 and Figure 11). Humans reach sexual maturity at 12.9 years of age on average (143). In contrast, mice become sexually mature the earliest, between 6-8 weeks, followed by pigs at 4-6 months of age (144-146). Once sexually mature, all these mammals continuously cycle until their ovarian follicle reserve has been depleted. In each of these mammalian species, their cyclicity is maintained by the hypothalamus-pituitary-gonadal (HPG) axis. The human menstrual cycle, pig and mouse estrous cycles all respond to gonadotropin feedback, which stimulates the production of ovarian endocrine hormones, estradiol and progesterone. One of the main differences is the type of cycle, classification and length. Humans have a menstrual cycle, which is indicative of changes within the ovary and endometrial lining, whereas pigs and mice do not menstruate, but instead both have characteristic estrous cycles that are dependent upon sexual receptiveness (143). The menstrual cycle in humans is about four weeks long, whereas the estrous cycle in mice lasts 3-5 days and

occurs every 19-21 days in pigs (*143*). Estrous is made up of four main stages: proestrus, estrus, metestrus and diestrus (*145, 147*). Proestrus is the first stage of the estrous cycle, during which follicles as well as the endometrial tissue begin developing. Proestrus is followed by estrus, which indicates the sexual receptivity of the animal. The third step in the estrous cycle is metestrus that signals the development of the corpus luteum and is followed by diestrus that stimulates the production of progesterone. Although these species share different types of reproductive cycles they all maintain a follicular phase and luteal phase; however, their durations vary between mammals (*143*). The follicular phase in humans lasts approximately 14 days followed by the luteal phase, which is an additional 12-15 days (*105*). In contrast pigs, have a shorter follicular phase (5-6 days) with a longer luteal phase (15-17 days) (*147*). Finally, due to their relatively quick 4-5 day estrous cycles, mice have the shortest follicular (2 days) and luteal (2-3 days) phase (*145*).

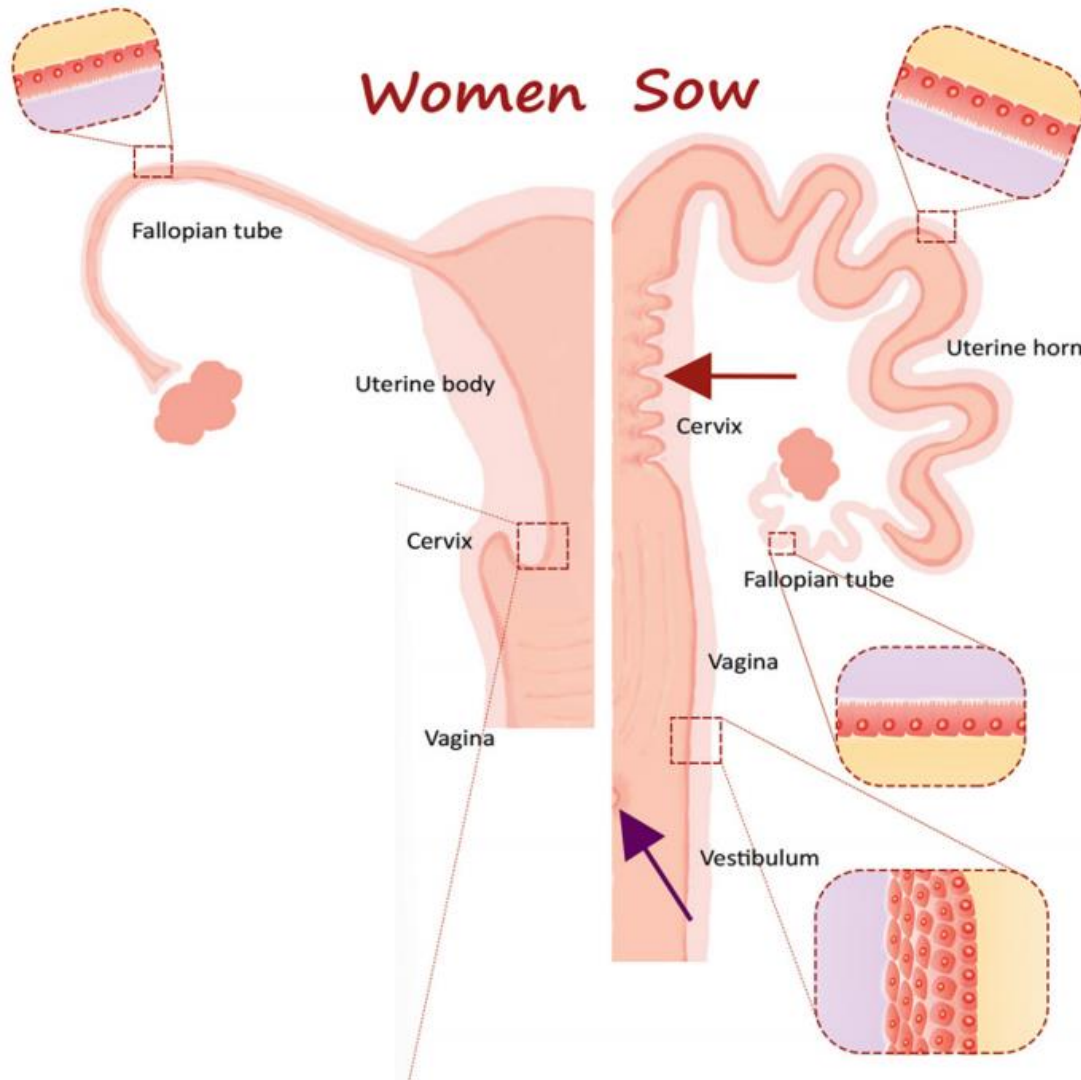


Figure 8 Human vs. Pig Reproductive Anatomy

The porcine uterus differs macroscopically from the human simplex uterus by having bilateral horns (bicornuate).

The porcine cervix displays a characteristic feature, not found in women; the cervical pulvini (red arrow).

Furthermore, the porcine urethra opens on the ventral surface of the vagina (purple arrow) creating an urogenital sinus that opens to the outside through the common urogenital orifice. In women, the urethra and vagina have its

own separate openings to the outside. Otherwise the porcine vagina is similar to the human one.

[Figure and text reproduced from (143). Open-access - Creative Commons Attribution License.]

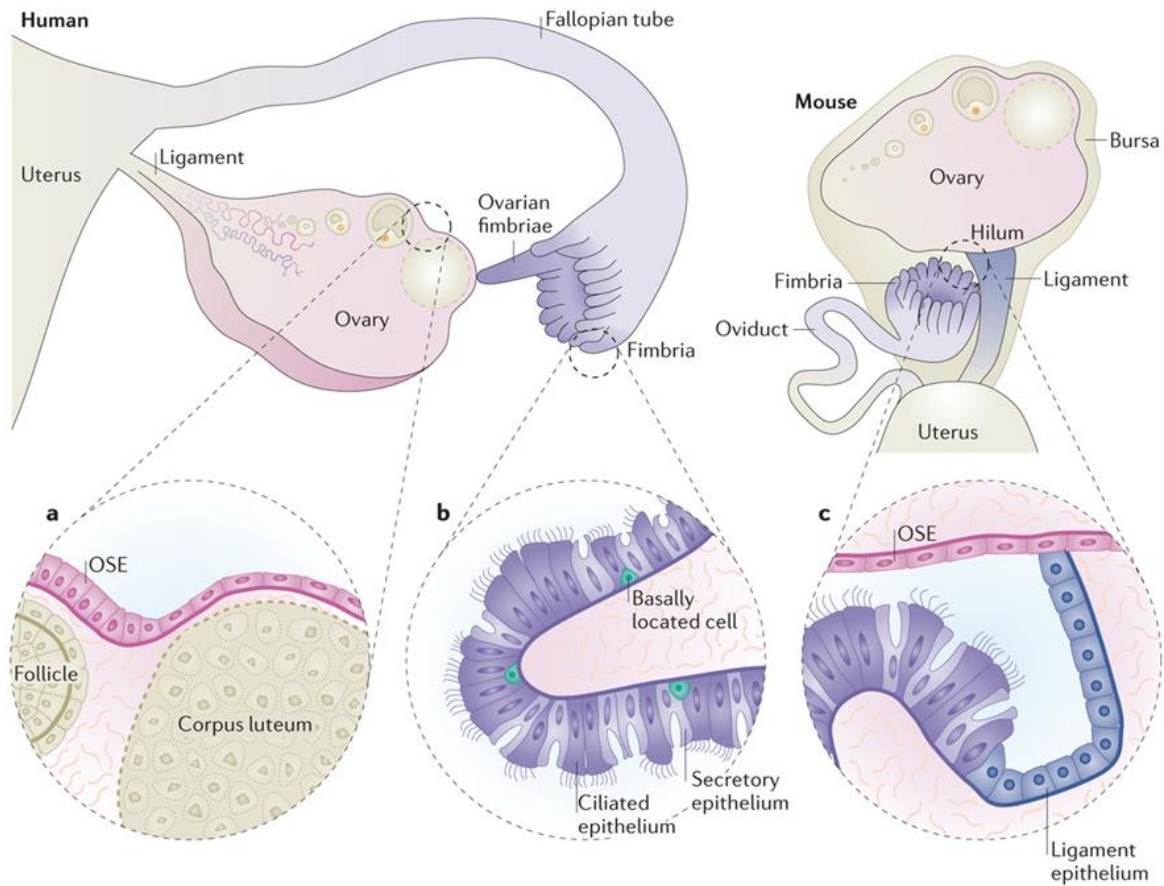


Figure 9 Human vs Mouse Reproductive Anatomy

The diagrams show the organization and anatomy of the adult human and mouse ovary; the fallopian tube (also known as the oviduct), including finger-like fimbria; the ovary ligament; and the uterus. A thin bursa membrane encapsulates the mouse ovary but is absent in humans. The placement of the ovary ligament differs between humans and mice. In humans, the ovary and the fimbria are anatomically contiguous at the ovarian fimbriae, whereas the ovary ligament abridges the ovary–fimbria connection in mice. A single-layered epithelium lines the ovary, fimbria and ovary ligament.

[Figure and text reproduced from (101). License obtained from Springer Nature – No. 4842620174150]

Table 1 Differences in Reproductive Cycle of Mammals

[Table adapted from (143). Open-access - Creative Commons Attribution License.]

Characteristic	Women (menstrual)	Non-humane primates (menstrual)	Minipigs (estrous)	Mice (estrous)
Cyclicity	Continuous cycling	Baboons: continuous cycling in captivity Rhesus Macaque: seasonal poly-oestral.	Continuous cycling	Continuous cycling
Age of sexual maturity	12.9 years	3 years	4–6 months	6–8 weeks
Length of cycle	28 days	28–33 days (highly variable)	19–21 days	3–5 days (highly variable)
Follicular/luteal phase	10–14 days/ 12–15 days	8 days/19 days	5-6 days/ 15–17 days	2 days/ 2–3 days
Endometrial sloughing/ menstruation	Yes	Yes	No	No

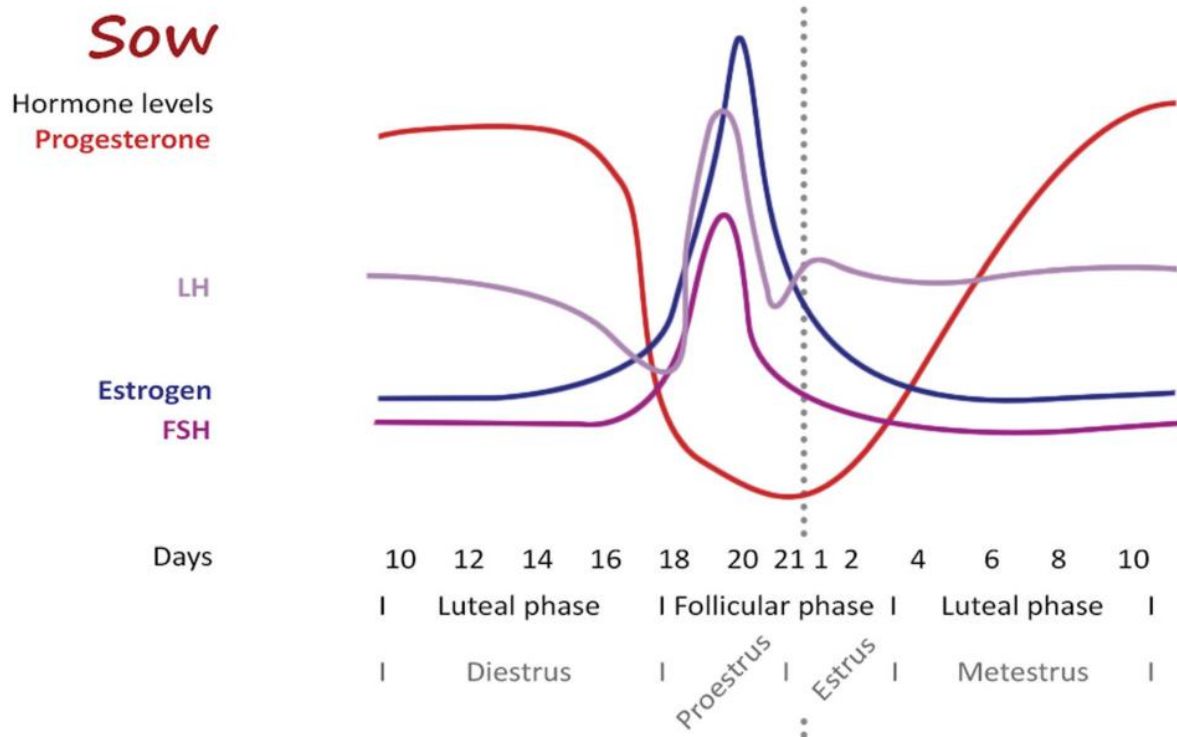


Figure 10 Porcine Estrous Cycle

The estrous cycle in pigs begins and ends with ovulation/ estrus. The menstrual cycle in women begins and ends with the start of menses, with the ovulation in the middle of the cycle. Otherwise, the length of the cycle and the hormonal fluctuations are very similar.

[Figure and text reproduced from (143). Open-access - Creative Commons Attribution License.]

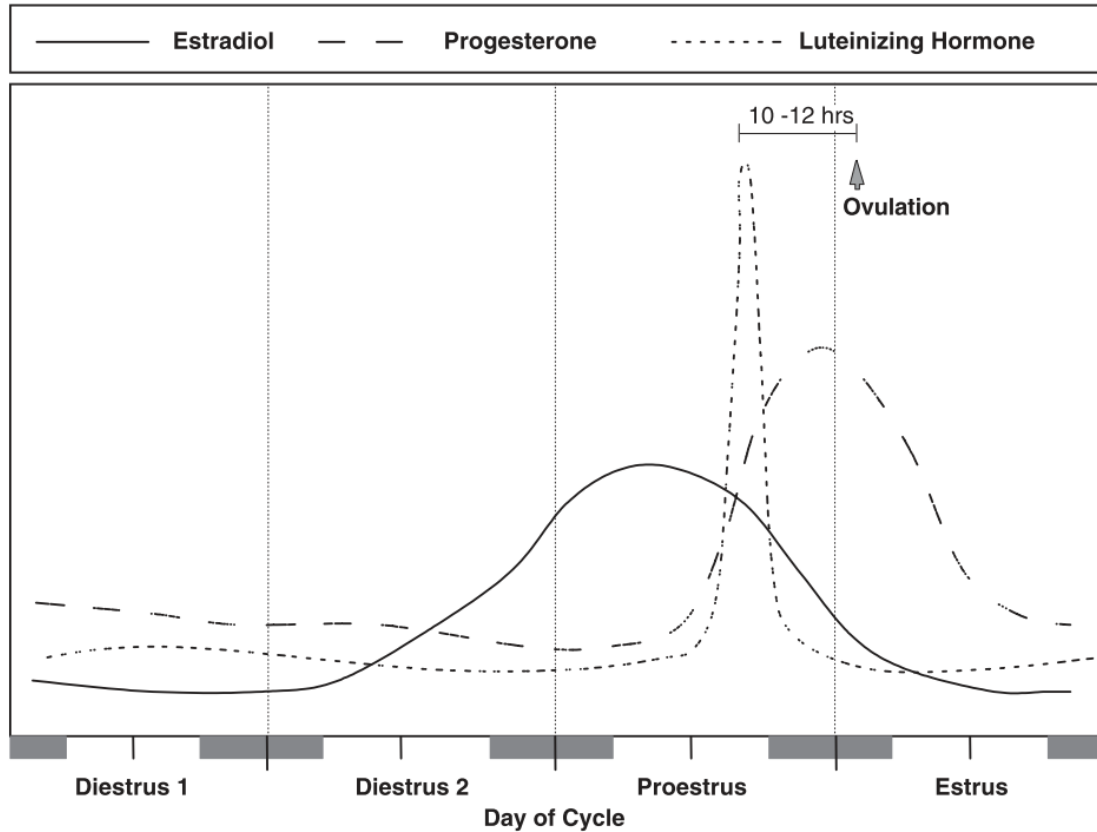


Figure 11 Rodent Estrous Cycle

Schematic pattern of the 4-day estrous cycle in the rat depicting serum estradiol and progesterone concentrations as they relate in time to the surge of luteinizing hormone (LH). Ovulation will typically occur during the early morning hours of estrus, approximately 10–12 hours after the rise in LH. Shaded blocks at the base of the figure indicate the dark portion of a 14:10 hr light:dark photoperiod.

[Figure reproduced from (145). License obtained from John Wiley and Sons – 4842600937042.]

1.2 Female Fertility Preservation

Fertility preservation is primarily dedicated to conserving the reproductive function of female and male cancer patients (148-151). A growing number of patients are surviving metastatic disease, which has also increased the clinical need for methods of fertility preservation. Cancer treatments, such as chemotherapy, radiation and gynecologic surgery can directly cause iatrogenic premature ovarian failure (POF), which lead to a loss of fertility (149). As a proactive effort to preserve fertility in women, oocytes and embryos are collected and cryopreserved prior to treatment using hormone stimulation. After these patients are cleared of cancer, their cryopreserved cells may be used for in vitro fertilization (IVF) and embryo transfer to induce pregnancy. However, there is another population of young girls and women, who cannot afford to delay cancer treatments and therefore are unable to undergo hormone stimulation for egg collection. As an alternative, ovarian cortical tissues are cryopreserved, which can be used for autotransplantation (152). This procedure is the primary method for fertility preservation; however, there remain risks associated with this approach including malignant cell transmission and surgical complications (153). A number of experimental cell and tissue engineering approaches have been developed to address these issues including in vitro/in vivo follicle maturation, an artificial ovary and the future potential for ovarian stem cell therapy (154). The following sub-sections will review the causes of infertility, specifically the effects of cancer treatments that can induce iatrogenic POF, and the progress of next generation therapies for female fertility preservation.

1.2.1 Female Infertility

Approximately 9% of world is infertile, which amounts to roughly 50 to 80 million people (155, 156). Infertility can be caused by several confounding factors including age, diet, genetic defects, and exposure to environmental hazards (157). Ovarian-associated pathologies, such as ovarian cancer, premature ovarian failure (POF), polycystic ovarian syndrome (PCOS) and endometriosis can also contribute to a loss of fertility (157). In each case, infertile patients looking to restore fertility may now have options due to improvements in assisted reproductive technologies, such as hormone stimulation, in vitro fertilization and embryo transfer. However, patients that do not have viable eggs of their own may turn to a surrogate or adoption.

1.2.2 Premature Ovarian Failure

Premature ovarian failure (POF), or primary ovarian insufficiency (POI) is the sudden or gradual loss of reproductive function and fertility prior to normal menopause (158-160). POF is generally caused by a loss or dysfunction of ovarian follicles, which can be attributed to genetic disorders or a malfunction within the HPG axis. Further, iatrogenic damage to the gonadal cells through surgical or chemical intervention can also result in POF. Specifically, cancer treatments, such as chemotherapy and radiotherapy are cytotoxic, which can rapidly induce follicle apoptosis and impair fertility. Female patients with abnormally high levels of follicle stimulating hormone (FSH) can be used as an indicator of POI (161). In the presence of healthy growing follicles, ovarian hormones provide a negative feedback to the GnRH neurons, which reduce the concentrations of FSH, however, with a lack of follicles, FSH remains constitutively active.

Additionally, anti-Müllerian hormone (AMH) can be predictive of the remaining ovarian reserve as it is expressed by small growing follicles.

1.2.3 Causes of Iatrogenic POF

Iatrogenic premature ovarian failure (POF) can be defined as any form of physical or chemical procedure that directly causes a significant loss or dysfunction of ovarian follicles (158). For example, cancer patients who are treated with chemotherapy, radiation or gynecologic surgery are at risk for developing POF. Chemotherapy agents and radiation are cytotoxic in moderate to high doses, which can depopulate the ovarian reserve, which is composed of the remaining immature follicles that indicate future fertility potential (162). Similarly, surgical methods to reduce malignant ovarian tissues can also damage the environment and trigger follicle atresia (151). To further elucidate these effects, the chemical agents and procedures that can induce POF will be reviewed in the following sub-sections.

1.2.3.1 Chemotherapy-Induced POF

It is estimated that 1 in 18 premenopausal women will be diagnosed with an invasive form of cancer (163). Chemotherapy is a common treatment for the ablation of malignant disease. However, there are side effects that can significantly reduce the quality of life for cancer patients. One of the major side effects is the disruption of normal reproductive function. Chemotherapeutic agents are notoriously cytotoxic and can severely damage the ovarian tissues and cells (Figure 12). Several studies that performed histological sampling of ovarian tissues exposed to chemotherapy, have provided evidence of a depreciated ovarian reserve and reduction in overall tissue volume (164-166). There are a number of different types of chemotherapy agents with varying mechanisms

of action including alkylating agents, platinum-based compounds, antimetabolites, vinca alkaloids and anthracycline antibiotics (162). The most significant risk of incurring infertility is caused by alkylating agents. This group consists of cyclophosphamide, busulfan, mechlorethamine, chlorambucil, and melphalan (162). Alkylating agents primarily induce apoptosis within the oocytes of ovarian follicles. Specifically, guanine bases within DNA are compromised by the addition of an alkyl group that results in unreparable double stranded DNA breaks that trigger cell death (167, 168). Further, these agents can cause disruption of developing follicles, which can prevent menstrual cycling. Chemotherapy exposure may also negatively impact the ovarian vasculature, which is critical in follicle maintenance and viability (169, 170). Additionally, increased fibrosis throughout the stroma can be observed within treated ovaries leading to further dysfunction (169, 171).

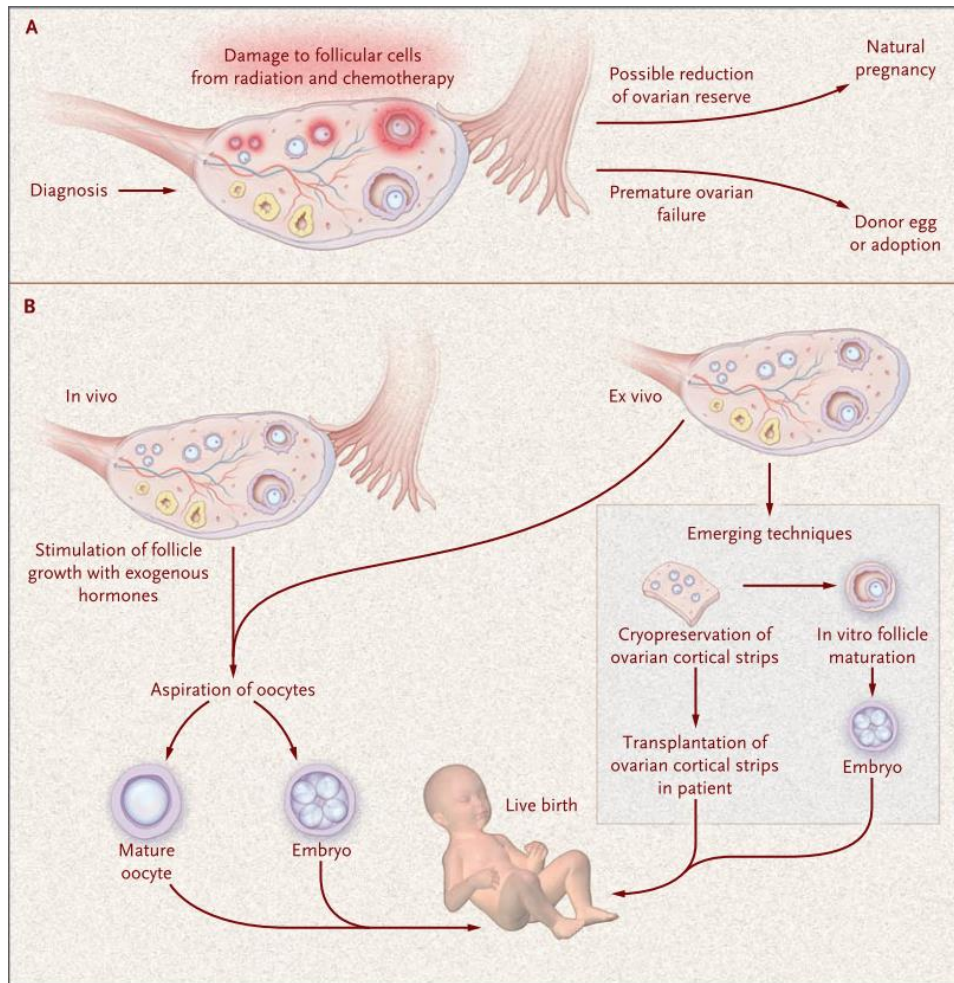


Figure 12 Iatrogenic Premature Ovarian Failure and Fertility Preservation

As shown in Panel A, high-dose radiation and most chemotherapeutic agents damage the growing cells in mature and immature follicles and, depending on the type of drug, the dose, and the age of the patient, may result in depletion of many or all follicles. This depletion may result in a short-term loss of reproductive function and an inability to attain a natural pregnancy after treatment. As shown in Panel B, if fertility interventions are warranted, the patient can delay treatment and undergo hormonal induction for 2 to 3 weeks to stimulate follicle development and recover mature oocytes. The oocytes can be frozen or fertilized, depending on the wishes of the patient. If there is insufficient time or if there are contraindications, one ovary can be removed, and ovarian cortical strips can be cryopreserved for use in tissue transplantation or emerging techniques such as in vitro follicle maturation.

[Figure and text reproduced with permission from (150), Copyright Massachusetts Medical Society.]

1.2.4 Current Fertility Preservation Techniques

Over the past several years, there have been significant advancements toward improving female fertility preservation (Figure 13). One of the major accomplishments was the development of cryopreservation protocols that dramatically improved the viability of ovarian tissues and cells for long-term storage (172). Without reliable cryopreservation, natural pregnancy would not be an option for POF patients. During the early 2000s, another outstanding achievement was made as ovarian tissue transplantation led to live-births in multiple human patients (173-175). To this day, orthotopic transplantation of ovarian cortical tissue remains the standard for female patients with iatrogenic POF. Due to the diversity of clinical outcomes and reporting, it has been difficult to gauge the effectiveness of ovarian tissue transplantation; however, it is anticipated that this procedure will soon be elevated from an experimental approach to the primary standard of care. Although this technique has shown undeniable clinical success, there remain concerns for patients with aggressive forms of cancer, which could lead to the transmission of malignant cells upon transplantation. Further, ovarian transplantation requires an invasive surgical procedure that could lead to complications. As a result, researchers have been working to develop new methods to reduce the potential for cancer transmission by isolating immature follicles from the surrounding stroma. In vitro and in vivo follicle maturation has been used with biomaterials to recapitulate folliculogenesis to obtain mature oocyte for downstream assisted-reproductive technologies (ARTs). Several of these techniques have directly resulted in live-births in mice; however, further research must be conducted to better replicate the highly dynamic conditions observed within the native ovary to improve fertility outcomes for human patients.

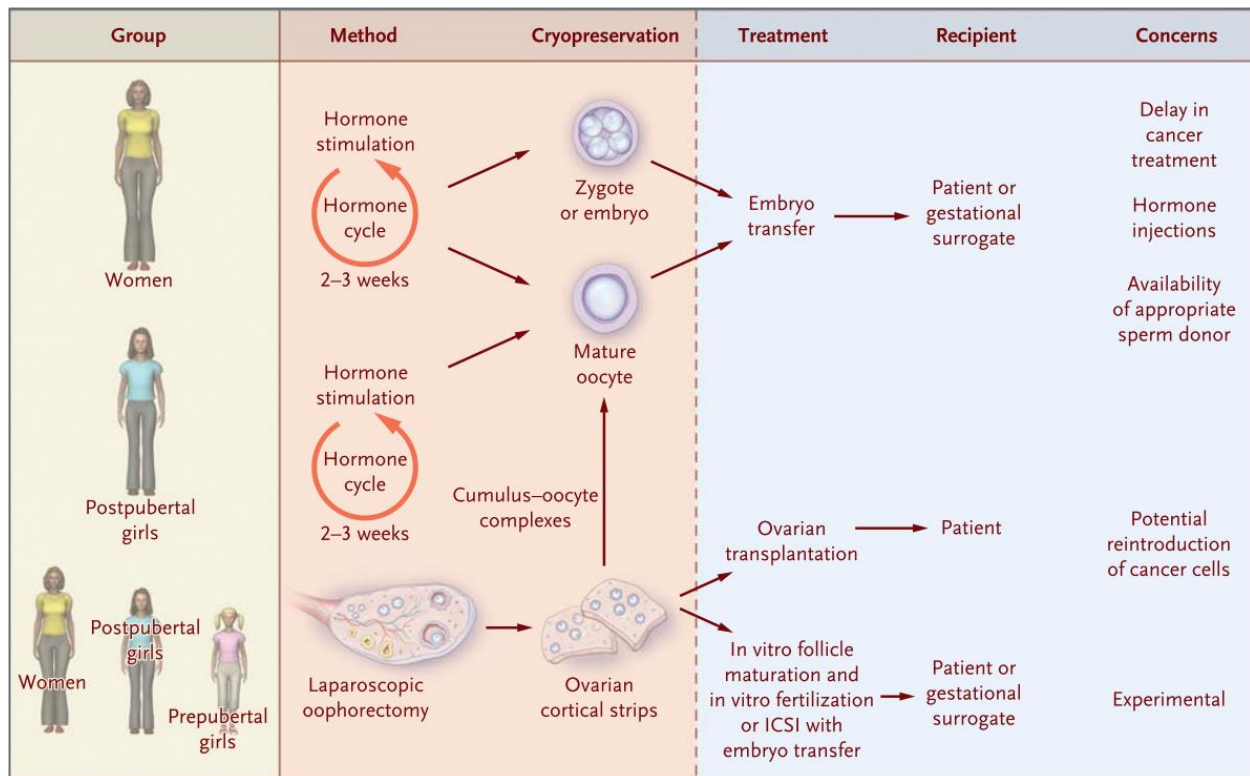


Figure 13 Fertility Preservation Options for Female Cancer Patients

Fertility-preserving options for young women with cancer include hormonal stimulation with cryopreservation of oocytes or embryos and laparoscopic oophorectomy with tissue storage and later use in transplantation or in vitro follicle maturation. At the time of tissue harvest, mature follicles may exist and cumulus–oocyte complexes may be harvested and matured in vitro to provide another source of mature eggs for storage. Depending on the patient’s uterine status, a gestational surrogate may be required. Tissue cryopreservation is the only option for girls who are not candidates for hormone stimulation.

[Figure and text reproduced with permission from (150), Copyright Massachusetts Medical Society.]

1.2.4.1 Cryopreservation

One of the most critical parts of fertility preservation is the capacity to store and retain the viability of ovarian tissues and cells. To accomplish this, cryopreservation techniques have been developed for ovarian tissues and follicles over the past 60 years (176, 177). The success of this process is now generally recognized internationally as the standard of care for female cancer

patients (178). The initial cryopreservation approach was to use slow-freezing with cryoprotectants, such as glycerol, dimethyl sulfoxide (DMSO), 1,2-propanediol (PROH) and sucrose (179-182). However, these methods led to poor cell viability and fertility outcomes after ovarian tissue transplantation. More recently, the use of vitrification, or rapid freezing after dehydration, has become the preferred method for cryopreservation (183, 184). Briefly, ovarian tissues are sequentially placed in graded concentrations of ethylene glycol and DMSO, supplemented with handling medium (HEPES-buffered TCM-199 solution with 20% synthetic serum substitute) in the primary incubation and sucrose in the secondary incubation. Tissues are subsequently added directly to liquid nitrogen and stored until further use. Just as tissues are rapidly frozen, the tissues are also rapidly warmed to 37°C in handling medium with decreasing concentrations of sucrose solution. This procedure demonstrates excellent oocyte viability and represents a feasible method for long-term storage of ovarian tissues and cells that offer patients an opportunity to restore fertility(184).

1.2.4.2 Ovarian Tissue Transplantation

The most common treatment for restoring fertility in female cancer patients is the use of ovarian cortical strip transplantation. This method has generated greater than 130 live-births worldwide (149). The decision to use ovarian tissue transplantation is generally predicated by a severe cancer diagnosis that requires immediate treatment. Therefore, prior to treatment, the patient undergoes a laparoscopic procedure to remove a small piece of the ovarian cortex, which is then cryopreserved until patients are ready for autotransplantation. Patients that can afford to delay potentially gonadotoxic treatments are able to use normal ARTs, such as hormone stimulation, to collect and cryopreserve oocytes and embryos prior to treatment. The primary form of this procedure is orthotopic transplantation, where ovarian cortical tissues are introduced into

the pelvic region, preferably onto the ovary, to promote natural conception; however, heterotopic procedures, with subcutaneous transplantation within the forearm and abdomen, are also used for *in vivo* follicle maturation and restoring endocrine function (185). Although this treatment has been successful, there are some considerable limitations including, follicle ischemia, malignant cell transmission and surgical complications. Overall, this method is a promising form of restoring both fertility and endocrine function for POF patients.

1.2.4.3 Biomaterial-Facilitated Approaches

A concern for using intact ovarian cortical tissues is the potential presence of residual malignant cells. For this reason, many researchers have begun testing the efficacy of using isolated follicles to reduce the reintroduction of cancer cells back to the patient upon transplantation. Several experimental techniques, such as *in vitro* and *in vivo* follicle maturation and artificial ovarian transplantation, are now being tested to support oocyte maturation from early-stage ovarian follicles that may be used to restore fertility. In order to promote follicle survival and maturation, a variety of biomaterials have been used to mimic the ovarian microenvironment. The following sub-sections will document the current research and outlook for these experimental therapies.

1.2.4.3.1 In Vitro Follicle Maturation

In vitro follicle maturation (IVM) is a popular experimental approach used for the support of follicle development to obtain meiotically competent oocytes for IVF. Follicles are isolated from the surrounding stroma and cultured in media supplemented with specific ovarian hormones and growth factors. Ideally, immature follicles will be activated under the influence of follicle

stimulating hormone and granulosa cells will start to proliferate. After substantial follicle growth over the course of several days to weeks, human chorionic gonadotropin (hCG) is used to stimulate the resumption of meiosis and the release of metaphase II (MII) oocytes. MII oocytes are then artificially inseminated to form an embryo for implantation and pregnancy.

The concept of IVM was initially examined by Eppig and O'Brien, who implemented a two-step culture system to develop mouse primary oocytes into meiotically-competent MII oocytes, which were used to generate live-births (186, 187). To improve maturation efficiency of two dimensional follicle culture (188), biomaterials have been used to provide a supportive three-dimensional culture environment and better mimic the conditions observed *in vivo* (Figure 14) (111, 189). Xu et al. 2006 used an alginate matrix to encapsulate mouse secondary follicles, which were cultured for eight days in growth medium (190). Upon enzymatic extraction from the alginate bead, follicles were placed in maturation medium, consisting of hCG and epidermal growth factor (EGF), to simulate ovulation. Results from this study indicated that a 3D culture environment could retain normal follicle morphology and yield a high percentage (70.9%) MII oocytes. Further, the fertilization rate of MII oocytes, which developed into a zygote, was 68.2%, which only differed by approximately 13% from *in vivo* superovulated control oocytes. Pseudopregnant female rats that received an embryo transfer, derived from *in vitro* culture, gave birth to healthy offspring. This study gave the impetus for an increased focus on advancing the field of female reproductive tissue engineering, with an emphasis on designing biomaterials that could mimic the ovarian microenvironment.

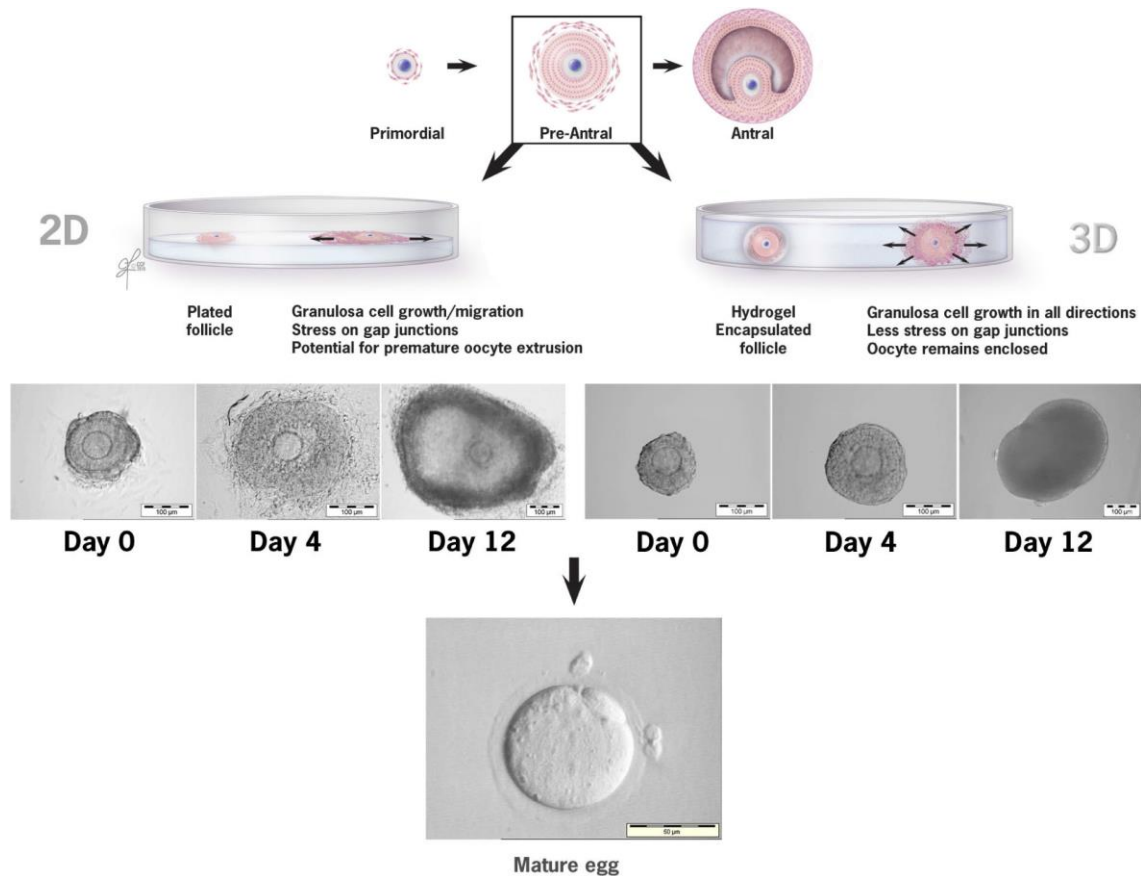


Figure 14 Hydrogel-facilitiated Follicle Encapsulation for 3D Culture

With 2-D growth granular cell migration away from the oocyte is evident with time in culture, leaving the oocyte vulnerable for premature extrusion. Pre-antral follicles embedded in hydrogel maintain their 3-D architecture.

Granular cell expansion occurs in all directions resulting in less stress on gap junctions.

[Figure and text reproduced from (191). Open-access - Creative Commons Attribution License.]

To date, alginate has been the primary biomaterial studied and used for 3D encapsulation of ovarian follicles for IVM across several species, including mouse (189, 190, 192-195), goat (196, 197), dog (198), cow (199), primate (200) and human (201). However, other popular biomaterials have emerged in an attempt to demonstrate in vitro folliculogenesis, such as collagen (202-207), fibrin (208-210), Matrigel (211), hyaluronic acid (212) and poly-ethylene glycol (PEG) (213). Adjustments in material properties and composition, as well as culture conditions, have led

to improved outcomes, which has made IVM a common practice for obtaining mature oocytes in lower species. However, efficiency for the maturation of immature human follicles remains poor and must be significantly improved for clinical translation.

1.2.4.3.2 In Vivo Follicle Maturation

In vivo follicle maturation is an experimental strategy using the body's natural environment to improve developmental outcomes after follicle isolation. Additionally, this technique would offer a protective barrier to prevent the transmission of malignant cells. The study by Xu et al. 2006 demonstrated that it was possible to recover encapsulated follicles from alginate hydrogels and continue with oocyte maturation(190). Therefore, Rios et al. 2019 examined the potential of using alginate encapsulation to create a retrievable implant to assess follicle maturity for fertilization(214). Primordial, primary, and secondary follicles were mechanically isolated and encapsulated within a 0.5% alginate bead. Encapsulated follicles were transplanted into ovariectomized mice at both orthotopic (subcutaneous) and heterotopic (ovarian bursa) sites. Alginate hydrogels were retrieved after seven days and upon follicle release, the antral follicles were exposed to hCG and EGF for 16 hours to induce ovulation. Among the recovered follicles, survival rates were low with the smallest number of follicles transplanted leading to the great recovery (76%). The subcutaneous transplants appeared to dramatically improve follicle survival in comparison to the transplants from the ovarian bursa. Although the survival rates were low, of the antral follicles recovered from subcutaneous implants, 63% achieve MII stage. Follicles obtained from the ovarian bursa yielded only 20% MII oocytes. After intracytoplasmic sperm injection (ICSI), 36% of the oocytes developed into 2-cell and 7% into 4-cell embryos. Standard IVF resulted in 40% of oocytes becoming 2-cell embryos. Finally, cancer cell transmission was

evaluated using luciferase-expressing malignant cells and detection via *in vivo* imaging. After removal of the alginate implant, there was no indication of neoplastic cells within the recipient mice. This strategy could be an effective way to promote improved follicle development while limiting the potential for cancer recurrence.

1.2.4.3.3 Artificial Ovary

The artificial ovary is a concept that uses biomaterials to facilitate the transplantation of isolated follicles to restore reproductive function and fertility. Recently, there have been several groups that have incorporated different strategies and biomaterials to prepare a supportive material to enhance follicle survival upon transplantation. Shikanov et al. 2011 introduced a combination system consisting of a fibrin gel supplemented with vascular endothelial growth factor (VEGF) to stimulate angiogenesis and promote graft survival. Transplanted mouse ovarian tissues supported by the fibrin/VEGF material improved follicle survival when compared to no biomaterial control. The transplanted material was also able to give rise to a litter of pups (215). Similarly, Smith et al. 2014 characterized the use of a fibrin gel for the transplantation of ovarian follicles. Early-stage follicles were enzymatically isolated, encapsulated within fibrin gels and transplanted into an ovariectomized mouse. Fibrin graft explants were performed at 0, 3, 9 and 21 days with follicles populations being significantly reduced by day 9 (216). Kniazeva et al. 2015 tested multiple biomaterials combinations, including variable concentration of fibrin, alginate and collagen, to improve follicle survival upon *in vivo* transplantation in an ovariectomized mouse model. Successful litters resulted solely from follicles encapsulated within fibrin gels that were supplemented with VEGF (217). Laronda et al. 2015 detailed a procedure for the decellularization of both human and bovine ovaries. Primary ovarian cells were seeded onto decellularized grafts,

which were then transplanted into ovariectomized mice. Post-transplantation, recipient mice showed evidence of initiating puberty(218). Paulini et al. 2016 tested an artificial ovary using a fibrin gel showing the efficacy of xenografting isolated preantral follicles within the peritoneum. Results showed that follicles had survived and were proliferating up to 7 days post-transplantation (219). Kim et al. 2016 implemented a poly-ethylene glycol vinyl sulfone (PEG-VS) hydrogel to support the transplantation of immature follicles and showed a restoration of endocrine function for up to 60 days post-transplantation (220). Laronda et al. 2017 established a bioprosthetic 3D printed ovary composed of gelatin to restore ovarian function in sterilized mice. As a result of the transplanted scaffold, GFP pups were born from the exogenous follicle transplant (221). These strategies have delivered exceptional results in a short time, which bodes well for the field of female fertility preservation. The next step for the development of artificial ovarian tissues is to test these materials in higher order mammalian species that could better evaluate their efficacy for human use.

1.2.4.4 Ovarian Stem Cells

The testis contains mitotically active spermatogonia that can produce sperm indefinitely throughout the course of a man's life. However, in contrast, oogonia complete mitosis and enter meiosis during prenatal development, which produces a finite number of oocytes in the ovary at birth. Within the past two decades, there have been several claims suggesting that a population of mitotically-active, female germline stem cells (FGSCs) may exist within the ovary (222). However, there have also been conflicting studies that oppose these findings (223). Nevertheless, multiple studies have shown that the intraovarian microinjection of FGSCs can support the birth of healthy pups post-chemotherapy (224-226). Although the mechanism behind this technique is

not well understood, the results suggest that ovarian stem cell populations may be a valuable tool to study the development of human oocytes and could offer a potential therapy to treat infertility.

2.0 Overview of Decellularized ECM Biomaterials

The field of tissue engineering and regenerative medicine uses various biomaterials to create a microenvironment that promotes a desired cell function. One of the most promising types of biomaterials are decellularized extracellular matrices (dECM) and their derivatives (ie. hydrogels, etc.). The benefit of using dECM materials is their tissue-specific molecular and biochemical composition, which has been shown to promote cellular infiltration and tissue remodeling. These materials are prepared using the process of decellularization that removes immunogenic material to avoid rejection upon transplantation *in vivo*. A diverse portfolio of decellularization agents have been used in combination to remove cells, while retaining tissue specificity. However, tissues are inherently different and thus, materials and method selection, along with significant optimization, are required to obtain a tissue-specific bioactive dECM scaffold. Recently, an increasing number of decellularization protocols and resultant dECM materials have been developed for ovarian tissues with potential for restoring fertility in female patients. Although great strides have been made in this area, there are several challenges and limitations remaining for the clinical translation of ovarian dECM materials for fertility preservation.

2.1 The Extracellular Matrix

The extracellular matrix (ECM) is a critical component of the cell microenvironment and is essential to maintaining homeostasis. The ECM is a diverse, tissue-specific network of proteins, proteoglycans and glycoproteins that are secreted by cells to provide structural support and act as a reservoir of small molecules to facilitate cell signaling. ECM composition varies based upon desired organization and functions of local cells. In the following section, we will look at some of the most common ECM components and how they directly impact cell behavior.

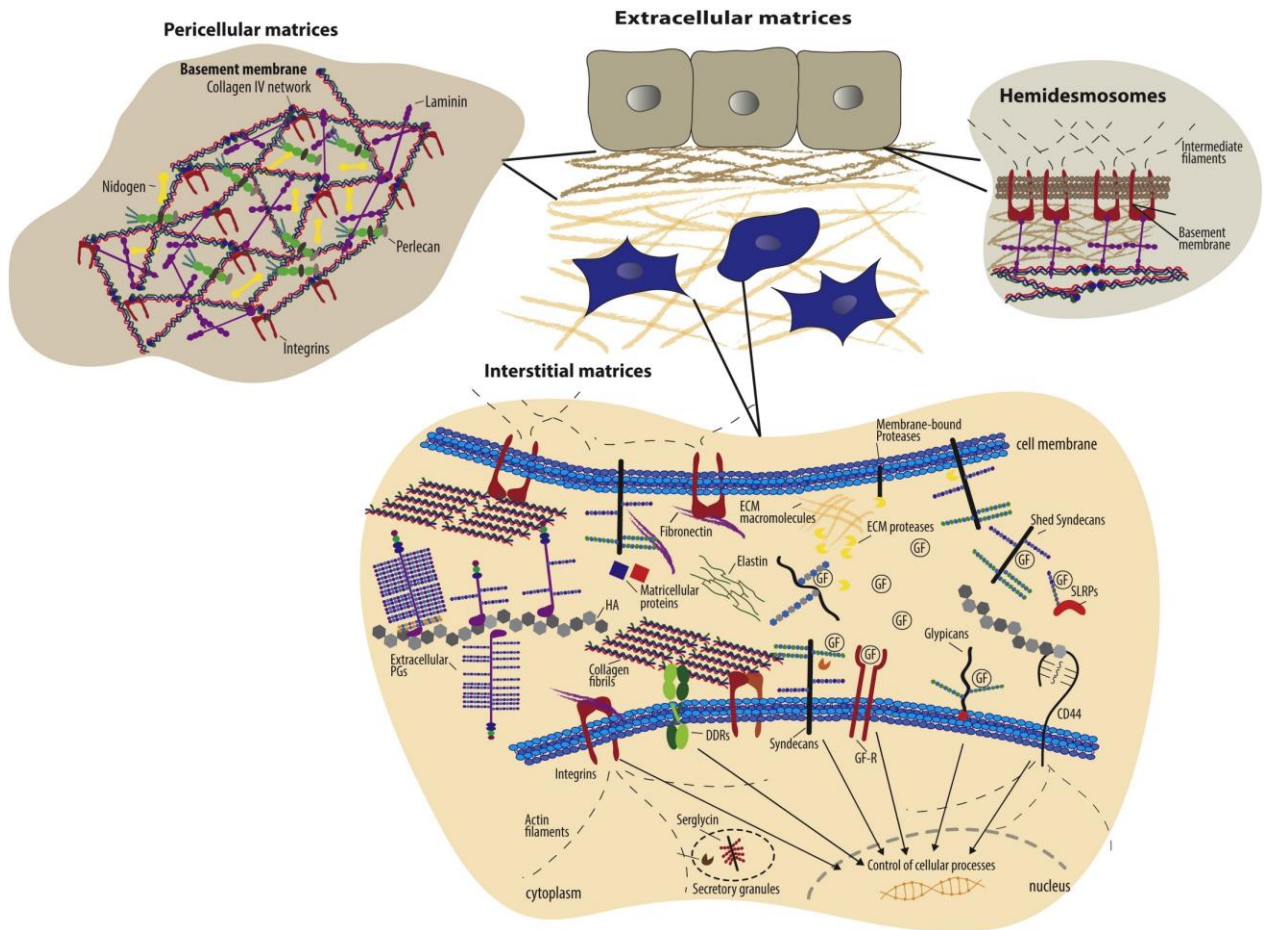


Figure 15 Extracellular Matrix Composition

ECMs are classified into two major types, the interstitial and pericellular matrices. Basement membrane, a type of pericellular matrix, is found between epithelial cells and connective tissue. This layer is composed of a collagen IV network that associates with ECM components including nidogen, laminin, perlecan, and minor collagens like collagen XV and XVIII. Epithelial cells are anchored to basement membranes by hemidesmosomes formed via interactions of integrins with laminins. Interstitial matrices are composed of collagen fibrils, elastin, secreted PGs and HA, and matricellular proteins. They interact with each other creating a dynamic and complex three-dimensional network. Cells bind to ECM components by specific cell surface receptors, such as integrins; cell surface PGs; syndecans and glypicans; the HA receptor CD44; and DDRs. They transduce signals into cells that regulate various cellular functions.

[Figure was reproduced from (227). License obtained from Elsevier – 4842610157190]

2.1.1 ECM Components

The extracellular matrix (ECM) is composed of a diverse set of biomolecules, such as proteins, glycoproteins, and proteoglycans that provide a structural framework to accommodate the function of resident cells (Figure 15) (228-231). A large portion of the ECM is made up of fibrous collagen proteins and are primarily recognized by their distinct triple helix configuration, which help to build supramolecular structures that are essential for establishing mechanical strength of a tissue (232, 233). Elastin fibers, composed of crosslinked tropoelastin molecules, and microfibrils provide elasticity within tissues (234). Glycoproteins are another class of ECM molecules that act as structural bridges between the ECM and their cellular inhabitants. The major glycoproteins of the ECM are laminins, fibronectin, and tenascins. Laminins are generally found within the basement membrane of tissues and can directly interact with cellular surface molecules (235). Fibronectin is a large molecule that can associate and bind to other ECM molecules, cell adhesion molecules and growth factors depending on its diverse and dynamic conformation (236). Similar to other glycoproteins, tenascin-C can also interact with ECM molecules and assist with cell migration through binding with cell adhesion molecules (237). A sub-class of glycoproteins are proteoglycans, which are distinguished by multiple chains of repeating, unbranched disaccharides referred to as glycosaminoglycans (GAGs). Proteoglycans containing GAGs, such as heparin, heparan sulfate, chondroitin sulfate, dermatan sulfate, keratan sulfate, and hyaluronic acid play a significant role in water retention, growth factor and cytokine binding, as well as cell adhesion (238-242). The ECM communicates with the cells via cell surface molecules, such as integrins and syndecans, which facilitates adhesion and cell migration (243-246). Recently, it was demonstrated that fibrillar components of the ECM can sequester proteins, microRNA and lipids within matrix-bound nanovesicles (MBVs), which can influence immune cell phenotype and stem

cell differentiation (247-249). Matrix metalloproteinases (MMPs), along with other proteolytic enzymes, can actively degrade ECM components to remodel the extracellular niche and facilitate the release of angiogenic, chemotactic, mitogenic and anti-inflammatory factors to influence resident cells (250-259).

2.1.2 Role of the ECM

The biochemical profile of the ECM can change dynamically within certain organs or can remain relatively static in others depending on their function. In general, the ECM plays a significant role in mediating homeostasis as it can provide mechanical and biochemical cues that trigger cell proliferation and differentiation. This process is facilitated by a phenomenon referred to as dynamic reciprocity, which is the continuous feedback between cells and the ECM to support the spatiotemporal functions of a given tissue (260-262). As a result, environmental stimuli may trigger the cells to generate a diverse milieu of proteins and soluble factors, which can then influence downstream processes, such as gene expression and protein synthesis (263). The ECM also is known to play a regulatory role in facilitating normal biological functions, such as stem cell differentiation, angiogenesis, innervation and healing response due to injury or disease (264-270). Due to these intrinsic properties, the ECM has become a desirable biomaterial, which has several applications for tissue engineering and regenerative medicine.

2.2 Decellularization

To obtain acellular ECM scaffolds, tissues must first undergo the process of decellularization. Decellularization is a procedure that disrupts and removes the cellular components of a tissue of interest using physical and/or chemical treatments. A critical factor of decellularization is the ability to obtain a non-immunogenic scaffold while retaining tissue-specific components, such as prominent ECM proteins and growth factors. In addition, it is important to consider the impact of the decellularization treatments on tissue morphology, especially if acellular ECM scaffolds will be re-seeded with cells. To achieve these outcomes, the materials and tissue processing must be carefully selected based upon tissue type to effectively remove endogenous cellular content while preserving the desired tissue-specific characteristics. To date, a wide range of tissues and organs have been decellularized using a diverse combination of materials and processing methods. The use of decellularization has grown dramatically due to successful application for tissue engineering and regenerative medicine. This technique has recently been demonstrated for use within female reproductive tissue engineering to mimic the ovarian microenvironment to support both follicle culture and in vivo transplantation. The following section will provide a general overview on the materials, methods and processing for successful decellularization to prepare dECM biomaterials for fertility preservation.

2.2.1 Methods

As mentioned above, there have been a significant number of decellularization approaches designed to obtain dECM scaffolds from almost every tissue and organ in the body (271). These approaches generally include treatments that fall into three main categories: (1) physical

treatments, (2) chemical treatments, and (3) enzymatic treatments (271-280). Tissues may only require one or a combination of these treatments in order to remove cellular content and preserve the integrity of the ECM. Processing methods, as well as incubation times, wash steps, and temperature, can dramatically alter the decellularization outcomes and dECM biomaterial efficacy. To improve the effectiveness of decellularization, tissues may be perfused or diced to increase surface area exposure to chemical or enzymatic reagents. Perfusion uses the existing vasculature of an organ to penetrate deep within the tissues and allows the organ to remain intact. This is beneficial for whole organ recellularization. However, if intact dECM scaffolds are not required, then dicing is also an option to enhance the quality of the decellularization. Ultimately, the selection of decellularization methods creates a tradeoff between the cell removal and preservation of bioactive components, which makes it critical to optimize protocols for non-standardized tissues. The following sub-sections will look at the most common types of treatments and their use for decellularization.

2.2.1.1 Physical Treatments

A variety of physical treatments are used to aid in the removal of cells including freeze-thaw cycles, mechanical delamination and hydrostatic pressure. Freeze-thaw cycles enhance the decellularization effects of detergents and enzymes when compared to chemical treatments alone (281). This process helps to loosen the cells within the tissues making it easier for their removal. Mechanical delamination is used to remove unwanted cellular layers to leave behind an acellular matrix. This strategy has been implemented in the preparation of ECM grafts and sheets, such as small intestinal submucosa (SIS) and urinary bladder matrix (UBM) (282-285). Hydrostatic pressure is another technique used to avoid the negative effects of detergents and reduce the total time of decellularization (286, 287). This process uses high-hydrostatic pressure, induced by a

pressurized and temperature-controlled chamber, to uniformly disrupt the cellular membranes of a tissues without compromising the structural components of the ECM.

2.2.1.2 Chemical Treatments

A common strategy for decellularization is to use chemical treatments, which includes detergents, acid and bases, hypo- and hypertonic solutions, solvents and chelators (288). Detergents are highly effective decellularization agents and are grouped based upon the net charge of the molecule. Many times, more than one type of detergent is used to improve both cell removal and clearance of residual chemicals (289, 290). Ionic detergents, such as sodium dodecyl sulfate (SDS) and sodium deoxycholate (SDC), are popular decellularization agents that are proficient at lysing cell and nuclear membranes (286, 287, 291-329). However, there are some negative consequences of using these detergents as they can also disrupt native ECM ultrastructure and can significantly reduce the presence of GAGs and tissue-specific growth factors (295, 302-304). Non-ionic detergents, such as Triton X-100, have been shown to be less aggressive than SDS, which can result in residual cellular content in thicker tissues, but it is more favorable for GAG and growth factor preservation (286, 287, 289, 291, 292, 294, 295, 299-301, 303-307, 311, 315, 319-324, 326, 328, 330-335). Finally, zwitterionic detergents such as, CHAPS (3-((3-cholamidopropyl)dimethylammonio)-1-propanesulfonate) and sulfobetaine-10,16 are primarily used for preservation of proteins and can also be used for the ablation of cells but are less effective cellular removal agents than ionic and non-ionic detergents (293, 299, 313, 323). Acids and bases are frequently used in decellularization to facilitate hydrolysis within the tissues. Acetic acid has been used to delipidize and increase porosity of acellular scaffolds, directly attributed to a loosening of collagen structural proteins, which promotes greater cell infiltration (331). Peracetic acid is commonly used a disinfectant of animal tissues and can further dissociate remnant nucleic acids

without compromising the ECM (336-338). Bases can also be used in the pre-processing of tissues, but they can have a detrimental impact on mechanical properties, which is caused by a dissociation of collagen networks (295, 339, 340). Hypo- and hypertonic solutions are used generally to rinse and remove cells and detergents from a tissue (288). Generally, phosphate buffered saline (PBS) is used in high concentrations (hypertonic) to remove water from a cell and lower concentrations (hypotonic) to cause swelling of cell and can purify proteins through nucleic separation (341). Alternating washes of hypo- and hypertonic solutions can also lyse cells due to increasing osmotic pressure, which can directly aid in decellularization without observable depreciation of tissue-specific components within the ECM (342). Solvents, such as alcohols (ie. ethanol, methanol, etc.), acetone and tributyl phosphate, can also be utilized for decellularization by similar mechanisms of dehydration and cell lysis (339). These chemicals can also be used for lipid removal in some decellularization protocols; however, solvents are known fixatives that can have irreversible effects on the structural integrity of the acellular scaffolds (330, 340, 343-346). Chelators are commonly paired with enzymes to help disrupt cell-ECM adhesions due to their ability to sequester essential ions (347, 348). Specifically, EDTA (ethylenediaminetetraacetic acid), a calcium (Ca^{2+}) chelator, and trypsin, an enzyme used for the cleavage of peptides associated with cell adhesion molecules, are used in tandem to free cells from a given substrate (287, 301, 308, 321, 333, 349).

2.2.2 Enzymatic Treatments

The last category of decellularization agents involves the use of enzymes, specifically nucleases and proteases (288). Nucleases, like DNase and RNase, are used to augment decellularization after cell permeabilization by cleaving nucleotides, which make up DNA and RNA strands within cells (287, 293, 297, 301). Proteases, such as trypsin, can also be used to

cleave naturally occurring peptides within cell adhesion molecules, with enhanced effects in the presence of a chelating agent (288). Although trypsin is useful for cell removal, it has off-target effects, which can reduce the integrity of ECM molecules, such as collagen and elastin (289, 304, 324, 332). Overall, the use of nucleases and proteases alone is not ideal for complete decellularization of a tissue; however, their use may improve the initial detachment of cells as well as the breakdown of large DNA/RNA fragments for a more thorough removal of immunogenic components. Other less common enzymes used for decellularization are collagenase, to reduce collagen fibers, and lipase, for improved lipid removal (330, 350).

2.2.3 dECM Derivatives

The immediate end-product of decellularization is an dECM scaffold that can be used for a number of potential tissue engineering applications. Acellular dECM scaffold materials can be used as a substrate for 3D cell-culture, recellularized for in vitro cell differentiation or as an acellular graft to promote healing and remodeling at the site of injury. Further, acellular tissues may be enzymatically digested, using pepsin and hydrochloric acid, to solubilize the tissue. Solubilized dECM is temperature-sensitive and once neutralized will form a hydrogel, which is primarily the product of a physical crosslinking of collagen molecules. dECM hydrogels provide a versatile biomaterial with several advantageous properties including tissue-specific bioactivity (diverse ECM composition, growth factors, hormones, etc.), injectability and degradability. Further, solubilized dECM components may be isolated and enriched to create highly concentrated forms of the tissue-specific ECM bioactive components.

2.2.4 Current Decellularization Approaches for Fertility Preservation

Decellularization has recently been used to generate ovarian-specific dECM biomaterials for fertility preservation applications. Ovarian tissues were first decellularized by Laronda et al. 2015 to restore puberty within an ovariectomized mouse (218). Human and bovine ovaries were decellularized in 500 micron slices then incubated in a 0.1% sodium dodecyl sulfate (SDS) solution on a rotator at room temperature for 24 hours. Whole bovine ovaries were immersed in 0.1% SDS at 4°C for 3 weeks to keep ovaries intact. Primary ovarian cells were isolated from CD1 female mice and seeded onto the acellular bovine ovarian scaffold then cultured for 2 days. Two weeks following ovariectomy of young CD1 female mice, recellularized ovarian scaffolds, were transplanted underneath the kidney capsule. Ovarian grafts showed no significant difference in circulating estradiol and inhibin A levels, which indicated that the decellularized graft supported ovarian cell function. Additionally, ovariectomized mice, that did not undergo ovarian graft transplantation, retained a hymen, whereas the vaginal orifices of graft recipients opened 4 weeks post-surgery, similar to non-ovariectomized control mice. Similar methods were used by Jakus et al. 2017, to prepare ovarian tissue paper (OTP) composites, using small pieces of decellularized bovine ovaries and poly-lactic-co-glycolic acid (PLGA) (351). OTP was used to culture both secondary mouse follicles as well as human and bovine ovarian cortical strips. Secondary follicles cultured on OTP maintained normal spherical morphology after 4 days. In addition, ovarian cortical strips, cultured for up to 8 weeks on OTP demonstrated healthy primordial and primary follicles and increasing estradiol production from 1 to 6 weeks. In another study, Hassanpour et al. 2018 used sodium lauryl ester sulfates (SLES) to decellularize human ovaries and evaluated efficacy for primary ovarian cell transplantation (352). Slices (2 mm thick) of human ovarian cortex were decellularized for 48 hours within a 1% SLES solution and agitated on a magnetic stir

plate at room temperature. Ovarian tissues were then treated with 500 units/mL of DNase I for 24 hours at 36°C. Halved ovaries were also decellularized with the 1% SLES with longer incubation times (30-40 days). Upon decellularization, scaffolds were reseeded with isolated primary ovarian cells from 8-day old female rats and cultured for 24 hours. Reseeded ovarian grafts were transplanted into the renal fat pad of 4-week old ovariectomized female rats. Ovariectomized female rats receiving the ovarian transplant showed evidence of somatic cells as well as significant differences in estradiol and progesterone within the serum when compared to non-grafted controls. Alshaikh et al. 2019 compared three different protocols for the decellularization of mouse ovaries (353). Three decellularization agents were examined including 0.5% SDS, 2% SDC and 1% Triton X-100. The results showed that SDS was superior for cellular removal but did not retain ECM components as well as SDC. Additionally, it was determined that decellularization with Triton X-100 was incomplete; however, this is to be expected at lower concentrations. Eivazkhani et al. 2019 compared the effects of SDS and sodium hydroxide (NaOH) for the decellularization of mouse, sheep and human ovaries (354). Acellular human ovarian scaffolds were reseeded with mouse ovarian cells and transplanted into ovariectomized mice. Ovarian cells transplanted onto scaffolds decellularized using NaOH showed improved metabolic activity and follicle structure reorganization in comparison to SDS treated scaffolds. Pors et al. 2019 used a decellularized human ovarian scaffold to examine recellularization of isolated human and murine stromal cells and pre-antral follicles (355). Ovarian scaffolds were prepared using 0.1% SDS for 18-24 hours with an additional 24-hour wash in 1 mg/mL DNase. Successful reseeded and transplantation of the ovarian scaffold resulted in follicle growth toward antral stage with follicle recovery rates ranging from 21-25% for murine and human cells respectively. Finally, Pennarossa et al. 2020 generated a multi-step protocol for the decellularization of whole porcine ovaries (356). Porcine

ovaries were frozen for at least 24 hours at -80°C and thawed at 37°C for 30 minutes. Thawed tissues were transferred to a solution of 0.5% SDS for 3 hours then washed in 1% Triton X-100 overnight, with each step occurring on an orbital shaker at 200 rpm. After a 9-hour washing step in deionized water (dIH₂O), the ovaries were moved to a 2% SDC solution for 12 hours. The tissues were then subjected to three final washes in dIH₂O for 2 hours each. Decellularized ovarian tissues displayed >98% reduction in comparison to native tissues with preservation of ECM components, such as collagen, elastin and GAGs. Acellular scaffolds reseeded with fibroblasts were shown to be non-cytotoxic and cytocompatible after 7-day culture. In summary, decellularization for ovarian tissues has shown promise for follicle culture and transplantation, which may lead to improved clinical outcomes for fertility preservation.

2.2.5 Regulatory Pathways for dECM Clinical Translation

[Section adapted from Buckenmeyer et al. 2020 (357)]

In general, any new biomedical therapy must be evaluated during pre-clinical animal studies prior to conducting clinical trials in human patients. Several dECM-based materials have been successfully commercialized and therefore may be used as a template to simplify the regulatory process (358). Historically, most dECM products declare as 510(k) medical devices or biologics with the Food and Drug Administration (FDA). Products classified as medical devices or biologics must satisfy several pre-clinical and clinical requirements that unequivocally demonstrates safety and efficacy. After the pre-clinical studies have occurred, either an Investigational Device Exemption (IDE), for medical devices, or an Investigational New Drug (IND) application, for biologics, must be approved by the FDA before proceeding into clinical studies, which can occur in several phases.

Each phase level is designed to carefully examine specific effects of the product after treating a set of eligible patients. Phase I generally consists of a small cohort of test subjects and is primarily focused on evaluating material safety and identifying any potential side effects. In Phase II, the number of test subjects increases and further examines the safety and efficacy. Phase III is used to directly compare the experimental material to similar products with a much larger test population to determine its effectiveness and compile safe-use information. The data obtained from the varying phase levels are then used to support a Biological Product License (BLA) or a Premarket Approval (PMA) application. Once the application is approved, the product can be marketed, as it is considered to have satisfied the FDA requirements.

2.2.6 Future Considerations for dECM Biomaterial Development

[Sections adapted from Buckenmeyer et al. 2020 (357)]

Pre-clinical and clinical success of dECM materials in various disease models have made them an intriguing option for applications within tissue engineering and regenerative medicine. Although they appear to have many advantages, there are still several challenges remaining for the appropriate design and implementation of these materials. Some of the major limiting factors that must be considered to maximize the effectiveness of this emerging approach are highlighted below.

Tissue selection, based upon both source and age, can have a significant impact on dECM materials (359). Site-specific tissues or organs harvested from exclusive regions are inherently different, as their microenvironments are designed to promote a specific cell function. Therefore, these native tissues have unique mechanical, biochemical and topographical properties that can illicit vastly different cellular responses. The age of the source tissue has been implicated in

temporal changes to ECM composition, molecular profiles and mechanical properties, such as an increase in fibrosis, tissue stiffening and inflammation with aging (359). Furthermore, if tissues are non-human, there are additional concerns related to species-specific differences that could negatively impact dECM material integration. For example, xenogeneic transplantation poses a risk of host immune rejection and incompatible homology (360). The ECM composition of sourced tissues must also be factored into the selection process. Specifically, the ECM proteins and proteoglycans that comprise healthy native tissues. Organs throughout the body have vastly different ECM contents and therefore, may require matching the appropriate ECM constituents to improve remodeling outcomes within a tissue-specific disease model. Another related element to ECM organization is the material stiffness, porosity and fiber orientation, which have all been shown to impact cell fate (361).

Once the ideal source of tissue has been selected, the decellularization method, reagents and post-decellularization treatments can further enhance or deplete critical biological signatures, such as tissue-specific growth factors and hormones. The use of enzymatic digestion to form hydrogel-based dECM materials can additionally alter the ultrastructural and mechanical properties. Particularly, stiffness and local ECM fiber organization within a hydrogel can change dramatically in comparison to native tissues. After dECM materials are implanted, they undergo a natural degradation process, with degradation times varying as a function of concentration and material composition. Therefore, dECM products must be carefully designed to optimize degradation times to promote regeneration of the damaged site.

Next generation dECM materials will require an in depth understanding of the diseased tissue and the ideal conditions that will initiate robust tissue remodeling. The goal is to create biomimetic materials to support the physiological profile observed within healthy tissues. To

accomplish this, researchers must consider testing a range of decellularization methods and techniques that preserve both the structural and functional components of the tissues. Tissue selection and processing should be carefully determined as well as the effects of dECM supplementation with growth factors and stem cells. Isolation and enrichment of the soluble fraction from decellularized nervous system tissues may also help stimulate functional regeneration. Finally, the addition of crosslinking agents and advancements in 3D printing may allow for improved tunability of the mechanical, topographical and structural properties of dECM materials with user-specified micropatterning and porosity to help support normal cell function and development.

3.0 Biomaterial-Assisted Follicle Microinjection as an Alternative Therapy for Fertility Preservation

3.1 Introduction

3.1.1 Rationale

Fertility preservation is an effort to restore fertility in young girls and women with cancer. Cytotoxic cancer treatments, such as chemotherapy, can significantly reduce the number of healthy follicles within the ovarian reserve, which may result in an impairment of fertility. Orthotopic transplantation of cryopreserved ovarian tissues have led to greater than 130 live-births worldwide; however, there remain risks associated with this procedure, including surgery-induced complications and potential transmission of residual malignant cells upon transplantation (149). To address the concern of malignant cells transmission, several groups have attempted to isolate ovarian follicles from the stromal cells to significantly reduce the chances for cancer recurrence. In vitro follicle maturation (IVM) has been recapitulated successfully from pre-antral follicles with the use of a variety of biomaterials, the most common being alginate. However, there has been limited success using IVM for human follicles with low rates of meiotically competent oocytes from immature follicles. Since it is difficult to accurately mimic the highly regulated ovarian environment that is necessary during folliculogenesis, several groups have turned to in vivo follicle maturation. In vivo follicle transplantation has led to live births in ovariectomized mice and has also showed efficacy for follicle maturation after subcutaneous implantation. Although these methods have shown the ability to restore fertility within ovariectomized mice, they have not been

tested within a chemotherapy model of infertility. Further, transplantation of follicles sequestered within a fibrin clot, would be infeasible in human patients due to the absence of a bursa within higher order mammals. Additionally, these approaches do not address the potential surgical complications that may result from follicle transplantation. Extracellular matrix-based biomaterials may have the potential to support the *in vitro* development and *in vivo* delivery of isolated follicles to restore fertility. Previously, decellularized ovarian ECM (dECM) scaffolds have been demonstrated to support short-term culture and transplantation of ovarian cells to effectively restore reproductive cycling in mice. Although these studies have resulted in functional hormone-producing ovarian follicles, they have not examined the use of dECM biomaterials to treat iatrogenic infertility. Therefore, we aim to develop methods to prepare ovarian-specific ECM hydrogels that can facilitate intraovarian follicle microinjection and support *in vivo* follicle development within chemotherapy-treated mice.

3.1.2 Innovation

The primary innovation of this work is the development of a decellularization protocol for the preparation of an ovarian-specific ECM (OECM) hydrogel. The second innovation is to implement the OECM hydrogel to facilitate the intraovarian microinjection of isolated follicles to establish an *in situ* ovary (ISO), which would allow the follicles to naturally integrate within the ovarian cortex. There are several advantages of using a hydrogel-facilitated microinjection approach. First, hydrogels have the ability to form *in situ* at physiological conditions. This would allow for a minimally invasive form of delivery, such as microinjection. The procedure could be similar to transvaginal oocyte retrieval for IVF; however, rather than collecting oocytes, follicles would be delivered into the ovary. This procedure is performed under ultrasound guidance and

could be done less-invasively than ovarian tissue transplantation. Secondly, microinjection can accommodate a high concentration of immature follicles within a small volume of hydrogel. Further, a successful *in situ* delivery may improve long-term follicle viability, maturation and natural pregnancy. This could also permanently replace the need for *in vitro* follicle culture, which has proven to be difficult for immature follicles. Primordial follicles, which reside within the ovarian cortex, are the most abundant follicle type within cryopreserved tissues. Therefore, it is imperative to implement methods that have the potential to support their maturation *in vivo* to improve fertility outcomes. The ability to inject follicles immediately upon isolation may also reduce the amount of time follicles are exposed to unfavorable culture conditions. This could make a significant difference in follicle viability upon transplantation. Finally, current biomaterial approaches reported in the literature have not performed ovarian follicle/tissue transplantation within animals treated with chemotherapy. If successful, this approach would not require patients to undergo an ovariectomy procedure. Instead, patients in remission could receive a minimally invasive follicle microinjection procedure to repopulate the ovarian reserve.

3.1.3 Central Hypothesis and Specific Aims

The central hypothesis for this thesis work is that ovarian tissue-derived hydrogels retain ovarian-specific components and provide a natural biomaterial to support the delivery of follicles in a chemotherapy-induced POF mouse (Figure 16). There are two main aims that were examined to test this central hypothesis.

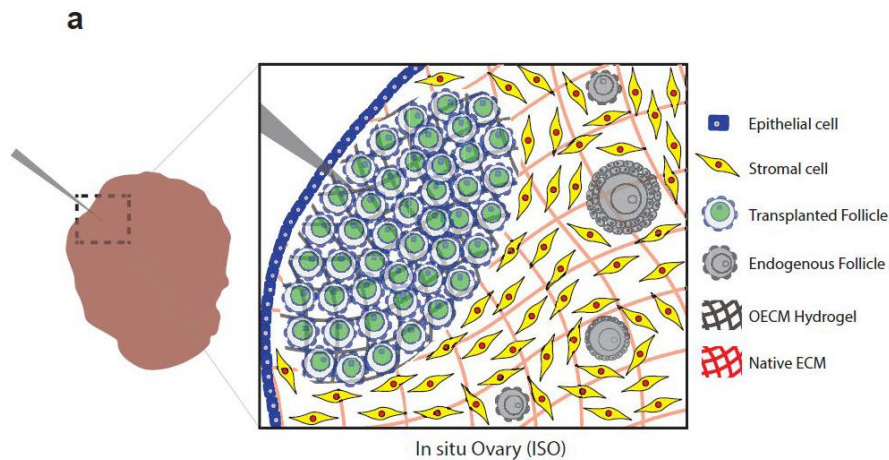


Figure 16 Central Hypothesis

The graphical representation shows our hypothesis for restoring fertility in patients with chemotherapy-induced premature ovarian failure (ciPOF). Intraovarian microinjection of an ovarian-specific ECM (OECM) hydrogel can support the delivery and long-term survival of exogenous primordial follicles (green) within an in situ ovary (ISO). The damaged ovarian tissue primarily consists of stromal cells (yellow) and a depleted population of endogenous follicles (gray).

Specific-aim 1: To decellularize porcine ovarian tissues for the derivation of an ovarian-specific ECM hydrogel.

Specific-aim 2: To determine the efficacy of ovarian hydrogels to support intraovarian follicle microinjection in a chemotherapy-induced POF mouse model.

4.0 Aim 1: Development of an Ovarian-Specific Extracellular Matrix Hydrogel

4.1 Introduction

Ovarian-related pathologies, such as infertility, ovarian cancer, polycystic ovarian syndrome and endometriosis, significantly reduce the quality of life for female patients, which produces a tremendous clinical and economic burden. Advancements in tissue engineering, specifically the development of tissue-specific extracellular matrix (ECM) biomaterials, may be used as both a diagnostic tool and therapeutic to help study and treat ovarian disease. One application for ovarian-specific ECM materials may be for female cancer patients that are negatively impacted by the effects of chemotherapy, radiation or gynecologic surgery. Specifically, alkylating agents used for chemotherapy are cytotoxic to cells and can significantly reduce the ovarian follicle population, which may result in either fertility impairment or a complete loss of fertility. This condition is classified as iatrogenic premature ovarian failure (POF) or primary ovarian insufficiency (POI).

Current strategies to restore function rely upon the cryopreservation of ovarian tissues and autotransplantation upon remission. However, patients who are at elevated risk for malignant cell contamination may be advised to avoid this therapy altogether to eliminate their chance for cancer cell transmission and recurrence. An alternative approach to restore fertility for cancer patients is through the isolation of immature follicles from the surrounding stromal cells, which may contain residual cancer cells. Ovarian follicles contain a basement membrane that protects the growing follicle from malignant cell invasion; therefore, the cancer risk can be significantly reduced, allowing follicles to be developed and fertilized in vitro. In vitro follicle maturation (IVM) has

been used successfully in several species, including humans. However, although our current understanding of folliculogenesis has improved, it remains incomplete. Therefore, in order to enhance the maturation efficiency of immature follicles toward meiotically competent oocytes it is important to recapitulate the ovarian microenvironment.

ECM biomaterials have been shown to improve healing through the ECM's intrinsic remodeling capability. Several tissue types have shown beneficial effects after treatment with ECM and most recently decellularized ovarian ECM (OECM) scaffolds have been used to facilitate the culture and transplantation of isolated follicles. However, ECM derivatives, such as hydrogels have yet to be tested as a three-dimensional substrate for IVM. To test the efficacy of this approach, we have developed a protocol for the decellularization of porcine ovaries to obtain an acellular ovarian-specific scaffold. Decellularized tissues were characterized to show the removal of immunogenic content without significantly disrupting the native architecture and ECM components of the ovary. Detection of residual ovarian-specific hormones also indicated that the decellularization process was mild enough to preserve native biomolecules. Solubilized acellular ovarian scaffolds successfully formed into hydrogels at physiological conditions. In vitro follicle maturation was tested to determine OECM hydrogel cytocompatibility and led to meiotically competent oocytes that could be fertilized up to the two-cell embryo stage. This outcome demonstrates the ability of the natural OECM hydrogel to support follicle development.

4.2 Objectives

The objectives of the first aim are: (1) to develop an effective decellularization protocol for porcine ovarian tissues using mild detergents to remove immunogenic material and preserve an ovarian-specific ECM components; (2) to characterize the acellular ovarian tissue in comparison to native porcine ovaries to examine the effects of decellularization including: ovarian tissue morphology, cell presence and distribution, double stranded DNA (dsDNA) quantification, DNA size, collagen and glycosaminoglycan content, ovarian-specific ECM and ovarian-specific hormones and growth factors; (3) to derive a hydrogel from decellularized ovarian ECM and define its viscoelastic properties, gelation kinetics and ultrastructure; (4) to evaluate the application of ovarian ECM hydrogels for both whole ovary culture and *in vitro* follicle maturation.

4.3 Methods

4.3.1 Ovarian Tissue Decellularization

Porcine ovaries from adolescent pigs (< 1 year old) were obtained from the local abattoir (*Thoma Meat Market, Saxonburg, PA*) and immediately stored on ice and frozen at -20°C. Ovaries were thawed, cleared of surrounding connective and adipose tissues, diced into cubes (~0.125 cm³) and transferred to a flask containing cold Milli-Q water (MQ). The diced tissues were shaken manually with MQ until residual blood was visibly removed then replaced with fresh MQ and stored overnight at 4°C. The tissues were then rinsed in fresh MQ on an orbital shaker for 30 minutes at 300 rpm. The flask containing tissue was then replaced with a pre-warmed solution of

0.02% trypsin and 0.05% EDTA then agitated on a magnetic stir plate for one hour at 37°C. Ovaries were then rinsed three times with MQ for 15 minutes each at 300 rpm. A 3% solution of Triton X-100 was then added to the flask and shaken for one hour at 300 rpm. A subsequent wash cycle was implemented to remove any residual detergents from the tissues. Each wash cycle consisted of several distilled water rinses with manual shaking (until no bubbles were observed), then alternating washes of MQ and 1X PBS to neutralize and release detergent that was bound to the tissues. After the wash cycle was completed, the fluid was replaced with fresh MQ and stored overnight at 4°C. A 4% sodium deoxycholate solution was added to the flask and agitated for 1 hour at 300 rpm. A subsequent wash cycle was performed then the tissue was replaced with fresh MQ and stored overnight at 4°C. The ovarian tissues were then depyrogenated and disinfected with a 0.1% peracetic acid and 4% ethanol solution for two hours at 300 rpm. This step was followed by three rinses in MQ, 1X PBS, MQ for 15 minutes each at 300 rpm then stored in fresh MQ at 4°C overnight. To ensure adequate removal of detergents and other chemical reagents one final series of washes with MQ, 1X PBS, MQ were performed for 15 minutes each at 300 rpm. The decellularized tissues were then stored at -80°C prior to lyophilization.

4.3.2 Detergent Assay

A commercial detergent assay kit (G-Biosciences - CMC-535) was used to assess the level of residual detergents during the decellularization protocol for ovarian tissues. Initial attempts at preparing decellularized ovarian tissues yielded hydrogels with poor cytocompatibility in the presence of macrophages. The detergent assay was used to ensure complete detergent removal from the decellularization effluent washes. Briefly, effluents were collected starting after the first Triton X-100 wash, and each subsequent wash step (12 steps in total), throughout the remainder

of the decellularization process. The assay sensitivity could detect detergent concentrations as high as 0.1% down to as little as 0.0016%. 50 μ L of standards, Triton X-100 and sodium deoxycholate (SDC), and samples from each effluent step were added to the a 96 well plate in duplicate. 100 μ L of 1X CMC-535 Fluorescent Dye was added to each well and mixed for 2 minutes on a shaker followed by the addition of 50 μ L of 1X CMC-535 Reagent 2 to each well, which was also mixed for 2 minutes. The plate fluorescence intensity was excited at 485 nm and read at an emission of 535 nm. Separate standard curves for both Triton X-100 and SDC were prepared and sample detergent concentrations were calculated.

4.3.3 Functional Assessment of Macrophages

A focus of the Brown lab is to evaluate the innate immune response to biomaterials. To study this, protocols have been established in the lab to isolate primary macrophages from the bone marrow and study their phenotype and function. To this end, we used these protocols to evaluate the cytocompatibility of ovarian hydrogels to replicate similar results regarding macrophage behavior in the presence of other common tissue-specific ECM hydrogels. The following subsections describe these methods.

4.3.3.1 Isolation of Bone Marrow-Derived Macrophages

Bone marrow-derived macrophages were harvested from 2 month or 18-20 month-old C57BL/6 mice as previously described (362). Briefly, femurs and tibiae were collected and were stripped of muscle and connective tissue. Bones were cut at either end to expose bone marrow. Sterile syringe and needles were used to extract bone marrow using macrophage differentiation media. Bone

marrow lysate was reconstituted in media and filtered through a sterile cell filter. Cells were cultured for 7 days in media to induce macrophage differentiation, with media changes once every 2 days.

4.3.3.2 Macrophage Treatment

Following 7 days of differentiation culture as described above, macrophages were treated with acute polarizing regimens to distinguish phenotypes over 24 hours. Naïve macrophage (M0) controls were treated with basal media for 24 hours. M1 (20 ng/mL IFN- γ and 100 ng/mL LPS) and M2 (20 ng/mL IL-4) polarizing cytokines were used to create positive controls for classical pro- and anti-inflammatory macrophages. ECM degradation products were neutralized and diluted to 250 μ g/mL in macrophage media to isolate biochemical effects of degradation products and prevent structural moieties from forming. Pepsin buffer (1 mg/mL pepsin in 0.01 M HCl) diluted in macrophage media was used as a control. Another set of treatment groups involved 24-hour exposure of ECM degradation products followed by 24-hour treatment with either the M1 or M2 treatment regimen, referred to as ECM \rightarrow M1 or ECM \rightarrow M2, respectively.

4.3.3.3 Indirect Immunolabeling for Arginase and iNOS Expression

Cells were fixed with 2% paraformaldehyde (PFA) for 30 minutes then washed in 1XPBS. Cells were incubated in blocking buffer (2% donkey serum, 1% bovine serum albumin (BSA), 0.1% Triton X-100, 0.1% Tween-20) for 1 hour at room temperature. Primary antibodies were diluted in this blocking buffer as follows and incubated overnight at 4 °C: iNOS (1:100, Abcam 3523) or Arginase-1 (1:200, Abcam 91279). iNOS is a classical M1 macrophage marker whereas Arginase-1 is a classical M2 macrophage marker. Cells were washed in 1XPBS then incubated in the appropriate fluorescently-labeled secondary antibody solution in blocking buffer for 1 hour at room temperature (donkey anti-rat Alexa Fluor 488, Invitrogen, 1:200; donkey anti-rabbit Alexa Fluor 488, Invitrogen, 1:300). Cell nuclei were counterstained with DAPI. Cells from 2 month old mice were imaged nine times in the

center of each well at 10X magnification using automated position capture function to remove bias from subjective image location acquisition. All imaging was performed on an Axio observer T1 microscope. Mean fluorescence intensity of cells was analyzed using Cell Profiler software (Broad Institute). Briefly, DAPI images were used by the program to identify cell nuclei then FITC images were used to identify cell borders around the identified nuclei. The mean fluorescent intensity was calculated by averaging the pixel intensities (scale of 0 to 1) across the entire cell area. Mean fluorescence intensity values were averaged for all imaged cells in each well.

4.3.3.4 Phagocytosis Assay

Following treatments, cells were assayed for phagocytic ability using Vybrant Phagocytosis Assay Kit (Invitrogen). Cells were incubated in FITC-labeled dead E. Coli particles for 2 hours in the cell culture incubator. Following washing, the cells were fixed with 2% PFA for 30 minutes then washed with 1X PBS. Cells were counterstained with DAPI then imaged and analyzed as described above.

4.3.3.5 Nitric Oxide Assay

Following treatments, 50 μ L of supernatant from macrophages were transferred into a fresh plate. Nitric oxide content was assayed using a Greiss Reagent system. Briefly, 50 μ L of sulfanilamide (1% in 5% phosphoric acid) was added to supernatants for 10 minutes. Then, 50 μ L of 0.1% N-1-naphthylethylenediamine in water was added to the mixture for an additional 10 minutes. The absorbance at 540 nm was measured using a BioTek SYNERGY HTX spectrophotometer.

4.3.4 Characterization of Decellularized Tissues

Decellularized ovarian tissues were characterized using a number of qualitative and quantitative measures to verify the removal of genetic material and maintenance of ovarian specific proteins. Native and decellularized ovarian tissues were formalin-fixed, paraffin-embedded, sectioned and stained using several histological procedures including DAPI (4',6-diamidino-2-phenylindole), Hematoxylin and Eosin (H&E), and Periodic Acid-Schiff (PAS). Antibodies specific for ECM proteins Collagen I (Abcam, ab34710) and IV (Abcam, ab6586), Fibronectin (Abcam, ab23751), and Laminin (Abcam, ab11575) were evaluated using DAB (3,3'-Diaminobenzidine) immunohistochemistry (IHC) staining to show conservation after decellularization. IHC tissue sections were counterstained using Hematoxylin QS (Vector Labs, Cat No. H-3404) to show cell nuclei in contrast with resident ECM proteins. DNA removal was quantified using a PicoGreen dsDNA assay kit (Invitrogen, Cat No. P11496). A 2.5% agarose gel was used to detect DNA fragments at a resolution between 25 and 1000 bp. Hydroxyproline (HYP) and sulfated glycosaminoglycans (sGAG) assays were performed to approximate collagen and sGAG content. Native and decellularized ovarian tissues were placed in M tubes and homogenized using a gentleMACS dissociator (Milltenyi) in a High Salt Buffer (pH 7.5, 50 mM Tris base, 150 mM NaCl, 5 M CaCl₂, 1% Triton-X-100, 1% Halt protease inhibitor cocktail, Pierce Biotechnology, Rockford, IL). After homogenization, M tubes containing samples were centrifuged at 4000 x g at 4°C for 5 minutes. Decellularized tissues required more starting mass for homogenization to have a higher concentration of total protein to more closely match native samples. Protein concentrations of the extracted tissues were determined using the BCA Protein Assay Kit (Pierce Biotechnology, Rockford, IL) and 50 µg total protein was used per sample for all assays. Ovarian specific growth factors including insulin growth factor (IGF-1) (R&D Systems,

Minneapolis, MN), 17 β -estradiol (R&D Systems, Minneapolis, MN), progesterone (Abcam, Cambridge, MA), anti-Müllerian hormone (AMH) (R&D Systems, Minneapolis, MN), and vascular endothelial growth factor (VEGF) (Abcam, Cambridge, MA), were quantified using enzyme-linked immunosorbent assays (ELISA).

4.3.4.1 Hematoxylin & Eosin (H&E) Staining

Tissue sections were deparaffinized in a series of re-hydrating steps to water. Slides were placed in Harris Hematoxylin for 8 minutes, followed by two 30 second washes in distilled water (dH₂O). Tissues were then placed in a solution of acid alcohol (5% glacial acetic acid and 95% ethanol) for 1 minutes, then washed twice in dH₂O for 30 seconds each. The next step was a 15 second dip in Scott's H₂O and 2 washes in dH₂O for 1 minute each. The final step was a stain in Eosin for 2 minutes before the tissues were dehydrated in a series of graded alcohols and xylenes. The slides were coverslipped using Permount and allowed to dry prior to imaging. All reagents were prepared fresh and filtered to remove concentrated particulate.

4.3.4.2 Periodic Acid Schiff (PAS) Staining

Periodic acid Schiff (PAS) staining was used to identify glycogens within the extracellular matrix of ovarian follicles. Native and decellularized ovarian tissues were fixed in 10% formalin for a minimum of 24 hours then paraffin-embedded. Tissue sections were cut at 5 micron and deparaffinized prior to staining. Slides were dipped in 0.5% periodic acid for 5 minutes then rinsed in distilled water. Tissues were then transferred to Schiff reagent for 15 minutes then washed in lukewarm tap water for 5 minutes. Ovarian sections were then counterstained with Harris modified hematoxylin (4 dips), washed for 1 minute in running water and treated with acid alcohol (95% Ethanol and 1% HCl) for an additional minute (3 dips). Tissues were washed in running water for

another minute then placed in saturated lithium carbonate (15 mg/mL water) for 6 dips. Tissues were washed in running water then dehydrated prior to being coverslipped with Permount. The PAS stain will show glycogen, mucin, fungi and basement membranes in a red/purple color and cell nuclei in a blue color.

4.3.4.3 Hydroxyproline (HYP) and Sulfated Glycosaminoglycans (sGAG) Assays

Native and decellularized ovarian tissues biochemical assays were performed to assess hydroxyproline (HYP) and sulfated glycosaminoglycan (sGAG) content. Lyophilized native and decellularized ovarian tissues were digested at 10 mg/mL in a papain solution (0.125 mg/mL papain; 0.100 M cysteine; 0.100 M Na₂HPO₄; 0.010 M Na₂EDTA) overnight at 50°C. HYP content was assessed by adding 50 µL of 2N NaOH to 50 µL of the papain digests and hydrolyzing the samples at 110 °C for 18 hours. Samples were neutralized with 5N HCl. After neutralization, each of the following reagents were added to each sample and vortexed sequentially: 100 µL of 0.01M copper sulfate, 2.5N NaOH and 6% H₂O₂. 400 µL of 3N sulfuric acid was then added to each sample, vortexed and incubated at 80°C for 5 minutes, then allowed to cool. Once the samples had cooled, 200 µL of 5% DMAB (dimethylamino benzaldehyde) solution in propanol was added to each tube. Samples were incubated at 70°C for 15 minutes then transferred to a 96 well plate. To detect HYP content, the absorbance was read at 525 nm. sGAG content was assessed by adding 50 µL of papain digested samples (in triplicate) onto a 96 well plate. A standard curve was prepared using chondroitin-6-sulfate. 250 µL of dimethylmethylene blue (DMMB) reagent was added to each sample and standard well and the absorbance was read at 540 nm to detect sGAG content.

4.3.4.4 Immunohistochemistry

Paraffin tissue sections were deparaffinized using xylenes and graded alcohols and rehydrated in water. Proteinase K was added to tissues and incubated in a humidity chamber for 5 minutes at room temperature. Slides were transferred into citric acid buffer (2.1 g/L citric acid; 500 uL Tween 20; Type I H₂O up to 1 L; pH: 6.0) at 100°C for 20 minutes, then moved to ice for an additional 20 minutes. Tissues were washed in 1X PBS 3 times for 3 minutes each and then moved to a 3% hydrogen peroxide solution in 1X PBS for 30 minutes at room temperature. This was followed by two 1X TBST (tris-buffered saline + 0.1% Tween 20) washes for 5 minutes each. A 1X PBS wash was performed two times for 3 minutes each. The non-specific epitopes were blocked using blocking buffer (5% Donkey Serum; 2% BSA; 0.1% Tween 20; 0.1% Triton X-100; 1X PBS) for 2 hours at room temperature, followed by the addition of primary antibodies diluted in the same blocking buffer and allowed to incubate overnight at 4°C in a humidified chamber. After overnight incubation the tissues were washed three times in 1X PBS for 3 minutes each. Once the unbound primary antibodies were washed away, biotinylated-secondary antibodies (in blocking buffer) were added for 30 minutes at room temperature in a humidified chamber. The unbound secondary antibodies were removed with another three washes in 1X PBS for 3 minutes each. Vecta-Shield ABC (avidin-biotinylated enzyme complex) Reagent (Vector Laboratories) was added to the tissues for 30 minutes at room temperature then washed three times in 1X PBS for 3 minutes each. A 4% DAB (3, 3'-diaminobenzidine) solution, acting as a substrate, produces a brown precipitate in the presence of ABC reagent, which is bound to the target antibody complex. The incubation time was variable; however, it generally did not exceed 1 minute. The DAB solution was quickly removed by rinsing in water for about two minutes then counterstained using Hematoxylin QS for about 45 seconds. The Hematoxylin was also washed immediately in water

to avoid overstaining. Slides were dehydrated using graded alcohols and xylenes then coverslipped in Permount before imaging.

4.3.5 Ovarian ECM Digestion and Hydrogel Formation

Lyophilized ovarian ECM powder was solubilized via enzymatic digestion. A stock ECM digest concentration of 10 mg/mL was prepared by adding 200 mg of ECM powder to a 20 mL solution of pepsin (Sigma P7012) at a concentration of 1 mg/mL ($\geq 2,500$ units/mg) dissolved in 0.01 N hydrochloric acid (HCl). Digestion was facilitated with an overhead mixer between 700-2000 RPM for less than 48 hours. Hydrogels were formed after neutralizing and buffering the solubilized ovarian ECM to physiological conditions. Two hydrogel concentrations (4 and 8 mg/mL) were prepared for testing and experimentation. A pre-gel solution was made on ice using the following components: (i) 10 mg/mL OEMC digest stock (volume determined by desired final concentration) (ii) 0.1 N NaOH (1/10th the volume of the digest), (iii) 10X PBS (1/9th the volume of the digest), and (iv) 1X PBS or L-15 medium (brought up to final volume). The solution was pulsed 3 times on a vortexer to mix then stored at 4°C until further use.

4.3.6 Hydrogel Characterization

Ovarian hydrogel ultrastructure was assessed using scanning electron microscopy (SEM). Hydrogels were fixed using 2.5% glutaraldehyde, washed with 1X PBS and post-fixed with osmium tetroxide (OsO₄). Samples were washed again in 1X PBS to dilute the OsO₄ then they were slowly exsiccated through a series of increasing ethanol concentrations. Complete dehydration was achieved using a critical point dryer. Dried hydrogels were sputter-coated with

gold/palladium particles and imaged at 8,000X magnification. A proprietary Matlab code was used to analyze SEM images to determine various hydrogel fiber network characteristics (363). Ovarian hydrogel bulk viscoelastic properties were determined using a dynamic parallel plate (40 mm) rheometer (AR-2000 TA instruments). A time sweep (5% strain, 1 rad/s) was used to demonstrate the effect of ECM concentration on both the storage (G') and loss (G'') modulus. Turbidimetric gelation kinetics were performed on the ovarian hydrogels as previously described (364, 365).

4.3.7 Whole Ovary Culture

Sohlh1-mCherry transgenic newborn mouse (Rajkovic Lab) ovaries were excised and cultured using ovarian ECM hydrogels at varying ECM concentrations to determine the impact on ovarian follicle development. Ovarian hydrogels were prepared in Millicell Cell Culture Inserts – PTFE, 0.4 μ m pore size (Millipore Sigma) at concentrations of 2, 5 and 10 mg/mL. Similarly, collagen and PTFE were used as controls. Sohlh1 newborn mouse ovaries were removed and placed on top of the various substrates and cultured for 7 days in ovarian culture medium (Appendix Table 3) in a cell culture incubator at 37°C (95% air, 5% CO₂). Media was changed every 2-3 days and ovaries were monitored carefully. After 7 days, whole ovaries were imaged under confocal microscopy to determine the presence of Sohlh1+ cells, which is a marker of primordial follicles. Sohlh1+ cells were quantified based upon the volume of the cells using Volocity software (Appendix Figure 20). Subsequently, ovaries were fixed in paraformaldehyde and embedded in paraffin wax. Ovaries were serial sectioned and stained using a variety of histological methods, including H&E, PAS, and IF/IHC. IHC was performed to identify cells expressing NOBOX, which is an oocyte-specific marker. IF was used to identify additional oocyte markers, Sohlh1 (oocyte cytoplasm) and Sohlh2 (oocyte nucleus), after cell culture.

4.3.8 In Vitro Follicle Culture

Follicle culture media was prepared and sterile filtered prior to follicle isolation (Appendix Table 4). Ovaries were excised from 14-16 day old C57BL/6 or B6/D2 female mice and transferred into warmed Dissection Media. Note: Dissection Media containing L-15 medium is pH stable out of cell culture incubator and was pre-warmed to 37°C in a water bath or incubator without CO₂. Once the ovaries were excised and the bursa was removed, ovaries were moved to a 9-well glass plate containing fresh Dissection Media. Secondary follicles were mechanically isolated from the ovaries using 27-½ gauge insulin syringes. One needle was used to secure the ovary while the other needle as used to gently scrape away the stromal cells and connective tissues to free the follicles. After 20-40 secondary follicles were isolated from each ovary, they were selected using an oocyte transfer pipette and placed in a 30 mm petri dish containing Maintenance Media then transferred to the cell culture incubator. This step was repeated until follicles had been removed from each ovary. Each isolation was performed at room temperature and limited to 30 minutes of exposure outside of the incubator to improve follicle viability. Prior to culture, follicles were encapsulated in 8 mg/mL ovarian hydrogels or 0.5% alginate. 8 mg/mL OECM pre-gel was prepared on ice, then multiple 100 µL droplets or a single 500 µL droplet were pipetted into a 35 mm petri dish on ice. Secondary follicles were then picked up with minimal volume, 5 at a time, and placed on top of each OECM droplet. A 100 µL positive displacement pipette was set to 25 µL and picked up about half of the total volume of OECM pre-gel then the other portion of the volume was used to pick up the follicle in the OECM droplet. The 25 µL follicle-OECM was perpendicularly pipetted into sterile and warmed 1X PBS or L-15 in a 35 mm petri dish. After 10 follicle-OECM hydrogel droplets were formed the petri dish was transferred into an incubator at 37°C (no CO₂) for an additional 20 minutes. After 20 minutes, the encapsulated follicles were

transferred into fresh Maintenance Media. This process was repeated until all follicles were encapsulated. Alginate encapsulation was performed similarly. First, 4-5 mL of calcium solution (50 mM CaCl₂; 140 mM NaCl; 500 mL Type I H₂O; pH:7.4) was pipetted into a 35 mm petri dish. Then, 500 μ L of 0.5% alginate was placed in the center of another 35 mm petri dish. After all follicles were encapsulated, they were transferred to a 96-well plate containing pre-warmed/equilibrated Growth Media (100 μ L). Follicles were cultured for 11 days, with Growth Media changes every two days (50 μ L removed and frozen for hormone analysis), adding 50 μ L of freshly prepared Growth Media. After every media change, follicles were imaged under a bright field microscope (with a humidified chamber) to assess follicle morphology and growth. Follicle diameters were determined using ImageJ to track development throughout the culture period. At day 11, antral follicles that surpassed 300 μ m in diameter were transferred to Maturation Media for 14-16 hours to induce ovulation and the resumption of meiosis. After 16 hours, follicles were nicked with a insulin needle to free the oocyte. Oocyte meiotic competence was evaluated morphologically and characterized into three categories: (1) Germinal Vesicle (GV) Stage – oocytes retain nuclear membrane and do not re-enter meiosis (2) Germinal Vesicle Breakdown (GVBD) – oocytes resume meiosis without a nuclear membrane, and (3) Metaphase II (MII) which extrudes the first polar body. In vitro fertilization (IVF) studies of MII oocytes produced from follicle cultures were conducted by Dr. Yi Sheng (Orwig Laboratory).

4.3.9 Statistical Analysis

All data were expressed as mean \pm s.e.m and plotted using GraphPad Prism 7.02. To detect differences between native and decellularized tissues for dsDNA, HYP, and sGAG concentrations as well as changes in hydrogel fiber network characteristics, the individual means were compared

using an unpaired, two-tailed, t-test. To detect differences in hormone retention between native tissues (ovary vs. bladder) and decellularized (OECM vs. UBM), the mean ranks were compared using an unpaired, one-way ANOVA (Kruskal-Wallis) with adjusted P-values calculated based upon Dunn's multiple comparisons test. Exact P-values resulting from the statistical analysis are presented within each figure.

4.4 Results and Discussion

4.4.1 Biomaterial Selection and Tissue Processing

The damaging effects of chemotherapy on ovarian tissues significantly reduces a patient's follicle population, which has a direct impact on fertility and endocrine function (162, 366, 367). In addition, chemical treatments have been implicated in microvasculature and stromal cell irregularities culminating in a compromised environment for cell survival (162). These unfavorable conditions cause a depletion of ovarian follicles and may reduce follicle viability post-transplantation (76, 221). Therefore, to re-establish the ovarian tissue microenvironment and repopulate the depleted endogenous follicle pool, we have bioengineered an ISO using an OECM hydrogel to facilitate intraovarian follicle transplant and provide a temporary niche to aid follicle engraftment and survival (Figure 16).

To prepare acellular ovarian scaffolds, porcine ovaries (Figure 17b) were diced (Figure 17c) then processed using a series of enzymatic and detergent-based washes to remove immunogenic material (Figure 17d). Trypsin and EDTA were used in tandem to disrupt cell adhesions to the ECM prior to treatments with Triton X-100 and sodium deoxycholate, which act

to permeabilize cell membranes. Tissues transitioned from an initial opaque appearance to translucent at the conclusion of the decellularization steps (Figure 17e). Intermediate water washing steps proved to be critical for the complete removal of residual cells and detergent from the tissues. Once the tissues were completely decellularized they were frozen, lyophilized (Figure 17f) and milled into a powder (Figure 17g) prior to biochemical testing and downstream processing.

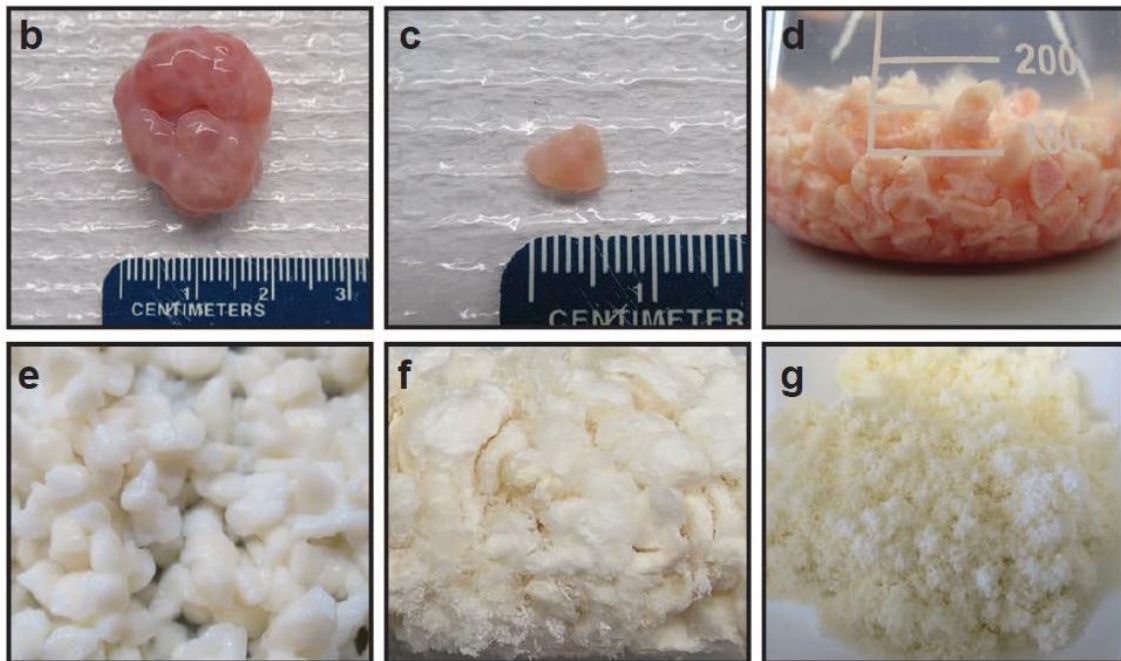


Figure 17 Ovarian Tissue Processing

b, Young (< 1 year old) porcine ovaries were sourced for decellularization. c, Ovaries were diced into small cubes (~0.125 cm³). d, Cubed ovaries were added to a flask and decellularized using enzymes and detergents. e, Decellularized ovarian tissues appeared white. f, Ovaries were frozen then lyophilized to remove their water content. g, Powdered OECM was prepared using a mill.

To demonstrate the effective removal of immunogenic components and preservation of extracellular matrix (ECM) components, we performed a set of histological stains and biochemical assays. Fluorescence staining with 4',6-diamidino-2-phenylindole (DAPI) showed few, if any nuclei present within the decellularized tissues in comparison to native ovarian tissue controls (Figure 18h). H&E (Figure 18i) and PAS (Figure 18j) staining showed a clear retention of ovarian microarchitecture, such as structural aspects of follicles, zona pellucida and corpora lutea, while sparse cellular content was visible. This highlights the effectiveness of our method to successfully remove cellular content, while causing limited disruption of tissue-specific morphology. Scanning electron micrographs (SEM) further detailed the dense cellular content within native ovarian tissues, whereas decellularized tissues appeared to show vacated follicular compartments surrounded by a porous scaffold (Figure 18k). A PicoGreen assay demonstrated greater than 98% reduction of dsDNA between native (9126 ± 1988 ng/mg) and decellularized (262.4 ± 59.96 ng/mg) samples (Figure 19l). Gel electrophoresis further showed a lack of DNA (Appendix Figure 10) within the decellularized tissues in comparison to native controls, suggesting a reduced potential for disease transmission and adverse immune reaction to cellular contents. Collagen and sulfated glycosaminoglycans (sGAG) were also examined to determine their retention post-decellularization. A hydroxyproline (HYP) assay was used to estimate the total collagen content within the scaffold. Native tissues (61.95 ± 6.064 ug/mg) contained significantly less HYP as a percentage of dry weight than decellularized tissues (153.3 ± 8.564 ug/mg) due to the loss of cellular mass; however, under this assumption the total collagen content within the decellularized scaffold as a fraction of the dry weight of all components was enriched after decellularization (Figure 19m). sGAG content was also preserved with no significant difference observed between native (5.24 ± 1.03 ug/mg) and decellularized (3.59 ± 0.436 ug/mg) samples (Figure 19n).

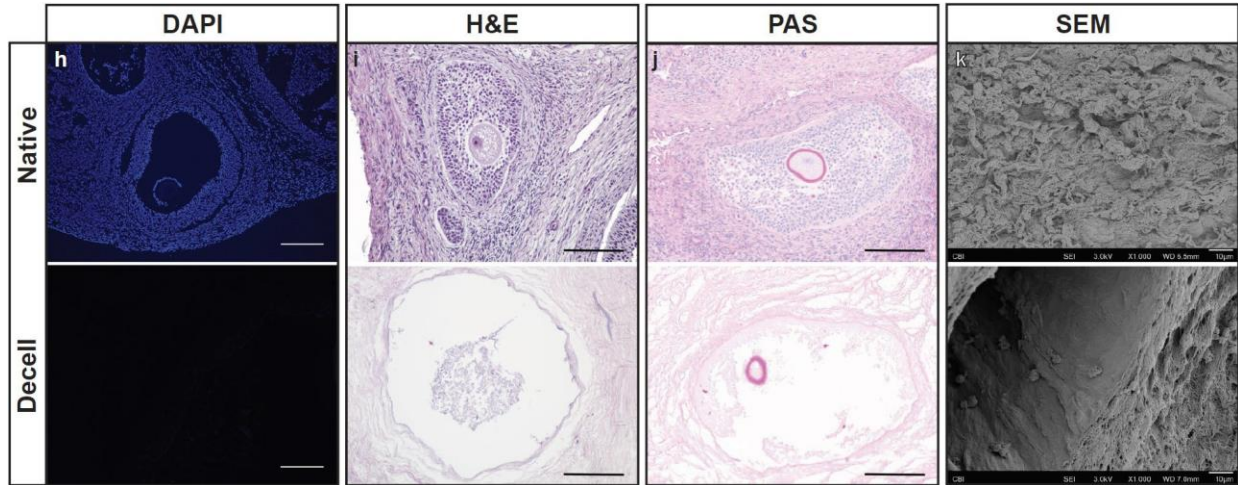


Figure 18 Histological and Ultrastructural Evaluation of Native and Decellularized Ovarian Tissues

h-j, Native (top row) and decellularized (bottom row) images of DAPI (200 μm scale), H&E (100 μm scale), and periodic acid-Schiff (PAS) (100 μm scale) staining determined that decellularized tissues removed cellular content while preserving ovarian tissue morphology. k, Scanning electron micrographs (SEM) show a dense cellular ultrastructure in native ovaries in comparison to a porous decellularized scaffold (10 μm scale).

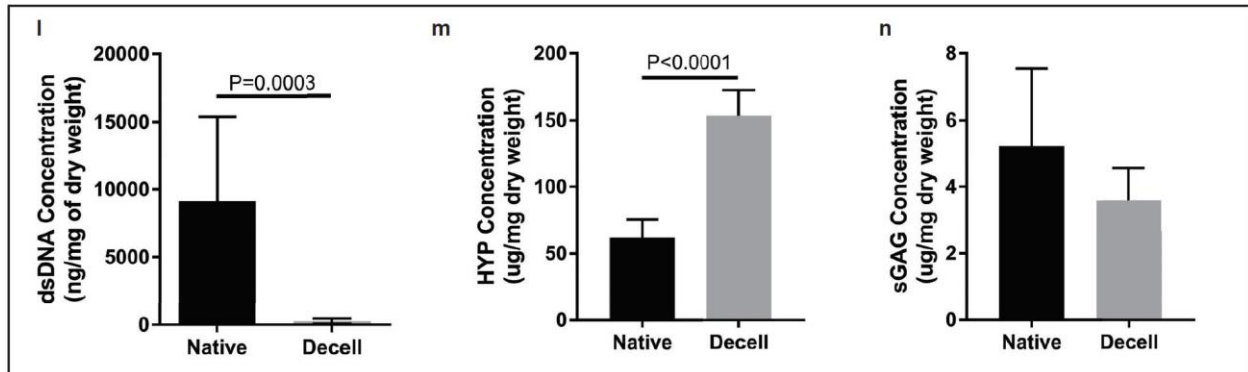


Figure 19 DNA and ECM Component Quantification

l, PicoGreen assay indicated that decellularized ovarian tissues significantly reduced the dsDNA concentration. Data represent mean \pm s.e.m. of ng/mg dry weight. P values by unpaired, two-tailed t-test. m, Hydroxyproline (HYP) concentration was significantly enriched in decellularized tissues and n, sulfated-Glycosaminoglycans (sGAG) levels did not differ significantly between native and decellularized samples. Data represent mean \pm s.e.m. of $\mu\text{g}/\text{mg}$ dry weight. P values by unpaired, two-tailed t-test.

4.4.2 Ovarian Tissue Specificity Present Post-Decellularization

The ECM is composed of a tissue-specific milieu of secreted proteins and proteoglycans that support the desired functions of a tissue (271, 288, 330). In the ovary, the ECM undergoes dynamic remodeling throughout the reproductive life span and is essential for regulating folliculogenesis and ovulation (2, 368). Specifically, OECM provides mechanical support, maintains normal cell morphology, promotes cell proliferation and steroidogenesis (2). Additionally, the OECM can sequester hormones and growth factors within the follicle niche to facilitate paracrine and endocrine signaling (2, 369). Therefore, the retention of OECM proteins would be ideal for supporting follicles within the ISO. To determine the effects of decellularization on ECM retention, we characterized a subset of the most highly expressed OECM proteins: Collagen I, Collagen IV, laminin and fibronectin (2, 368, 370, 371). Immunohistochemistry revealed that Collagen I was distributed uniformly in the native samples, with a slight enrichment surrounding the thecal compartments of the follicles in decellularized samples (Figure 20a). Collagen IV was also labeled, showing definitive staining within the basement membrane of the epithelial layer and the basal lamina of individual follicles in both the native and decellularized groups (Figure 20b). Similar to Collagen IV, laminin was predominantly found within the basal lamina adjacent to the theca interna surrounding follicles (Figure 20c). Finally, fibronectin appeared to be conserved throughout the ovarian tissues with little to no differences in distribution noted between the native and decellularized groups (Figure 20d).

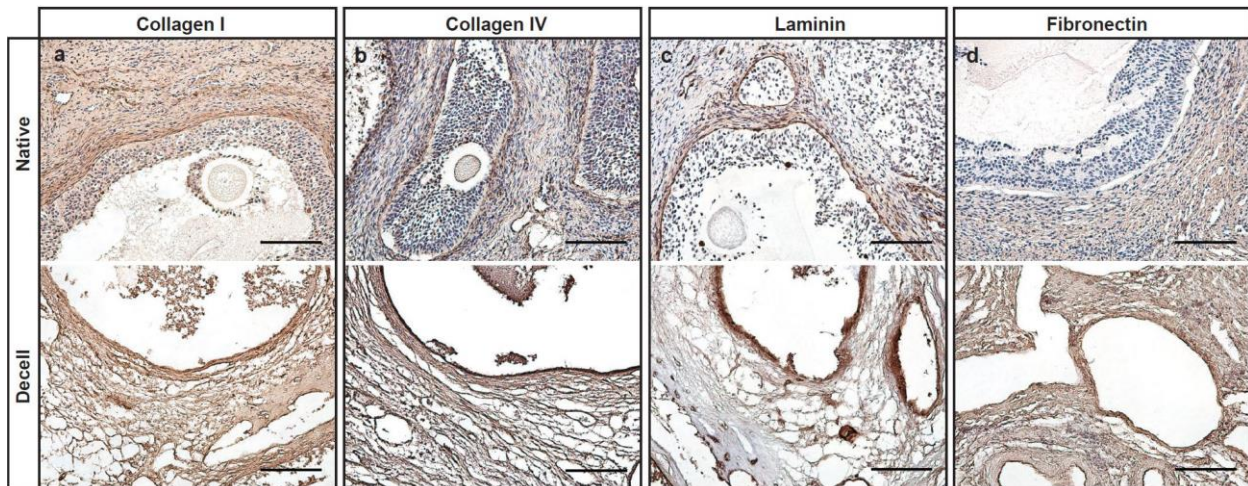


Figure 20 Characterization of Ovarian-specific ECM Proteins

Immunohistochemistry (IHC) images of native (top row) and decellularized (bottom row) ovarian tissues shows the distribution of extracellular matrix proteins: a, Collagen I was uniformly expressed throughout each of the tissues. b, Collagen IV appeared to concentrate in the basal lamina of the follicles and the basement membrane surround the epithelial layer of the ovary. c, Laminin was present within the thecal compartment and d, Fibronectin was evenly expressed in lower concentrations; however, antibody staining was enriched in decellularized tissues. Scale, 100 μ m.

Ovarian hormones and growth factors sequestered in the OECM orchestrate both local and systemic endocrine function. The hypothalamic-pituitary-gonadal (HPG) axis stimulates the production of ovarian hormones, which act to modulate hormone production in a cyclic manner (13). The hypothalamus produces gonadotropin releasing hormone (GnRH), which stimulates the secretion of follicle stimulating hormone (FSH) and luteinizing hormone (LH) (13). FSH and LH trigger the production of estradiol, follicle development and ovulation. Estradiol from the ovulatory follicle and progesterone from the resulting corpus luteum provide feedback to either inhibit or stimulate hormone secretion from the hypothalamus and pituitary (13). Spatiotemporal production of these reproductive hormones primarily facilitates follicle development, ovulation and pregnancy (13).

For this study, we were particularly interested in hormones produced by the ovary due to their roles in follicle selection. Specifically, anti-Müllerian hormone (AMH), estradiol and progesterone. AMH is produced by granulosa cells of pre-antral and antral follicles (120). As AMH levels increase, it can inhibit the recruitment of primordial follicles and decrease the responsiveness of large pre-antral/antral follicles to FSH. AMH is one of the few hormones that are produced during the early stages of folliculogenesis, which are widely recognized as gonadotropin-independent (4). Estradiol is also produced by follicular cells and is most commonly known for its role in the LH surge which triggers ovulation; however, at low concentrations, estradiol can function as a negative regulator of FSH, which inhibits follicle growth (4, 10). The corpus luteum, which arises from the cells of ovulatory follicles and is present during the late luteal phase, produces high levels of progesterone, which is necessary for maintaining pregnancy. Like estradiol, progesterone can also inhibit FSH production further delaying follicle growth (4).

We hypothesized that these ovarian hormones may be important for the survival of transplanted immature follicles within the ISO. Therefore, to elucidate the effects of decellularization on the disruption of these components, we processed a large batch of 100 ovaries separated into five groups (n = 20 per group) analyzed as independent samples (Appendix Figure 1). As controls, we used both native and decellularized urinary bladder matrix (UBM), collected from female pigs and prepared as previously described (372), to determine if there were significant differences in the hormone concentrations based upon tissue source. After tissue homogenization, protein was extracted from each group and tested using biochemical assays for AMH, estradiol and progesterone. ELISA quantification determined that decellularized OECM samples contained low concentrations of each of the ovarian-specific analytes: AMH (1031 ± 192.9 pg/mg), estradiol (113.8 ± 19.63 pg/mg) and progesterone (2697 ± 1890 pg/mg) (Figure 21e-g). Native ovaries

contained significantly higher levels of estradiol and progesterone when compared to native bladder. Furthermore, decellularized OECM had significantly higher progesterone values than UBM. Additional analytes associated with follicle development, insulin-growth factor (IGF-1) and vascular endothelial growth factor (VEGF), were also tested but were undetectable within the decellularized samples (Appendix Figure 12).

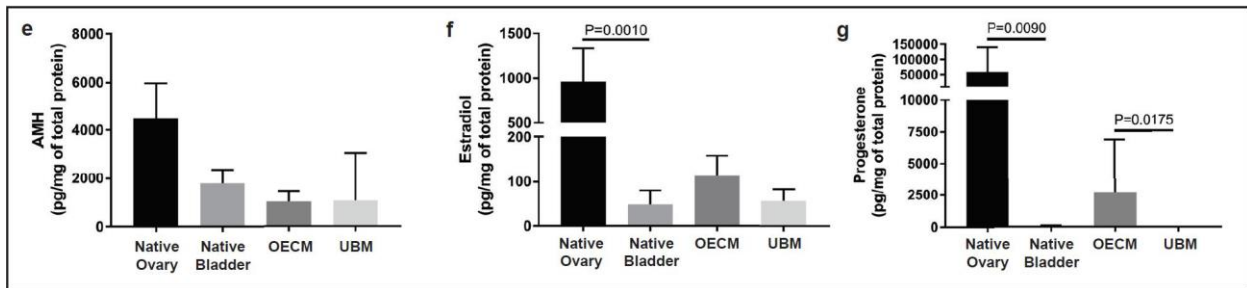


Figure 21 Quantification of Ovarian-specific Hormones after Decellularization

Ovarian hormones secreted by follicular cells were quantified from total protein using enzyme-linked immunosorbent assays (ELISAs). e, Anti-Müllerian hormone (AMH) was measured at high concentrations within native ovarian tissues but was reduced by >50% within decellularized OECM. f, Estradiol concentrations were significantly higher in native ovary in comparison to native bladder and OECM was two-fold greater than UBM. g, Progesterone levels were significantly greater in both native ovary and OECM in comparison to native bladder and UBM, respectively. ELISAs were conducted using 100 ovaries batched into 5 independent samples (n = 20 ovaries). Data represent mean \pm s.e.m. of pg/mg of total protein. P values by one-way ANOVA using Kruskal-Wallis with Dunn's multiple comparisons test. Native (ovary and bladder) and decellularized groups (OECM and UBM) were compared separately.

4.4.3 Ovarian Hydrogel Properties Modified with Changes in ECM Concentration

Once the decellularized tissues were processed and characterized, we solubilized the OECM then neutralized the digested material to prepare the hydrogels. Visibly transparent hydrogels were formed after exposure to physiological conditions for approximately 20 minutes (Figure 22a). We used SEM to evaluate the hydrogel ultrastructural properties at 4 and 8 mg/mL ECM concentrations (Figure 22b,c). Fiber network characteristics were quantified using SEM imaging and digital image analysis (363) with concentration dependent effects observed with a significant increase in fiber diameter, fiber length and bulk porosity in the 8 mg/mL OECM hydrogel group (Figure 23d-h). These results indicate that individual fiber and large-scale network properties such as the bulk porosity are dependent on ECM concentration.

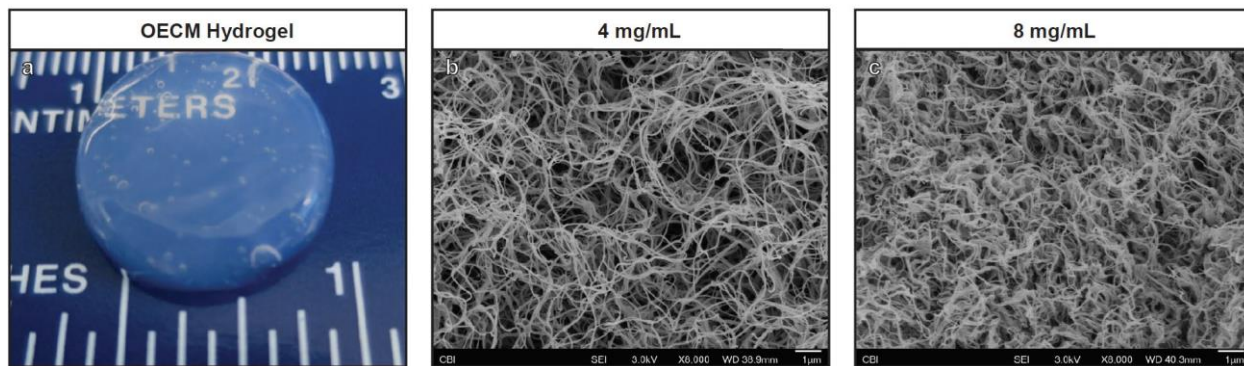


Figure 22 Ovarian ECM Hydrogel Formation and Ultrastructure

a, Solubilized ovarian ECM (OECM) formed transparent hydrogels upon neutralization and exposure to physiologic conditions. b-c, Scanning electron micrographs (SEM) show a fibrous and porous architecture at both 4 and 8 mg/mL OECM concentrations.

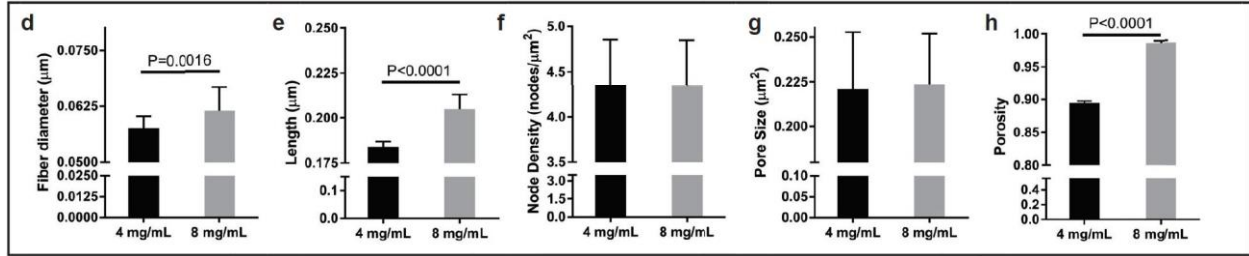


Figure 23 OEEM Hydrogel Fiber Network Analysis

d-h, Hydrogel fiber network characteristics were quantified using a Matlab algorithm with significant increases in fiber diameter, fiber length and porosity directly correlating with an increase in OEEM concentration. Data represent mean \pm s.e.m. for all parameters. P values by unpaired, two-tailed t-test.

To determine the viscoelastic properties of the OEEM hydrogel, we performed a rheological time sweep on varying ECM concentrations. An increase in ECM concentration from 4 to 8 mg/mL appeared to correlate with an elevated storage (G') and loss (G'') moduli (Figure 24i,j). However, there were no observable differences in turbidimetric gelation kinetics with a change in ECM concentration (Figure 24k). Gelation time varied based upon the test conditions. Specifically, direct conduction with the Peltier plate achieved complete gelation approximately 15 minutes prior to the samples heated via convection during gelation kinetics testing. However, once gelation initiated, hydrogels from both test formats consistently solidified within 20 minutes.

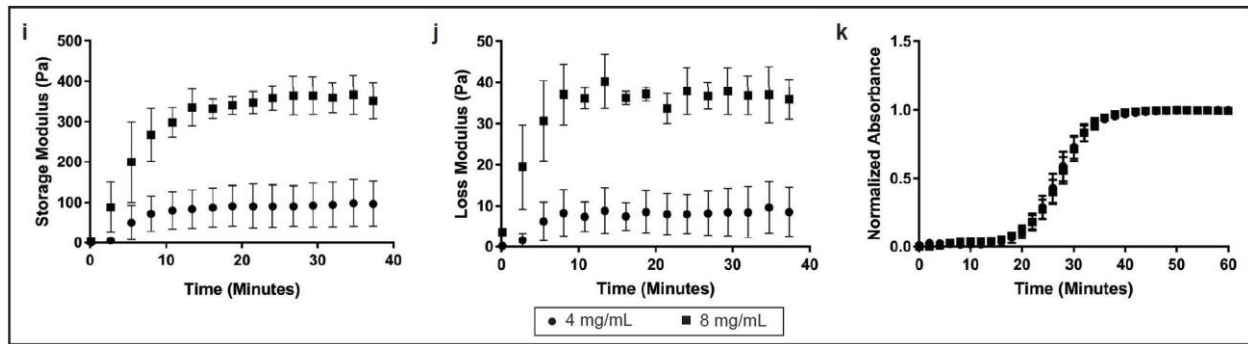


Figure 24 OECEM Hydrogel Viscoelastic Properties and Gelation Kinetics

Viscoelastic material properties were quantified using a rheological time sweep. i, Storage (G') and j, Loss (G'') moduli increased dramatically with the higher 8 mg/mL OECEM concentration. k, Turbidimetric gelation kinetics showed that gelation was conserved with a change in OECEM concentration.

4.4.4 In Vitro Applications

4.4.4.1 Whole Ovary Culture

Ovarian hydrogels were prepared in a sterile environment in a cell culture hood at three ECM concentrations: 2, 5 and 10 mg/mL. Pre-casted hydrogels were immersed in either Waymouth's MB 7521 or DMEM/F12 media then moved into the incubator at 37°C (95% air; 5% CO₂). Ovaries were microdissected from day 0 Sohlh1-mCherry (S1CF) newborn mice and placed in warmed 1X PBS. mCherry fluorescent protein was used to track primordial follicles indicated by the presence of Sohlh1⁺ cells in the nucleus and cytoplasm of oocytes. Extracted ovaries were trimmed to remove the outer membrane as well as any remaining tissues then transferred on top of the hydrogels at each concentration and returned to the incubator. Media was changed every 2-3 days and follicle development was assessed after 7 days in culture. Ovaries cultured in Waymouth's media were characterized after 7 days using several staining and imaging techniques. Ovaries were fixed in paraformaldehyde (PFA), serial-sectioned and stained. PAS staining was

used to validate follicle morphology and viability showing that ovaries cultured on top of the hydrogels maintained a normal structure and size at each concentration, however there was little growth evident. (Figure 25A) Primordial follicles appeared to dominate at 2 mg/mL ECM concentration and slightly decrease in number at 5 mg/mL concentration. This was verified quantitatively using confocal imaging of the whole ovary. A volumetric analysis was performed using Volocity software by measuring the fluorescence signal from *Sohlh1*+ cells indicating the presence of early oocytes. Volocity parameters were set to classify a minimum fluorescence intensity volume of $500 \mu\text{m}^3$ as a detectable viable oocyte for detection (+/- 10 micron threshold for oocyte diameter). No significant differences were observed between the total number of *Sohlh1*+ cells in the 2 mg/mL ovary culture compared to the wild-type mouse ovary extracted at day 7 suggesting that lower ECM concentration or stiffness represents similar culture conditions to in vivo follicle development. (Figure 25A) The decrease of detectable *Sohlh1*+ cells in the 5 mg/mL hydrogel culture may indicate that an increase in stiffness could drive follicle maturation. As a comparative study, a second experimental group of ovaries were cultured in Dulbecco's Modified Eagle Medium/F-12 Nutrient Mixture (DMEM/F-12) to determine how a change in culture conditions affected follicle growth. Immunohistochemistry (IHC) using a NOBOX oocyte-specific marker was used to qualitatively diagnose oocyte viability and follicle development. NOBOX is a homeobox gene that is present in oocytes from early to late stage follicles throughout development. IHC results from these experimental groups showed little to no oocyte growth across all hydrogel cultured ovaries (Figure 25B). NOBOX stain in the wild-type ovary was indicative of follicle growth with several primary follicles migrating towards the center of the ovary and multiple primordial follicles populated at the perimeter cortex.

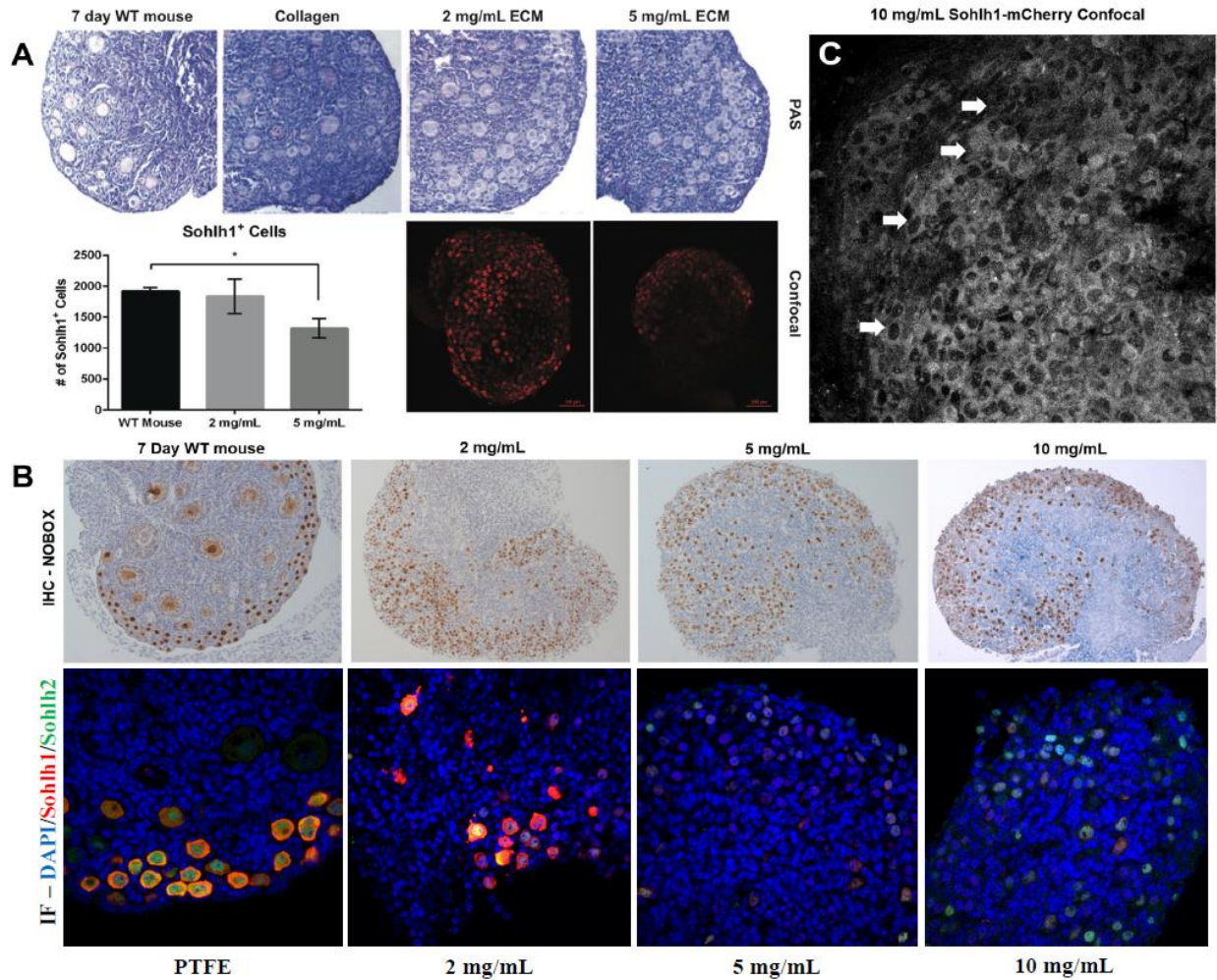


Figure 25 In Vitro Culture of Newborn Mouse Ovaries

Newborn mouse ovaries were cultured on top of ovarian hydrogels for 7 days. (A) Periodic acid Schiff (PAS) staining shows a comparison of ovarian tissue morphology at varying hydrogel ECM concentrations in comparison to normal WT mouse ovary extracted at day 7. Confocal imaging of Sohlh1+mCherry cells indicated by red fluorescence. Sohlh1+ cells were quantified using Volocity software. (B) Immunohistochemistry (IHC) and immunofluorescence (IF) staining show oocyte presence using three oocyte markers: NOBOX, Sohlh1, and Sohlh2. (C) 60X magnified B&W confocal image showing arrows indicating Sohlh1+ staining in the cytoplasm of the oocytes.

This data suggests that the ovarian hydrogels inhibit development, which contradicted the previous cultures immersed in Waymouth's media. Immunofluorescence (IF) imaging was performed using *Sohlh1* (spermatogenesis and oogenesis specific basic helix-loop-helix 1) and *Sohlh2* markers, which appear in early primordial follicles. Images taken at 60X magnification support the qualitative IHC data showing both *Sohlh1*⁺ (red) and *Sohlh2*⁺ (green) oocytes, which confirms the presence of early oocytes (Figure 25B).

4.4.4.2 In Vitro Follicle Maturation

One of the potential techniques for restoring fertility is the use of *in vitro* follicle maturation (IVM). Therefore, we hypothesized that OECM hydrogels would be a cytocompatible biomaterial that could support follicle maturation. To test this hypothesis, we developed methods to isolate, encapsulate and culture secondary mouse follicles using OECM hydrogels (Figure 26). This process was significantly improved over multiple trials by altering the material properties, follicle encapsulation methods and culture conditions. In the first trial, 2 mg/mL OECM hydrogels (100 μ L) were used to encapsulate a single or group (8) of mechanically isolated primary to secondary follicles. The ECM concentration was selected based upon the results from the whole ovary culture, which produced the several viable follicles within the ovary after 7-day culture. Once the follicle(s) were resuspended in the OECM hydrogel they were pipetted into a 96 well plate. 100 μ L of growth media was added to the top of the encapsulated follicles and they were cultured for 6 days. After 6 days, all the follicles in both the single and grouped samples had atypical morphology and showed minimal to no growth (Appendix Figure 25 and Appendix Figure 27). In addition, the OECM hydrogel appeared to be shriveled and degenerating.

We observed that the OECM hydrogels used in the whole ovary cultures led to poor outcomes from higher ECM concentrations, which we initially attributed to their corresponding

mechanical properties. However, the initial mechanical properties of the OECM hydrogels were not significantly different (Appendix Figure 21). This conclusion led us to test the cytocompatibility of the original OECM hydrogel with a non-ovarian cell type. We hypothesized that the initial protocol for ovarian decellularization did not clear residual detergents, which could lead to poor cell viability. To test this hypothesis, we cultured primary macrophages in the presence of our OECM hydrogel. After running several standard macrophage functional assays, we determined that the initial decellularization protocol did not sufficiently remove detergents and caused cytotoxic effects on macrophages. A revised ovarian decellularization protocol, with additional washes, was developed to remove residual detergents (Ovarian Tissue Decellularization). Upon repeating these macrophages assays, with the new OECM hydrogel, the results showed similar outcomes to other tissue-specific materials, such as porcine small intestine submucosa (SIS) and urinary bladder matrix (UBM) (Appendix Figure 5, Appendix Figure 6, Appendix Figure 7, Appendix Figure 8). In addition, an unintended byproduct of the revised decellularization protocol was a significant increase in the storage and loss modulus of the OECM hydrogel (Figure 24). This allowed us to better evaluate the effects of biomaterial stiffness on follicle cultures.

During the second trial of IVM, we implemented the newly refined OECM hydrogel at two ECM concentrations (4 and 8 mg/mL) as well as a 0.5% alginate as a control material. The OECM hydrogels and follicles were prepared similarly to the first trial, whereas the alginate was used in a droplet form, floating within the growth media (Appendix Figure 30). The results of this second trial showed that rather than degenerating, the follicles grew slightly within the OECM hydrogel groups with greater growth observed in the 4 mg/mL in comparison to the 8 mg/mL OECM group (Appendix Figure 31 and Appendix Figure 32). Interestingly, the 0.5% alginate group did not grow

after 6 days in culture. After repeating these experiments under the same conditions, we saw similar outcomes, with modest growth after six days of culture. However, mouse follicles generally experience exponential growth around 6 days, which was not observed in our second trial.

One of the main factors in follicle recruitment and growth is follicle stimulating hormone (FSH). Therefore, we hypothesized that using a human recombinant FSH (Gonal-F), which is a clinical-grade FSH used for human patients in the IVF clinics, would stimulate exponential growth of the follicles encapsulated in OECM hydrogels. In addition, we changed the follicle encapsulation method to a droplet form of OECM to improve the diffusion of nutrients into the follicle, which also mimics the alginate encapsulation (Appendix Figure 29). These changes were applied in the third trial of IVM, using an 8 mg/mL OECM hydrogel (n = 13 follicles), 8 mg/mL UBM hydrogel (n = 5) and 0.5% alginate hydrogel (n = 5) to encapsulate the follicles. After encapsulation, the follicle diameters were measured and averaged, with initial mean follicles diameters of the following: OECM = 104.14 μm ; UBM = 97.54 μm ; Alginate = 124.44. On day 8 of follicle culture, the mean diameters, showed little to no growth across all the groups; however, one of the follicles from the OECM group retained normal morphology and grew exponentially after day 6 of culture (Figure 27 and Figure 28). By day 10, this follicle surpassed 300 μm in diameter and retained excellent morphological integrity, which clearly demonstrated follicle support. Further, this follicle successfully resumed meiosis I and released a polar body, indicative of a meiotically-competent MII oocyte (Figure 29). A follow up study was conducted to test the fertilization potential for MII oocytes derived from OECM encapsulated follicles. A group of 97 follicles (127.72 mean starting diameter) were isolated from B6/D2 female mice and encapsulated within 8 mg/mL OECM hydrogels then cultured for 12 days. By day 12, 20 of the follicles reached antral stage (20.6%), but only 14 of the oocytes were able to be released for in vitro fertilization

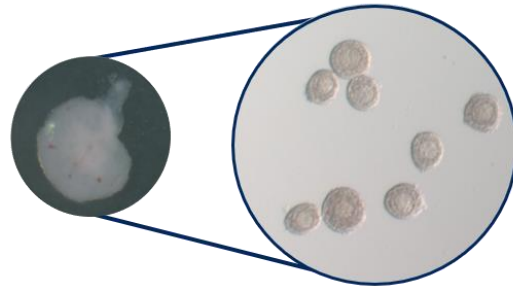
(IVF). Of the 14 oocytes undergoing IVF, only one was successfully fertilized and developed into a two-cell embryo (Figure 30). These results suggest that OECM hydrogels are a suitable substrate for *in vitro* follicle maturation. Although, further improvements in follicle isolation and encapsulation methods would be necessary to promote greater follicle maturation efficiency.

Excise ovaries

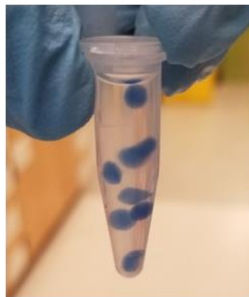


C57BL/6/J or B6D2
female mouse

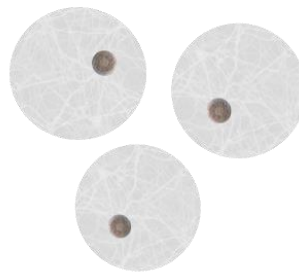
Mechanical isolation of secondary follicles (125-160 μm)



Encapsulate secondary follicles in OECM droplets



OECM Droplets



Encapsulated Follicles

Figure 26 Mechanical Follicle Isolation and Encapsulation in OECM Hydrogels

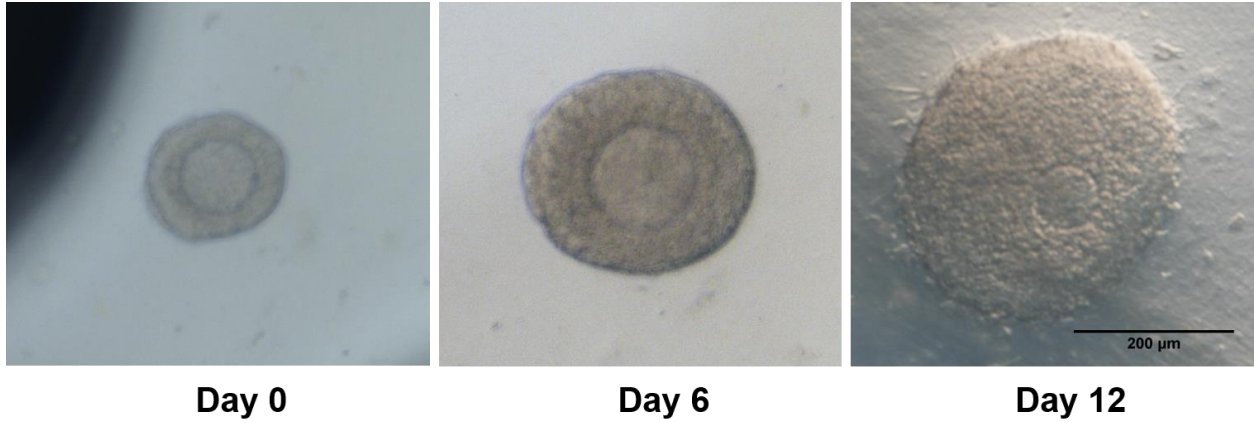


Figure 27 IVM OECM Follicle Morphology

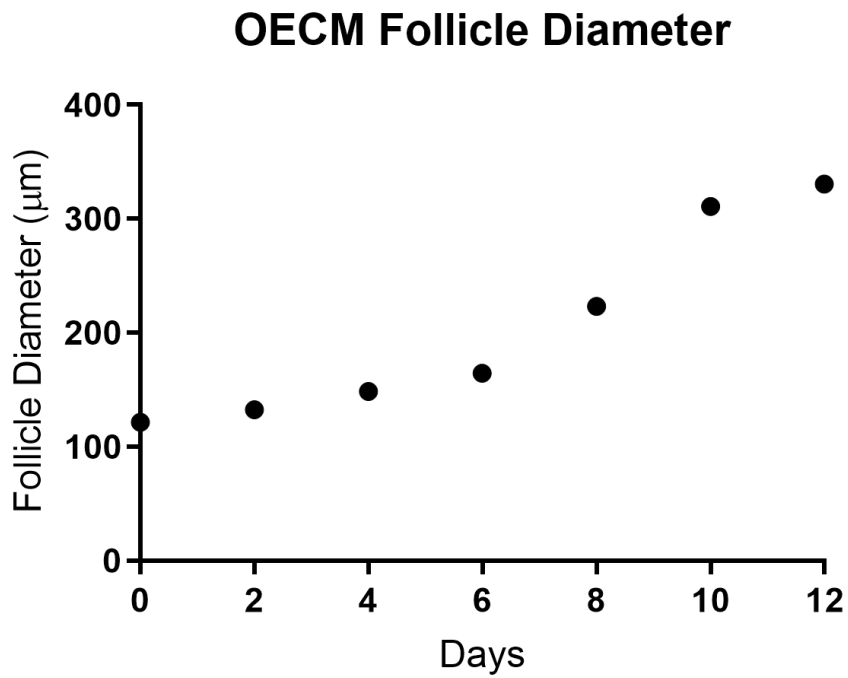


Figure 28 IVM OECM Follicle Diameter

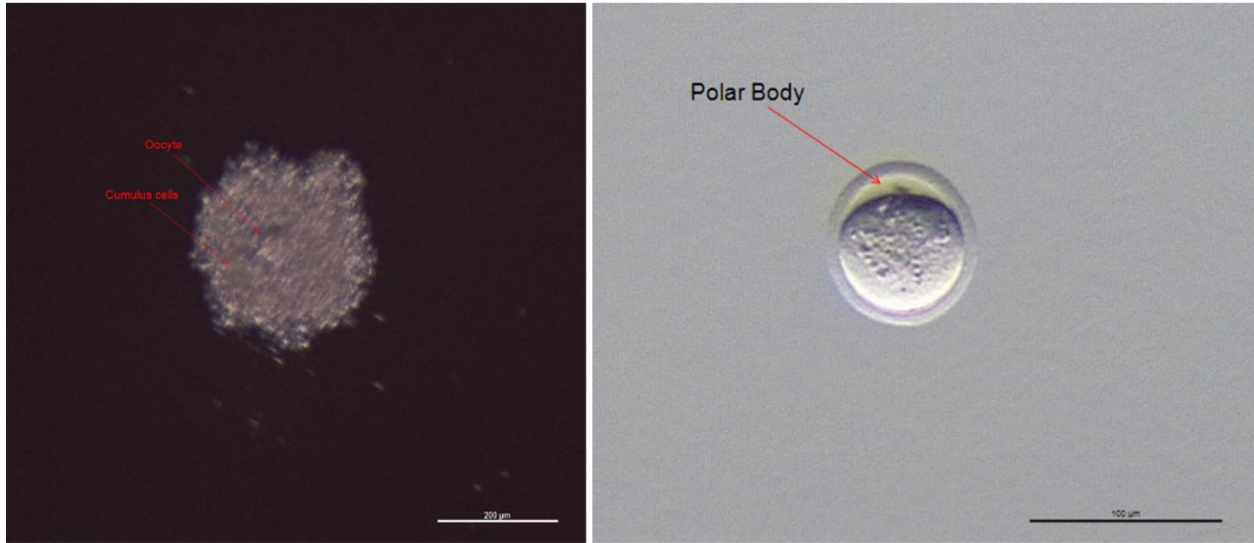


Figure 29 Cumulus Oocyte Complex (COC) and MII Oocyte



Day 2 post IVF

Figure 30 Two-cell Embryo Produced After IVF

4.5 Conclusion

In aim 1, we developed a decellularization method to obtain an acellular porcine ovarian scaffold. We demonstrated that a protocol combining physical agitation with a series of enzymes, detergent, acids and alcohols was an effective strategy to remove cells while preserving ovarian-specific components. Specifically, histological comparisons between native and decellularized ovarian tissues showed cellular ablation in decellularized samples with evidence of evacuated follicle structures. A quantitative decellularization assessment resulted in >98% reduction of dsDNA as well as a severe fragmentation of DNA. In addition, hydroxyproline and glycosaminoglycan content was not significantly different native samples. Ovarian-specific ECM proteins were also evaluated using immunohistochemical staining and clearly showed the presence of collagen I, collagen IV, laminin and fibronectin within decellularized samples. Additionally, decellularized tissues retained detectable levels of ovarian-specific hormones, such as anti-Müllerian hormone, progesterone and estradiol. Acellular ovarian-specific ECM scaffolds were enzymatically digested and successfully formed into hydrogels. SEM image analysis showed significant differences between 4 and 8 mg/mL OECM hydrogel concentration changes in hydrogel fiber network properties, including fiber diameter, length and porosity. Hydrogel viscoelastic properties were assessed and showed that increased ECM concentration can result in a direct increase of both the storage and loss modulus. However, gelation kinetics determined that there was no difference in the rate of turbidity between changing ECM hydrogel concentrations. Finally, OECM hydrogels were tested for compatibility for both whole newborn mouse ovary culture and in vitro follicle maturation (IVM). Newborn mouse ovaries cultured on top of 2mg/mL OECM hydrogels showed no significant difference in Sohlh1-positive oocytes in comparison to native tissues. Further, 8 mg/mL OECM hydrogel droplets were used to encapsulate pre-antral

follicles for IVM. This platform led to the maturation of meiotically-competent MII oocytes after 12 days of culture. In addition, in vitro fertilization of MII oocytes obtained from OECM hydrogel-mediated IVM resulted in a two-cell embryo.

5.0 Aim 2: Ovarian ECM Hydrogel-Facilitated Intraovarian Follicle Microinjection

5.1 Introduction

Ovarian follicles are the major functional component of the ovary that produce hormones (e.g., estrogen) and mature eggs for ovulation (13, 373). Chemotherapy or radiation treatments for cancer or other conditions can deplete the ovarian follicle pool, which can result in premature ovarian failure (POF), compromising ovarian hormone production and fecundity (162, 366, 367). Ovarian tissue cryopreservation is an experimental option used to preserve the fertility of patients who cannot afford to delay gonadotoxic treatment. Upon remission, the ovarian cortex, which is rich in primordial follicles, can be transplanted back into patient survivors and ovulate eggs to establish natural pregnancies or be stimulated to produce eggs for *in vitro* fertilization (IVF) (172-175, 219, 374-377). However, ovarian tissue transplantation remains an invasive surgical procedure and may not be appropriate in cases where there are concerns that ovarian tissues may harbor malignant cells (e.g., leukemia). To address these concerns, other experimental alternatives, such as *in vitro* follicle maturation (IVM) and artificial ovaries, use isolated immature follicles from the stroma to reduce the potential for co-transplantation of cancer cells. These methods have been used to achieve complete folliculogenesis and have led to live-births in mouse models of infertility, but several challenges must be addressed prior to their clinical translation for human patients.

A major obstacle for restoring reproductive function and fertility has been the inability to accurately mimic the dynamic environment of the human ovary. While our understanding of the spatiotemporal biochemical and mechanical signaling cues is improving, it remains poorly defined.

However, a potential solution may be to simply use the ovary as a transplantation site for isolated immature follicles. Intraovarian transplantation has successfully been used to generate live-births from infertile mice after the delivery of female germline stem cells (224-226). However, the existence and characterization of ovarian stem cells in the human adult ovary remains controversial (223, 378). Alternatively, intraovarian transplantation of isolated primordial follicles may have potential to replenish the ovarian reserve of cancer patients post-chemotherapy. A previous attempt to restore fertility after chemotherapy using this approach resulted in follicle apoptosis (379). However, we hypothesized that immature follicles may benefit from the additional support of a biomaterial to facilitate integration within the ovary to promote long-term survival and function.

One option to improve the effectiveness of intraovarian follicle transplantation, integration and survival could be the use of a tissue-specific extracellular matrix (ECM) hydrogel. ECM hydrogels have been used to treat a spectrum of diseases due to their intrinsic ability to promote tissue remodeling (359). To obtain ECM hydrogels, tissues must be first be decellularized to remove immunogenic components. This process can be used to preserve an ovarian-specific acellular scaffold, which is composed of a unique profile of ECM proteins, proteoglycans, glycoproteins and sequestered biomolecules (ie. growth factors) (380, 381). Recently, bovine ovaries were decellularized using sodium dodecyl sulfate (SDS) to obtain a tissue-specific scaffold, which was re-seeded with healthy follicles and transplanted to restore cycling in an ovariectomized mouse (218). Similarly, porcine and bovine ovaries were decellularized then processed into ECM composite “tissue papers”, demonstrating a versatile approach for short-term *in vitro* culture of nonhuman primate and human ovarian cortical strips (351). Another group has cited the use of SDS to decellularize human ovarian medulla and cortical tissues, but observed low follicle recovery rates upon recellularization and xenotransplantation after three weeks (382).

Although SDS is highly proficient at cellular ablation, acellular scaffolds prepared with SDS have led to adverse cytocompatibility, which has been directly linked to the disruption of matrix composition (330, 383-386). Therefore, we aimed to develop a new decellularization method using less abrasive detergents to obtain acellular scaffolds that can be processed into an ovarian-specific ECM (OECM) hydrogel to facilitate intraovarian follicle transplant.

5.2 Objectives

Here, we report a strategy to enhance intraovarian microinjection of isolated immature follicles using an OECM hydrogel. Porcine ovaries were decellularized then characterized to evaluate the effects on ovarian tissue-specificity. Solubilized acellular ovaries were formed into OECM hydrogels to facilitate the delivery of primordial follicles and establish an *in situ* ovary (ISO). Chemotherapy-induced POF (ciPOF) mice were prepared using busulfan and cyclophosphamide to observe the impact on follicle populations. Intraovarian microinjection of immature follicles resuspended in OECM hydrogels were performed using ciPOF mice to examine the efficacy of this approach for donor follicle survival and reproductive outcomes. Transplanted ciPOF female mice were bred to fertile males and produced donor follicle (GFP+)-derived progeny. In human patients, the OECM/follicle suspension could be injected non-invasively under the ovarian cortex using a transvaginal ultrasound-guided approach similar to how eggs are retrieved from the ovary for *in vitro* fertilization (IVF). Therefore, this approach may offer a minimally-invasive method to support and enhance the transplantation of immature follicles to restore reproductive function in female cancer patients.

5.3 Methods

5.3.1 Chemotherapy-Induced POF Model

Busulfan (Sigma) and cyclophosphamide (MP BioMedicals LLC) were combined to induce POF in 6-week old female mice (NCR nu/nu). Recipient mice were given a single intraperitoneal injection (IP) and allowed to recover up to 3 weeks prior to treatment. To initially identify the most appropriate chemotherapy regimen, four doses of busulfan/cyclophosphamide (mg/kg) were tested: (1) 12-100 (2) 12-200 (3) 24-100 (4) 24-200. Ovaries were excised, fixed in 4% paraformaldehyde (PFA), paraffin embedded and serial sectioned.

5.3.2 Weigert's Hematoxylin Picric Methyl Blue Staining

To evaluate the effects of chemotherapy on ovarian follicle populations, ovarian tissues were stained using Weigert's hematoxylin picric acid methyl blue. Tissues were deparaffinized to water and then placed in Weigert's Iron Hematoxylin for 10 minutes. Weigert's Iron Hematoxylin was prepared by making a 1:1 mixture of Solution A (1 gram of Hematoxylin in 95% ethanol in 100 mL) and Solution B (Ferric Chloride – 29% aqueous 4 mL; dH₂O 95 mL; HCl 1 mL). Slides were washed in running tap water for 2 minutes until a blue-purple color is visible. The tissues were counterstained with Picric Acid Methyl Blue (Picric acid saturated (aqueous) 250 mL; Methyl Blue 100 mg) for 6 minutes and washed three times in 95% ethanol for 3-5 minutes each. The stained tissues were dehydrate in a series of graded alcohols and xylenes then coverslipped using Permount. After staining, the tissues were imaged under an upright bright field microscope.

5.3.3 Ovarian Follicle Classification and Quantification

Ovarian tissue sections stained with Weigert's Hematoxylin Picric Methyl Blue were evaluated based on the reduction of follicle populations due to chemotherapy dosing. Every 10 sections were examined for total follicle number and classified by stage and quantified. The following criteria was used to count the follicles: (1) each follicle contains a visible oocyte (2) Primordial follicles have a single layer of squamous granulosa cells (3) Primary follicles have single layer of cuboidal granulosa cells (4) Secondary follicles contain two to four layers of granulosa cells without the development of an antrum (5) Antral follicles have greater than four layers of granulosa cells as well as definitive antrum. The total number of follicles were quantified then the sum was multiplied by 10 to provide an estimate of the entire follicle population of each ovary.

5.3.4 Enzymatic Follicle Isolation

Ovarian donor follicles were prepared using a physical and enzymatic isolation procedure adapted from Kim et al. (220). First, ovaries were excised from 6-14 day old female (DBA GFP/nu) mice and placed into pre-warmed L-15 (Leibovitz's) medium. The ovaries were freed from the bursa using a pair of forceps and an insulin needle. Ovaries were then minced using insulin needles into small fragments to aid in digestion. The ovarian fragments were then added to 1.5 mL microcentrifuge tube containing 500 μ L of pre-warmed L-15 medium and 50 μ L of Liberase TM (13 Wünsch units/mL). The tubes were then placed on an orbital shaker and agitated at 200 rpm for 5 minutes at 37°C. After incubation, the mixture was then pipetted gently for one minute to help free the ovarian follicles from connective tissue. This process was repeated once more until

the ovaries had been completely dissociated. After digestion, 10% fetal bovine serum was added to the mixture to halt enzyme activity. The tubes were placed in an upright position for 15 minutes at 37°C to allow follicles to sediment. After 15 minutes, 200 µL of the mixture was carefully pipetted off the top to remove singular ovarian cells. The samples were centrifuged at 100g for 5 minutes to loosely concentrate the follicles. A syringe needle was used to gently remove the medium from the tube without disturbing the follicle pellet. Finally, the pellet was resuspended in a chilled 4 mg/mL OECM pre-gel and kept on ice in preparation for follicle microinjection.

5.3.5 Ovarian Tissue Decellularization

Porcine ovaries from adolescent pigs (< 1 year old) were obtained from the local abattoir (*Thoma Meat Market, Saxonburg, PA*) and immediately stored on ice and frozen at -20°C. Ovaries were thawed, cleared of surrounding connective and adipose tissues, diced into cubes (~0.125 cm³) and transferred to a flask containing cold Milli-Q water (MQ). The diced tissues were shaken manually with MQ until residual blood was visibly removed then replaced with fresh MQ and stored overnight at 4°C. The tissues were then rinsed in fresh MQ on an orbital shaker for 30 minutes at 300 rpm. The flask containing tissue was then replaced with a pre-warmed solution of 0.02% trypsin and 0.05% EDTA then agitated on a magnetic stir plate for one hour at 37°C. Ovaries were then rinsed three times with MQ for 15 minutes each at 300 rpm. A 3% solution of Triton X-100 was then added to the flask and shaken for one hour at 300 rpm. A subsequent wash cycle was implemented to remove any residual detergents from the tissues. Each wash cycle consisted of several distilled water rinses with manual shaking (until no bubbles were observed), then alternating washes of MQ and 1X PBS to neutralize and release detergent that was bound to the tissues. After the wash cycle was completed, the fluid was replaced with fresh MQ and stored

overnight at 4°C. A 4% sodium deoxycholate solution was added to the flask and agitated for 1 hour at 300 rpm. A subsequent wash cycle was performed then the tissue was replaced with fresh MQ and stored overnight at 4°C. The ovarian tissues were then depyrogenated and disinfected with a 0.1% peracetic acid and 4% ethanol solution for two hours at 300 rpm. This step was followed by three rinses in MQ, 1X PBS, MQ for 15 minutes each at 300 rpm then stored in fresh MQ at 4°C overnight. To ensure adequate removal of detergents and other chemical reagents one final series of washes with MQ, 1X PBS, MQ were performed for 15 minutes each at 300 rpm. The decellularized tissues were then stored at -80°C prior to lyophilization.

5.3.6 Ovarian ECM Digestion and Hydrogel Formation

Lyophilized ovarian ECM powder was solubilized via enzymatic digestion. A stock ECM digest concentration of 10 mg/mL was prepared by adding 200 mg of ECM powder to a 20 mL solution of pepsin (Sigma P7012) at a concentration of 1 mg/mL ($\geq 2,500$ units/mg) dissolved in 0.01 N hydrochloric acid (HCl). Digestion was facilitated with an overhead mixer between 700-2000 RPM for less than 48 hours. Hydrogels were formed after neutralizing and buffering the solubilized ovarian ECM to physiological conditions. Two hydrogel concentrations (4 and 8 mg/mL) were prepared for testing and experimentation. A pre-gel solution was made on ice using the following components: (i) 10 mg/mL OEMC digest stock (volume determined by desired final concentration) (ii) 0.1 N NaOH (1/10th the volume of the digest), (iii) 10X PBS (1/9th the volume of the digest), and (iv) 1X PBS or L-15 medium (brought up to final volume). The solution was pulsed 3 times on a vortexer to mix then stored at 4°C until further use.

5.3.7 Fluorescent-Labeling of Ovarian ECM Hydrogels

A fluorescently-tagged TRITC-labeled ovarian ECM hydrogel was prepared to track the gel post-injection and determine whether the gel localized within the site of injection (Appendix Figure 35). To prepare the labeled gel, 40 μ L tetramethylrhodamine isothiocyanate (TRITC) stock solution was added to 160 μ L of dimethylformamide (DMF) and vortexed to solubilize the TRITC. The TRITC solution was added to 5 mL of 10 mg/mL ovarian digest within a 25 mL flask. The pH was adjusted to 10 through the addition of 0.1 N NaOH, approximately 4.8 mL. The TRITC and OECM were mixed on a magnetic stir plate overnight at 4°C to allow TRITC conjugation to the free amines within the OECM digest. The pH was then re-adjusted to 2 to halt the reaction. The TRITC-OECM hydrogel was dialyzed for one week to remove unbound TRITC from the OECM digest. TRITC-OECM was then frozen and lyophilized for long-term storage. Lyophilized TRITC-OECM was resuspended in water and evaluated at various dilutions. To prepare a TRITC-labeled gel, 1:20 of the total hydrogel volume was replaced with the TRITC-OECM stock, which provided a strong signal under a TRITC fluorescent filter to track the OECM hydrogel.

5.3.8 In Vivo Follicle Microinjection

The experimental design and rationale for animal use (described in IACUC Protocol #: 18103002) were reviewed and approved by the University of Pittsburgh Institutional Animal Care and Use Committee (IACUC). Eight-week old ciPOF female mice (NCR nu/nu) mice were anesthetized and placed on the operating table with their back exposed. A single midline dorsal incision (0.5 cm) was made using small scissors. Subcutaneous connective tissue was then freed from the underlying muscle on each side using blunt forceps. Once the ovary was located under

the thin muscle layer, a small incision (<1 cm) was made to gain entry to the peritoneal cavity. The edge of the incision was held with tooth forceps, while the ovarian fat pad was removed to expose the ovary and surrounding bursa. A small volume (<10 μ L) of chilled follicle-OECM pre-gel was transferred to a glass needle (filament Cat#: FB245B and borosilicate glass micro pipette Cat#: B100-75-10) then secured to a pressurized microinjection system. Eppendorf microinjection system (TransferMan NK2 and FemtoJet) was used for follicle delivery and surgical manipulation observed under a Nikon SMZ stereomicroscope. The loaded needle was positioned perpendicular to the ovary and guided into the ovarian cortex, where the follicle-OECM mixture was slowly injected at a constant pressure ranging from 50-250 hPa. For each injection, approximately 1.0×10^3 follicles were transplanted. The same surgical and injection procedures were performed contralaterally. The follicle-injected ovaries were placed back into the abdominal cavity, the muscle layers were sutured, and the skin incision was stapled.

5.3.9 Mating Study

Two weeks after injection both the follicle recipient and non-injected control ciPOF nude female mice were bred to male nude mice (NCR nu/nu, Taconic). The breeding was conducted for three cycles, which concluded at 106 days on average. Pups born were fostered within 1 day with NCR nu/+ (Taconic) females due to the lack of developed mammary glands in the nude mouse strain used for recipients, then they were weaned at 3-4 weeks old. Pups (DBA-GFP/nu-, Orwig Lab) inherited from the follicle injected recipients were selected based on physical traits consisting of fur, dark eyes or GFP expression. Genotyping was performed using mouse tail DNA and standard PCR with the following primers: GFP forward primer sequence (GAA CGG CAT CAA GGT GAA CT); GFP reverse primer sequence (TGC TCA GGT AGT GGT TGT CG); β -actin

forward primer sequence (CGG TTC CGA TGC CCT GAG GCT CTT); β -actin reverse primer sequence (CGT CAC ACT TCA TGA TGG AAT TGA) (primers prepared by Integrated DNA Technologies, inc.). PCR products were run on a 2.5% agarose gel and imaged under UV light. The resulting pups were grown to 8 weeks and bred for fertility status. Second generation breeding pairs consisted of a GFP/nu- experimental female and DBA/2 control male (Jackson), a GFP/nu- experimental female and GFP/nu- experimental male, and a DBA/2 control female and GFP/nu- experimental male. Breeding pairs were separated after two weeks.

5.3.10 Immunofluorescence Staining and Imaging of Microinjected Ovaries

Ovaries were excised at the conclusion of the third breeding cycle and fixed in 4% PFA overnight then embedded in paraffin. Tissues were serial sectioned and stained with DAPI and α -GFP antibody to evaluate the presence of endogenous and transplanted (GFP+) cells/follicles. Sectioned tissues were deparaffinized and placed in citric acid buffer (2.1g/L citric acid; 500 μ L of Tween 20; 1L of dH₂O at pH: 6.0) at 100°C for 20 minutes and then on ice for an additional 20 minutes. The slides were removed and washed twice in dH₂O for two minutes each the twice in 1X PBS for 2 minutes each. The tissue sections were then placed in a solution of copper sulfate (10 mM) and ammonium acetate (50 mM) in 1 L of dH₂O for 20 minutes in a water bath at 37°C. Following this step, the tissues were washed twice in 1X TBST (tris-buffered saline and 0.1% Tween 20) for 3 minutes each and repeated using 1X PBS for two washes of 2 minutes each. The tissue sections were circles with a PAP pen and then covered with blocking buffer (5% Donkey Serum; 2% BSA; 0.1% Tween 20; 0.1% Triton X-100; 1X PBS) for 2 hours at room temperature, followed by the addition of primary antibodies diluted in the same blocking buffer and allowed to incubate overnight at 4°C in a humidified chamber. The primary antibodies were removed and

tissues were washed five times in 1X PBS for 2 minutes each. Fluorescently-tagged secondary antibodies (diluted in blocking buffer) were added to the tissues and incubated for 30 minutes at room temperature protected from light. The tissues were washed five times in 1X PBS for 2 minutes, mounted in FluoroGel plus DAPI and coverslipped prior to imaging. Four ovaries were evaluated per treatment group. Nikon Eclipse Ti-U inverted microscope and NIS Elements software was used to capture representative images of GFP-positive structures within each tissue section. DAPI and FITC channels were taken separately and merged to demonstrate the population of endogenous and GFP expressing cells, respectively.

5.3.11 Ovarian Single-Cell Isolation, Antibody Staining, and Flow Cytometry

To characterize the cellular populations over time, whole ovaries were excised and placed in chilled L-15 medium. Insulin syringes were used to free the ovaries from the bursa. Ovaries were transferred into 500 μ L of warmed 1X Hank's Balanced Salt Solution (HBSS) where they were minced and placed into a 2 mL screw top tube. 50 μ L of Liberase TM (13 Wünsch Units/mL) (Roche) was added to the tube and the minced ovaries were incubated in a water bath set to 37°C for 15 minutes. After incubation, 950 μ L of FACS buffer was added to each tube to stop the enzymatic reaction and the tubes were then placed in a bead homogenizer then agitated for 30 seconds at 2.10 m/s. Samples were filtered through a 100 μ m cell strainer to prepare a single cell suspension and then cells were washed in 1X HBSS then pelleted in a centrifuge at 350 x g for 5 minutes at 4°C. Cells were resuspended in 1 mL of 1X HBSS and 1 μ L of BD Horizon Fixable Viability Stain 780 was added to cells and positive ArC Amine Compensation beads. Viability dye was incubated for 30 minutes at 4°C. Cells were washed twice with 2 mL of FACS buffer and supernatant was decanted. 2 μ L of α -CD16/32 (Fc Block – Biolegend 101302) was added to each

sample and incubated for 10 minutes at room temperature. 1 mL of FACS buffer was added to each sample and spun down at 4°C. Supernatant was decanted from each sample and 2 µL of each extracellular antibody (Zp3, CD45, CD68, CD206, CD86) was added to the cells and allowed to incubate for 20 minutes at 4°C. AbC total antibody compensation tubes (Invitrogen) were stained with 1 µL of each corresponding antibody. Cells were washed twice with 2 mL of FACS buffer and supernatant decanted. Sample pellets were vortexed briefly to disrupt the cells, which were then fixed in 1 mL of 5% neutral buffered formalin and incubated for 40-60 minutes at 4°C protected from light. Cells were then permeabilized using 2 mL of 1X Permeabilization buffer (eBioscience) and spun at 400-600 x g for 5 minutes at 4°C. The supernatant was discarded and then permeabilization was repeated. The cell pellet was then resuspended in the residual volume (~100 µL after decanting) of 1X Permeabilization buffer. Without additional washes, 2 µL of intracellular markers (NOBOX, GFP, ki67, Caspase3) were added to the cells and incubated overnight at 4°C. For compensation, 1 µL of each intracellular antibody was added to AbC total compensation beads. After overnight incubation, 2 mL of 1X Permeabilization buffer was added to each tube and samples were centrifuged at 400-600 x g for 5 minutes at room temperature, supernatant discarded and wash repeated. Stained cells were resuspended in 200 µL and compensation beads in 500 µL of FACS buffer then analyzed by flow cytometry. First, we gated on non-debris (forward side scatter area vs side scatter area) and then on single cells (forward scatter area vs height plots) (Appendix Figure 39). From the population of single cells, we gated on total viable cells (viability dye). Out of the viable cells, we could then select the population of apoptotic (Caspase3) and proliferative (ki67) cells. From viable cells, we could also gate on CD45+ (immune cells) and CD45- (non-immune) cells. The CD45+ cell population would allow us to examine the population of resident macrophages (CD68) and macrophage phenotypes (CD86

and CD206). The CD45- cell population would allow us to quantify oocyte-expressing cells (Zp3 and NOBOX). In addition, cells expressing GFP would indicate cells that were donated from transgenic mice for follicle microinjection.

5.3.12 Statistical Analysis

All data were expressed as mean \pm s.e.m and plotted using GraphPad Prism 7.02. In order to detect differences in follicle populations after chemotherapy, the individual means were compared using an unpaired, two-tailed, t-test. Exact P-values resulting from the statistical analysis are presented within each figure.

5.4 Results and Discussion

5.4.1 Alkylating Agents Significantly Reduce Endogenous Follicle Population

After developing and characterizing the OECM hydrogel as a carrier for follicle injection, we created a clinically relevant ciPOF mouse model. We chose to induce POF using alkylating agents, busulfan and cyclophosphamide, due to their known cytotoxic effects on ovarian tissues and cells (162, 367, 387, 388). Briefly, a single intraperitoneal (IP) injection was given to 6-week old nude female mice. Dosing was titrated to determine an appropriate treatment that would significantly reduce the endogenous follicle pool to lower or eliminate the chances of fertility. The following doses were tested, abbreviated as busulfan-cyclophosphamide (mg/kg): (1) 12-100 (2) 12-200 (3) 24-100 (4) 24-200.

At three weeks post-IP injection, histological staining with Weigert's Hematoxylin-Picric Methyl Blue clearly illustrated the damaging effects of each chemotherapy regimen on the follicle population within the ovaries (Figure 31a-e). Dose dependent effects were observed with elevated levels of busulfan and cyclophosphamide reducing the follicle numbers (Figure 32a). Follicles were counted based upon developmental stage (Appendix Table 5 and Appendix Figure 33). Primordial and primary follicles were significantly reduced after exposure to all treatments in comparison to non-treated control mice (Figure 32b and Appendix Table 6). The outcomes of chemotherapy titration suggested that a range of doses could impair fertility outcomes or lead to ovarian insufficiency. Therefore, we determined that it was important to evaluate the efficacy of hydrogel-assisted follicle microinjection using female mice treated across each dosage of chemotherapy. We selected the 12-100, 12-200 and 24-100 doses of busulfan-cyclophosphamide to prepare our ciPOF mice for follicle transplantation because these doses caused significant follicle loss and the animals retained good overall health. Although the 24-200 treatment resulted in the greatest follicle reduction, we excluded this group from follicle transplantation due to the poor health of the mice post-chemotherapy.

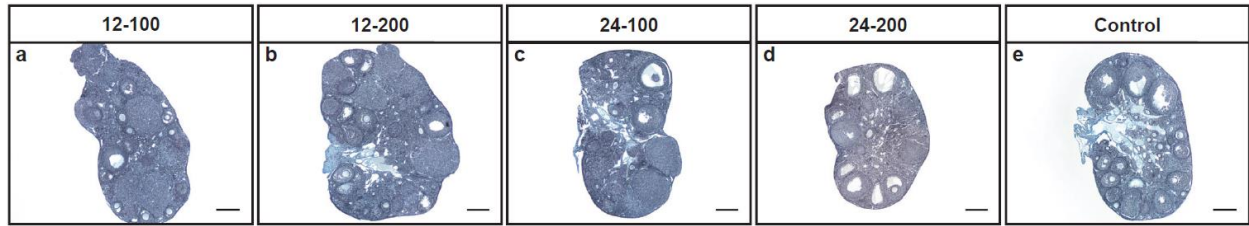


Figure 31 Effects of Chemotherapy Dosing on Ovarian Tissues

Four doses of busulfan-cyclophosphamide **a**, 12-100 mg/kg **b**, 12-200 mg/kg **c**, 24-100 mg/kg **d**, 24-200 mg/kg **e**, non-injected (control) were administered via single IP injection. Ovaries were excised at 3 weeks post treatment and stained using Weigert's Hematoxylin Picric Acid Methyl Blue. Scale, 250 μ m.

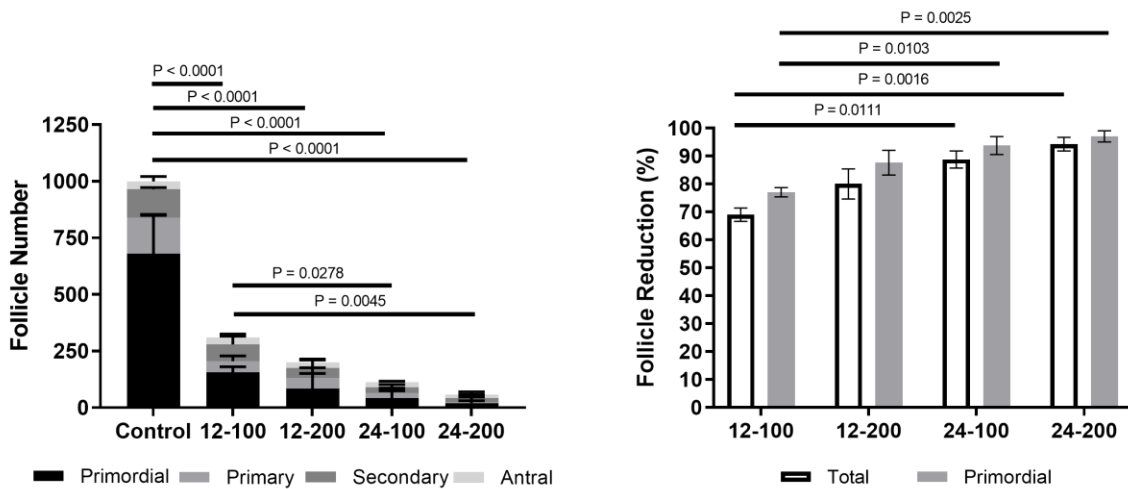


Figure 32 Endogenous Follicle Populations Post-Chemotherapy

a, Follicles were manually counted, quantified and classified by developmental stage showing a steady decline of the total follicle number with increasing dose. Additionally, busulfan appeared to have an enhanced effect on follicle depletion in comparison to cyclophosphamide. **b**, Significant reduction of primordial follicles across all doses indicated a severe depletion of the ovarian reserve, decreasing potential fertility.

5.4.2 Enzymatic Follicle Isolation and Microinjection Provides an Efficient Transplant

Procedure

Follicle incubation time from isolation to transplant is a concern for cell therapy applications as it can directly impact viability (389). Therefore, we adapted an existing enzymatic isolation protocol (220) to reduce the time needed to obtain a large pool of immature follicles for transplant. To enable identification of transplanted versus endogenous follicles, we isolated follicles from transgenic mice exhibiting ubiquitous GFP under the chicken β -actin (CAG) promoter. We tested enzyme concentrations of 10% and 20% for both Liberase TM and DH (13 Wünsch units/mL) to determine their effects on follicle disaggregation and quality. Briefly, Liberase TM or DH was added to the minced ovaries then two five-minute cycles of physical agitation at 37°C were performed with a minute of pipetting after each cycle. After assessing each sample, we determined that the best formulation was the 10% Liberase TM, which released a large population of morphologically normal GFP follicles during the 12-minute isolation procedure (Figure 33). In order to estimate the number of follicles isolated with this procedure, follicles were manually counted using a hemocytometer. There were approximately 1.5×10^3 total follicles isolated per ovary with 74.4% of this population identified at the primordial stage.

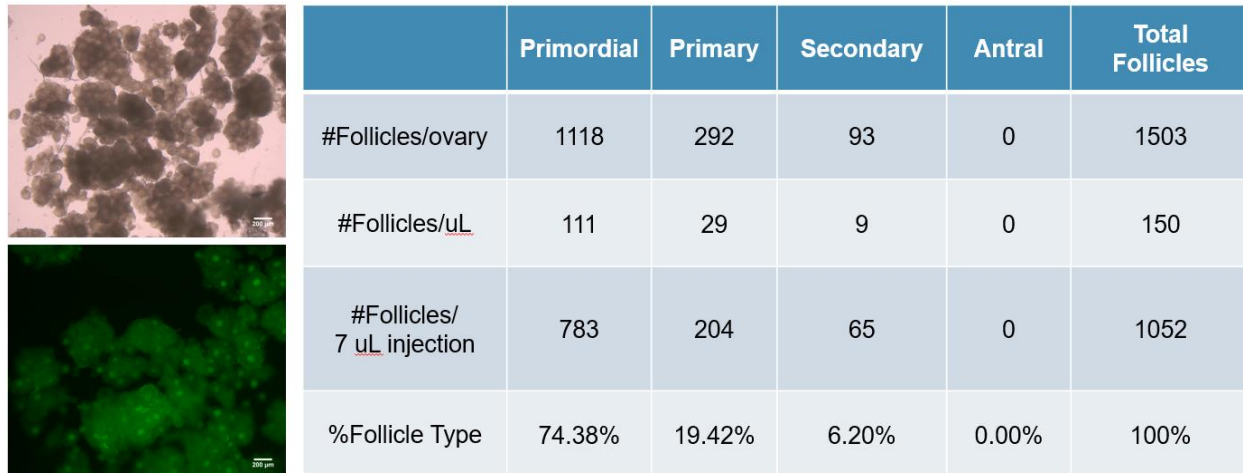


Figure 33 Follicle Isolation and Quantification

Intact GFP follicles were enzymatically isolated using Liberase TM and imaged under bright field (top) and fluorescence (bottom). Scale, 500 μ m. Isolated follicles were quantified using a hemocytometer demonstrating a predominantly primordial follicle population with approximately 1.0×10^3 follicles per intraovarian injection.

Once we showed that it was feasible to efficiently obtain follicles, we wanted to test the efficacy of using microinjection to transplant follicles into the ovarian cortex of ciPOF mice. Immature follicles naturally reside within the ovarian cortex, as this region of the ovary has mechanically distinct properties that support maintenance of immature follicles (76, 390). Therefore, we wanted to precisely dispense follicles into or near the cortex. Previously, intragonadal cell delivery has been shown successfully using microinjection (224-226). So, we decided to implement this technique to facilitate intraovarian follicle transplant to establish an ISO. First, we tested the delivery of the OECM hydrogel alone via microinjection. A small volume of hydrogel was injected into the ovarian cortex, and the recipient animal was sacrificed to visualize the injection site (Figure 34i top). Bright field images clearly illustrated Trypan blue dye at the site of injection at the tissue surface (Figure 34i bottom). Furthermore, the use of a TRITC-labeled OECM hydrogel allowed us to identify the hydrogel at the ovarian surface post-injection (Figure

34j). These results confirmed this method as a suitable delivery mechanism for the viscous OECM within a specific anatomical location of the ovary. Finally, we performed the same experiment with the addition of isolated GFP follicles to determine if the gel and follicles could be delivered simultaneously, resulting in the formation of an ISO. Ovaries excised from the TRITC-OECM hydrogel and GFP follicle microinjection clearly indicated a co-localization of the OECM and follicles within the ovarian cortex (Figure 34k).

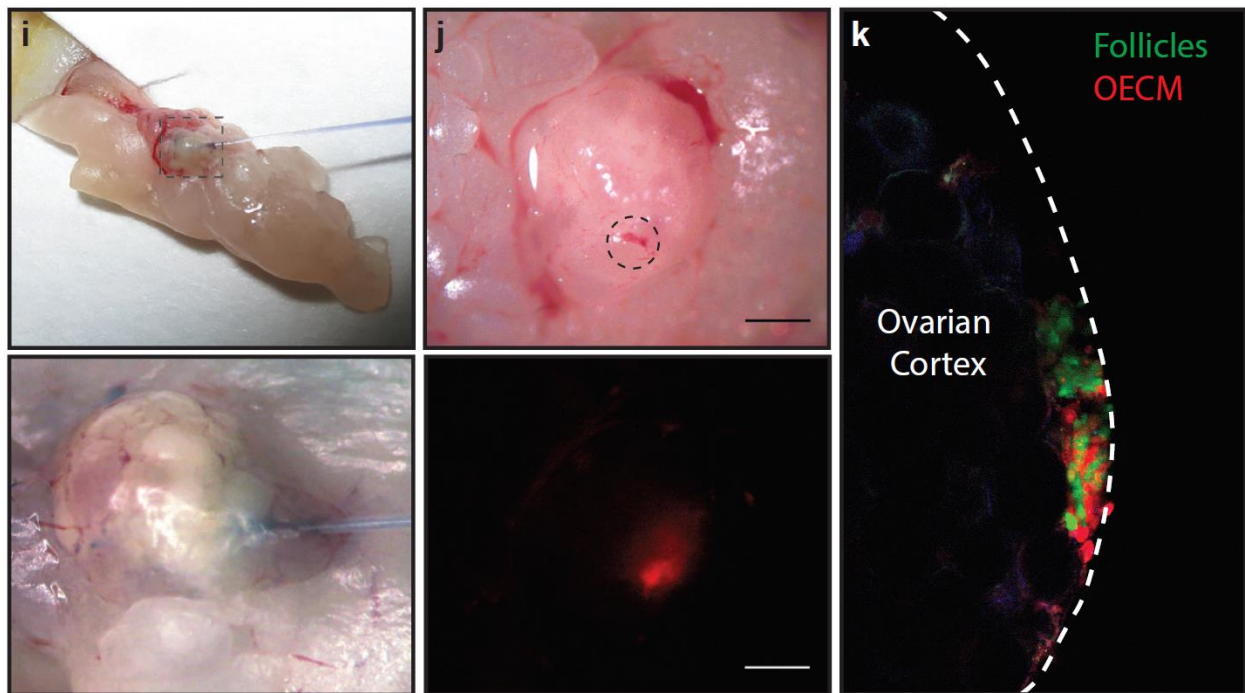


Figure 34 Intraovarian Follicle Microinjection

i, Brightfield images show the gross morphology of the ovary during microinjection (top) and magnified to show the injection site for follicle transplant (bottom). j, Pressurized microinjection was tested as a potential technique to deliver the OECM hydrogel (TRITC-labeled) and visualized under bright field (top) and fluorescence (bottom).

Scale, 500 μm . k, Multiphoton images confirmed that intraovarian follicle microinjection of the isolated GFP follicles (green) and OECM (red) co-localized within the ovarian cortex to form an in situ ovary. The dotted line

(white) indicates the outer surface of the ovarian epithelium.

5.4.3 Microinjected Follicles Give Rise to Multiple Generations of GFP Pups

We used our ciPOF mice to investigate the therapeutic potential of an ISO to support follicle survival after intraovarian microinjection. Approximately 1.0×10^3 GFP⁺ follicles resuspended in 7 μ L of OECM hydrogel were microinjected into the ovarian cortex of ciPOF nude female mice: 12-100 (n = 2), 12-200 (n = 2) and 24-100 (n = 2). Non-injected ciPOF nude female mice were used as controls: 12-100 (n = 3), 12-200 (n = 2) and 24-100 (n = 2). To reduce tissue damage due to needle puncture, only a single follicle injection was performed on each ovary. Freshly isolated GFP follicles from 6-14 day female (DBA-GFP/nu-) mice were used to ensure a predominantly immature follicle population at the time of injection.

To determine the effects of follicle microinjection on fertility, follicle recipient and non-injected control ciPOF nude female mice were mated with nude male mice for three breeding cycles (~100 days). The breeding strategy was designed to definitively distinguish between pups derived from transplanted or endogenous follicles (Appendix Table 7). Pups from endogenous follicles would be nude, lacking fur, whereas pups from transplanted GFP follicles would have fur with a 50% chance of glowing green (GFP/nu-). After three breeding cycles, ciPOF follicle transplant recipients produced a total of three GFP⁺/nu- pups within three separate litters (Appendix Table 8). The first breeding cycle yielded one GFP pup (GFP/nu-001) out of three healthy offspring followed by a single GFP pup (GFP/nu-002) with no littermates during the second cycle (Figure 35a,b). As a note, when litters were small, the pups were fostered into nude litters (as shown by the additional nude pups in Figure 35b). Each of the first two GFP pups were born from the same ciPOF mouse treated with a dose of 24-100 mg/kg. This observation demonstrates that intraovarian follicle transplant has the potential to lead to multiple births from a

single injection. During the third and final breeding cycle, one GFP pup (GFP/nu-003) was born out of five healthy offspring from a ciPOF mouse in the 12-100 mg/kg group (Figure 35c). This result suggests that transplanted follicles are viable for at least 90 days post-injection. Overall, eight litters and a total of 35 pups were born from ciPOF mice that received a follicle transplant (n = 6). In comparison, seven litters with a total of 36 pups were born from non-injected ciPOF control mice (n = 7). A follow-up mating study was performed to test the reproductive health of the GFP pups generated from follicle transplantation. The GFP offspring resulting from follicle transplant (DBA-GFP^{+/nu-}) were bred with DBA wild-type (GFP^{-/nu+}) (Appendix Table 9) and inbred with each mating pair (Appendix Table 10) producing multiple large litters of hemizygous (GFP^{+/-}) and homozygous (GFP^{+/+}) genetic backgrounds (Figure 35d,e and Appendix Table 11). In each of the litters, GFP expression was clearly observed in the presence of a UV lamp and confirmed with genotyping (Figure 36).

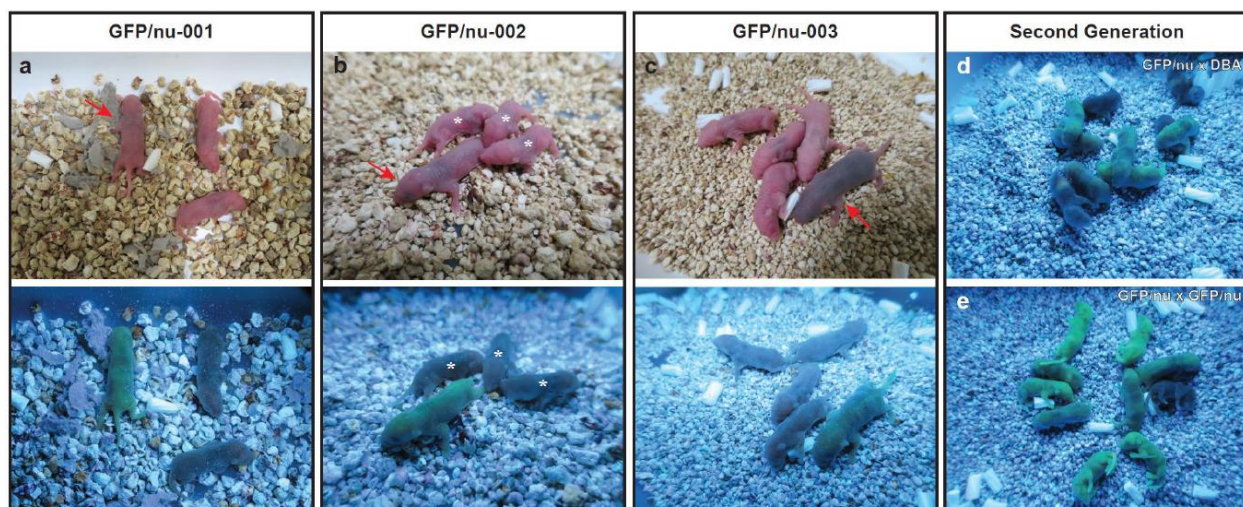


Figure 35 Microinjected Follicles Give Rise to Multiple GFP Litters

The efficacy of intraovarian follicle transplant for fertility preservation was tested by injecting a pool of isolated GFP follicles within an OECM hydrogel into a ciPOF nude female mice. The follicle recipient mice were then mated to male mice of the same genetic background (nu/nu) to distinguish between progeny derived from exogenous (GFP+) or endogenous (GFP-) follicles. a-b, Two GFP pups (GFP/nu-001 and GFP/nu-002) were born in consecutive litters from the same mother (24-100 mg/kg dose) as a direct result of the follicle transplantation. c, Another GFP pup (GFP/nu-003) was derived from a ciPOF female mouse (12-100 mg/kg dose) during the third mating cycle (>100 days post-transplant). This demonstrates that an ISO can support injected follicles in a dose-independent manner and have long-term viability post-injection. Multiple litters of second generation pups were derived from both d, outbred (GFP/nu x DBA) and e, inbred (GFP/nu x GFP/nu) mice, which indicates that intraovarian follicle transplantation did not disrupt reproductive development.

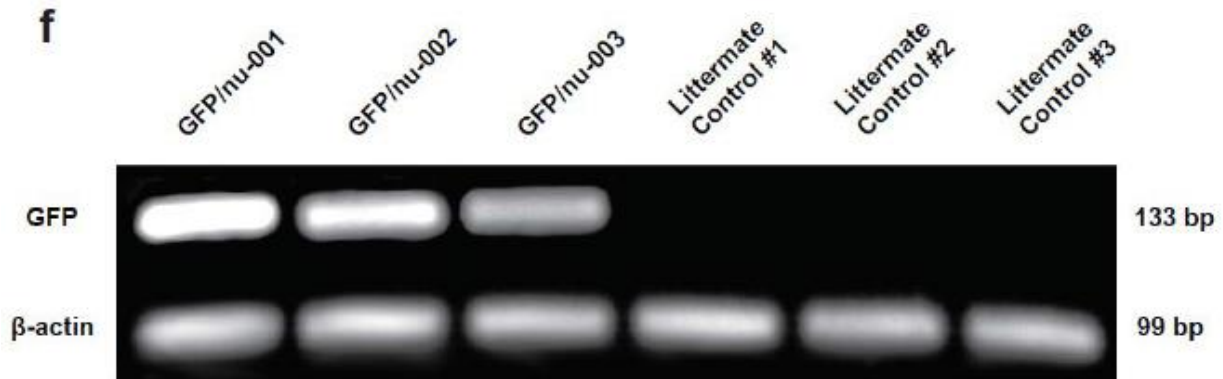


Figure 36 Genotyping of GFP Pups and Littermates

Genotyping of the GFP pups and littermate controls was confirmed using standard PCR and gel electrophoresis. GFP bands only appeared within the GFP mouse samples and none within the littermate samples. β -actin was used as an internal control appearing in each of the samples tested. Gels were cropped and processed to highlight the bands of interest.

5.4.4 Intraovarian Microinjection Supports Follicle Longevity Post-Transplant

Finally, we wanted to determine the effects of this therapy on follicle longevity post-transplant. To answer this question, we performed immunofluorescent labeling of ovaries excised from ciPOF nude female mice after three breeding cycles (~100 days). Comprehensive imaging demonstrated significant GFP expression throughout the transplanted tissues and suggests that multiple follicles remained viable post-transplantation (Figure 37a). Transplanted ovaries also retained growing endogenous follicles (Figure 37b). Non-injected control tissues lacked GFP expression and endogenous follicles appeared to be reduced in comparison to ovaries from transplanted mice (Appendix Figure 36). However, we could not confirm any definitive differences between residual endogenous follicles based solely upon the immunofluorescence

images. Finally, we were able to identify follicles at various stages of development including primordial (Figure 37c), secondary (Figure 37d), antral (Figure 37e), and corpus luteum (Figure 37f), which indicates that the ISO is compatible with engraftment and long-term development of transplanted follicles.

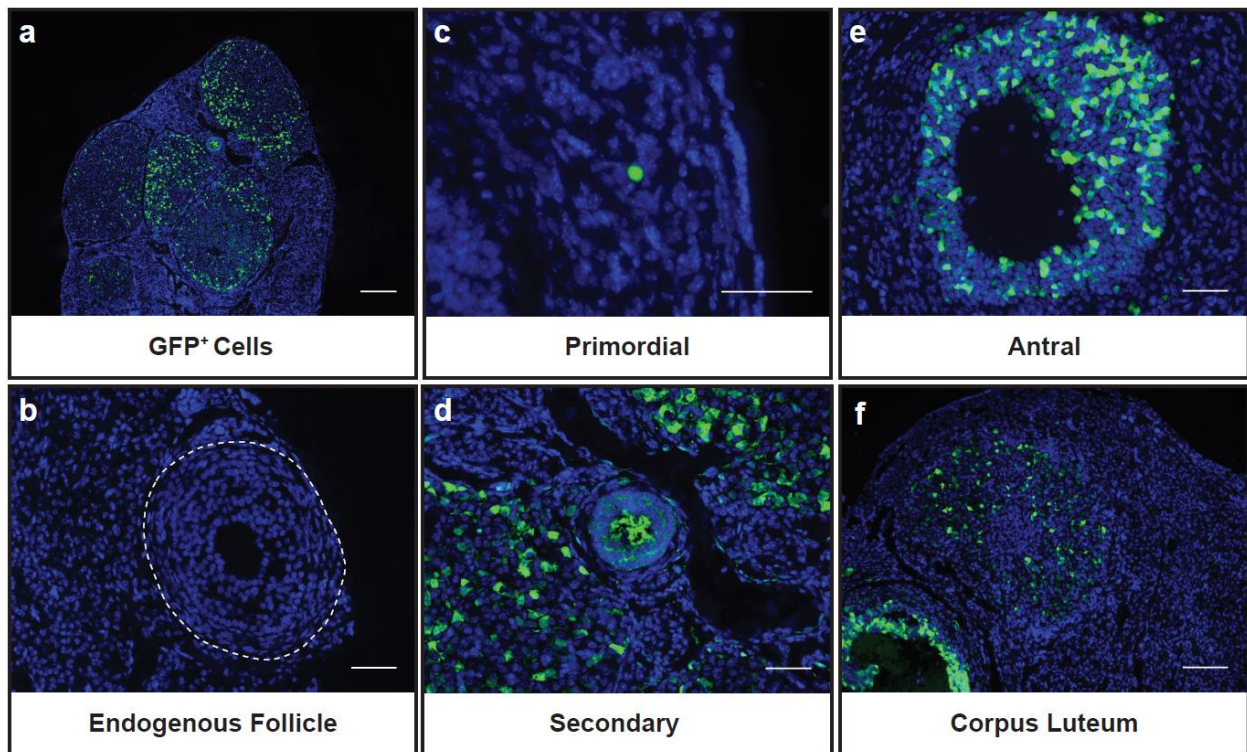


Figure 37 Survival of GFP+ Cells Post-Transplantation

Ovarian tissues were excised from ciPOF follicle recipient mice after three breeding cycles (106 days on average).

Immunofluorescence staining was performed using DAPI (endogenous cells) and GFP (transplanted cells) to evaluate follicle survival. a, A representative image of a transplanted ovary suggests that GFP+ cells integrated within the tissues and were actively proliferating. Scale, 200 μ m. b, Presence of an endogenous secondary follicle (GFP-), indicated by dotted line (white). Scale, 50 μ m. Various stages of follicle development were also present among the transplanted tissues, including: c, Primordial (Scale, 50 μ m) d, Secondary (Scale, 50 μ m) e, Antral (Scale, 50 μ m) and f, Corpus Luteum (Scale, 100 μ m).

5.5 Conclusion

In aim 2, the primary goal was to evaluate the efficacy of the OEEM hydrogel to aid in the delivery, engraftment and survival of isolated ovarian follicles. In addition, we wanted to examine this approach in a clinically relevant chemotherapy treated mouse model. First, we assessed the effects of busulfan and cyclophosphamide dosing on ovarian follicle populations. Ovarian follicles were evaluated histologically, classified by developmental stage and quantified. Each dose of chemotherapy caused a significant reduction in total follicles in comparison to the non-treated control mice. The 24-200 dose resulted in the greatest depletion of endogenous follicles, however, this treatment group also resulted in small ovaries and poor overall health of the mice. Next, we showed the ability to efficiently isolate a predominantly immature follicle pool that could be for transplantation. Ovaries from transgenic DBA/GFP female mice were excised and follicles were isolated. Follicle quantification determined that a 7 μ L injection would contain an estimated 1.0×10^3 total follicles, 74% of which would be primordial follicles. Multi-photon imaging demonstrated feasibility of hydrogel-facilitated intraovarian follicle microinjection, showing a co-localization of TRITC-labeled OEEM hydrogel and GFP+ follicles with the ovarian cortex. Finally, chemotherapy treated female mice were given a single intraovarian follicle microinjection within each ovary facilitated by the OEEM hydrogel to evaluate follicle engraftment and survival. Mating studies resulted in three healthy GFP+ pups in three separate litters over the span of three breeding cycles generated from mice treated with 12-100 and 24-100 mg/kg busulfan-cyclophosphamide. Second generation breeding of GFP progeny derived from intraovarian follicle microinjection resulted in several large litters. In addition, immunofluorescence imaging of ovaries excised 100+ days post-follicle transplantation showed the presence of GFP+ cells, which were

integrated into follicle structures. These results demonstrate that hydrogel-facilitated intraovarian follicle microinjection can support follicle delivery, engraftment and long-term survival.

6.0 Discussion

Women who cryopreserve oocytes or embryos prior to gonadotoxic treatments can use assisted-reproductive technologies (ART), such as IVF and embryo transfer to start a family (391, 392). To preserve eggs or embryos, the patient must first undergo hormone stimulation to collect mature oocytes. Controlled ovarian stimulation requires two or more weeks and is not a viable option for patients who have not reached reproductive maturity or who cannot afford to postpone treatment (150, 151, 393). For these girls and women, cryopreservation of intact ovarian tissues prior to treatment is the only potential option to naturally restore endocrine function and fertility. The current gold standard for fertility preservation in patients in remission is the autologous surgical transplantation of cryopreserved ovarian cortical strips (152, 153, 172-175, 185, 374, 377, 394). To date, there have been numerous successful procedures performed in humans, resulting in greater than 130 live-births; however, the efficiency of this method remains low, with live-birth rates ranging from 23-36% of patients achieving live-births (149, 395). Although ovarian tissue transplantation has shown promise, it is an invasive procedure and carries a potential risk of reintroducing malignant cells back into the body (396). To address these concerns, several pre-clinical experimental approaches have been proposed, including *in vitro* follicle maturation (IVM), the development of an artificial ovary and stem cell transplantation (Table 2).

Table 2 Summary of Notable Pre-Clinical Fertility Preservation Studies

Several therapeutic approaches have been explored to ameliorate the effects of infertility. In general, these can be divided into three main categories: (1) Ovarian engraftment (2) Biomaterial-facilitated and (3) Intraovarian transplantation methods. Ovarian engraftment can be equated to cortical strip autotransplantation, which is currently considered as the gold-standard in the field. Biomaterial-facilitated methods have recently progressed toward the development of a functional artificial ovary, which uses a scaffold or hydrogel to support follicle transplantation. Intraovarian transplantation has been primarily focused on the delivery of oogonial stem cells (OSCs). Each of the in vivo studies listed have used varied models of infertility, induced either by ovariectomy or chemotherapy, with a limited number showing the ability to produce pups (highlighted in green). However, the clinical translation of these approaches may be hindered by invasive surgical procedures and ex vivo follicle and stem cell manipulation. To overcome these barriers to the clinic, we have proposed a minimally invasive technique to facilitate the delivery and support of ovarian follicles within an in situ ovary (ISO), which promotes a natural solution for restoring fertility.

Approach	Source Material	Processed Form	Study type	Model of Infertility	Summary	Reference
Ovarian engraftment	Healthy Ovarian Tissue	N/A	In vivo	Yes (Chemotherapy)	Batchvarov et al. use a chemotherapy regimen of busulfan and cyclophosphamide to induce infertility. Grafted ovarian tissue was able to rescue host fertility although non-grafted hosts also gave rise to litters 200+ days post treatment.	(397)
Biomaterial-facilitated	Sodium Alginate	Alginate gel	In vivo	No	Rios et al. examine the potential of immunisolating and encapsulating ovarian follicles within alginate hydrogels for subcutaneous transplant. Hydrogels were retrieved and mature oocytes were collected then successfully fertilized with 7% of the embryos reaching 4 cell stage.	(214)
	Human Ovary	OECM Scaffold	In vitro/ In vivo	No	Hassanpour et al. develop a decellularization protocol incorporating SLES to prepare an ovarian tissue specific scaffold.	(352)
	Gelatin	3D Printed Scaffold	In vivo	Yes (Ovariectomy)	Laronda et al. establish a bioprosthetic 3D printed ovary to restore ovarian function in sterilized mice. GFP pups born from exogenous follicle transplant.	(221)
	Synthetic PEG	PEG hydrogel	In vivo	Yes (Ovariectomy)	Kim et al. implement a PEG-VS hydrogel to support the transplantation of immature follicles and restore endocrine function for up to 60 days.	(220)
	Fibrinogen/Thrombin	Fibrin gel	In vivo	No	Paulini et al. test an artificial ovary using a fibrin gel showing the efficacy of xenografting isolated preantral follicles within the peritoneum. Results showed follicles survival and proliferation up to 7 days post-transplant.	(219)
	Human/Bovine Ovary	OECM Scaffold	In vivo	Yes (Ovariectomy)	Laronda et al. detail a procedure for the decellularization of both human and bovine ovaries. Primary ovarian cells seeded onto decellularized grafts were transplanted into ovariectomized mice and showed evidence of initiating puberty.	(218)
	Fibrinogen/Thrombin	Fibrin gel + VEGF	In vitro/ In vivo	Yes (Ovariectomy)	Kniazeva et al. test several biomaterial graft systems in an ovariectomized mouse. Successful litters resulted solely from fibrin gel supplemented with VEGF.	(217)
	Fibrinogen/Thrombin	Fibrin gel	In vivo	Yes (Ovariectomy)	Smith et al. characterize the use of a fibrin gel for the transplant of ovarian follicles. Early-stage follicles were enzymatically isolated, encapsulated within fibrin gels and transplanted into an ovariectomized mouse. Tissue explants were performed at 0, 3, 9 and 21 days with follicles populations being significantly reduced by day 9.	(216)
	Fibrinogen/Thrombin	Fibrin gel	In vivo	Yes (Ovariectomy)	Luyckx et al. prepare an artificial ovary from fibrin gel that promotes survival and proliferation of preantral follicles 1 week post-transplant.	(398)
	Fibrinogen/Thrombin	Fibrin gel + VEGF	In vivo	Yes (Ovariectomy)	Shikanov et al. introduce a combination system consisting of Fibrin gel supplemented with VEGF to stimulate angiogenesis and promote graft survival. Transplanted mouse ovarian tissues supported by the Fibrin/VEGF material improved follicle survival when compared to no biomaterial control. The transplant material was also able to give rise to a litter of pups.	(215)
Intraovarian Transplantation	Female germline stem cells (FGSCs)	PBS	In vivo	Yes (Chemotherapy)	Xiong et al. implement a stem cell therapy to reverse the effects observed with exposure to chemotherapy. FGSC microinjection led to healthy pups post-chemotherapy.	(224)
	Primordial Follicles	PBS	In vivo	Yes (Chemotherapy)	Park et al. show significant genetic changes within primordial follicle markers after exposure to chemotherapy. Intraovarian primordial follicle transplantation did not restore fertility.	(379)

IVM consists of the isolation and culture of immature follicles to obtain meiotically-competent oocytes for IVF. IVM approaches have predominantly shifted from two-dimensional culture toward three-dimensional hydrogel-based follicle encapsulation, which has improved follicle morphology and intercellular signaling (191). The most commonly used hydrogel for IVM is alginate (190, 200, 375, 399-403); although, there are several other options that have been examined including, fibrin (209), fibrin-alginate (208, 215), and polyethylene glycol (PEG) (213, 404). Each of these materials provide a unique set of physical and biochemical properties, which allows them to support the growth and maturation of follicles *in vitro*. Successful application of IVM has been shown in mice leading to live-births (190); however, the pre-clinical translation of this approach for human follicles has been limited (405). Recently, follicle maturation has been attempted *in vivo* through the heterotopic subcutaneous transplant of a retrievable hydrogel seeded with immature follicles (214). Antral follicles developed in the hydrogel and germinal vesicle stage oocytes could be extracted, matured to MII stage and fertilized, leading to the development of two and four cell embryos. However, embryos were not transferred in this study and pregnancies were not established.

As IVM has proven to be a major challenge for human follicles, several groups have pursued the development of an artificial ovary. This concept involves the isolation and sequestering of immature follicles in a bio-supportive scaffold that can be transplanted to recover ovarian function. Similar to IVM, various biomaterials are being examined as options to support the delivery, survival and function of ovarian follicles *in vivo*. Recently, a fibrin gel supplemented with vascular endothelial growth factor (VEGF) was used to facilitate the transplantation of primordial follicles into the bursa of ovariectomized mice and gave rise to a healthy litter of pups (217). In another study, a 3D printed gelatin scaffolds were used to examine the effects of pore

geometry on follicle survival and achieved healthy pups through natural mating post-implantation in sterilized mice (221). Since each of these studies used ovariectomized mice as transplant recipients, they were unable to evaluate the suitability of the endogenous ovary as a transplant site or the impact that chemotherapy would have on transplant follicle engraftment, survival and development.

The objective of the present study was to develop a method to transplant ovarian follicles into the endogenous ovary using a supportive OECM hydrogel. Our approach required minimal *in vitro* manipulation of follicles and short-term exposure to *ex vivo* conditions prior to intraovarian microinjection. This was accomplished by solubilizing acellular ovarian scaffolds to create a thermo-responsive, injectable material which was able to form *in situ* following injection under physiological conditions. In addition, we proposed an adapted method for efficiently isolating follicles to reduce the total time *ex vivo* prior to transplantation. To mimic ciPOF experienced in the clinic, a single intraperitoneal injection of busulfan and cyclophosphamide was used to significantly reduce the endogenous follicle population in female recipient mice. The OECM hydrogel combined with freshly isolated GFP⁺ ovarian follicles were successfully delivered into the ovarian cortex, forming an ISO. Intraovarian follicle transplant aided by the OECM hydrogel gave rise to multiple, consecutive litters containing at least one pup expressing GFP.

This study demonstrates a potential strategy for restoring fertility after chemotherapy, but we acknowledge that there are several limitations. A major benefit of isolating follicles from the ovarian stroma is the potential to reduce malignant cells that could be introduced during transplantation and there have been reports suggesting that follicle isolation can significantly decrease cancer cells prior to implantation (217, 406). However, since our primary aim was to improve intraovarian follicle transplant and survival, we did not filter out stromal cells within our

follicle suspension after isolation. Therefore, it is possible that stromal cells or other cell types may have contributed to ovarian follicle survival within the ciPOF ovaries. In addition, donor follicles were isolated from whole allogeneic ovaries rather than autologously sourced ovarian tissue. We also acknowledge that the wide age range (6-14 days) of mice used to collect donor follicles could yield drastically different follicle and stromal cell populations. In future experiments, it would be ideal to use donor mice from the same age to reduce variability. However, in order to increase the number of available donor follicles, isolated follicles were combined into a single batch and equally distributed for transplantation. One of the main goals of this therapy is to eventually restore fertility in human patients. However, as a first attempt, we were interested in examining the effects of this method on donor follicle survival after intraovarian microinjection. Although the ciPOF mice had a significantly reduced follicle number they were not infertile, as non-injected control mice had multiple litters. In addition, the presence of endogenous follicles could also aid exogenous follicle integration and survival within the ovarian niche. Another significant limitation of this study was the size of the mouse ovaries. The current animal model restricted the use of larger volumes of injected gel during a single treatment making it difficult to deliver a greater quantity of follicles. Theoretically, as the number of injected follicles increases it could also improve the potential fertility outcomes. In addition, the ratio of gel to follicles may also be a decisive factor in long-term follicle survival. For example, a higher follicle concentration could inhibit access to nutrients within the ISO triggering apoptosis or atresia. Finally, to improve the outcomes observed in this report, multiple hydrogels with varying compositions and mechanical properties will be tested to evaluate *in situ* follicle-hydrogel interactions over time. To this end, a comprehensive follow up study will be conducted in a larger animal model using follicles isolated

from cryopreserved, autologous ovarian tissues to evaluate the therapeutic and translational potential of this approach.

OECM hydrogels, paired with intraovarian microinjection created an environment that supported survival and development of transplanted follicles. This therapeutic approach employs the innate remodeling capacity of the ECM to establish an ISO to facilitate follicle transplant. In the human clinic, this technique could be deployed using the same minimally-invasive ultrasound-guided approach used to aspirate follicles from the ovary in IVF clinics. Instead of aspirating eggs, follicles could be injected directly into the ovarian cortex. Overall, the restorative reproductive outcomes observed in this study suggest that this platform could be used to address current unmet clinical needs.

7.0 Concluding Remarks

7.1 Study Summary

The overarching goal of this work was to improve upon the current therapies used to treat fertility preservation. Our hypothesis was that ovarian ECM hydrogels could facilitate the intraovarian delivery and engraftment of isolated follicles in chemotherapy-treated mice. To test this hypothesis, we developed a decellularization protocol to obtain ovarian-specific acellular tissues. We found that decellularized ovaries removed greater than 97% of dsDNA while retaining ECM components and hormones. Further, we found that decellularized ovarian tissues could be solubilized and formed into a hydrogel at physiological conditions. Hydrogel properties were examined at two different ECM concentrations using rheology, gelation kinetics and ultrastructure analyses. We found that increasing ECM concentration led to greater viscoelastic properties, while gelation times remained constant. Ovarian hydrogels were also tested as a candidate substrate for *in vitro* follicle culture. After 12 days in culture, pre-antral follicles transitioned into fully mature, fertilizable oocytes, which yielded a two-cell embryo.

To create a clinically relevant chemotherapy model of premature ovarian failure, we treated young female mice with varying doses of busulfan and cyclophosphamide. Ovarian tissues were examined three weeks after injection to evaluate the effects of chemotherapy on follicle populations. Chemotherapy treatments resulted in a significant reduction in total follicles in comparison to untreated controls and indicated that primordial and primary follicles were the most sensitive to treatments. To assess the efficacy of intraovarian follicle microinjection, isolated follicles were resuspended in hydrogels then microinjected into the ovarian cortex. Confocal

microscopy showed that OECM hydrogels and follicles colocalized with the cortical region, establishing an *in situ* ovary. Finally, hydrogel-facilitated intraovarian follicle microinjection was tested using ciPOF mice to determine the impact on follicle survival. Transgenic (GFP+/DBA) female mice were used as follicle donors and nude ciPOF female mice were used as follicle transplant recipients. After three breeding cycles, with nude male mice, three litters contained three pups derived from donor follicle microinjection. Second generation breeding of the GFP+ progeny resulted in multiple healthy litters, indicating that follicle microinjection did not compromise their reproductive health. Additionally, histological analysis using immunofluorescence showed GFP+ cells within ciPOF treated tissues at greater than 100 days post-transplantation. These results suggest that hydrogel-facilitated follicle microinjection could promote the long-term survival of transplanted follicles.

7.2 Limitations

Although this study produced exciting results, there were several limitations that could have been improved. One of the major limitations of this work was the use of a mouse model. The size of the mouse ovary limited the total amount of hydrogel and follicles that could be injected. Theoretically, if a greater number of follicles are delivered into the ovary, the fertility potential would increase. Even though we only injected a small volume of gel, we were able to establish pregnancies from a small pool of transplanted follicles within each ovary. In addition, the transgenic backgrounds of the mice and breeding strategy could have been improved to yield offspring with only a single definitive trait (ie. GFP, hair/eye color, etc.). This would improve initial detection and differentiate between pups derived from transplanted follicles versus

endogenous follicles. It was also difficult to assess the variability in live-births between mice, which could have been attributed to uneven distribution of follicles and the efficiency of follicle injection. Methods for assessing donor follicle counts post-transplantation would have provided critical information to better evaluate breeding results within transplanted ciPOF mice.

Another limitation of the study was that chemotherapy treated mice were not completely infertile making it difficult to assess whether supportive cells of the endogenous ovary played a role in facilitating donor follicle survival and development. To ensure infertility, follicle microinjections could have been delayed by eight weeks post-chemotherapy, which did not yield any litters during the third breeding cycle in higher doses of busulfan and cyclophosphamide. However, it is interesting that fertility was lost in ciPOF control animals shortly after the first two breeding cycles, which may be a sign there are residual effects of chemotherapy that may contribute to rapid follicle loss, rather than natural atresia. Therefore, it may suggest that the ovarian ECM hydrogel does have some chemoprotective properties that shield transplanted follicles from immediate apoptosis as they displayed GFP signals at 100 days post-transplantation.

Additionally, the follicle isolation procedure did not filter out loose stromal or somatic cells, which could have provided additional support for follicle survival and development. In order to accurately evaluate the effects of the ovarian hydrogel, a pure follicle population should be used. Further, for cancer patients with suspicious ovarian tissues that may contain malignant cells, it is important to develop and test an efficient protocol that completely eliminates the stromal cells from the follicle pool.

Finally, the clinical translation of this type of procedure would need to be tested using minimally invasive methods such as intravaginal follicle injection under ultrasound guidance. At this initial stage development, this study was primarily focused on evaluating the efficacy of

hydrogel-facilitated microinjection and to determine if the hydrogel-follicle suspension colocalized within the ovarian cortex. To accommodate these initial tests, we performed an invasive surgical procedure to expose the ovaries and used a microinjection system to deliver the follicles. Therefore, we were unable to determine the feasibility of a minimally invasive application of this technique.






















7.3 Future Directions

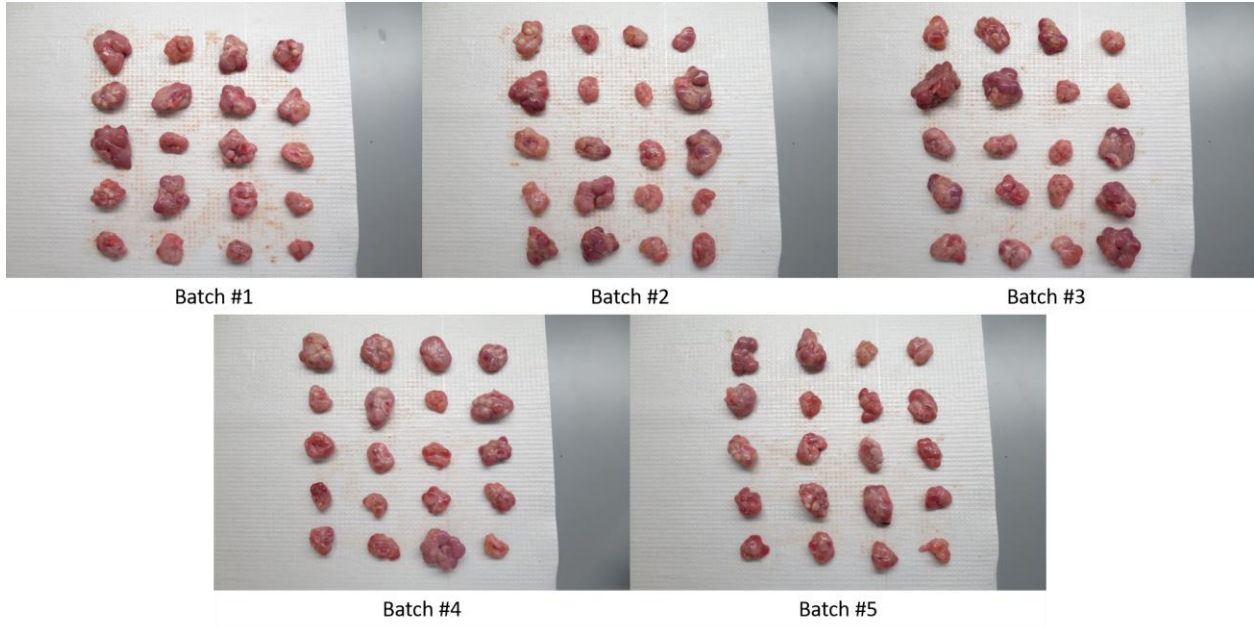
To improve upon the studies performed within the scope of the current dissertation, future experiments would be required to assess some of the outstanding questions regarding the effects of hydrogel-facilitated follicle microinjection. Ideally, this study should be performed in a higher order mammal, such as a non-human primate. Ovarian cortical strips should be collected and cryopreserved prior to chemotherapy, radiation or equivalent model to mimic the effects of iatrogenic infertility. After cytotoxic treatments are performed, donor follicles should be isolated from the same cryopreserved tissue to mimic the process of autologous follicle transplantation in humans. Further, methods should be developed to rapidly isolate a pure follicle pool, free from somatic and stromal cells. Multiple biomaterial compositions should be tested with varying viscoelastic properties along with sham controls. The mechanics of follicle delivery via microinjection should be characterized to evaluate the effects of shear stress and biomaterial viscosity on viability post-transplantation. Additionally, feasibility studies should be performed using transvaginal follicle delivery under ultrasound guidance. Finally, ovarian tissues should be explanted at both acute and long-term time points post-transplantation to determine the local and systemic effects using quantitative metrics, such as flow cytometry, Luminex assays and

immunohistochemistry. Most importantly, the success of future experiments approach will be evaluated based upon the rate of healthy pregnancy and live-births, which demonstrate efficacy for a model of infertility.

Appendix A Decellularization Processing

Appendix Table 1 Mass Conservation of Initial Decellularization Protocol

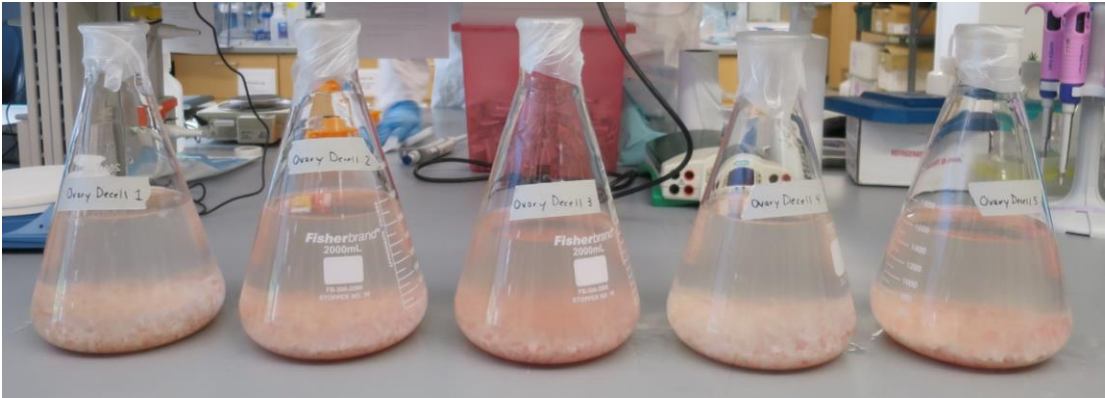
Ovary Sample	Native Ovary	Decelled Ovary	Lyophilized Ovary	Native Wet Weight	Decelled Wet Weight	Decelled Dry Weight	Mass Percent Loss Post-Decellularization	Mass Percent Loss Post-Lyophilization
1				12.215 g	6.785 g	0.567 g	44%	92%
2				8.063 g	4.511 g	0.403 g	44%	91%
3				3.595 g	2.614 g	0.204 g	27%	92%
4				7.088 g	4.435 g	0.356 g	37%	92%
5				7.778 g	5.202 g	0.444 g	33%	91%
6				13.620 g	8.965 g	0.763 g	34%	91%
7-30				8.295 g	3.828 g	0.354 g	54%	91%
Overall Average				8.381 g	4.146 g	0.374 g	50%	91%



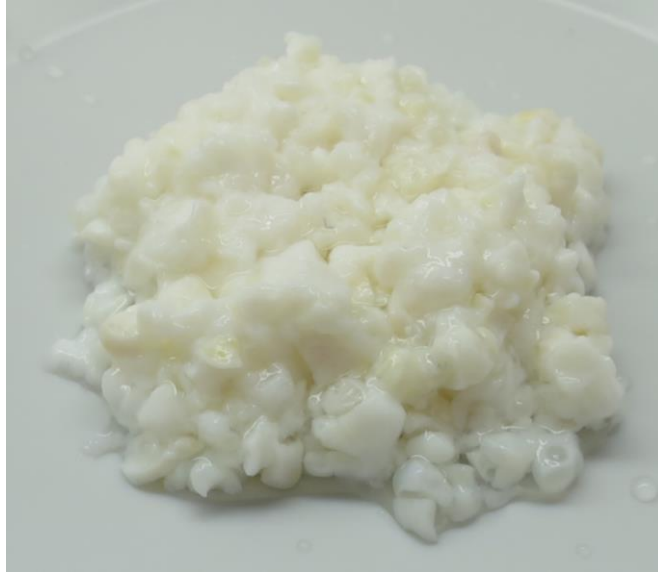
Appendix Figure 1 Porcine Ovaries for Batch Decellularization



Appendix Figure 2 Batch of Diced Porcine Ovaries



Appendix Figure 3 Tissues in Flasks Before and After Decellularization



Appendix Figure 4 Decellularized Porcine Ovaries

Appendix B Decellularization Mass Conservation

Appendix Table 2 Effects of Decellularization on Tissue Mass

Ovary #	Native Wet Weight (g)	Starting Ovary Batch Mass (g)	Native Diced Wet Mass (g)	Native Tissue Wet Mass (g)	Native Tissue Dry Mass (g)	Decelled Wet Mass (g)	Decelled Dry Mass (g)	Native Mass Percent Reduction (Wet vs. Lyophilized)	Decell Mass Percent Reduction (Wet vs. Lyophilized)	Grams of ECM/native mass	% ECM mass
1	8.053										
2	3.406										
3	6.724										
4	3.480										
5	1.674										
6	4.604										
7	5.168										
8	6.884										
9	2.350										
10	4.604	109.752	87.663	5.257	0.834	37.711	2.23	84%	94%	0.0302	3.02%
11	8.204										
12	8.094										
13	5.062										
14	5.771										
15	2.963										
16	9.097										
17	5.401										
18	2.284										
19	10.775										
20	5.154										

Appendix Table 2 (continued)

Ovary #	Native Wet Weight (g)	Starting Ovary Batch Mass (g)	Native Diced Wet Mass (g)	Native Tissue Wet Mass (g)	Native Tissue <u>D</u> ry Mass (g)	Decelled Wet Mass (g)	Decelled Dry Mass (g)	Native Mass Percent Reduction (Wet vs. Lyophilized)	Decell Mass Percent Reduction (Wet vs. Lyophilized)	Grams of ECM/ native mass	% ECM mass
21	2.537										
22	2.323										
23	3.307										
24	10.220										
25	4.996										
26	2.051										
27	5.007										
28	9.084										
29	5.400										
30	8.590	95.729	63.914	5.717	0.959	30.238	1.913	83%	94%	0.0360	3.60%
31	2.067										
32	3.176										
33	4.166										
34	3.004										
35	3.309										
36	1.648										
37	9.190										
38	8.428										
39	3.455										
40	3.771										

Appendix Table 2 (continued)

Ovary #	Native Wet Weight (g)	Starting Ovary Batch Mass (g)	Native Diced Wet Mass (g)	Native Tissue Wet Mass (g)	Native Tissue Dry Mass (g)	Decelled Wet Mass (g)	Decelled Dry Mass (g)	Native Mass Percent Reduction (Wet vs. Lyophilized)	Decell Mass Percent Reduction (Wet vs. Lyophilized)	Grams of ECM/native mass	% ECM mass
41	3.961										
42	6.579										
43	3.248										
44	4.591										
45	3.675										
46	2.545										
47	6.886										
48	14.079										
49	2.265										
50	1.853	105.533	75.218	5.878	1.104	32.295	1.975	81%	94%	0.0323	3.23%
51	4.955										
52	4.964										
53	2.470										
54	5.013										
55	10.078										
56	3.832										
57	3.942										
58	4.149										
59	7.072										
60	9.376										

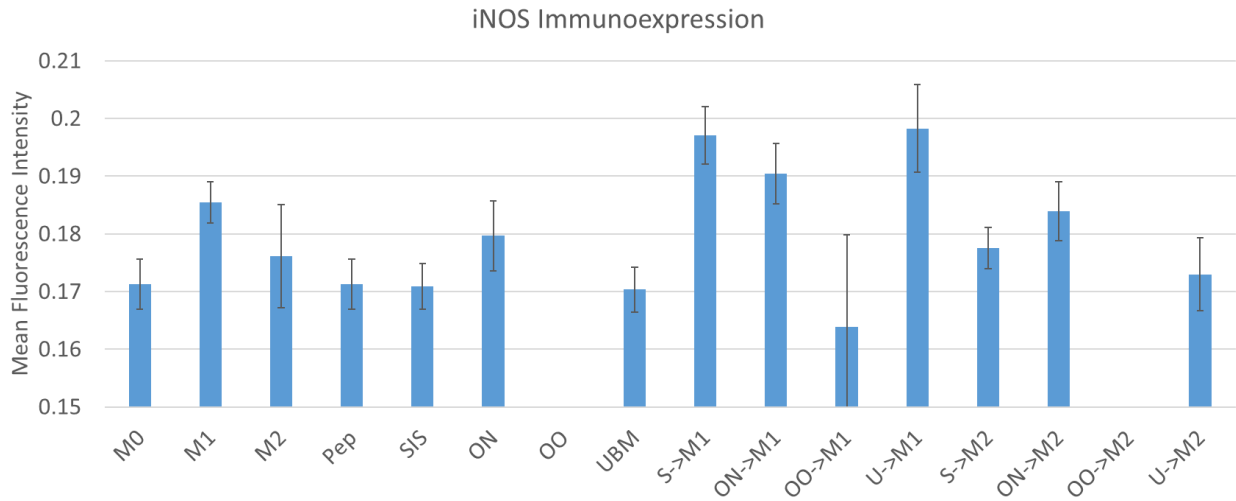
Appendix Table 2 (continued)

Ovary #	Native Wet Weight (g)	Starting Ovary Batch Mass (g)	Native Diced Wet Mass (g)	Native Tissue Wet Mass (g)	Native Tissue <u>D</u> ry Mass (g)	Decelled Wet Mass (g)	Decelled Dry Mass (g)	Native Mass Percent Reduction (Wet vs. Lyophilized)	Decell Mass Percent Reduction (Wet vs. Lyophilized)	Grams of ECM/ native mass	% ECM mass
61	1.969										
62	3.131										
63	9.058										
64	2.860										
65	3.068										
66	2.900										
67	1.976										
68	2.424										
69	3.721										
70	2.833	86.464	61.684	4.745	0.798	33.720	2.044	83%	94%	0.0398	3.98%
71	3.230										
72	4.077										
73	7.091										
74	1.953										
75	7.436										
76	2.592										
77	8.115										
78	7.551										
79	6.250										
80	4.229										

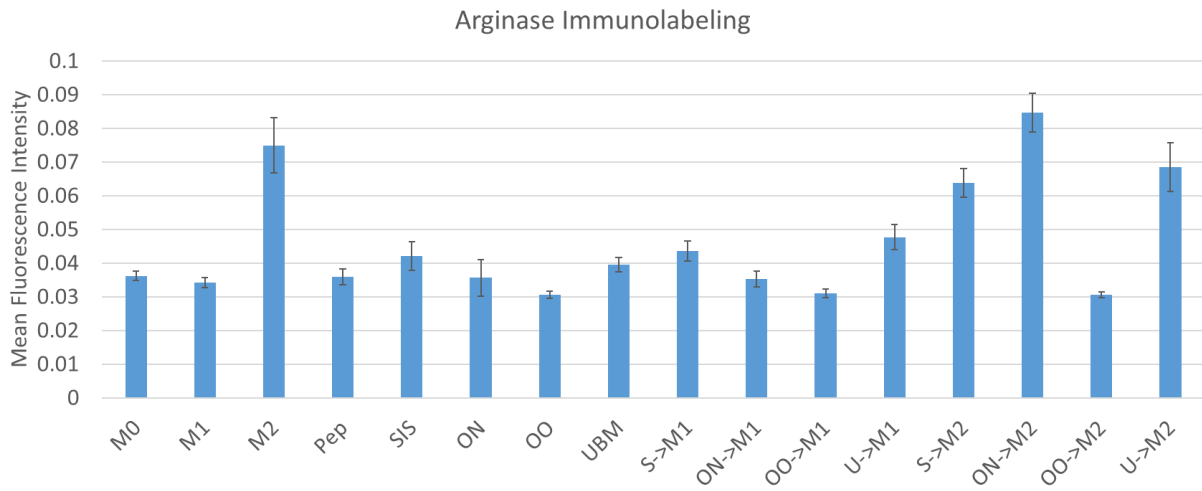
Appendix Table 2 (continued)

Ovary #	Native Wet Weight (g)	Starting Ovary Batch Mass (g)	Native Diced Wet Mass (g)	Native Tissue Wet Mass (g)	Native Tissue <u>D</u> ry Mass (g)	Decel ^l ed Wet Mass (g)	Decel ^l ed Dry Mass (g)	Native Mass Percent Reduction (Wet vs. Lyophilized)	Decell Mass Percent Reduction (Wet vs. Lyophilized)	Grams of ECM/ native mass	% ECM mass
81	1.694	75.899	51.402	5.993	0.946	25.607	1.491	84%	94%	0.0344	3.44%
82	2.981										
83	2.999										
84	2.486										
85	3.815										
86	5.041										
87	6.499										
88	2.780										
89	4.445										
90	3.201										
91	4.290										
92	2.770										
93	3.878										
94	5.621										
95	2.103										
96	2.954										
97	5.165										
98	8.071										
99	2.079										
100	3.027										
Total	473.377	473.377	339.881	27.59	4.641	159.571	9.653				
Overall Average	4.734	94.675	67.976	5.518	0.9282	31.914	1.9306	83%	94%	0.0346	3.456%

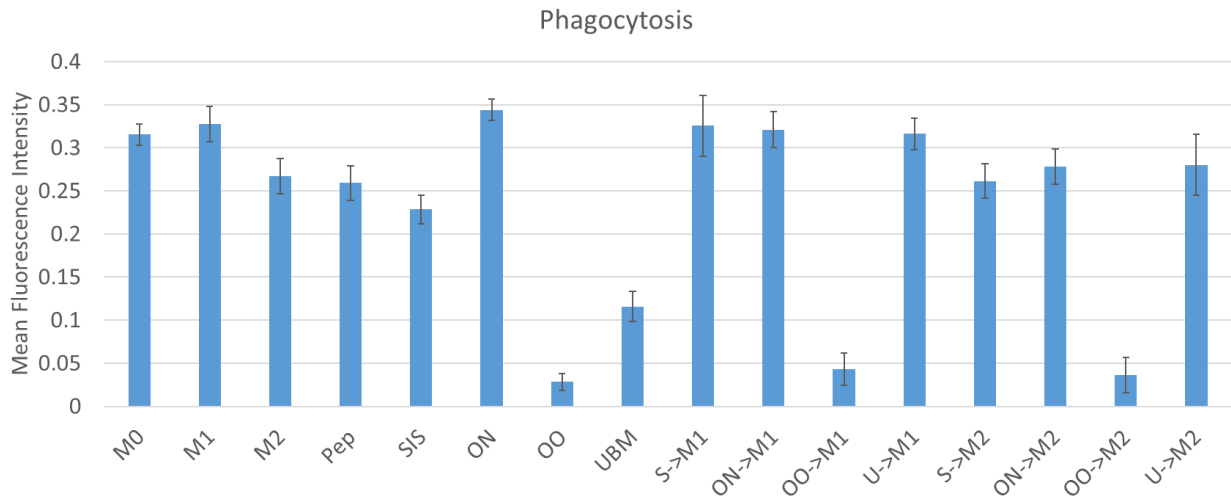
Appendix C Ovarian Hydrogel Cytocompatibility



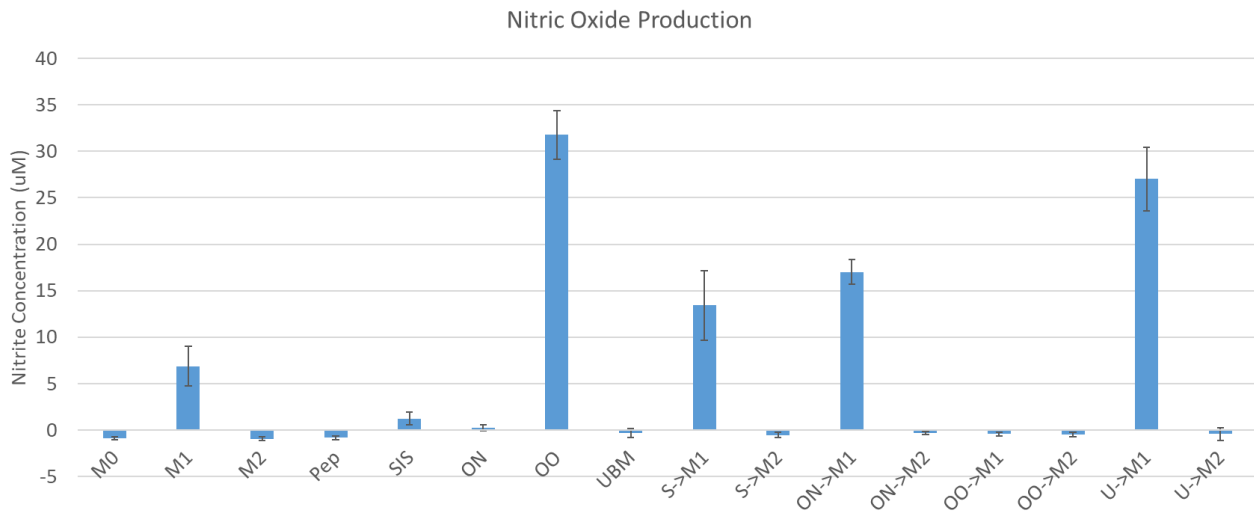
Appendix Figure 5 Macrophage iNOS Expression



Appendix Figure 6 Macrophage Arginase Expression

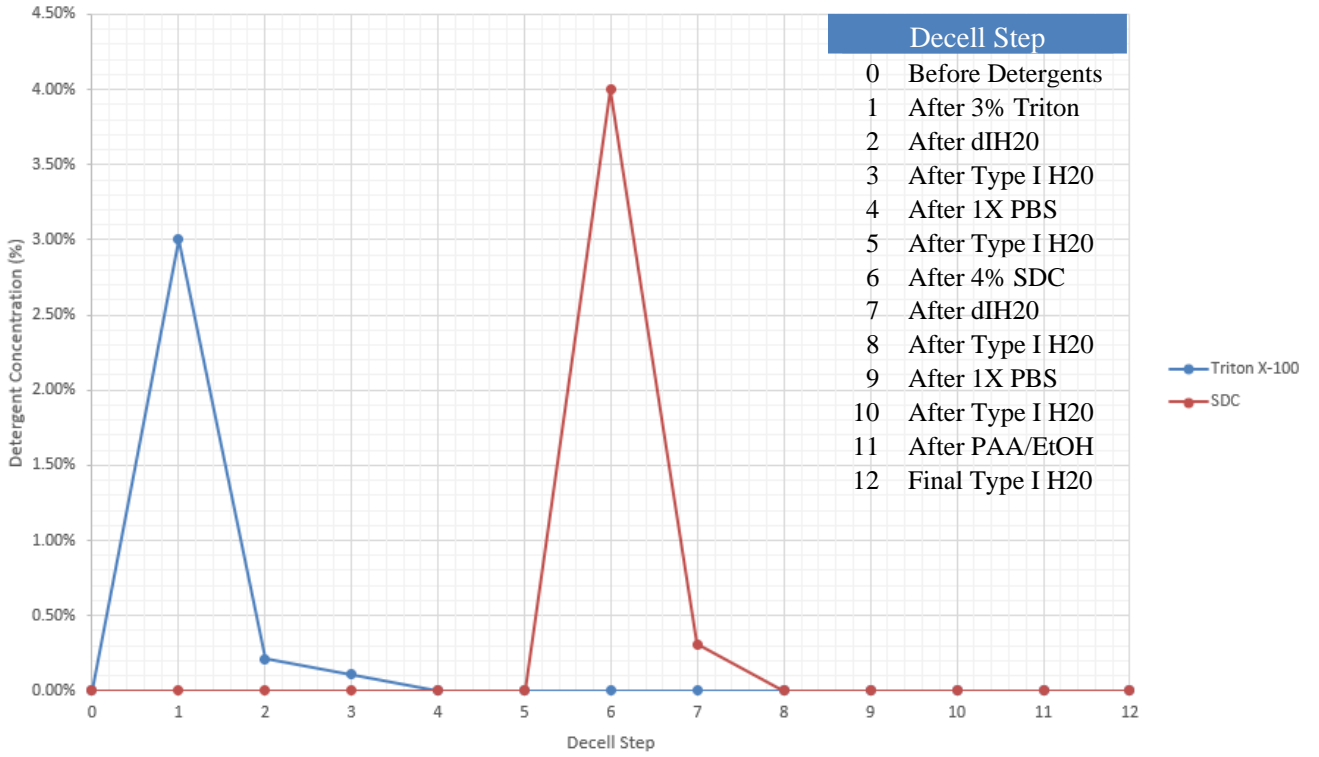


Appendix Figure 7 Macrophage Phagocytosis



Appendix Figure 8 Macrophage Nitric Oxide Production

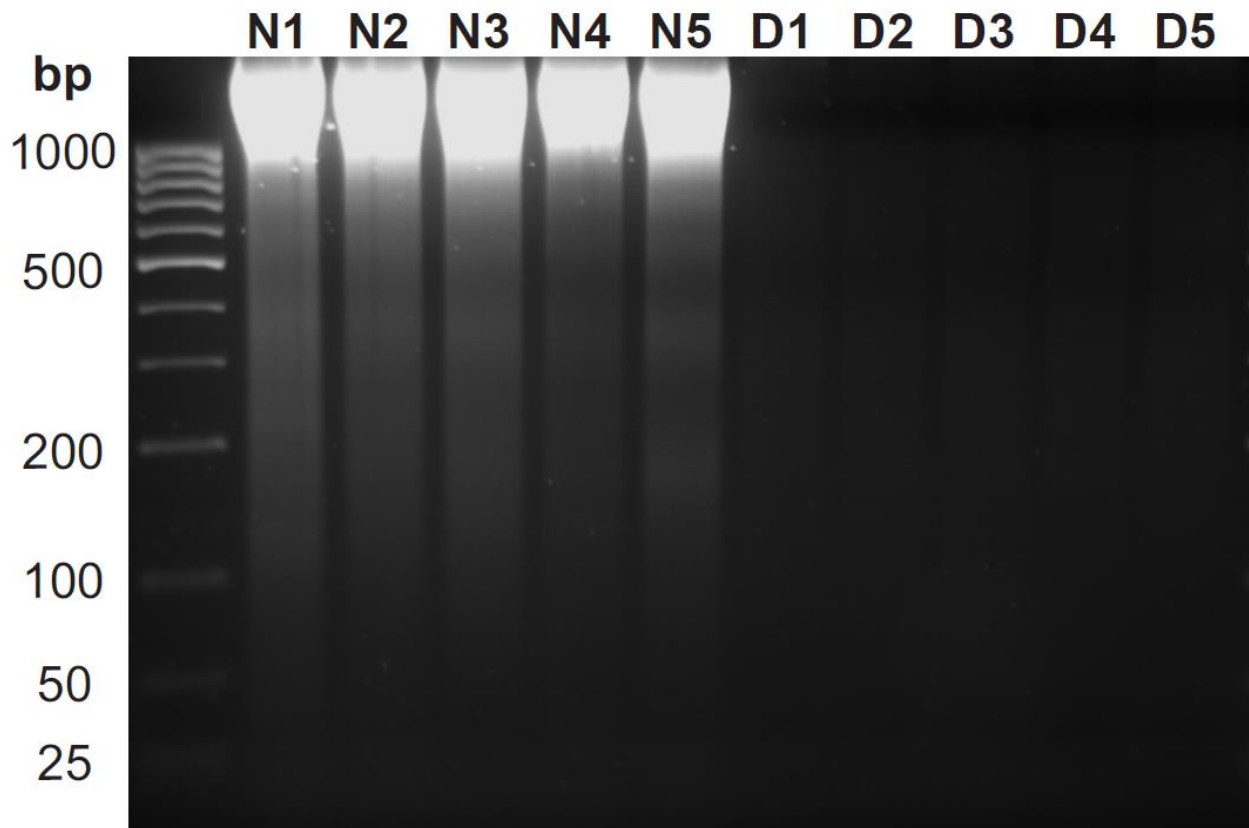
Appendix D Detergent Concentration During Decellularization



Appendix Figure 9 Effects of Washes on Detergent Concentrations

Effluents were collected after washes with Triton X-100 and sodium deoxycholate to determine if the amount of residual detergents.

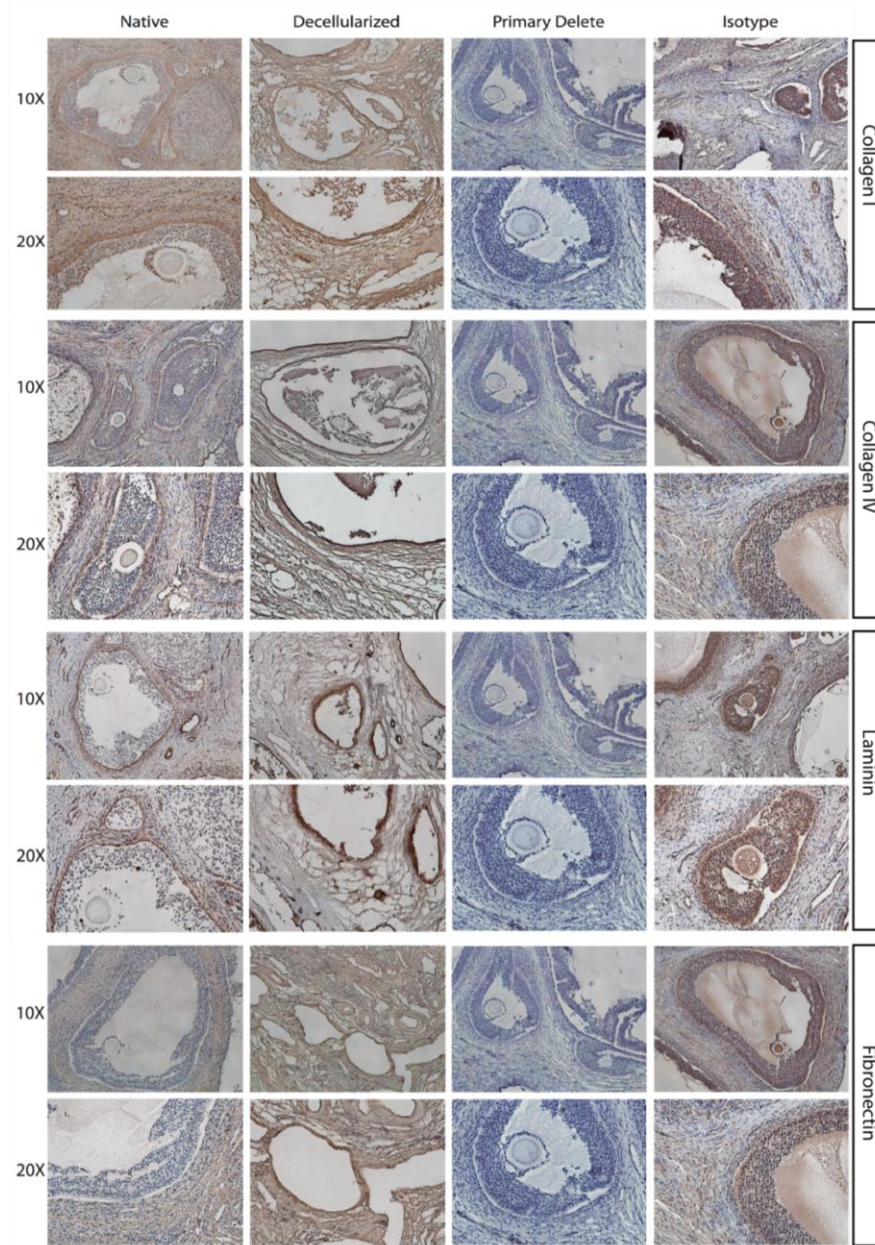
Appendix E DNA Fragmentation Post-Decellularization



Appendix Figure 10 Agarose Gel Electrophoresis

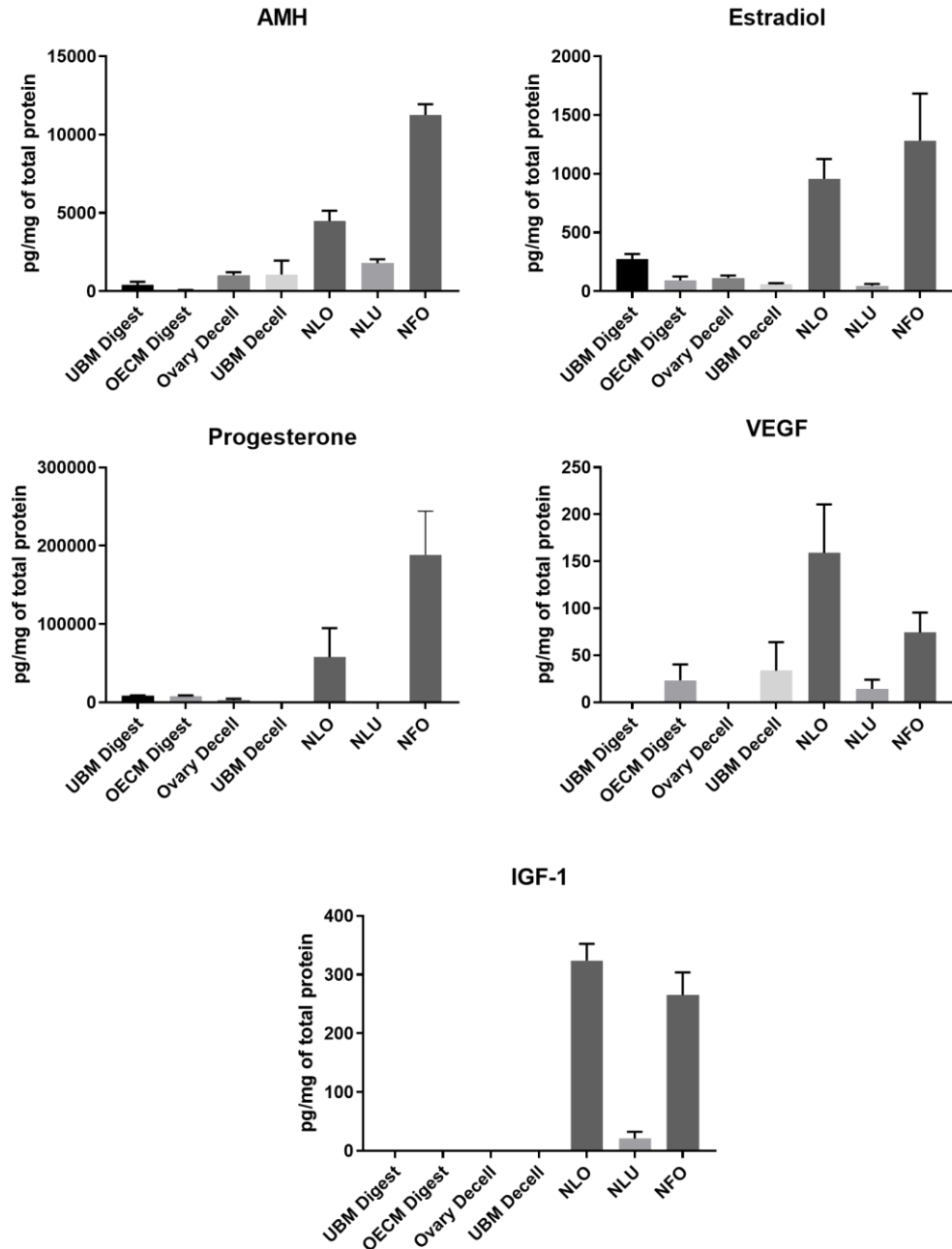
A 2.5% agarose gel was used to characterize the presence of DNA within ovarian tissues post-decellularization. No visible bands were observed within the decellularized ovarian tissues (D1-D5). Native ovarian tissues (N1-N5) were used as a positive control. Each lane represents an individual sample of DNA.

Appendix F Ovarian Tissue Immunohistochemistry



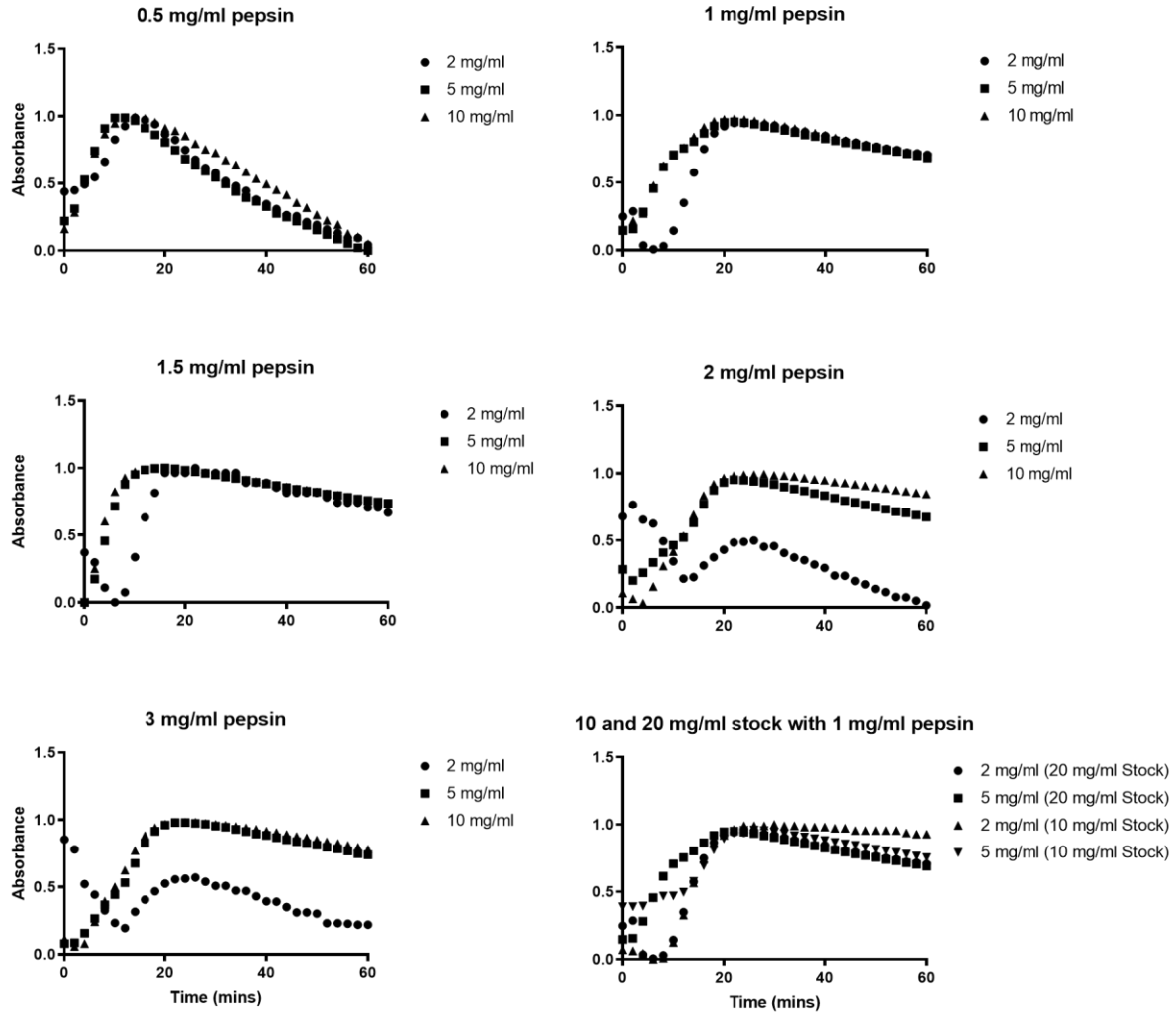
Appendix Figure 11 IHC Ovarian ECM Proteins

Appendix G Effect of Ovarian Tissue Processing on Hormones and Growth Factors



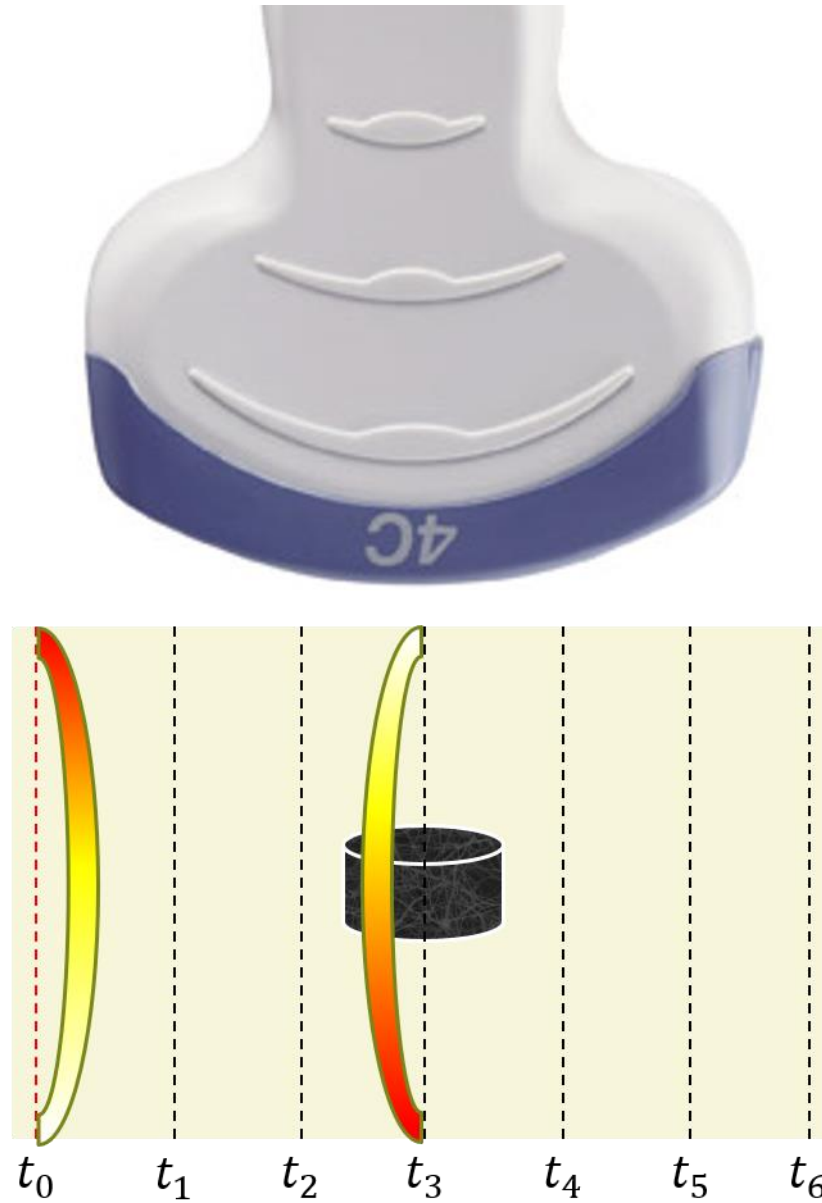
Appendix Figure 12 Retention of Ovarian-specific Hormones and Growth Factors

Appendix H Ovarian Hydrogel Optimization



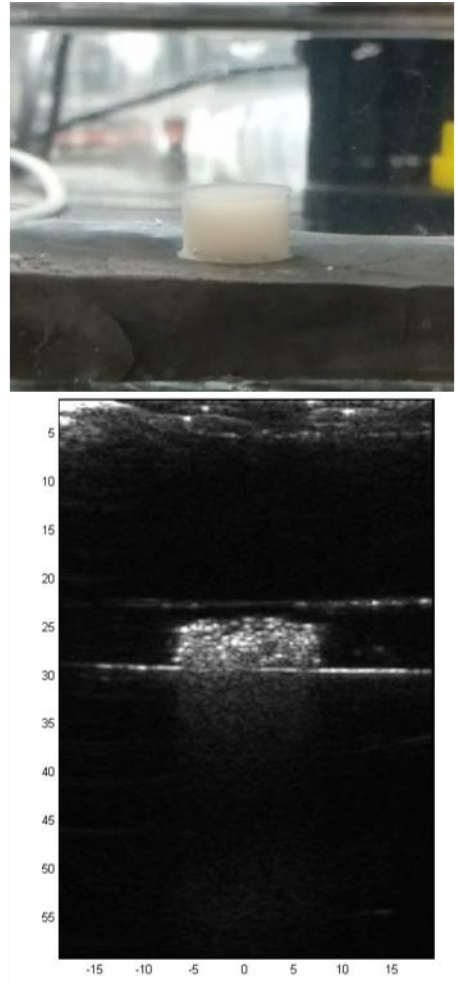
Appendix Figure 13 Effects of Pepsin on Gelation Kinetics

Appendix I Ovarian Hydrogel Mechanical Characterization



Appendix Figure 14 Ultrasound Elastography

Ultrasound elastography was tested as potential alternative technique to directly measure bulk mechanical properties of the native ovary vs ovarian hydrogels.



Appendix Figure 15 Ultrasound Elastography Experimental Setup



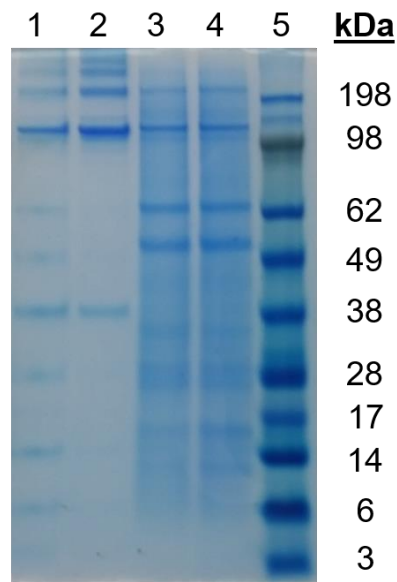
5 mg/mL 10 mg/mL 15 mg/mL



Appendix Figure 16 OECM Soluble/Insoluble Fraction

Lane Identification

- 1) Insoluble fraction (Pepsin Digest)
- 2) Ovarian ECM (Pepsin Digest)
- 3) Soluble fraction (filtered)
- 4) Soluble fraction (unfiltered)
- 5) SeeBlue2 Protein Ladder



Appendix Figure 17 Protein Gel Soluble vs Insoluble Fraction

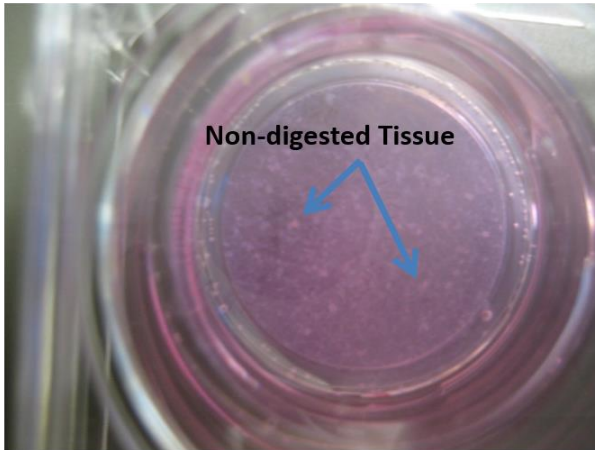
Urea extraction was used to enrich soluble fraction of the OECM components.

Appendix J *In Vitro* Newborn Mouse Ovary Culture

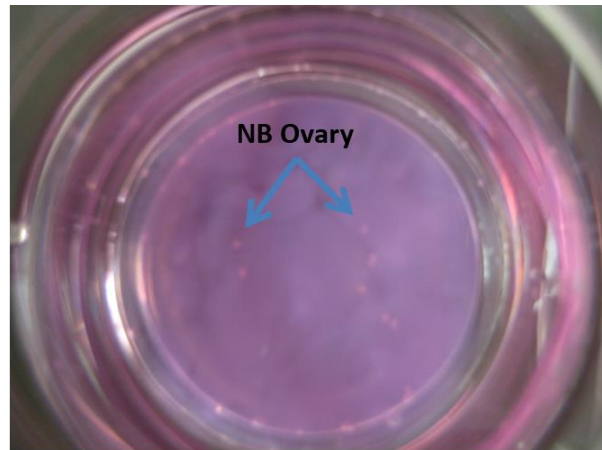
Appendix Table 3 Whole Ovary Culture Medium

Waymouth's MB 7521 Medium	DMEM/F-12 Medium
10% FBS	0.1% Albumax
50 U Penicillin/Streptomycin	50 U Penicillin/Streptomycin
0.23 mM Pyruvic Acid	1X Glutamax
	27.5 µg/mL Transferrin
	0.05 mg/mL L-ascorbic Acid
	1 µg/mL Insulin
	0.1% Bovine Serum Albumin (BSA)

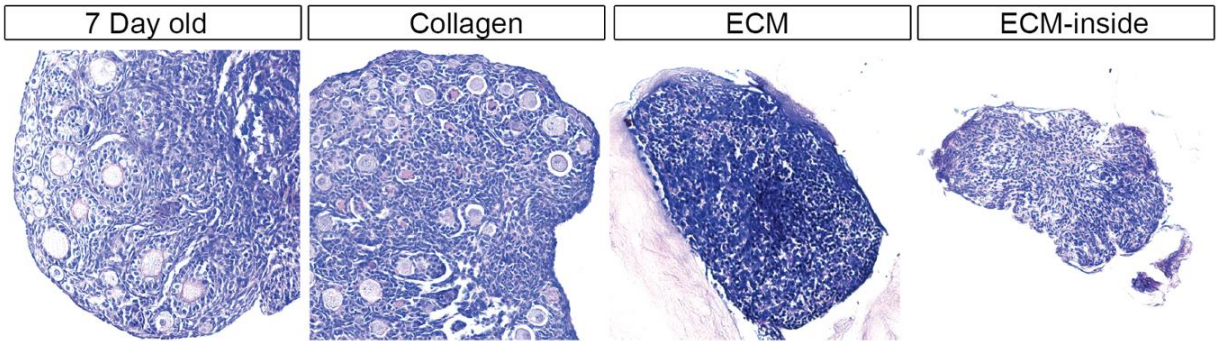
1st test



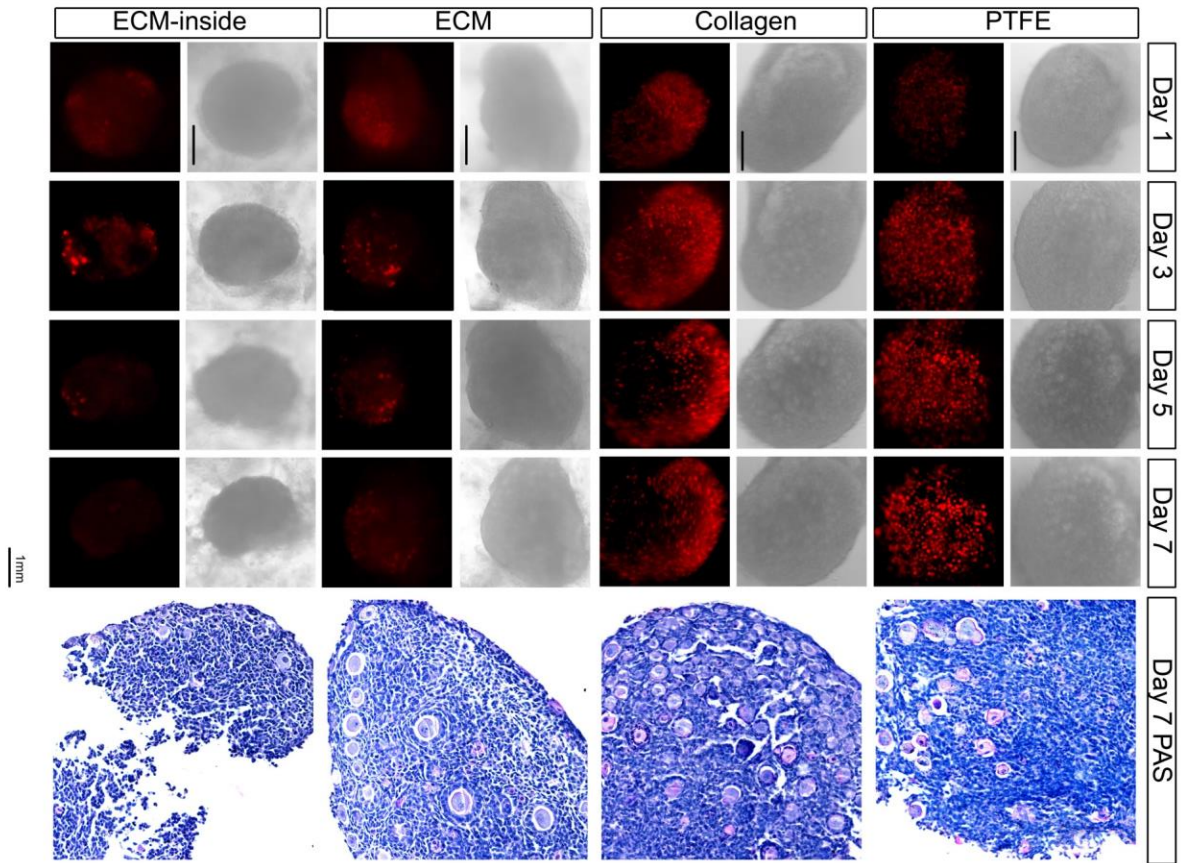
2nd test



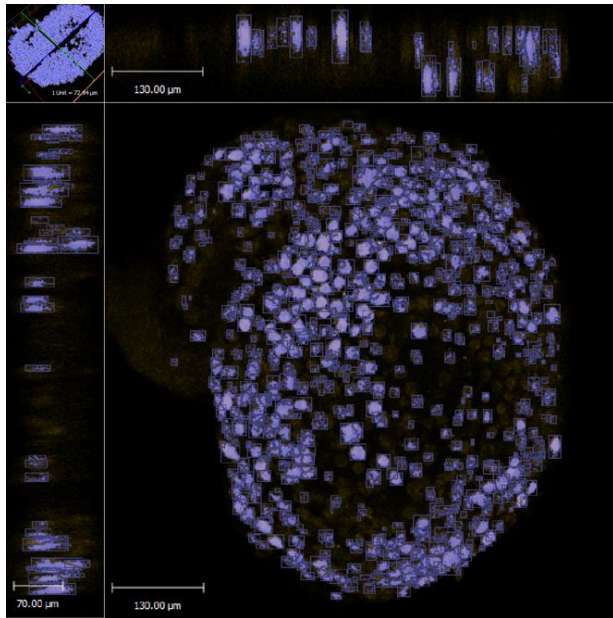
2nd 7day culture



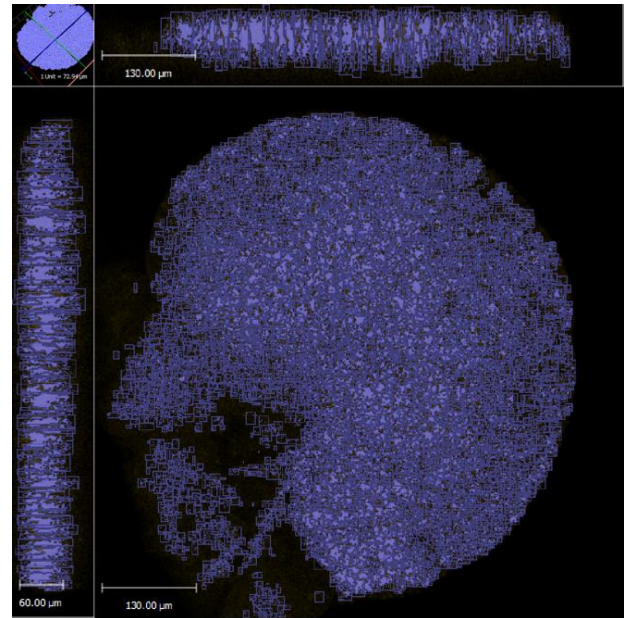
Appendix Figure 18 OECM Hydrogel Optimization for Whole Ovary Culture



Appendix Figure 19 Initial Results of Whole Ovary Culture



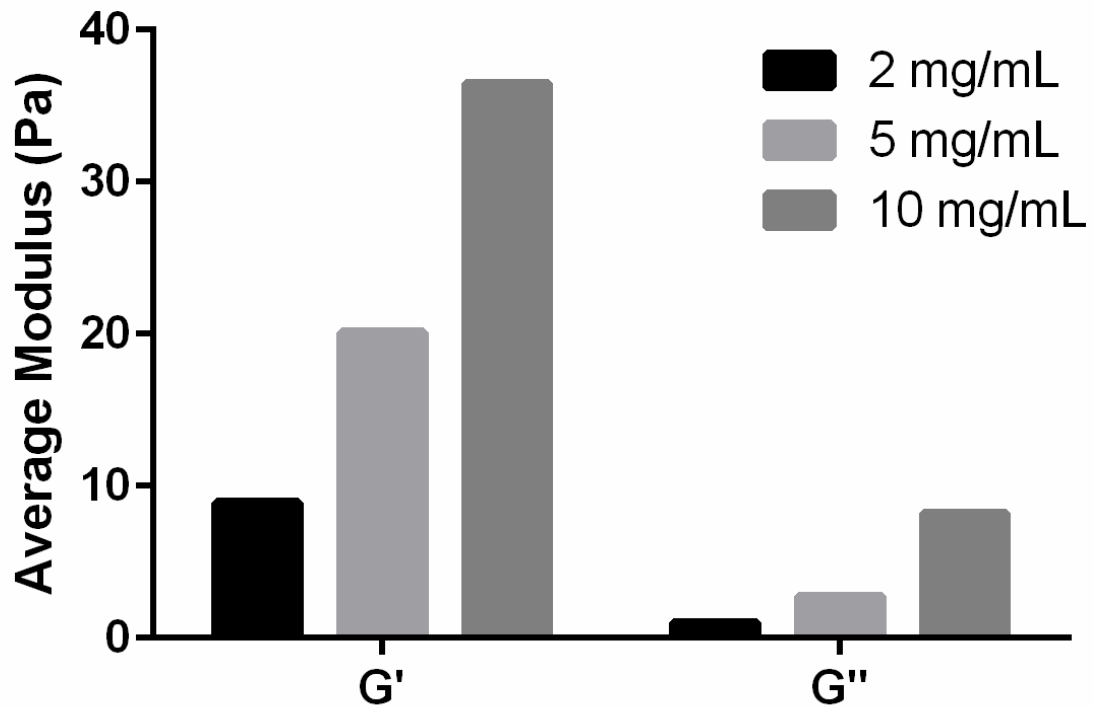
2 mg/mL



10 mg/mL

Appendix Figure 20 Follicle Quantification Using Volocity Software

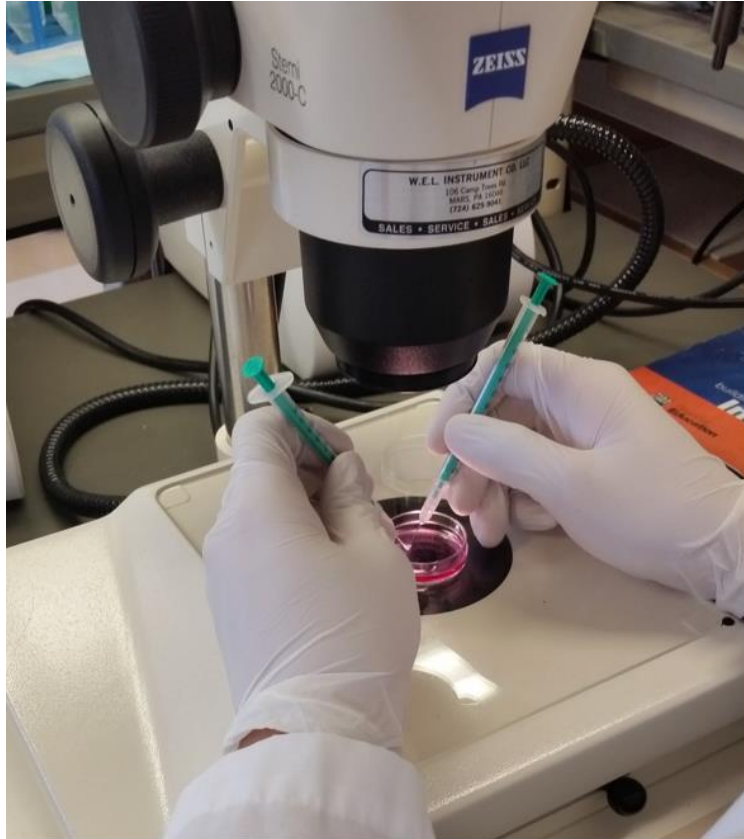
Hydrogel Viscoelastic Properties



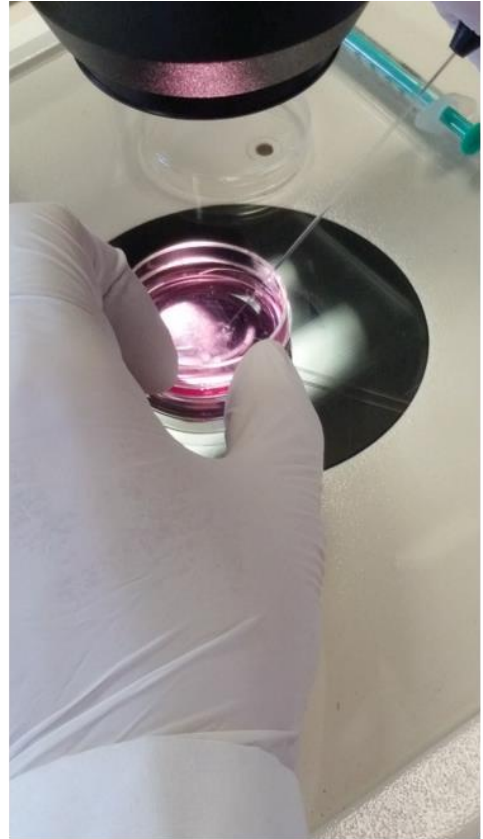
Appendix Figure 21 Viscoelastic Properties of OECM Hydrogel for Ovary Culture

The initial protocol used to decellularize ovarian tissues resulted in residual detergents within the scaffold and negatively impacted the viscoelastic properties (shown here). The revised protocol, which added wash steps, significantly improved the mechanical stiffness of the OECM hydrogels.

Appendix K *In Vitro* Mouse Follicle Cultures

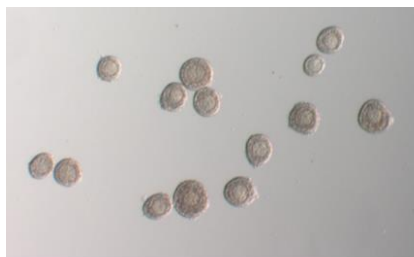


Mechanically dissociate follicles from day 16 female mice



Micropipette pre-antral follicles into fresh media

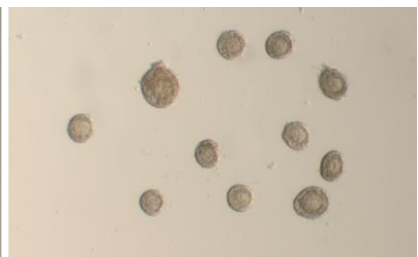
Appendix Figure 22 Mechanical Follicle Isolation for IVM



Mouse 1

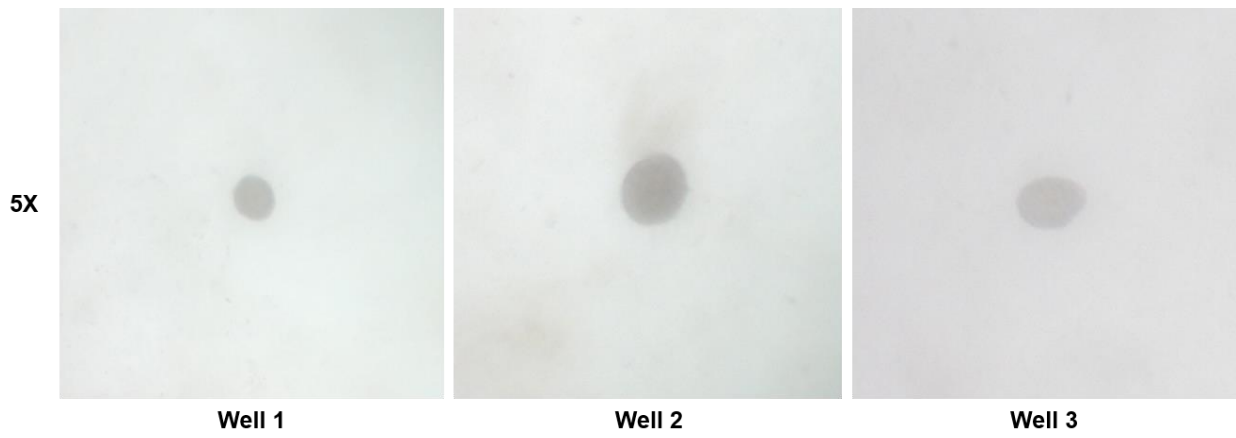


Mouse 2

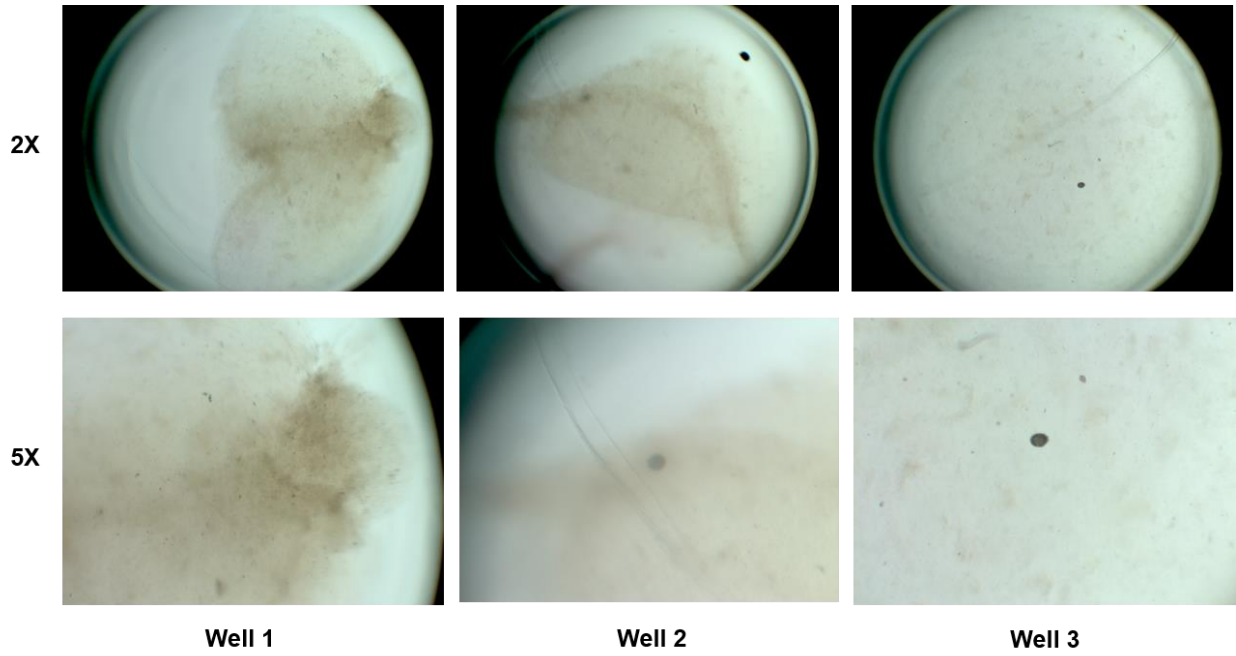


Mouse 3

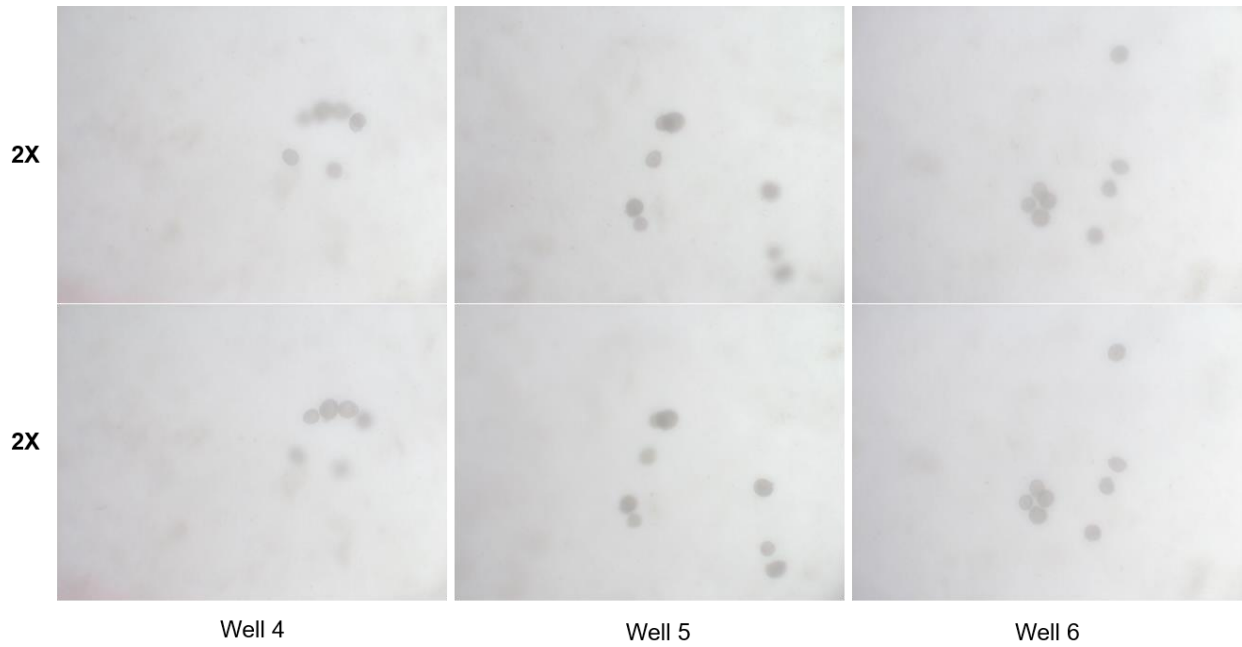
Appendix Figure 23 IVM Trial 1 – Isolated Follicles



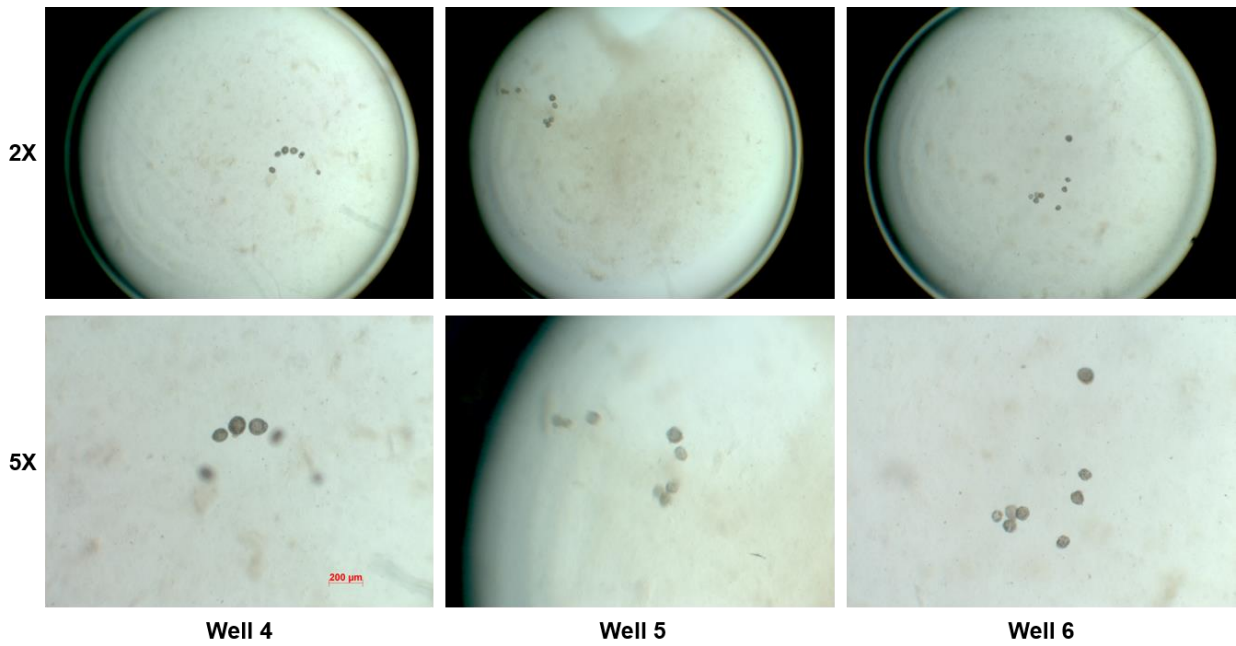
Appendix Figure 24 OECM-IVM Trial 1 - Single Follicle – Day 1



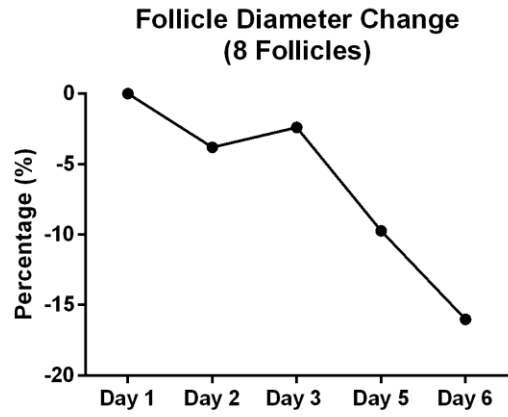
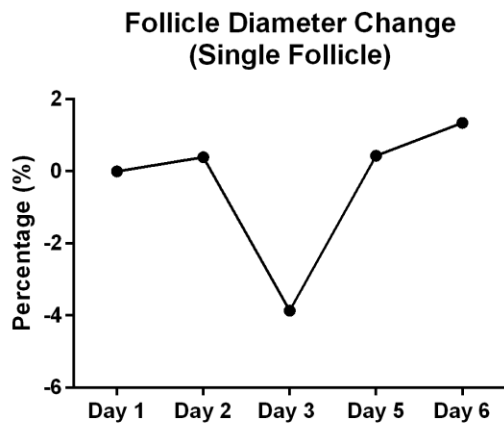
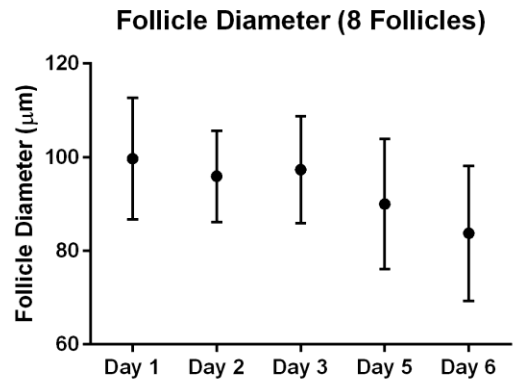
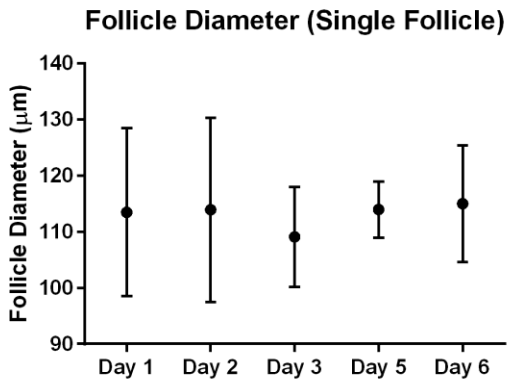
Appendix Figure 25 OECM-IVM Trial 1 – Single Follicle – Day 6



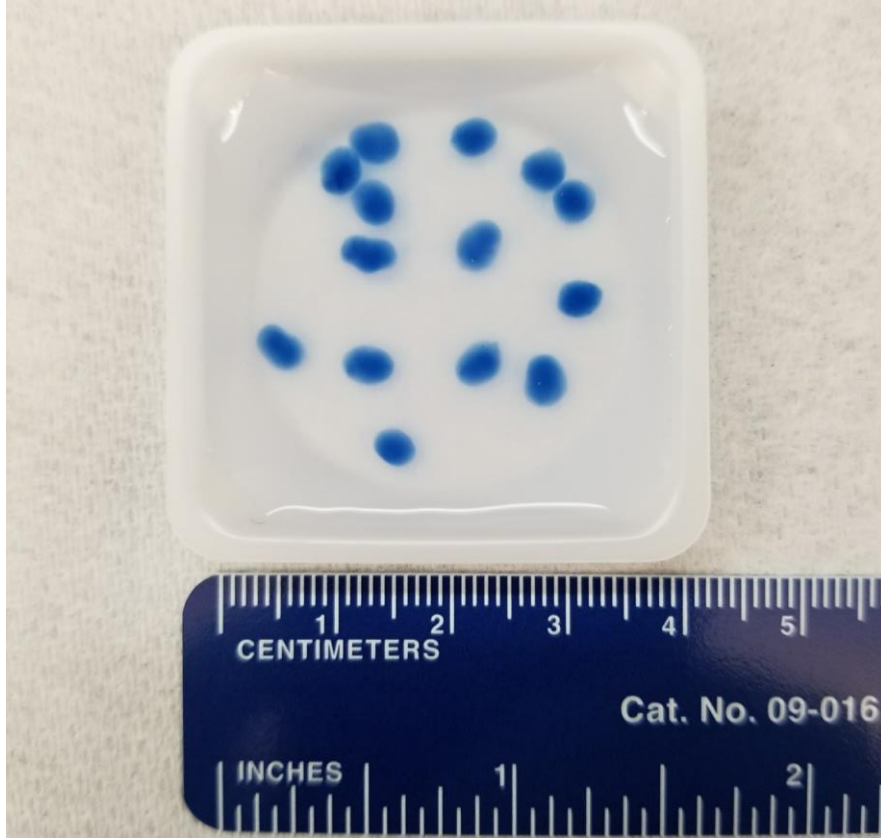
Appendix Figure 26 OECM-IVM Trial 1 – Grouped Follicles - Day 1



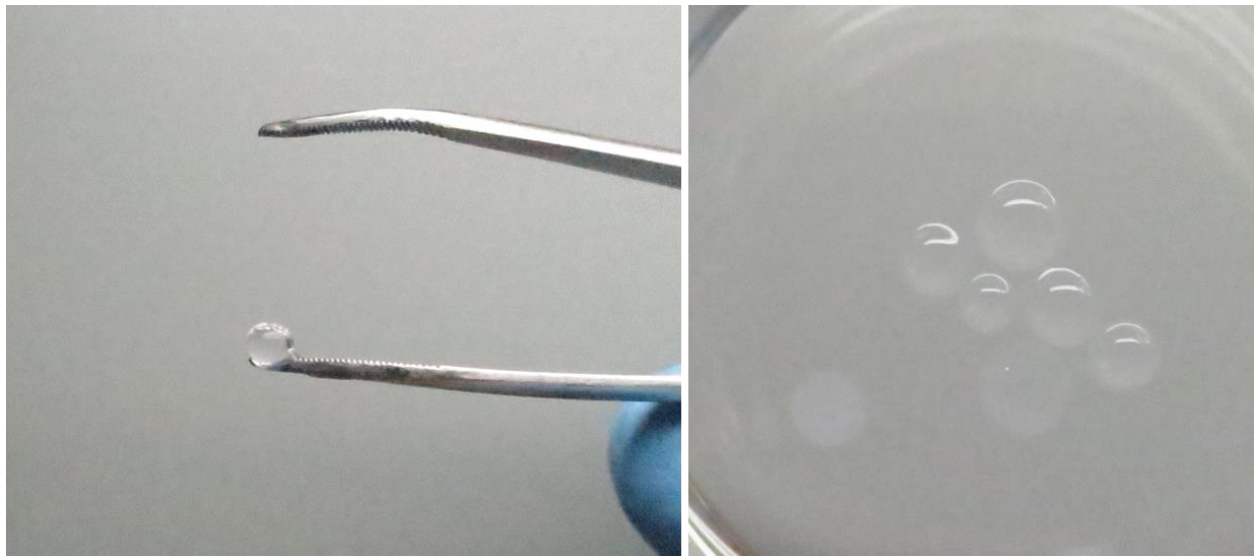
Appendix Figure 27 OECM-IVM Trial 1 – Grouped Follicles – Day 6



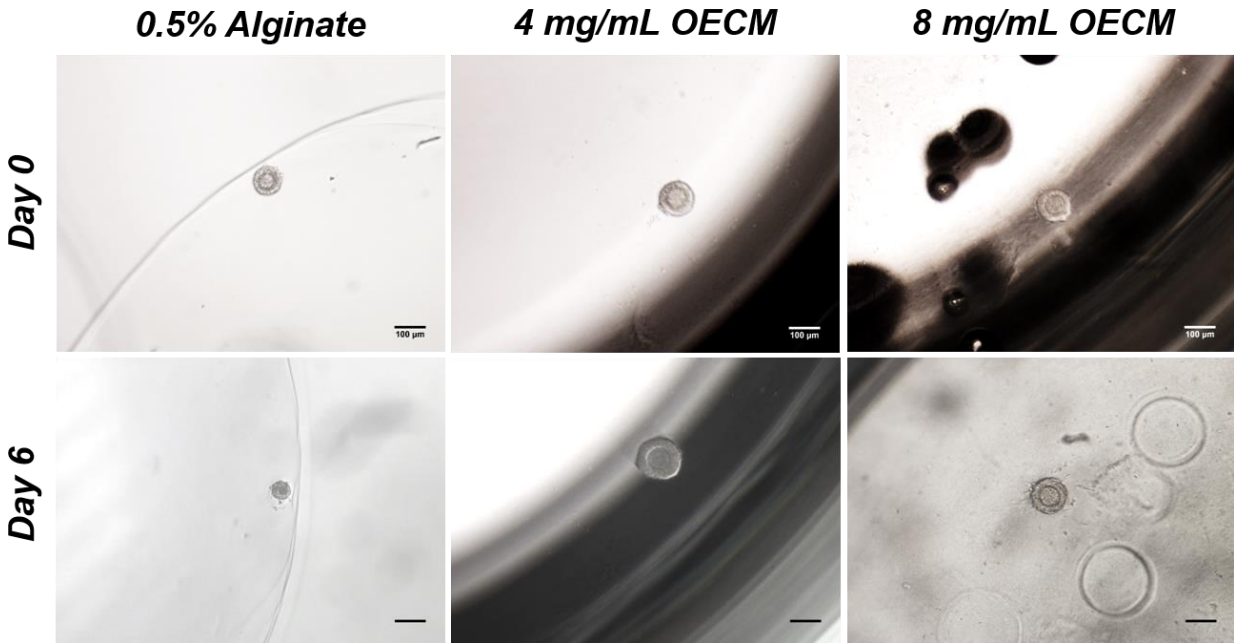
Appendix Figure 28 OECM-IVM Trial 1 – Follicle Diameter



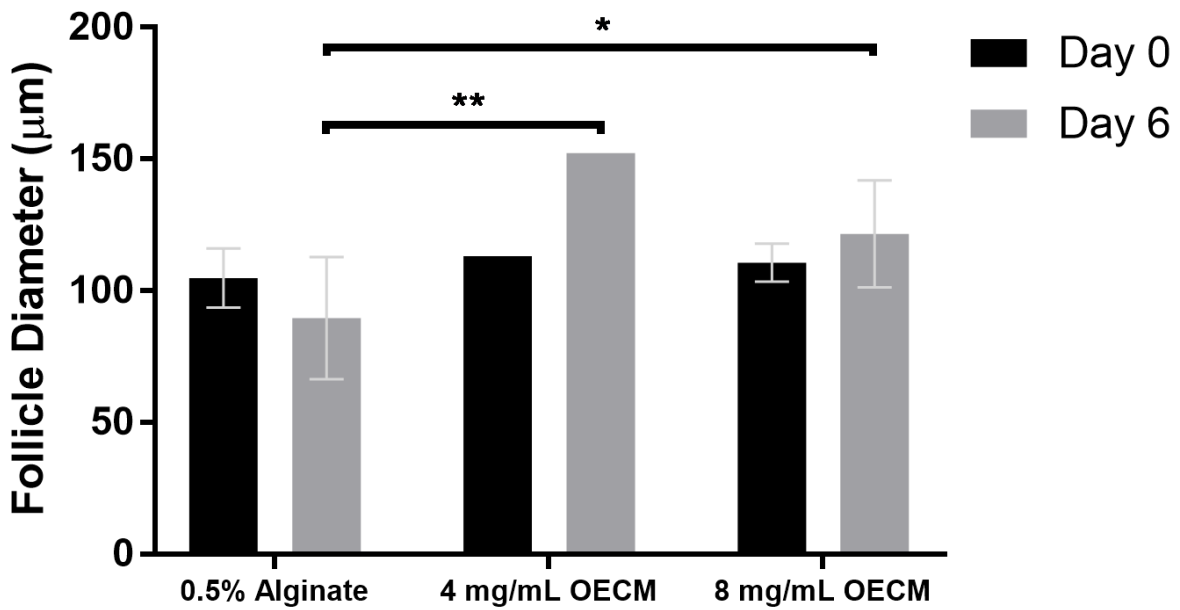
Appendix Figure 29 OECM Hydrogel Droplets



Appendix Figure 30 Alginate Microspheres



Appendix Figure 31 New OECM-IVM Trial 2 – Follicle Morphology

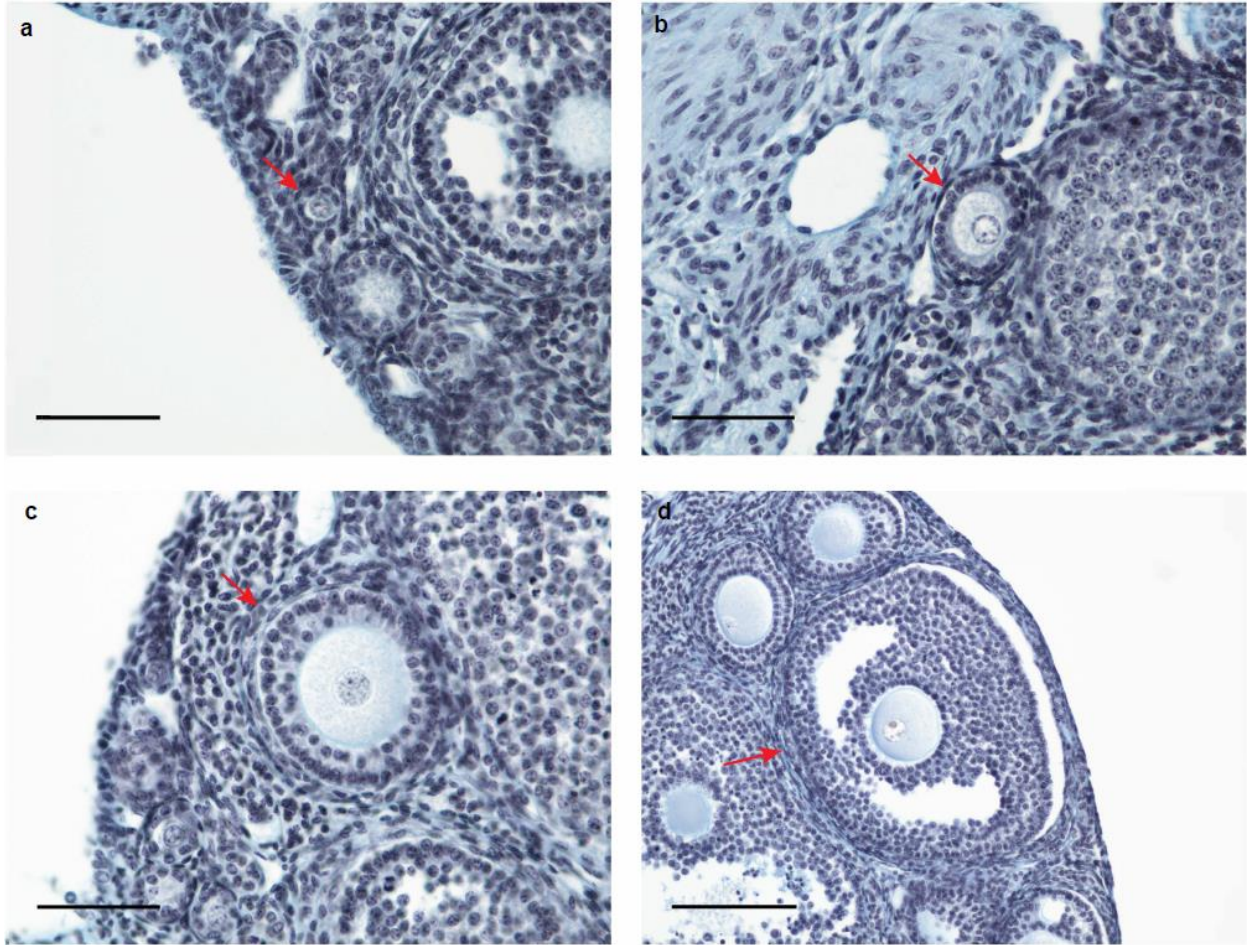


Appendix Figure 32 New OECM-IVM Trial 2 – Follicle Diameter

Appendix Table 4 In Vitro Follicle Culture Media

Dissection Media	Maintenance Media	Growth Media	Maturation Media
L-15 (Leibovitz's Media)	α -MEM (with Glutamax)	α -MEM (with Glutamax)	α -MEM (with Glutamax)
0.5% Pen/Strep	0.5% Pen/Strep	Bovine Fetuin (1 mg/mL)	10% FBS
1% FBS	1% FBS	1X ITS	EGF (10 ng/mL)
		BSA (3 mg/mL)	hCG (1.5 IU/mL)
		Gonal-F (10 mIU/mL)	Gonal-F (10 mIU/mL)

Appendix L Ovarian Follicle Stage Determination



Appendix Figure 33 Morphological Characterization of Follicle Stage

Follicles were quantified and developmental stage was determined by their morphology a, Primordial follicles were recognized by a central oocyte surrounded by a single layer of squamous granulosa cells. Scale, 50 μm . b, Primary follicles were counted if they contained a single oocyte with a layer of cuboidal granulosa cells. Scale, 50 μm . c, Secondary follicles contained an oocyte with 2-4 layers of cuboidal granulosa cells. Scale, 50 μm . d, Antral follicles were distinguished by an oocyte with several layers of cuboidal granulosa cells containing pockets of antral fluid.

Scale, 100 μm . Red arrows indicate counted follicles.

Appendix M Follicle Quantification Post-Chemotherapy

Appendix Table 5 Follicle Counts Post-Chemotherapy

The table (below) lists the means (bold) and standard deviations (SD) of quantified follicles at each of the tested dosages (busulfan-cyclophosphamide mg/kg). Total and primordial follicle reductions were calculated as a percentage of the follicles present within healthy control mice.

Follicle Stage	Control (n =2)	12-100 (n = 5)	12-200 (n = 5)	24-100 (n = 4)	24-200 (n = 4)
Primordial	680.0	156.0	84.0	42.5	20.0
Primordial SD	169.7	25.1	67.3	44.3	27.1
Primary	160.0	50.0	48.0	22.5	5.0
Primary SD	14.1	22.4	44.4	9.6	5.8
Secondary	125.0	74.0	44.0	25.0	17.5
Secondary SD	7.1	35.8	39.1	12.9	15.0
Antral	35.0	30.0	24.0	22.5	15.0
Antral SD	21.2	15.8	11.4	5.0	12.9
Total	1000.0	310.0	200.0	112.5	57.5
Total SD	155.6	53.4	121.0	61.3	48.6
% Reduction (Total)		69.0%	80.0%	88.8%	94.3%
% Reduction (Primordial Follicles)		77.1%	87.6%	93.8%	97.1%

Appendix N Statistical Differences Comparing Chemotherapy Dose

Appendix Table 6 Dose-Dependent Statistical Differences in Follicle Counts

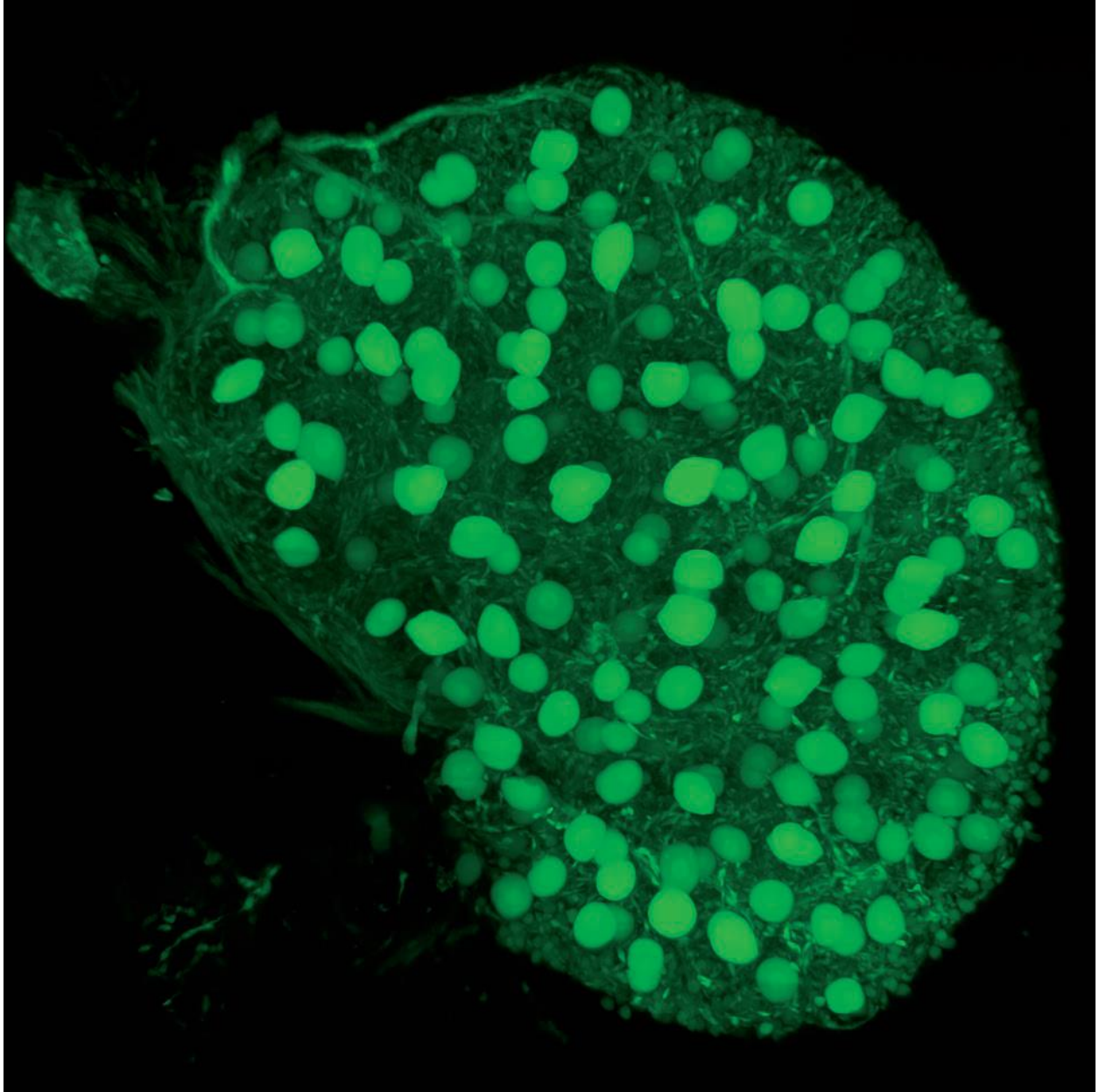
The table (below) displays statistical differences between follicle counts based upon chemotherapy treatment. One-way ANOVA with Tukey's multiple comparisons showed significant differences (highlighted in green) within each follicle stage and total follicles.

Follicle Stage	Group Comparison	Significant?	Summary	P-Value
Primordial	Control vs. 12-100	Yes	****	<0.0001
	Control vs. 24-100	Yes	****	<0.0001
	Control vs. 12-200	Yes	****	<0.0001
	Control vs. 24-200	Yes	****	<0.0001
	12-100 vs. 24-100	No	ns	0.0955
	12-100 vs. 12-200	No	ns	0.3891
	12-100 vs. 24-200	Yes	*	0.0352
	24-100 vs. 12-200	No	ns	0.8517
	24-100 vs. 24-200	No	ns	0.9846
	12-200 vs. 24-200	No	ns	0.5538
Primary	Control vs. 12-100	Yes	**	0.0013
	Control vs. 24-100	Yes	***	0.0002
	Control vs. 12-200	Yes	**	0.0011
	Control vs. 24-200	Yes	****	<0.0001
	12-100 vs. 24-100	No	ns	0.5468
	12-100 vs. 12-200	No	ns	>0.9999
	12-100 vs. 24-200	No	ns	0.1333
	24-100 vs. 12-200	No	ns	0.6133
	24-100 vs. 24-200	No	ns	0.8779
	12-200 vs. 24-200	No	ns	0.1611
Secondary	Control vs. 12-100	No	ns	0.2642
	Control vs. 24-100	Yes	**	0.0086
	Control vs. 12-200	Yes	*	0.03
	Control vs. 24-200	Yes	**	0.0048
	12-100 vs. 24-100	No	ns	0.1349
	12-100 vs. 12-200	No	ns	0.4933
	12-100 vs. 24-200	No	ns	0.0679
	24-100 vs. 12-200	No	ns	0.859
	24-100 vs. 24-200	No	ns	0.9957
	12-200 vs. 24-200	No	ns	0.6543

Appendix Table 6 (continued)

Follicle Stage	Group Comparison	Significant?	Summary	P-Value
Antral	Control vs. 12-100	No	ns	0.9899
	Control vs. 24-100	No	ns	0.7998
	Control vs. 12-200	No	ns	0.8471
	Control vs. 24-200	No	ns	0.4231
	12-100 vs. 24-100	No	ns	0.9076
	12-100 vs. 12-200	No	ns	0.9465
	12-100 vs. 24-200	No	ns	0.4535
	24-100 vs. 12-200	No	ns	0.9998
	24-100 vs. 24-200	No	ns	0.9222
	12-200 vs. 24-200	No	ns	0.8377
Total	Control vs. 12-100	Yes	****	<0.0001
	Control vs. 24-100	Yes	****	<0.0001
	Control vs. 12-200	Yes	****	<0.0001
	Control vs. 24-200	Yes	****	<0.0001
	12-100 vs. 24-100	Yes	*	0.0278
	12-100 vs. 12-200	No	ns	0.3087
	12-100 vs. 24-200	Yes	**	0.0045
	24-100 vs. 12-200	No	ns	0.5743
	24-100 vs. 24-200	No	ns	0.8932
	12-200 vs. 24-200	No	ns	0.1547

Appendix O Transgenic GFP Mouse Ovary



Appendix Figure 34 Tissue Cleared GFP Mouse Ovary

Appendix P Fluorescently Labeled Ovarian ECM Hydrogel



Non-labeled

1:20

1:10

Appendix Figure 35 TRITC-labeled Ovarian Hydrogel

Appendix Q Breeding Strategy and Outcomes Following Follicle Microinjection

Appendix Table 7 Breeding Strategy for Follicle Recipients

The table represents the potential breeding outcomes expected after intraovarian follicle microinjection. Genetic backgrounds may be derived from both endogenous and transplanted follicles. Pups born from the transplanted follicles were distinguished by GFP expression and/or fur with dark eyes.

		Female			
		Endogenous Nude Mouse Follicles		Transplanted GFP Mouse Follicles	
		Nu-	Nu-	DBA GFP+	DBA GFP-
Male	Nu-	NCR nu-/nu-: nude mice with red eyes	NCR nu-/nu-: nude mice with red eyes	GFP+/nu-: furry, dark eyes, glows green under UV	GFP-/nu-: furry, dark eyes, does not glow green
	Nu-	NCR nu-/nu-: nude mice with red eyes	NCR nu-/nu-: nude mice with red eyes	GFP+/nu-: furry, dark eyes, glows green under UV	GFP-/nu-: furry, dark eyes, does not glow green

Appendix Table 8 Breeding Outcomes of ciPOF Female Mice

Three cycles of breeding occurred with the transplanted ciPOF nude (nu-/nu-) female mice mated to nude (nu-/nu-) male mice. Three GFP pups were born as a result of the follicle transplantation. Non-injected control ciPOF mice are highlighted in red. Pups generated from the follicle transplant were bred to determine reproductive health.

Chemotherapy Dose	Animal ID	Cycle #1			Cycle #2			Cycle #3			Total Pups	Total GFP
		Live	Dead	GFP	Live	Dead	GFP	Live	Dead	GFP		
12-100	6194	4	0	0	0	0	0	0	0	0	4	0
	6195	2	4	0	3	0	0	5	0	1	14	1
	6196	2	0	0	1	4	0	0	0	0	7	0
	6197	0	0	0	3	0	0	6	0	0	9	0
	6198	0	0	0	0	0	0	0	0	0	0	0
12-200	6242	6	0	0	0	0	0	0	0	0	6	0
	6243	7	0	0	0	0	0	0	0	0	7	0
	6245	0	0	0	0	0	0	0	0	0	0	0
	6246	0	0	0	4	0	0	0	0	0	4	0
24-100	6237	0	0	0	0	0	0	0	0	0	0	0
	6238	3	0	1	1	0	1	0	0	0	4	2
	6240	11	0	0	5	0	0	0	0	0	16	0
	6241	0	0	0	0	0	0	0	0	0	0	0

Appendix Table 9 Outbreeding Strategy of GFP Progeny

Potential breeding outcomes shown for GFP/nu pups bred with DBA wild-type (GFP-/nu+) mice.

	GFP+/Nu+	GFP+/Nu-	GFP-/Nu+	GFP-/Nu-
GFP-/Nu+	GFP+/- Nu+/+	GFP+/- Nu+/-	GFP-/- Nu+/+	GFP-/- Nu+/-
GFP-/Nu+	GFP+/- Nu+/+	GFP+/- Nu+/-	GFP-/- Nu+/+	GFP-/- Nu+/-
GFP-/Nu+	GFP+/- Nu+/+	GFP+/- Nu+/-	GFP-/- Nu+/+	GFP-/- Nu+/-
GFP-/Nu+	GFP+/- Nu+/+	GFP+/- Nu+/-	GFP-/- Nu+/+	GFP-/- Nu+/-

Appendix Table 10 Inbreeding Strategy of GFP Progeny

Potential breeding outcomes shown for GFP/nu pups bred with GFP/nu pups. Cells outlined in red indicate nude offspring (nu-/nu-).

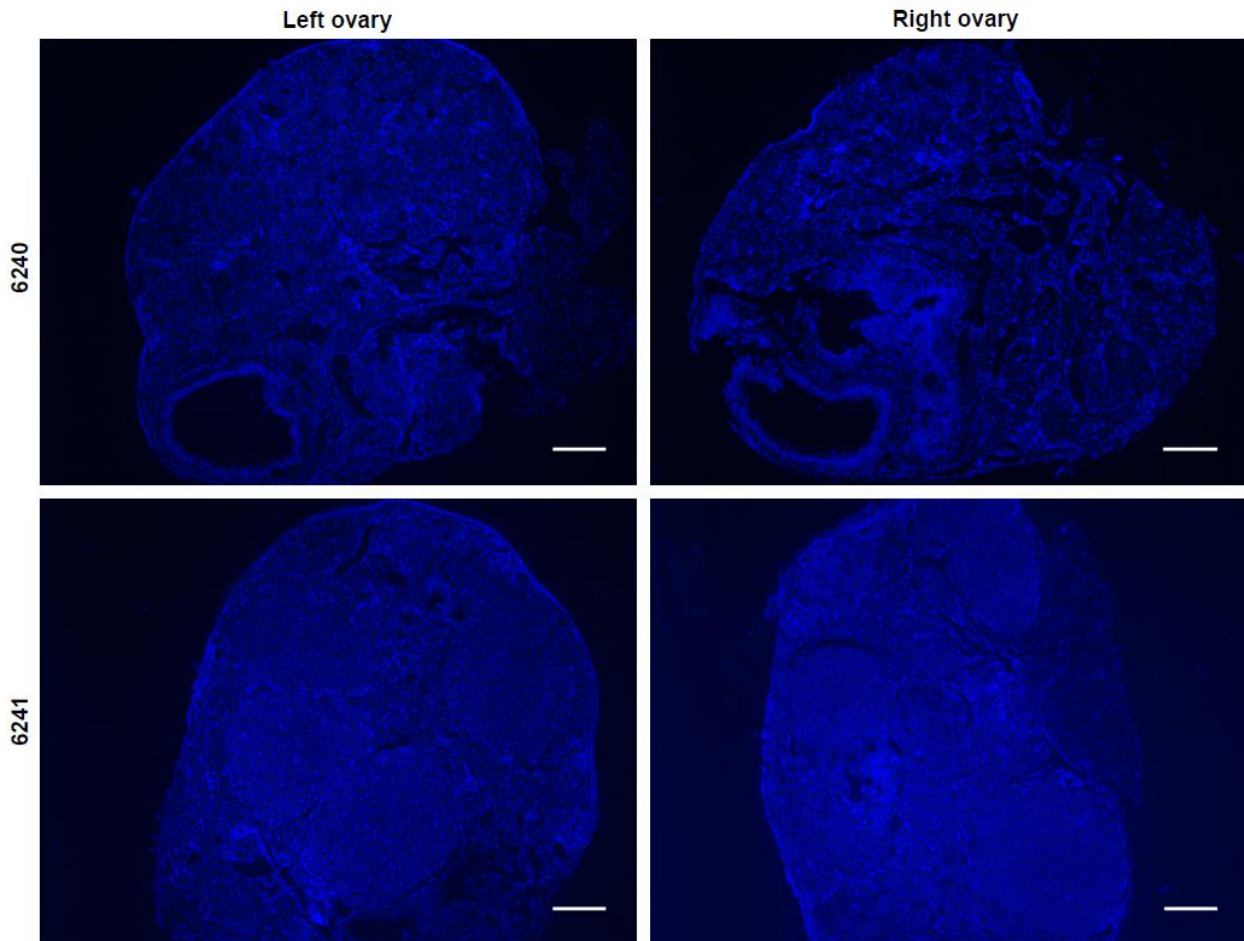
	GFP+/Nu+	GFP+/Nu-	GFP-/Nu+	GFP-/Nu-
GFP+/Nu+	GFP+/+ Nu+/+	GFP+/+ Nu+/-	GFP+/- Nu+/+	GFP+/- Nu+/-
GFP+/Nu-	GFP+/+ Nu+/-	GFP+/+ Nu-/-	GFP+/- Nu+/-	GFP+/- Nu-/-
GFP-/Nu+	GFP+/- Nu+/+	GFP+/- Nu+/-	GFP-/- Nu+/+	GFP-/- Nu+/-
GFP-/Nu-	GFP+/- Nu+/-	GFP+/- Nu-/-	GFP-/- Nu+/-	GFP-/- Nu-/-

Appendix Table 11 Second Generation Breeding Outcomes

Multiple breeding cycles with the follicle-transplant derived GFP mice resulted in a total of 43 second generation pups.

Animal ID	Breeding Partner ID	Cycle	Live	Dead	GFP
GFP/nu-001 (F)	DBA - 1683 (M)	1	10	0	5
	GFP/nu-003 (M)	2	8	1	6
GFP/nu-002 (F)	GFP/nu-003 (M)	1	10	0	9
	DBA - 1684 (M)	2	0	0	0
DBA/2-1644 (F)	B6D2 - 853 (M)	1	11	0	0
	GFP/nu-003 (M)	2	8	0	6
	GFP/nu-003 (M)	3	7	0	3
Total Second Generation Pups			43	1	29

Appendix R Control Non-Injected ciPOF Ovaries

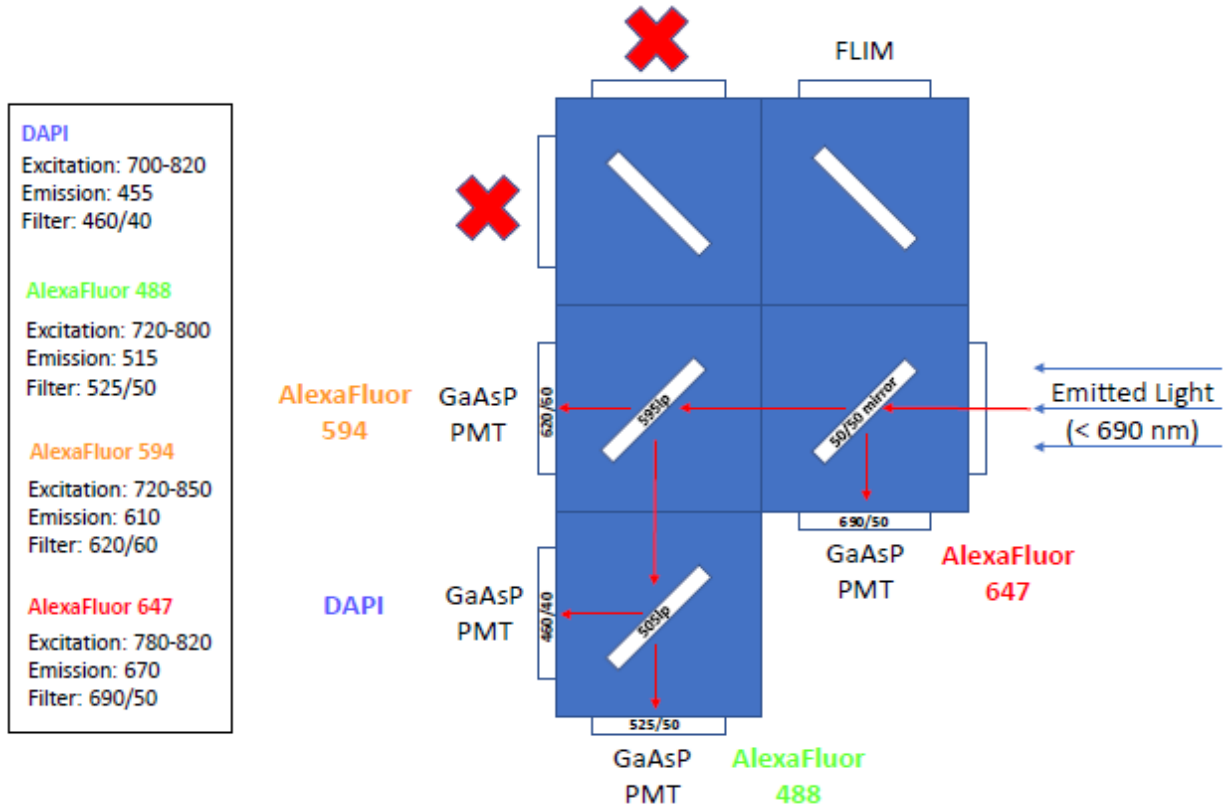


Appendix Figure 36 Immunofluorescence of Control ciPOF Ovaries

Merged DAPI and FITC immunofluorescence images of control ovaries (Animal ID: 6240 and 6241) Scale, 200 μ m.

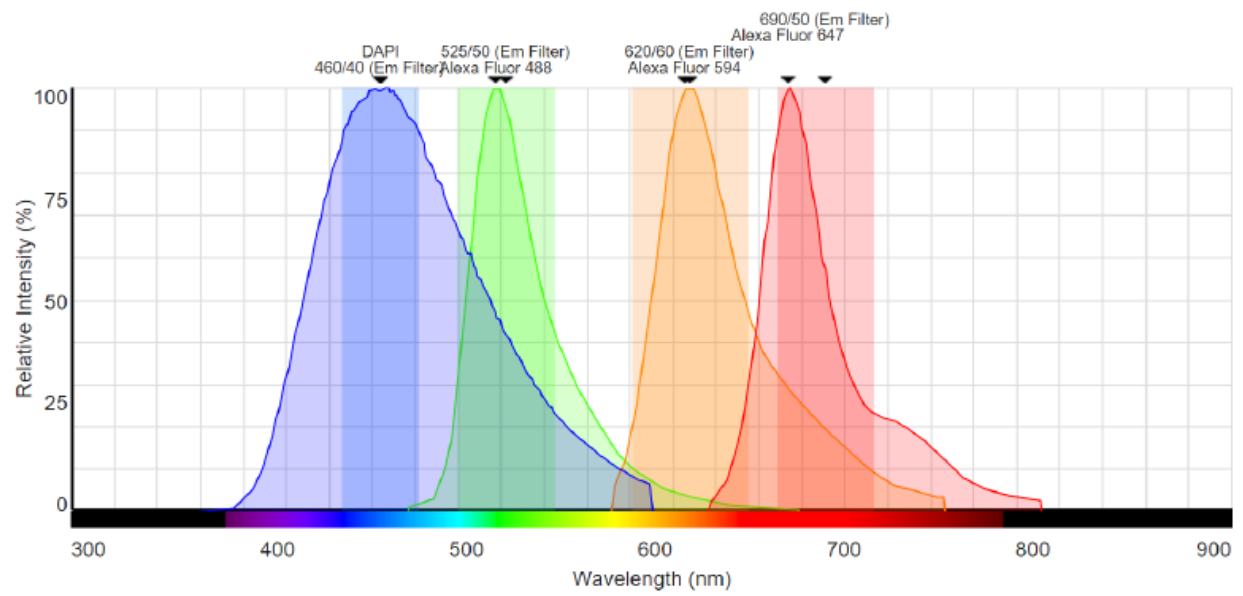
Non-injected control tissues showed endogenous follicle growth, but appeared to have a reduced population of immature follicles in comparison to ovaries that received follicle transplant. As expected, no cells within the control tissues expressed GFP.

Appendix S Two-Photon Imaging



Appendix Figure 37 Two-Photon Filter Cube Design

A future direction for the characterization of the ovarian microenvironment post-follicle microinjection would be to use tissue clearing with two-photon microscopy. Methods were being developed to establish a custom filter cube for the detection of four distinct fluorochemicals tagged to ovarian-specific antibodies.



Appendix Figure 38 Two-Photon Excitation and Emission Wavelengths/Filters

Appendix T Ovarian Flow Cytometry

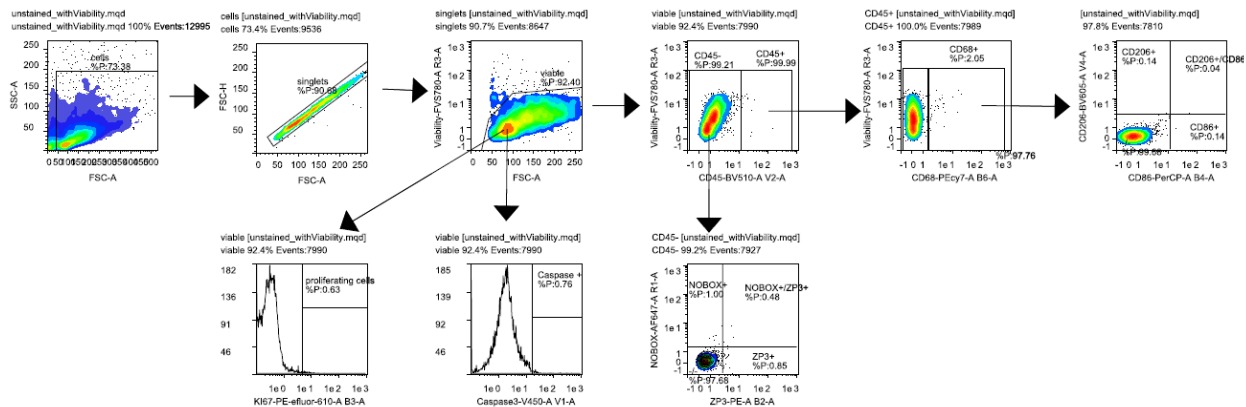
Appendix Table 12 Ovarian Flow Panel

Purpose: To evaluate and characterize cell population dynamics within the ovary in response to treatment

Populations

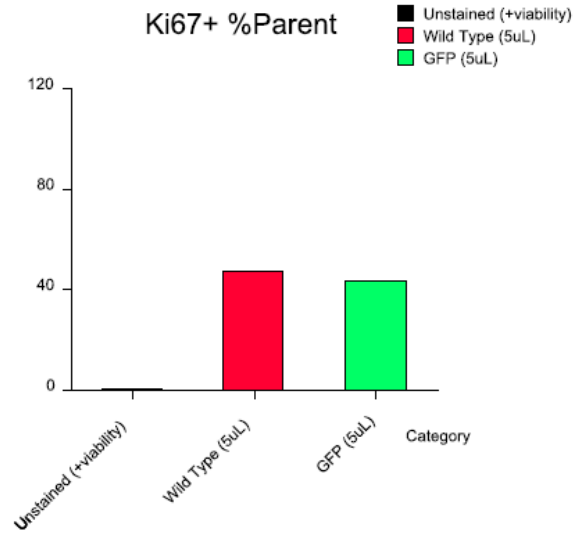
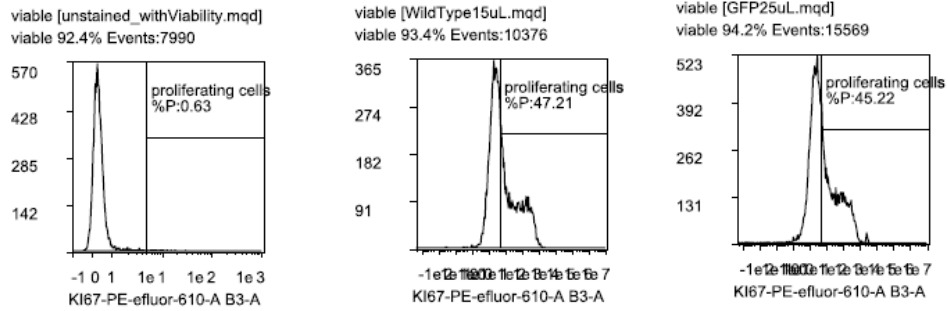
1. Viable Cells (Viability Dye)
2. Proliferating (ki67) and Apoptotic (Caspase3) Cells
3. Immune Response:
 - CD45 (Leukocytes)
 - CD68 (Macrophages)
 - CD86 (M1 Macs)
 - CD206 (M2 Macs)
4. Oocytes (NOBOX and Zp3)
5. Transplanted Cells (GFP+ Cells)

Channel	Marker	Cell Type	Antibody	Marker Expression
V1	Caspase-3	Apoptotic cells	Caspase-3-V450	Intracellular
V2	CD45	Leukocytes	BV510	Extracellular
V3				
V4	CD206	M2 Macs	CD206-BV605	Extracellular
V5				
B1	GFP	GFP+ cells	None (with compensation beads)	Ubiquitous
B2	Zp3	Oocytes	Zp3-PE	Extracellular
B3	ki67	Proliferating cells	ki67 PE-eFluor 610	Intracellular
B4	CD86	M1 Macs	PerCP	Extracellular
B5				
B6	CD68	Macrophages	PE/Cy7	Extracellular
R1	NOBOX	Oocytes	AF 647	Intracellular
R2				
R3	Viability	Viability	Fixable Viability Stain 780	Intracellular

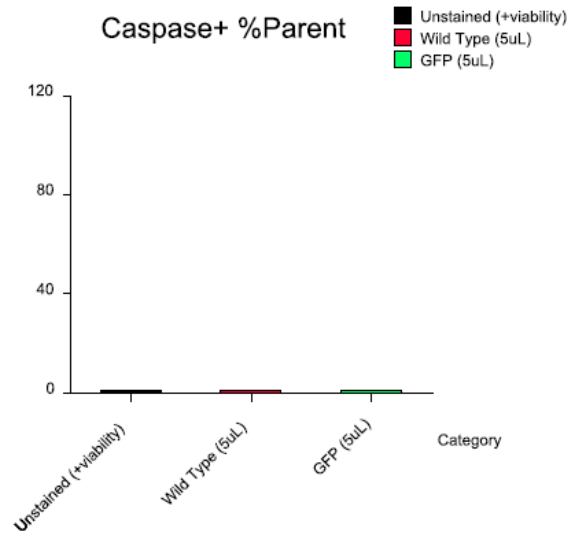
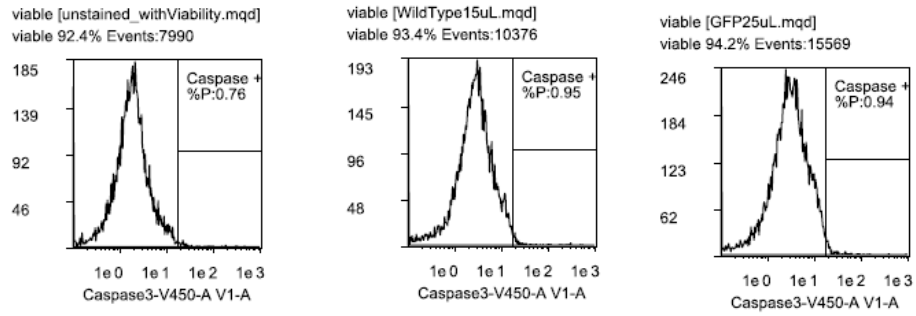


Appendix Figure 39 Ovarian Flow Gating Strategy

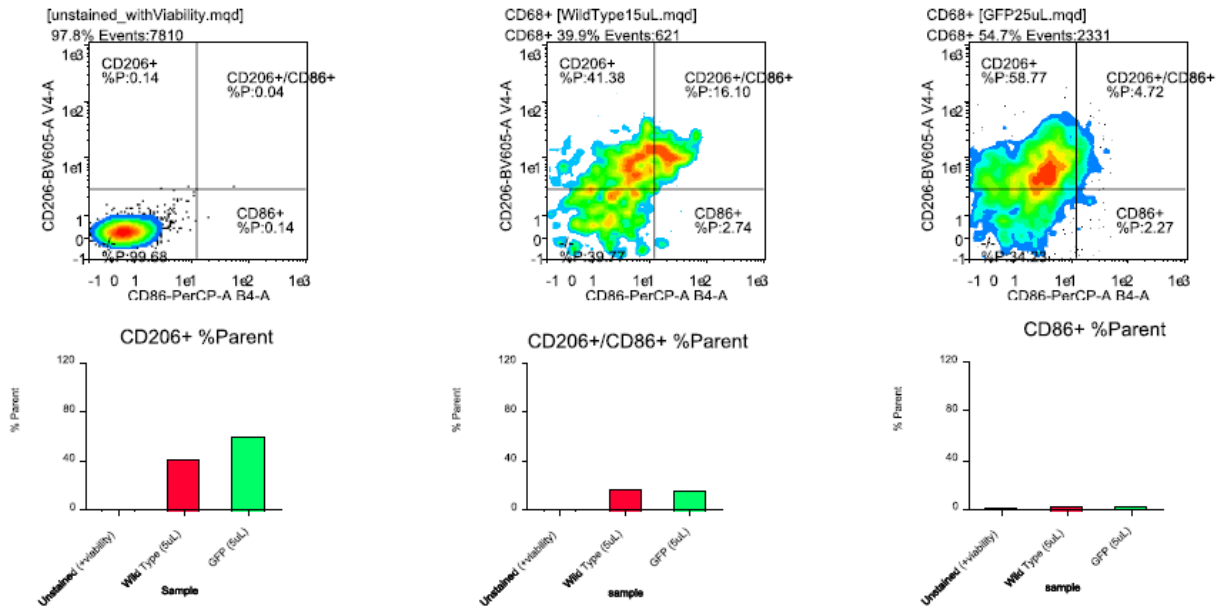
A flow panel and intracellular staining protocol was established to detect changes within the ovary post-follicle transplant to further characterize the tissue response after treatment.



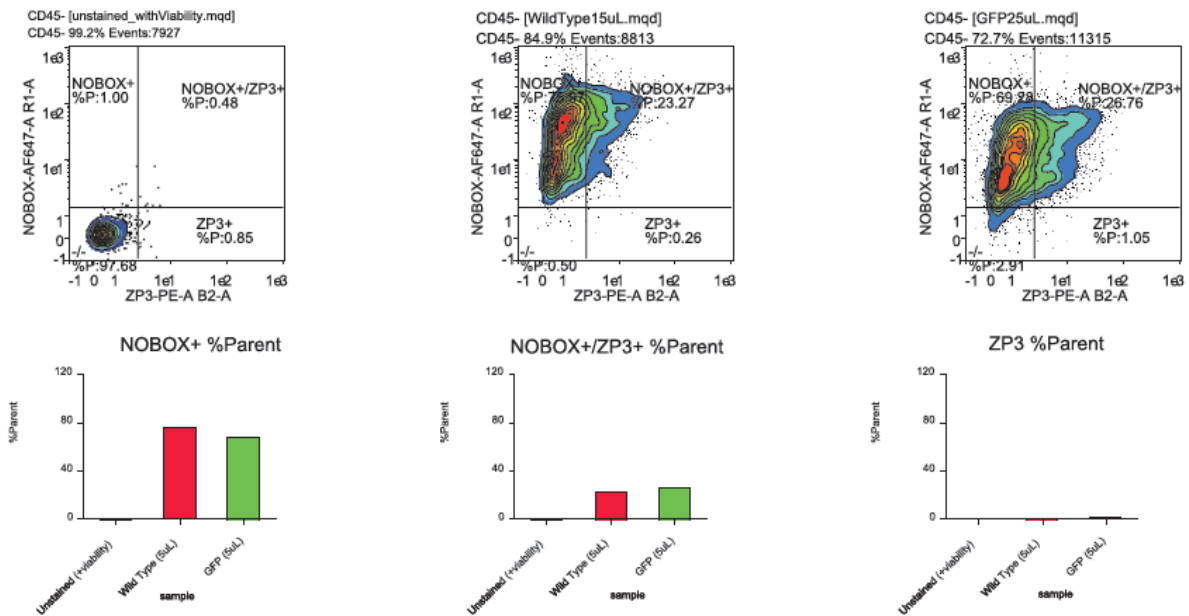
Appendix Figure 40 Proliferative Cells (Ki67+ Cells)



Appendix Figure 41 Percentage of Apoptotic Cells (Caspase3+ Cells)



Appendix Figure 42 Percentage of Macrophage Populations (CD206+ and CD86+ Cells)



Appendix Figure 43 Percentage of Oocytes (NOBOX+ and Zp3+ cells)

Bibliography

1. R. E. Jones, K. H. Lopez, in *Human Reproductive Biology (Fourth Edition)*, R. E. Jones, K. H. Lopez, Eds. (Academic Press, San Diego, 2014), pp. 23-50.
2. T. K. Woodruff, L. D. Shea, The role of the extracellular matrix in ovarian follicle development. *Reprod Sci* **14**, 6-10 (2007).
3. A. G. Byskov, Differentiation of mammalian embryonic gonad. *Physiological reviews* **66**, 71-117 (1986).
4. M. A. Edson, A. K. Nagaraja, M. M. Matzuk, The mammalian ovary from genesis to revelation. *Endocrine reviews* **30**, 624-712 (2009).
5. J. B. Kerr, M. Myers, R. A. Anderson, The dynamics of the primordial follicle reserve. *Reproduction* **146**, R205-215 (2013).
6. C. Thomas-Teinturier *et al.*, Ovarian reserve after treatment with alkylating agents during childhood. *Hum Reprod* **30**, 1437-1446 (2015).
7. W. H. Wallace, T. W. Kelsey, Human ovarian reserve from conception to the menopause. *PloS one* **5**, e8772 (2010).
8. M. A. Wood, A. Rajkovic, Genomic markers of ovarian reserve. *Semin Reprod Med* **31**, 399-415 (2013).
9. J. S. Richards, The Ovarian Cycle. *Vitamins and hormones* **107**, 1-25 (2018).
10. J. Rojas *et al.*, Physiologic Course of Female Reproductive Function: A Molecular Look into the Prologue of Life. *J Pregnancy* **2015**, 715735-715735 (2015).
11. J. Buratini, C. A. Price, Follicular somatic cell factors and follicle development. *Reproduction, fertility, and development* **23**, 32-39 (2011).
12. E. A. McGee, A. J. Hsueh, Initial and cyclic recruitment of ovarian follicles. *Endocrine reviews* **21**, 200-214 (2000).
13. G. W. Bates, M. Bowling, Physiology of the female reproductive axis. *Periodontol 2000* **61**, 89-102 (2013).
14. N. Chabbert Buffet, C. Djakoure, S. C. Maitre, P. Bouchard, Regulation of the human menstrual cycle. *Frontiers in neuroendocrinology* **19**, 151-186 (1998).
15. P. Limonta *et al.*, GnRH in the Human Female Reproductive Axis. *Vitamins and hormones* **107**, 27-66 (2018).

16. K. Hummitzsch *et al.*, A new model of development of the mammalian ovary and follicles. *PloS one* **8**, e55578 (2013).
17. N. A. Hanley *et al.*, SRY, SOX9, and DAX1 expression patterns during human sex determination and gonadal development. *Mechanisms of development* **91**, 403-407 (2000).
18. R. E. Jones, K. H. Lopez, in *Human Reproductive Biology*. (Elsevier, Elsevier Books, 2014), chap. 5, pp. 87-102.
19. D. Wilhelm, J. X. Yang, P. Thomas, Mammalian sex determination and gonad development. *Current topics in developmental biology* **106**, 89-121 (2013).
20. T. DeFalco, B. Capel, Gonad morphogenesis in vertebrates: divergent means to a convergent end. *Annual review of cell and developmental biology* **25**, 457-482 (2009).
21. R. E. Jones, K. H. Lopez, in *Human Reproductive Biology (Fourth Edition)*, R. E. Jones, K. H. Lopez, Eds. (Academic Press, San Diego, 2014), pp. 87-102.
22. S. Eggers, A. Sinclair, Mammalian sex determination—insights from humans and mice. *Chromosome research : an international journal on the molecular, supramolecular and evolutionary aspects of chromosome biology* **20**, 215-238 (2012).
23. P. M. Motta, S. Makabe, S. A. Nottola, The ultrastructure of human reproduction. I. The natural history of the female germ cell: origin, migration and differentiation inside the developing ovary. *Hum Reprod Update* **3**, 281-295 (1997).
24. H. Stoop *et al.*, Differentiation and development of human female germ cells during prenatal gonadogenesis: an immunohistochemical study. *Hum Reprod* **20**, 1466-1476 (2005).
25. A. M. Heeren *et al.*, Development of the follicular basement membrane during human gametogenesis and early folliculogenesis. *BMC developmental biology* **15**, 4 (2015).
26. I. Konishi, S. Fujii, H. Okamura, T. Parmley, T. Mori, Development of interstitial cells and ovigerous cords in the human fetal ovary: an ultrastructural study. *Journal of anatomy* **148**, 121-135 (1986).
27. R. A. Anderson, N. Fulton, G. Cowan, S. Coutts, P. T. Saunders, Conserved and divergent patterns of expression of DAZL, VASA and OCT4 in the germ cells of the human fetal ovary and testis. *BMC developmental biology* **7**, 136 (2007).
28. A. Bukovsky *et al.*, Oogenesis in adult mammals, including humans: a review. *Endocrine* **26**, 301-316 (2005).
29. K. Jagarlamudi, A. Rajkovic, Oogenesis: transcriptional regulators and mouse models. *Mol Cell Endocrinol* **356**, 31-39 (2012).

30. M. E. Pepling, Follicular assembly: mechanisms of action. *Reproduction* **143**, 139-149 (2012).
31. J. A. Alberts B, Lewis J, et al., in *Molecular Biology of the Cell. 4th Edition*. (Garland Science, New York, 2002), chap. Meiosis.
32. J. A. Alberts B, Lewis J, et al., in *Molecular Biology of the Cell. 4th Edition*. (Garland Science, New York, 2002), chap. Mitosis.
33. M. M. Viveiros, R. De La Fuente, in *The Ovary (Third Edition)*, P. C. K. Leung, E. Y. Adashi, Eds. (Academic Press, 2019), pp. 165-180.
34. J. A. Alberts B, Lewis J, et al., in *Molecular Biology of the Cell. 4th Edition*. (Garland Science, New York, 2002), chap. An Overview of the Cell Cycle.
35. J. A. Alberts B, Lewis J, et al., in *Molecular Biology of the Cell. 4th Edition*. (Garland Science, New York, 2002), chap. Cytokinesis.
36. J. J. Bromfield, R. L. Piersanti, in *The Ovary (Third Edition)*, P. C. K. Leung, E. Y. Adashi, Eds. (Academic Press, 2019), pp. 157-164.
37. M. Ginsburg, M. H. Snow, A. McLaren, Primordial germ cells in the mouse embryo during gastrulation. *Development (Cambridge, England)* **110**, 521-528 (1990).
38. K. Molyneaux, C. Wylie, Primordial germ cell migration. *The International journal of developmental biology* **48**, 537-544 (2004).
39. H. Peters, The development of the mouse ovary from birth to maturity. *Acta endocrinologica* **62**, 98-116 (1969).
40. X. Wu *et al.*, Zygote arrest 1 (Zar1) is a novel maternal-effect gene critical for the oocyte-to-embryo transition. *Nature genetics* **33**, 187-191 (2003).
41. Z. B. Tong *et al.*, Mater, a maternal effect gene required for early embryonic development in mice. *Nature genetics* **26**, 267-268 (2000).
42. H. J. Leese, Metabolic control during preimplantation mammalian development. *Hum Reprod Update* **1**, 63-72 (1995).
43. C. M. Dalton, J. Carroll, Biased inheritance of mitochondria during asymmetric cell division in the mouse oocyte. *Journal of cell science* **126**, 2955-2964 (2013).
44. Y. Yu, R. Dumollard, A. Rossbach, F. A. Lai, K. Swann, Redistribution of mitochondria leads to bursts of ATP production during spontaneous mouse oocyte maturation. *J Cell Physiol* **224**, 672-680 (2010).
45. K. Swann, Y. Yu, The dynamics of calcium oscillations that activate mammalian eggs. *The International journal of developmental biology* **52**, 585-594 (2008).

46. T. Ducibella, R. Fissore, The roles of Ca²⁺, downstream protein kinases, and oscillatory signaling in regulating fertilization and the activation of development. *Developmental biology* **315**, 257-279 (2008).
47. O. Yoshino, H. E. McMahon, S. Sharma, S. Shimasaki, A unique preovulatory expression pattern plays a key role in the physiological functions of BMP-15 in the mouse. *Proceedings of the National Academy of Sciences of the United States of America* **103**, 10678-10683 (2006).
48. K. J. Hutt, D. F. Albertini, An oocentric view of folliculogenesis and embryogenesis. *Reproductive biomedicine online* **14**, 758-764 (2007).
49. G. F. Erickson, C. Wang, A. J. Hsueh, FSH induction of functional LH receptors in granulosa cells cultured in a chemically defined medium. *Nature* **279**, 336-338 (1979).
50. N. Dekel, Spatial relationship of follicular cells in the control of meiosis. *Progress in clinical and biological research* **267**, 87-101 (1988).
51. L. B. Josefsberg *et al.*, Maturation-promoting factor governs mitogen-activated protein kinase activation and interphase suppression during meiosis of rat oocytes. *Biology of reproduction* **68**, 1282-1290 (2003).
52. A. Tsafiriri, S. Y. Chun, R. Zhang, A. J. Hsueh, M. Conti, Oocyte maturation involves compartmentalization and opposing changes of cAMP levels in follicular somatic and germ cells: studies using selective phosphodiesterase inhibitors. *Developmental biology* **178**, 393-402 (1996).
53. T. R. Coleman, W. G. Dunphy, Cdc2 regulatory factors. *Current opinion in cell biology* **6**, 877-882 (1994).
54. M. Kanatsu-Shinohara, R. M. Schultz, G. S. Kopf, Acquisition of meiotic competence in mouse oocytes: absolute amounts of p34(cdc2), cyclin B1, cdc25C, and weel in meiotically incompetent and competent oocytes. *Biology of reproduction* **63**, 1610-1616 (2000).
55. P. Marangos, J. Carroll, The dynamics of cyclin B1 distribution during meiosis I in mouse oocytes. *Reproduction* **128**, 153-162 (2004).
56. H. Rime *et al.*, Microinjection of Cdc25 protein phosphatase into *Xenopus* prophase oocyte activates MPF and arrests meiosis at metaphase I. *Biology of the cell* **82**, 11-22 (1994).
57. A. Hampl, J. J. Eppig, Analysis of the mechanism(s) of metaphase I arrest in maturing mouse oocytes. *Development (Cambridge, England)* **121**, 925-933 (1995).
58. E. Ledan, Z. Polanski, M. E. Terret, B. Maro, Meiotic maturation of the mouse oocyte requires an equilibrium between cyclin B synthesis and degradation. *Developmental biology* **232**, 400-413 (2001).

59. N. Rimon-Dahari, L. Yerushalmi-Heinemann, L. Alyagor, N. Dekel, Ovarian Folliculogenesis. *Results Probl Cell Differ* **58**, 167-190 (2016).
60. T. G. Baker, A QUANTITATIVE AND CYTOLOGICAL STUDY OF GERM CELLS IN HUMAN OVARIES. *Proceedings of the Royal Society of London. Series B, Biological sciences* **158**, 417-433 (1963).
61. S. K. Bristol-Gould *et al.*, Postnatal regulation of germ cells by activin: the establishment of the initial follicle pool. *Developmental biology* **298**, 132-148 (2006).
62. J. L. Tilly, Commuting the death sentence: how oocytes strive to survive. *Nature reviews. Molecular cell biology* **2**, 838-848 (2001).
63. J. B. Kerr *et al.*, DNA damage-induced primordial follicle oocyte apoptosis and loss of fertility require TAp63-mediated induction of Puma and Noxa. *Molecular cell* **48**, 343-352 (2012).
64. G. Livera *et al.*, p63 null mutation protects mouse oocytes from radio-induced apoptosis. *Reproduction* **135**, 3-12 (2008).
65. E. K. Suh *et al.*, p63 protects the female germ line during meiotic arrest. *Nature* **444**, 624-628 (2006).
66. H. Zhang *et al.*, Somatic cells initiate primordial follicle activation and govern the development of dormant oocytes in mice. *Current biology : CB* **24**, 2501-2508 (2014).
67. K. J. Hutt, E. A. McLaughlin, M. K. Holland, Kit ligand and c-Kit have diverse roles during mammalian oogenesis and folliculogenesis. *Molecular human reproduction* **12**, 61-69 (2006).
68. A. L. Durlinger *et al.*, Control of primordial follicle recruitment by anti-Müllerian hormone in the mouse ovary. *Endocrinology* **140**, 5789-5796 (1999).
69. H. Mizunuma *et al.*, Activin from secondary follicles causes small preantral follicles to remain dormant at the resting stage. *Endocrinology* **140**, 37-42 (1999).
70. J. K. Findlay *et al.*, in *The Ovary (Third Edition)*, P. C. K. Leung, E. Y. Adashi, Eds. (Academic Press, 2019), pp. 3-21.
71. J. S. Davis, H. A. LaVoie, in *The Ovary (Third Edition)*, P. C. K. Leung, E. Y. Adashi, Eds. (Academic Press, 2019), pp. 237-253.
72. G. F. Erickson, S. Shimasaki, The physiology of folliculogenesis: the role of novel growth factors. *Fertility and sterility* **76**, 943-949 (2001).
73. M. Soares *et al.*, The best source of isolated stromal cells for the artificial ovary: medulla or cortex, cryopreserved or fresh? *Hum Reprod* **30**, 1589-1598 (2015).

74. C. K. Hughes, J. L. Pate, in *The Ovary (Third Edition)*, P. C. K. Leung, E. Y. Adashi, Eds. (Academic Press, 2019), pp. 269-292.
75. H. M. Brown, D. L. Russell, Blood and lymphatic vasculature in the ovary: development, function and disease. *Hum Reprod Update* **20**, 29-39 (2014).
76. L. D. Shea, T. K. Woodruff, A. Shikanov, Bioengineering the ovarian follicle microenvironment. *Annu Rev Biomed Eng* **16**, 29-52 (2014).
77. A. Shikanov, M. Xu, T. K. Woodruff, L. D. Shea, A method for ovarian follicle encapsulation and culture in a proteolytically degradable 3 dimensional system. *J Vis Exp*, (2011).
78. R. P. Piprek, M. Kolasa, D. Podkowa, M. Kloc, J. Z. Kubiak, Transcriptional profiling validates involvement of extracellular matrix and proteinases genes in mouse gonad development. *Mechanisms of development* **149**, 9-19 (2018).
79. T. E. Curry, Jr., K. G. Osteen, The matrix metalloproteinase system: changes, regulation, and impact throughout the ovarian and uterine reproductive cycle. *Endocrine reviews* **24**, 428-465 (2003).
80. D. Aharoni, I. Meiri, R. Atzmon, I. Vlodaysky, A. Amsterdam, Differential effect of components of the extracellular matrix on differentiation and apoptosis. *Current biology : CB* **7**, 43-51 (1997).
81. K. Oktay, G. Karlikaya, O. Akman, G. K. Ojakian, M. Oktay, Interaction of extracellular matrix and activin-A in the initiation of follicle growth in the mouse ovary. *Biology of reproduction* **63**, 457-461 (2000).
82. M. Bortolussi *et al.*, Changes in the organization of the extracellular matrix in ovarian follicles during the preovulatory phase and atresia. An immunofluorescence study. *Basic and applied histochemistry* **33**, 31-38 (1989).
83. J. R. Figueiredo *et al.*, Extracellular matrix proteins and basement membrane: their identification in bovine ovaries and significance for the attachment of cultured preantral follicles. *Theriogenology* **43**, 845-858 (1995).
84. C. Huet, C. Pisselet, B. Mandon-Pépin, P. Monget, D. Monniaux, Extracellular matrix regulates ovine granulosa cell survival, proliferation and steroidogenesis: relationships between cell shape and function. *J Endocrinol* **169**, 347-360 (2001).
85. R. Rajah, G. S. Sundaram, Protein distribution and gene expression of collagen type IV in the neonatal rat ovary during follicle formation. *Cellular and molecular biology (Noisy-le-Grand, France)* **40**, 769-780 (1994).
86. Y. Zhao, M. R. Luck, Gene expression and protein distribution of collagen, fibronectin and laminin in bovine follicles and corpora lutea. *Journal of reproduction and fertility* **104**, 115-123 (1995).

87. R. A. Anderson, E. E. Telfer, Being a good egg in the 21st century. *British medical bulletin* **127**, 83-89 (2018).
88. Y. Chen, W. N. Jefferson, R. R. Newbold, E. Padilla-Banks, M. E. Pepling, Estradiol, progesterone, and genistein inhibit oocyte nest breakdown and primordial follicle assembly in the neonatal mouse ovary in vitro and in vivo. *Endocrinology* **148**, 3580-3590 (2007).
89. W. Y. Son, M. Das, E. Shalom-Paz, H. Holzer, Mechanisms of follicle selection and development. *Minerva Ginecol* **63**, 89-102 (2011).
90. H. M. Picton, S. E. Harris, W. Muruvi, E. L. Chambers, The in vitro growth and maturation of follicles. *Reproduction* **136**, 703-715 (2008).
91. O. Salha, N. Abusheikha, V. Sharma, Dynamics of human follicular growth and in-vitro oocyte maturation. *Human reproduction update* **4**, 816-832 (1998).
92. L. Mork *et al.*, Temporal differences in granulosa cell specification in the ovary reflect distinct follicle fates in mice. *Biology of reproduction* **86**, 37 (2012).
93. A. R. Baerwald, G. P. Adams, R. A. Pierson, Ovarian antral folliculogenesis during the human menstrual cycle: a review. *Hum Reprod Update* **18**, 73-91 (2012).
94. C. Liu, J. Peng, M. M. Matzuk, H. H. Yao, Lineage specification of ovarian theca cells requires multicellular interactions via oocyte and granulosa cells. *Nature communications* **6**, 6934 (2015).
95. J. F. Armstrong, K. Pritchard-Jones, W. A. Bickmore, N. D. Hastie, J. B. Bard, The expression of the Wilms' tumour gene, WT1, in the developing mammalian embryo. *Mechanisms of development* **40**, 85-97 (1993).
96. J. A. Kreidberg *et al.*, WT-1 is required for early kidney development. *Cell* **74**, 679-691 (1993).
97. E. E. Nilsson, M. K. Skinner, Bone morphogenetic protein-4 acts as an ovarian follicle survival factor and promotes primordial follicle development. *Biology of reproduction* **69**, 1265-1272 (2003).
98. W. S. Lee *et al.*, Effects of bone morphogenetic protein-7 (BMP-7) on primordial follicular growth in the mouse ovary. *Molecular reproduction and development* **69**, 159-163 (2004).
99. A. Kedem *et al.*, Activated ovarian endothelial cells promote early follicular development and survival. *Journal of ovarian research* **10**, 64-64 (2017).
100. N. Auersperg, A. S. Wong, K. C. Choi, S. K. Kang, P. C. Leung, Ovarian surface epithelium: biology, endocrinology, and pathology. *Endocrine reviews* **22**, 255-288 (2001).
101. A. Ng, N. Barker, Ovary and fimbrial stem cells: biology, niche and cancer origins. *Nature reviews. Molecular cell biology* **16**, 625-638 (2015).

102. W. J. Murdoch, A. C. McDonnell, Roles of the ovarian surface epithelium in ovulation and carcinogenesis. *Reproduction* **123**, 743-750 (2002).
103. R. Singavarapu, N. Buchinsky, D. J. Cheon, S. Orsulic, Whole ovary immunohistochemistry for monitoring cell proliferation and ovulatory wound repair in the mouse. *Reprod Biol Endocrinol* **8**, 98 (2010).
104. J. E. Burdette, S. J. Kurley, S. M. Kilen, K. E. Mayo, T. K. Woodruff, Gonadotropin-induced superovulation drives ovarian surface epithelia proliferation in CD1 mice. *Endocrinology* **147**, 2338-2345 (2006).
105. R. E. Jones, K. H. Lopez, in *Human Reproductive Biology (Fourth Edition)*, R. E. Jones, K. H. Lopez, Eds. (Academic Press, San Diego, 2014), pp. 51-66.
106. M. Mihm, S. Gangooly, S. Muttukrishna, The normal menstrual cycle in women. *Animal reproduction science* **124**, 229-236 (2011).
107. P. M. Conn, W. F. Crowley, Jr., Gonadotropin-releasing hormone and its analogs. *Annual review of medicine* **45**, 391-405 (1994).
108. F. Waldhauser, G. Weissenbacher, H. Frisch, A. Pollak, Pulsatile secretion of gonadotropins in early infancy. *European journal of pediatrics* **137**, 71-74 (1981).
109. J. L. Ross, D. L. Loriaux, G. B. Cutler, Jr., Developmental changes in neuroendocrine regulation of gonadotropin secretion in gonadal dysgenesis. *The Journal of clinical endocrinology and metabolism* **57**, 288-293 (1983).
110. J. K. Findlay, A. E. Drummond, Regulation of the FSH Receptor in the Ovary. *Trends Endocrinol Metab* **10**, 183-188 (1999).
111. P. K. Kreeger, N. N. Fernandes, T. K. Woodruff, L. D. Shea, Regulation of mouse follicle development by follicle-stimulating hormone in a three-dimensional in vitro culture system is dependent on follicle stage and dose. *Biology of reproduction* **73**, 942-950 (2005).
112. G. F. Erickson, D. A. Magoffin, C. A. Dyer, C. Hofeditz, The ovarian androgen producing cells: a review of structure/function relationships. *Endocrine reviews* **6**, 371-399 (1985).
113. K. Shrestha, D. Rodler, F. Sinowatz, R. Meidan, in *The Ovary (Third Edition)*, P. C. K. Leung, E. Y. Adashi, Eds. (Academic Press, 2019), pp. 255-267.
114. W. L. Miller, R. J. Auchus, The molecular biology, biochemistry, and physiology of human steroidogenesis and its disorders. *Endocrine reviews* **32**, 81-151 (2011).
115. J. F. Strauss, in *The Ovary (Third Edition)*, P. C. K. Leung, E. Y. Adashi, Eds. (Academic Press, 2019), pp. 83-94.
116. Y. M. Chan, J. P. Butler, V. F. Sidhoum, N. E. Pinnell, S. B. Seminara, Kisspeptin administration to women: a window into endogenous kisspeptin secretion and GnRH

- responsiveness across the menstrual cycle. *The Journal of clinical endocrinology and metabolism* **97**, E1458-1467 (2012).
117. J. J. Eppig, Oocyte control of ovarian follicular development and function in mammals. *Reproduction* **122**, 829-838 (2001).
 118. P. G. Knight, C. Glister, TGF-beta superfamily members and ovarian follicle development. *Reproduction* **132**, 191-206 (2006).
 119. J. Xu *et al.*, Anti-Müllerian hormone is produced heterogeneously in primate preantral follicles and is a potential biomarker for follicle growth and oocyte maturation in vitro. *Journal of assisted reproduction and genetics* **33**, 1665-1675 (2016).
 120. M. J. G. Gruijters, J. A. Visser, A. L. L. Durlinger, A. P. N. Themmen, Anti-Müllerian hormone and its role in ovarian function. *Molecular and cellular endocrinology* **211**, 85-90 (2003).
 121. S. L. P. Regan *et al.*, Involvement of Bone Morphogenetic Proteins (BMP) in the Regulation of Ovarian Function. *Vitamins and hormones* **107**, 227-261 (2018).
 122. K. A. Lawson *et al.*, Bmp4 is required for the generation of primordial germ cells in the mouse embryo. *Genes & development* **13**, 424-436 (1999).
 123. Y. Ying, G. Q. Zhao, Cooperation of endoderm-derived BMP2 and extraembryonic ectoderm-derived BMP4 in primordial germ cell generation in the mouse. *Developmental biology* **232**, 484-492 (2001).
 124. K. B. Lee *et al.*, Bone morphogenetic protein 2 and activin A synergistically stimulate follicle-stimulating hormone beta subunit transcription. *Journal of molecular endocrinology* **38**, 315-330 (2007).
 125. C. Glister, C. F. Kemp, P. G. Knight, Bone morphogenetic protein (BMP) ligands and receptors in bovine ovarian follicle cells: actions of BMP-4, -6 and -7 on granulosa cells and differential modulation of Smad-1 phosphorylation by follistatin. *Reproduction* **127**, 239-254 (2004).
 126. M. Khalaf *et al.*, BMP system expression in GCs from polycystic ovary syndrome women and the in vitro effects of BMP4, BMP6, and BMP7 on GC steroidogenesis. *European journal of endocrinology* **168**, 437-444 (2013).
 127. A. Pierre *et al.*, Molecular basis of bone morphogenetic protein-4 inhibitory action on progesterone secretion by ovine granulosa cells. *Journal of molecular endocrinology* **33**, 805-817 (2004).
 128. Y. T. Wu *et al.*, High bone morphogenetic protein-15 level in follicular fluid is associated with high quality oocyte and subsequent embryonic development. *Hum Reprod* **22**, 1526-1531 (2007).

129. G. Zhu *et al.*, Bone morphogenetic proteins (BMP) 2, 4, 6 and 7 affect ovarian follicular development through regulation of follicle-stimulating hormone receptor (FSHR) and luteinizing hormone receptor (LHR) expression in goat granulosa cells. *J Cell Biol Genet* **3**, 14-21 (2013).
130. S. Ogura-Nose *et al.*, Anti-Mullerian hormone (AMH) is induced by bone morphogenetic protein (BMP) cytokines in human granulosa cells. *Eur J Obstet Gynecol Reprod Biol* **164**, 44-47 (2012).
131. F. Otsuka, R. K. Moore, S. Shimasaki, Biological function and cellular mechanism of bone morphogenetic protein-6 in the ovary. *J Biol Chem* **276**, 32889-32895 (2001).
132. W. S. Lee, F. Otsuka, R. K. Moore, S. Shimasaki, Effect of bone morphogenetic protein-7 on folliculogenesis and ovulation in the rat. *Biology of reproduction* **65**, 994-999 (2001).
133. S. Shimasaki *et al.*, A functional bone morphogenetic protein system in the ovary. *Proceedings of the National Academy of Sciences of the United States of America* **96**, 7282-7287 (1999).
134. E. S. Feary *et al.*, Patterns of expression of messenger RNAs encoding GDF9, BMP15, TGFBR1, BMPR1B, and BMPR2 during follicular development and characterization of ovarian follicular populations in ewes carrying the Woodlands FecX2W mutation. *Biology of reproduction* **77**, 990-998 (2007).
135. K. Inagaki, S. Shimasaki, Impaired production of BMP-15 and GDF-9 mature proteins derived from proproteins WITH mutations in the proregion. *Mol Cell Endocrinol* **328**, 1-7 (2010).
136. F. Otsuka, S. Shimasaki, A novel function of bone morphogenetic protein-15 in the pituitary: selective synthesis and secretion of FSH by gonadotropes. *Endocrinology* **143**, 4938-4941 (2002).
137. M. M. Pulkki *et al.*, A covalently dimerized recombinant human bone morphogenetic protein-15 variant identifies bone morphogenetic protein receptor type 1B as a key cell surface receptor on ovarian granulosa cells. *Endocrinology* **153**, 1509-1518 (2012).
138. Y. Li *et al.*, Increased GDF9 and BMP15 mRNA levels in cumulus granulosa cells correlate with oocyte maturation, fertilization, and embryo quality in humans. *Reprod Biol Endocrinol* **12**, 81 (2014).
139. N. Kaivo-Oja *et al.*, Adenoviral gene transfer allows Smad-responsive gene promoter analyses and delineation of type I receptor usage of transforming growth factor-beta family ligands in cultured human granulosa luteal cells. *The Journal of clinical endocrinology and metabolism* **90**, 271-278 (2005).
140. J. Shi *et al.*, Growth differentiation factor 3 is induced by bone morphogenetic protein 6 (BMP-6) and BMP-7 and increases luteinizing hormone receptor messenger RNA expression in human granulosa cells. *Fertil Steril* **97**, 979-983 (2012).

141. S. Mazerbourg, P. Monget, Insulin-Like Growth Factor Binding Proteins and IGFBP Proteases: A Dynamic System Regulating the Ovarian Folliculogenesis. *Frontiers in endocrinology* **9**, 134 (2018).
142. A. V. Sirotkin, Growth factors controlling ovarian functions. *J Cell Physiol* **226**, 2222-2225 (2011).
143. E. Lorenzen, F. Follmann, G. Jungersen, J. S. Agerholm, A review of the human vs. porcine female genital tract and associated immune system in the perspective of using minipigs as a model of human genital Chlamydia infection. *Veterinary research* **46**, 116 (2015).
144. G. Bode *et al.*, The utility of the minipig as an animal model in regulatory toxicology. *Journal of pharmacological and toxicological methods* **62**, 196-220 (2010).
145. J. M. Goldman, A. S. Murr, R. L. Cooper, The rodent estrous cycle: characterization of vaginal cytology and its utility in toxicological studies. *Birth defects research. Part B, Developmental and reproductive toxicology* **80**, 84-97 (2007).
146. M. M. Swindle, A. Makin, A. J. Herron, F. J. Clubb, Jr., K. S. Frazier, Swine as models in biomedical research and toxicology testing. *Veterinary pathology* **49**, 344-356 (2012).
147. N. M. Soede, P. Langendijk, B. Kemp, Reproductive cycles in pigs. *Animal reproduction science* **124**, 251-258 (2011).
148. I. Ben-Aharon *et al.*, Optimizing the process of fertility preservation in pediatric female cancer patients - a multidisciplinary program. *BMC cancer* **16**, 620 (2016).
149. J. Donnez, M.-M. Dolmans, Fertility Preservation in Women. *The New England journal of medicine* **377**, 1657-1665 (2017).
150. J. S. Jeruss, T. K. Woodruff, Preservation of fertility in patients with cancer. *The New England journal of medicine* **360**, 902-911 (2009).
151. K. A. Wallberg, V. Keros, O. Hovatta, Clinical aspects of fertility preservation in female patients. *Pediatric blood & cancer* **53**, 254-260 (2009).
152. M. Salama, T. K. Woodruff, New advances in ovarian autotransplantation to restore fertility in cancer patients. *Cancer metastasis reviews* **34**, 807-822 (2015).
153. J. Donnez, M. M. Dolmans, Transplantation of ovarian tissue. *Best Pract Res Clin Obstet Gynaecol* **28**, 1188-1197 (2014).
154. E. Cho, Y. Y. Kim, K. Noh, S. Y. Ku, A new possibility in fertility preservation: The artificial ovary. *J Tissue Eng Regen Med*, (2019).
155. J. Boivin, L. Bunting, J. A. Collins, K. G. Nygren, International estimates of infertility prevalence and treatment-seeking: potential need and demand for infertility medical care. *Hum Reprod* **22**, 1506-1512 (2007).

156. Infections, pregnancies, and infertility: perspectives on prevention. World Health Organization. *Fertil Steril* **47**, 964-968 (1987).
157. W. G. Foster, A. M. Gannon, H. C. Furlong, in *The Ovary (Third Edition)*, P. C. K. Leung, E. Y. Adashi, Eds. (Academic Press, 2019), pp. 485-491.
158. J. S. Laven, Primary Ovarian Insufficiency. *Semin Reprod Med* **34**, 230-234 (2016).
159. L. Nelson *et al.*, in *Premature ovarian failure*. (Lippincott-Raven Philadelphia, 1996), pp. 1394-1410.
160. L. M. Nelson, Clinical practice. Primary ovarian insufficiency. *The New England journal of medicine* **360**, 606-614 (2009).
161. Testing and interpreting measures of ovarian reserve: a committee opinion. *Fertil Steril* **103**, e9-e17 (2015).
162. G. Bedoschi, P. A. Navarro, K. Oktay, Chemotherapy-induced damage to ovary: mechanisms and clinical impact. *Future oncology* **12**, 2333-2344 (2016).
163. R. L. Siegel, K. D. Miller, A. Jemal, Cancer statistics, 2019. *CA: a cancer journal for clinicians* **69**, 7-34 (2019).
164. G. Familiari *et al.*, Ultrastructure of human ovarian primordial follicles after combination chemotherapy for Hodgkin's disease. *Hum Reprod* **8**, 2080-2087 (1993).
165. R. Himmelstein-Braw, H. Peters, M. Faber, Morphological study of the ovaries of leukaemic children. *British journal of cancer* **38**, 82-87 (1978).
166. O. Oktem, K. Oktay, Quantitative assessment of the impact of chemotherapy on ovarian follicle reserve and stromal function. *Cancer* **110**, 2222-2229 (2007).
167. F. Li *et al.*, Sphingosine-1-phosphate prevents chemotherapy-induced human primordial follicle death. *Hum Reprod* **29**, 107-113 (2014).
168. R. Soleimani, E. Heytens, Z. Darzynkiewicz, K. Oktay, Mechanisms of chemotherapy-induced human ovarian aging: double strand DNA breaks and microvascular compromise. *Aging* **3**, 782-793 (2011).
169. M. F. Marcello *et al.*, Structural and ultrastructural study of the ovary in childhood leukemia after successful treatment. *Cancer* **66**, 2099-2104 (1990).
170. D. C. Doll, J. W. Yarbrow, Vascular toxicity associated with antineoplastic agents. *Seminars in oncology* **19**, 580-596 (1992).
171. S. V. Nicosia, M. Matus-Ridley, A. T. Meadows, Gonadal effects of cancer therapy in girls. *Cancer* **55**, 2364-2372 (1985).

172. M. A. Filatov *et al.*, Female fertility preservation strategies: cryopreservation and ovarian tissue in vitro culture, current state of the art and future perspectives. *Zygote (Cambridge, England)* **24**, 635-653 (2016).
173. J. Donnez *et al.*, Livebirth after orthotopic transplantation of cryopreserved ovarian tissue. *Lancet* **364**, 1405-1410 (2004).
174. D. Meirow *et al.*, Pregnancy after transplantation of cryopreserved ovarian tissue in a patient with ovarian failure after chemotherapy. *The New England journal of medicine* **353**, 318-321 (2005).
175. S. J. Silber *et al.*, Ovarian transplantation between monozygotic twins discordant for premature ovarian failure. *The New England journal of medicine* **353**, 58-63 (2005).
176. P. Delphine M. V, THE FERTILITY OF MICE WITH ORTHOTOPIC OVARIAN GRAFTS DERIVED FROM FROZEN TISSUE. *Reproduction* **1**, 230-241 (1960).
177. J. Carroll, D. G. Whittingham, M. J. Wood, E. Telfer, R. G. Gosden, Extra-ovarian production of mature viable mouse oocytes from frozen primary follicles. *Journal of reproduction and fertility* **90**, 321-327 (1990).
178. L. Nahata *et al.*, Ovarian tissue cryopreservation as standard of care: what does this mean for pediatric populations? *Journal of assisted reproduction and genetics*, (2020).
179. R. G. Gosden, D. T. Baird, J. C. Wade, R. Webb, Restoration of fertility to oophorectomized sheep by ovarian autografts stored at -196 degrees C. *Hum Reprod* **9**, 597-603 (1994).
180. D. A. Gook, D. H. Edgar, C. Stern, Effect of cooling rate and dehydration regimen on the histological appearance of human ovarian cortex following cryopreservation in 1, 2-propanediol. *Hum Reprod* **14**, 2061-2068 (1999).
181. R. G. Gosden, Low temperature storage and grafting of human ovarian tissue. *Mol Cell Endocrinol* **163**, 125-129 (2000).
182. D. A. Gook, D. H. Edgar, C. Stern, The effects of cryopreservation regimens on the morphology of human ovarian tissue. *Mol Cell Endocrinol* **169**, 99-103 (2000).
183. S. Silber, N. Kagawa, M. Kuwayama, R. Gosden, Duration of fertility after fresh and frozen ovary transplantation. *Fertil Steril* **94**, 2191-2196 (2010).
184. N. Kagawa, S. Silber, M. Kuwayama, Successful vitrification of bovine and human ovarian tissue. *Reproductive biomedicine online* **18**, 568-577 (2009).
185. M. Grynberg *et al.*, Ovarian tissue and follicle transplantation as an option for fertility preservation. *Fertil Steril* **97**, 1260-1268 (2012).

186. J. J. Eppig, M. J. O'Brien, Development in vitro of mouse oocytes from primordial follicles. *Biology of reproduction* **54**, 197-207 (1996).
187. M. J. O'Brien, J. K. Pendola, J. J. Eppig, A revised protocol for in vitro development of mouse oocytes from primordial follicles dramatically improves their developmental competence. *Biology of reproduction* **68**, 1682-1686 (2003).
188. R. Cortvrindt, J. Smits, A. C. Van Steirteghem, In-vitro maturation, fertilization and embryo development of immature oocytes from early preantral follicles from prepuberal mice in a simplified culture system. *Hum Reprod* **11**, 2656-2666 (1996).
189. S. A. Pangas, H. Saudye, L. D. Shea, T. K. Woodruff, Novel approach for the three-dimensional culture of granulosa cell-oocyte complexes. *Tissue Eng* **9**, 1013-1021 (2003).
190. M. Xu, P. K. Kreeger, L. D. Shea, T. K. Woodruff, Tissue-engineered follicles produce live, fertile offspring. *Tissue Eng* **12**, 2739-2746 (2006).
191. N. Desai *et al.*, Three-dimensional in vitro follicle growth: overview of culture models, biomaterials, design parameters and future directions. *Reprod Biol Endocrinol* **8**, 119 (2010).
192. P. K. Kreeger, J. W. Deck, T. K. Woodruff, L. D. Shea, The in vitro regulation of ovarian follicle development using alginate-extracellular matrix gels. *Biomaterials* **27**, 714-723 (2006).
193. E. R. West, M. Xu, T. K. Woodruff, L. D. Shea, Physical properties of alginate hydrogels and their effects on in vitro follicle development. *Biomaterials* **28**, 4439-4448 (2007).
194. M. Xu, E. West, L. D. Shea, T. K. Woodruff, Identification of a stage-specific permissive in vitro culture environment for follicle growth and oocyte development. *Biology of reproduction* **75**, 916-923 (2006).
195. S. Y. Jin, L. Lei, A. Shikanov, L. D. Shea, T. K. Woodruff, A novel two-step strategy for in vitro culture of early-stage ovarian follicles in the mouse. *Fertil Steril* **93**, 2633-2639 (2010).
196. I. R. Brito *et al.*, Alginate hydrogel matrix stiffness influences the in vitro development of caprine preantral follicles. *Molecular reproduction and development* **81**, 636-645 (2014).
197. G. M. Silva *et al.*, In vitro development of secondary follicles from pre-pubertal and adult goats cultured in two-dimensional or three-dimensional systems. *Zygote (Cambridge, England)* **23**, 475-484 (2015).
198. N. Songsasen, T. K. Woodruff, D. E. Wildt, In vitro growth and steroidogenesis of dog follicles are influenced by the physical and hormonal microenvironment. *Reproduction* **142**, 113-122 (2011).

199. V. R. Araújo, M. O. Gastal, A. Wischral, J. R. Figueiredo, E. L. Gastal, In vitro development of bovine secondary follicles in two- and three-dimensional culture systems using vascular endothelial growth factor, insulin-like growth factor-1, and growth hormone. *Theriogenology* **82**, 1246-1253 (2014).
200. M. Xu *et al.*, Encapsulated three-dimensional culture supports development of nonhuman primate secondary follicles. *Biology of reproduction* **81**, 587-594 (2009).
201. S. Xiao *et al.*, In vitro follicle growth supports human oocyte meiotic maturation. *Sci Rep* **5**, 17323 (2015).
202. C. Torrance, E. Telfer, R. G. Gosden, Quantitative study of the development of isolated mouse pre-antral follicles in collagen gel culture. *Journal of reproduction and fertility* **87**, 367-374 (1989).
203. Y. Hirao *et al.*, In vitro growth and maturation of pig oocytes. *Journal of reproduction and fertility* **100**, 333-339 (1994).
204. K. Schotanus, W. J. Hage, H. Vanderstichele, R. van den Hurk, Effects of conditioned media from murine granulosa cell lines on the growth of isolated bovine preantral follicles. *Theriogenology* **48**, 471-483 (1997).
205. K. Yamamoto *et al.*, Development to live young from bovine small oocytes after growth, maturation and fertilization in vitro. *Theriogenology* **52**, 81-89 (1999).
206. R. Abir *et al.*, Morphological study of fully and partially isolated early human follicles. *Fertil Steril* **75**, 141-146 (2001).
207. T. Itoh, M. Kacchi, H. Abe, Y. Sendai, H. Hoshi, Growth, antrum formation, and estradiol production of bovine preantral follicles cultured in a serum-free medium. *Biology of reproduction* **67**, 1099-1105 (2002).
208. A. Shikanov, M. Xu, T. K. Woodruff, L. D. Shea, Interpenetrating fibrin-alginate matrices for in vitro ovarian follicle development. *Biomaterials* **30**, 5476-5485 (2009).
209. J. Xu *et al.*, Fibrin promotes development and function of macaque primary follicles during encapsulated three-dimensional culture. *Hum Reprod* **28**, 2187-2200 (2013).
210. M. Xu *et al.*, In vitro oocyte maturation and preantral follicle culture from the luteal-phase baboon ovary produce mature oocytes. *Biology of reproduction* **84**, 689-697 (2011).
211. C. M. Higuchi, Y. Maeda, T. Horiuchi, Y. Yamazaki, A Simplified Method for Three-Dimensional (3-D) Ovarian Tissue Culture Yielding Oocytes Competent to Produce Full-Term Offspring in Mice. *PLoS one* **10**, e0143114 (2015).
212. N. Desai, F. Abdelhafez, A. Calabro, T. Falcone, Three dimensional culture of fresh and vitrified mouse pre-antral follicles in a hyaluronan-based hydrogel: a preliminary

- investigation of a novel biomaterial for in vitro follicle maturation. *Reprod Biol Endocrinol* **10**, 29 (2012).
213. A. Shikanov, R. M. Smith, M. Xu, T. K. Woodruff, L. D. Shea, Hydrogel network design using multifunctional macromers to coordinate tissue maturation in ovarian follicle culture. *Biomaterials* **32**, 2524-2531 (2011).
 214. P. D. Rios *et al.*, Retrievable hydrogels for ovarian follicle transplantation and oocyte collection. *Biotechnol Bioeng* **115**, 2075-2086 (2018).
 215. A. Shikanov *et al.*, Fibrin encapsulation and vascular endothelial growth factor delivery promotes ovarian graft survival in mice. *Tissue Eng Part A* **17**, 3095-3104 (2011).
 216. R. M. Smith *et al.*, Fibrin-mediated delivery of an ovarian follicle pool in a mouse model of infertility. *Tissue Eng Part A* **20**, 3021-3030 (2014).
 217. E. Kniazeva *et al.*, Primordial Follicle Transplantation within Designer Biomaterial Grafts Produce Live Births in a Mouse Infertility Model. *Sci Rep* **5**, 17709 (2015).
 218. M. M. Laronda *et al.*, Initiation of puberty in mice following decellularized ovary transplant. *Biomaterials* **50**, 20-29 (2015).
 219. F. Paulini *et al.*, Survival and growth of human preantral follicles after cryopreservation of ovarian tissue, follicle isolation and short-term xenografting. *Reproductive biomedicine online* **33**, 425-432 (2016).
 220. J. Kim *et al.*, Synthetic hydrogel supports the function and regeneration of artificial ovarian tissue in mice. *Npj Regenerative Medicine* **1**, 16010 (2016).
 221. M. M. Laronda *et al.*, A bioprosthetic ovary created using 3D printed microporous scaffolds restores ovarian function in sterilized mice. *Nature communications* **8**, 15261 (2017).
 222. J. Johnson, J. Canning, T. Kaneko, J. K. Pru, J. L. Tilly, Germline stem cells and follicular renewal in the postnatal mammalian ovary. *Nature* **428**, 145-150 (2004).
 223. M. Wagner *et al.*, Single-cell analysis of human ovarian cortex identifies distinct cell populations but no oogonial stem cells. *Nature communications* **11**, 1147-1147 (2020).
 224. J. Xiong *et al.*, Intraovarian Transplantation of Female Germline Stem Cells Rescue Ovarian Function in Chemotherapy-Injured Ovaries. *PloS one* **10**, e0139824 (2015).
 225. Y. Zhang *et al.*, Production of transgenic mice by random recombination of targeted genes in female germline stem cells. *J Mol Cell Biol* **3**, 132-141 (2011).
 226. K. Zou *et al.*, Production of offspring from a germline stem cell line derived from neonatal ovaries. *Nat Cell Biol* **11**, 631-636 (2009).

227. A. D. Theocharis, S. S. Skandalis, C. Gialeli, N. K. Karamanos, Extracellular matrix structure. *Adv Drug Deliv Rev* **97**, 4-27 (2016).
228. J. L. Young, A. W. Holle, J. P. Spatz, Nanoscale and mechanical properties of the physiological cell–ECM microenvironment. *Experimental cell research* **343**, 3-6 (2016).
229. R. T. Miller, Mechanical properties of basement membrane in health and disease. *Matrix Biology* **57**, 366-373 (2017).
230. L. D. Muiznieks, F. W. Keeley, Molecular assembly and mechanical properties of the extracellular matrix: A fibrous protein perspective. *Biochimica et Biophysica Acta (BBA)-Molecular Basis of Disease* **1832**, 866-875 (2013).
231. T. Stylianopoulos *et al.*, Diffusion of particles in the extracellular matrix: the effect of repulsive electrostatic interactions. *Biophysical journal* **99**, 1342-1349 (2010).
232. M. Van der Rest, R. Garrone, Collagen family of proteins. *The FASEB journal* **5**, 2814-2823 (1991).
233. S. Ricard-Blum, The collagen family. *Cold Spring Harbor perspectives in biology* **3**, a004978 (2011).
234. S. M. Mithieux, A. S. Weiss, Elastin. *Advances in protein chemistry* **70**, 437-461 (2005).
235. M. Aumailley, The laminin family. *Cell adhesion & migration* **7**, 48-55 (2013).
236. A. J. Zollinger, M. L. Smith, Fibronectin, the extracellular glue. *Matrix Biology* **60**, 27-37 (2017).
237. K. S. Midwood, M. Chiquet, R. P. Tucker, G. Orend, Tenascin-C at a glance. *Journal of cell science* **129**, 4321-4327 (2016).
238. A. Köwitsch, G. Zhou, T. Groth, Medical application of glycosaminoglycans: a review. *Journal of tissue engineering and regenerative medicine* **12**, e23-e41 (2018).
239. T. E. Hardingham, A. J. Fosang, Proteoglycans: many forms and many functions. *FASEB journal : official publication of the Federation of American Societies for Experimental Biology* **6**, 861-870 (1992).
240. R. V. Iozzo, L. Schaefer, Proteoglycan form and function: A comprehensive nomenclature of proteoglycans. *Matrix biology : journal of the International Society for Matrix Biology* **42**, 11-55 (2015).
241. K. Myhre, G. C. Blobel, Proteoglycan signaling co-receptors: roles in cell adhesion, migration and invasion. *Cellular signalling* **21**, 1548-1558 (2009).

242. Y. Choi, H. Chung, H. Jung, J. R. Couchman, E. S. Oh, Syndecans as cell surface receptors: Unique structure equates with functional diversity. *Matrix biology : journal of the International Society for Matrix Biology* **30**, 93-99 (2011).
243. D. S. Harburger, D. A. Calderwood, Integrin signalling at a glance. *Journal of cell science* **122**, 159-163 (2009).
244. J. D. Humphries, A. Byron, M. J. Humphries, Integrin ligands at a glance. *Journal of cell science* **119**, 3901-3903 (2006).
245. B. Leitinger, E. Hohenester, Mammalian collagen receptors. *Matrix biology : journal of the International Society for Matrix Biology* **26**, 146-155 (2007).
246. X. Xian, S. Gopal, J. R. Couchman, Syndecans as receptors and organizers of the extracellular matrix. *Cell and tissue research* **339**, 31-46 (2010).
247. L. Huleihel *et al.*, Matrix-bound nanovesicles within ECM bioscaffolds. *Science advances* **2**, e1600502 (2016).
248. A. Faust *et al.*, Urinary bladder extracellular matrix hydrogels and matrix-bound vesicles differentially regulate central nervous system neuron viability and axon growth and branching. *Journal of biomaterials applications* **31**, 1277-1295 (2017).
249. L. Huleihel *et al.*, Matrix-Bound Nanovesicles Recapitulate Extracellular Matrix Effects on Macrophage Phenotype. *Tissue Eng Part A* **23**, 1283-1294 (2017).
250. C. Bonnans, J. Chou, Z. Werb, Remodelling the extracellular matrix in development and disease. *Nature reviews. Molecular cell biology* **15**, 786-801 (2014).
251. A. Naba *et al.*, The matrisome: in silico definition and in vivo characterization by proteomics of normal and tumor extracellular matrices. *Molecular & Cellular Proteomics* **11**, (2012).
252. F. Li *et al.* (Taylor & Francis, 2004).
253. P. Banerjee, C. Shanthi, Cryptic peptides from collagen: a critical review. *Protein and peptide letters* **23**, 664-672 (2016).
254. G. E. Davis, K. J. Bayless, M. J. Davis, G. A. Meininger, Regulation of tissue injury responses by the exposure of matricryptic sites within extracellular matrix molecules. *The American journal of pathology* **156**, 1489-1498 (2000).
255. B. M. Sicari, L. Zhang, R. Londono, S. F. Badylak, in *Biomimetics and Stem Cells*. (Springer, 2013), pp. 103-110.
256. V. Agrawal *et al.*, Recruitment of progenitor cells by an extracellular matrix cryptic peptide in a mouse model of digit amputation. *Tissue engineering Part A* **17**, 2435-2443 (2011).

257. V. Agrawal *et al.*, An isolated cryptic peptide influences osteogenesis and bone remodeling in an adult mammalian model of digit amputation. *Tissue engineering Part A* **17**, 3033-3044 (2011).
258. J. J. Ames *et al.*, Identification of an endogenously generated cryptic collagen epitope (XL313) that may selectively regulate angiogenesis by an integrin yes-associated protein (YAP) mechano-transduction pathway. *Journal of Biological Chemistry* **291**, 2731-2750 (2016).
259. T. L. Adair-Kirk, R. M. Senior, Fragments of extracellular matrix as mediators of inflammation. *The international journal of biochemistry & cell biology* **40**, 1101-1110 (2008).
260. M. J. Bissell, H. G. Hall, G. Parry, How does the extracellular matrix direct gene expression? *Journal of theoretical biology* **99**, 31-68 (1982).
261. P. Bornstein, J. McPherson, H. Sage, in *Pathobiology of the Endothelial Cell*, H. L. Nossel, H. J. Vogel, Eds. (Academic Press, 1982), pp. 215-228.
262. G. S. Schultz, J. M. Davidson, R. S. Kirsner, P. Bornstein, I. M. Herman, Dynamic reciprocity in the wound microenvironment. *Wound Repair and Regeneration* **19**, 134-148 (2011).
263. B. Yue, Biology of the Extracellular Matrix: An Overview. *Journal of Glaucoma* **23**, S20-S23 (2014).
264. M. Ahmed, C. French-Constant, Extracellular Matrix Regulation of Stem Cell Behavior. *Current Stem Cell Reports* **2**, 197-206 (2016).
265. F. Gattazzo, A. Urciuolo, P. Bonaldo, Extracellular matrix: A dynamic microenvironment for stem cell niche. *Biochimica et Biophysica Acta (BBA) - General Subjects* **1840**, 2506-2519 (2014).
266. J. Sottile, Regulation of angiogenesis by extracellular matrix. *Biochimica et Biophysica Acta (BBA)-Reviews on Cancer* **1654**, 13-22 (2004).
267. V. Agrawal, B. N. Brown, A. J. Beattie, T. W. Gilbert, S. F. Badylak, Evidence of innervation following extracellular matrix scaffold-mediated remodelling of muscular tissues. *Journal of tissue engineering and regenerative medicine* **3**, 590-600 (2009).
268. G. S. Schultz, A. Wysocki, Interactions between extracellular matrix and growth factors in wound healing. *Wound repair and regeneration* **17**, 153-162 (2009).
269. M. S. Agren, M. Werthen, The extracellular matrix in wound healing: a closer look at therapeutics for chronic wounds. *The international journal of lower extremity wounds* **6**, 82-97 (2007).

270. M. Xue, C. J. Jackson, Extracellular matrix reorganization during wound healing and its impact on abnormal scarring. *Advances in wound care* **4**, 119-136 (2015).
271. T. J. Keane, I. T. Swinehart, S. F. Badylak, Methods of tissue decellularization used for preparation of biologic scaffolds and in vivo relevance. *Methods* **84**, 25-34 (2015).
272. P. M. Crapo, T. W. Gilbert, S. F. Badylak, An overview of tissue and whole organ decellularization processes. *Biomaterials* **32**, 3233-3243 (2011).
273. M. L. Wong, L. G. Griffiths, Immunogenicity in xenogeneic scaffold generation: antigen removal vs. decellularization. *Acta biomaterialia* **10**, 1806-1816 (2014).
274. C. L. Dearth *et al.*, The effect of terminal sterilization on the material properties and in vivo remodeling of a porcine dermal biologic scaffold. *Acta biomaterialia* **33**, 78-87 (2016).
275. M. L. Wong, J. L. Wong, N. Vapniarsky, L. G. Griffiths, In vivo xenogeneic scaffold fate is determined by residual antigenicity and extracellular matrix preservation. *Biomaterials* **92**, 1-12 (2016).
276. D. D. Cissell, J. C. Hu, L. G. Griffiths, K. A. Athanasiou, Antigen removal for the production of biomechanically functional, xenogeneic tissue grafts. *Journal of biomechanics* **47**, 1987-1996 (2014).
277. A. M. Matuska, P. S. McFetridge, The effect of terminal sterilization on structural and biophysical properties of a decellularized collagen-based scaffold; implications for stem cell adhesion. *Journal of Biomedical Materials Research Part B: Applied Biomaterials* **103**, 397-406 (2015).
278. T. J. Keane, S. F. Badylak, The host response to allogeneic and xenogeneic biological scaffold materials. *Journal of tissue engineering and regenerative medicine* **9**, 504-511 (2015).
279. D. O. Freytes, R. S. Tullius, S. F. Badylak, Effect of storage upon material properties of lyophilized porcine extracellular matrix derived from the urinary bladder. *Journal of Biomedical Materials Research Part B: Applied Biomaterials: An Official Journal of The Society for Biomaterials, The Japanese Society for Biomaterials, and The Australian Society for Biomaterials and the Korean Society for Biomaterials* **78**, 327-333 (2006).
280. D. O. Freytes, R. S. Tullius, J. E. Valentin, A. M. Stewart-Akers, S. F. Badylak, Hydrated versus lyophilized forms of porcine extracellular matrix derived from the urinary bladder. *Journal of Biomedical Materials Research Part A: An Official Journal of The Society for Biomaterials, The Japanese Society for Biomaterials, and The Australian Society for Biomaterials and the Korean Society for Biomaterials* **87**, 862-872 (2008).
281. J. Burk *et al.*, Freeze-thaw cycles enhance decellularization of large tendons. *Tissue Engineering Part C: Methods* **20**, 276-284 (2014).

282. S. F. Badylak, G. C. Lantz, A. Coffey, L. A. Geddes, Small intestinal submucosa as a large diameter vascular graft in the dog. *Journal of Surgical Research* **47**, 74-80 (1989).
283. S. Badylak, S. Meurling, M. Chen, A. Spievack, A. Simmons-Byrd, Resorbable bioscaffold for esophageal repair in a dog model. *Journal of pediatric surgery* **35**, 1097-1103 (2000).
284. S. F. Badylak *et al.*, Esophageal reconstruction with ECM and muscle tissue in a dog model. *The Journal of surgical research* **128**, 87-97 (2005).
285. B. Brown, K. Lindberg, J. Reing, D. B. Stolz, S. F. Badylak, The basement membrane component of biologic scaffolds derived from extracellular matrix. *Tissue Eng* **12**, 519-526 (2006).
286. S. Sasaki *et al.*, In vivo evaluation of a novel scaffold for artificial corneas prepared by using ultrahigh hydrostatic pressure to decellularize porcine corneas. *Molecular vision* **15**, 2022 (2009).
287. S. Funamoto *et al.*, The use of high-hydrostatic pressure treatment to decellularize blood vessels. *Biomaterials* **31**, 3590-3595 (2010).
288. P. M. Crapo, T. W. Gilbert, S. F. Badylak, An overview of tissue and whole organ decellularization processes. *Biomaterials* **32**, 3233-3243 (2011).
289. E. Rieder *et al.*, Decellularization protocols of porcine heart valves differ importantly in efficiency of cell removal and susceptibility of the matrix to recellularization with human vascular cells. *The Journal of thoracic and cardiovascular surgery* **127**, 399-405 (2004).
290. S. Cebotari *et al.*, Detergent decellularization of heart valves for tissue engineering: toxicological effects of residual detergents on human endothelial cells. *Artificial organs* **34**, 206-210 (2010).
291. H. C. Ott *et al.*, Perfusion-decellularized matrix: using nature's platform to engineer a bioartificial heart. *Nature medicine* **14**, 213-221 (2008).
292. B. E. Uygun *et al.*, Organ reengineering through development of a transplantable recellularized liver graft using decellularized liver matrix. *Nature medicine* **16**, 814-820 (2010).
293. T. H. Petersen *et al.*, Tissue-engineered lungs for in vivo implantation. *Science* **329**, 538-541 (2010).
294. K. H. Nakayama, C. A. Batchelder, C. I. Lee, A. F. Tarantal, Decellularized rhesus monkey kidney as a three-dimensional scaffold for renal tissue engineering. *Tissue Engineering Part A* **16**, 2207-2216 (2010).
295. J. E. Reing *et al.*, The effects of processing methods upon mechanical and biologic properties of porcine dermal extracellular matrix scaffolds. *Biomaterials* **31**, 8626-8633 (2010).

296. E. Rieder *et al.*, Decellularization protocols of porcine heart valves differ importantly in efficiency of cell removal and susceptibility of the matrix to recellularization with human vascular cells. *The Journal of thoracic and cardiovascular surgery* **127**, 399-405 (2004).
297. B. D. Elder, D. H. Kim, K. A. Athanasiou, Developing an articular cartilage decellularization process toward facet joint cartilage replacement. *Neurosurgery* **66**, 722-727 (2010).
298. R.-N. Chen, H.-O. Ho, Y.-T. Tsai, M.-T. Sheu, Process development of an acellular dermal matrix (ADM) for biomedical applications. *Biomaterials* **25**, 2679-2686 (2004).
299. L. Du, X. Wu, K. Pang, Y. Yang, Histological evaluation and biomechanical characterisation of an acellular porcine cornea scaffold. *British journal of ophthalmology* **95**, 410-414 (2011).
300. S. B. Lumpkins, N. Pierre, P. S. McFetridge, A mechanical evaluation of three decellularization methods in the design of a xenogeneic scaffold for tissue engineering the temporomandibular joint disc. *Acta biomaterialia* **4**, 808-816 (2008).
301. B. Yang *et al.*, Development of a porcine bladder acellular matrix with well-preserved extracellular bioactive factors for tissue engineering. *Tissue Engineering Part C: Methods* **16**, 1201-1211 (2010).
302. H. C. Ott *et al.*, Regeneration and orthotopic transplantation of a bioartificial lung. *Nature medicine* **16**, 927 (2010).
303. D. W. Courtman *et al.*, Development of a pericardial acellular matrix biomaterial: biochemical and mechanical effects of cell extraction. *Journal of biomedical materials research* **28**, 655-666 (1994).
304. M.-T. Kasimir *et al.*, Comparison of different decellularization procedures of porcine heart valves. *The International journal of artificial organs* **26**, 421-427 (2003).
305. T. Woods, P. F. Gratzer, Effectiveness of three extraction techniques in the development of a decellularized bone–anterior cruciate ligament–bone graft. *Biomaterials* **26**, 7339-7349 (2005).
306. C. Deeken *et al.*, Method of preparing a decellularized porcine tendon using tributyl phosphate. *Journal of Biomedical Materials Research Part B: Applied Biomaterials* **96**, 199-206 (2011).
307. J. S. Cartmell, M. G. Dunn, Effect of chemical treatments on tendon cellularity and mechanical properties. *Journal of Biomedical Materials Research: An Official Journal of The Society for Biomaterials, The Japanese Society for Biomaterials, and The Australian Society for Biomaterials and the Korean Society for Biomaterials* **49**, 134-140 (2000).

308. I. Tudorache *et al.*, Tissue engineering of heart valves: biomechanical and morphological properties of decellularized heart valves. *The Journal of heart valve disease* **16**, 567-573; discussion 574 (2007).
309. D. J. Rosario *et al.*, Decellularization and sterilization of porcine urinary bladder matrix for tissue engineering in the lower urinary tract. (2008).
310. J. Cortiella *et al.*, Influence of acellular natural lung matrix on murine embryonic stem cell differentiation and tissue formation. *Tissue Engineering Part A* **16**, 2565-2580 (2010).
311. E. A. Ross *et al.*, Embryonic stem cells proliferate and differentiate when seeded into kidney scaffolds. *Journal of the American Society of Nephrology* **20**, 2338-2347 (2009).
312. S. Cebotari *et al.*, Detergent decellularization of heart valves for tissue engineering: toxicological effects of residual detergents on human endothelial cells. *Artificial organs* **34**, 206-210 (2010).
313. L. Gui, S. A. Chan, C. K. Breuer, L. E. Niklason, Novel utilization of serum in tissue decellularization. *Tissue Engineering Part C: Methods* **16**, 173-184 (2010).
314. B. N. Brown *et al.*, Comparison of three methods for the derivation of a biologic scaffold composed of adipose tissue extracellular matrix. *Tissue Engineering Part C: Methods* **17**, 411-421 (2011).
315. T. Shupe, M. Williams, A. Brown, B. Willenberg, B. E. Petersen, Method for the decellularization of intact rat liver. *Organogenesis* **6**, 134-136 (2010).
316. F. Bolland *et al.*, Development and characterisation of a full-thickness acellular porcine bladder matrix for tissue engineering. *Biomaterials* **28**, 1061-1070 (2007).
317. J. A. DeQuach *et al.*, Simple and high yielding method for preparing tissue specific extracellular matrix coatings for cell culture. *PloS one* **5**, (2010).
318. E. K. Merritt *et al.*, Functional assessment of skeletal muscle regeneration utilizing homologous extracellular matrix as scaffolding. *Tissue Engineering Part A* **16**, 1395-1405 (2010).
319. B. N. Brown, J. E. Valentin, A. M. Stewart-Akers, G. P. McCabe, S. F. Badylak, Macrophage phenotype and remodeling outcomes in response to biologic scaffolds with and without a cellular component. *Biomaterials* **30**, 1482-1491 (2009).
320. M. Ozeki *et al.*, Evaluation of decellularized esophagus as a scaffold for cultured esophageal epithelial cells. *Journal of Biomedical Materials Research Part A* **79A**, 771-778 (2006).
321. J. M. Wainwright *et al.*, Preparation of cardiac extracellular matrix from an intact porcine heart. *Tissue Eng Part C Methods* **16**, 525-532 (2010).

322. T. L. Sellaro *et al.*, Maintenance of human hepatocyte function in vitro by liver-derived extracellular matrix gels. *Tissue Eng Part A* **16**, 1075-1082 (2010).
323. T. W. Hudson, S. Y. Liu, C. E. Schmidt, Engineering an improved acellular nerve graft via optimized chemical processing. *Tissue Eng* **10**, 1346-1358 (2004).
324. M. Yang, C.-Z. Chen, X.-N. Wang, Y.-B. Zhu, Y. J. Gu, Favorable effects of the detergent and enzyme extraction method for preparing decellularized bovine pericardium scaffold for tissue engineered heart valves. *Journal of Biomedical Materials Research Part B: Applied Biomaterials* **91B**, 354-361 (2009).
325. P. W. Henderson *et al.*, Development of an Acellular Bioengineered Matrix with a Dominant Vascular Pedicle1. *Journal of Surgical Research* **164**, 1-5 (2010).
326. A. P. Price, K. A. England, A. M. Matson, B. R. Blazar, A. Panoskaltsis-Mortari, Development of a decellularized lung bioreactor system for bioengineering the lung: the matrix reloaded. *Tissue Eng Part A* **16**, 2581-2591 (2010).
327. M. T. Conconi *et al.*, Homologous muscle acellular matrix seeded with autologous myoblasts as a tissue-engineering approach to abdominal wall-defect repair. *Biomaterials* **26**, 2567-2574 (2005).
328. S. Z. Guo, X. J. Ren, B. Wu, T. Jiang, Preparation of the acellular scaffold of the spinal cord and the study of biocompatibility. *Spinal Cord* **48**, 576-581 (2010).
329. M. T. Conconi *et al.*, Tracheal matrices, obtained by a detergent-enzymatic method, support in vitro the adhesion of chondrocytes and tracheal epithelial cells. *Transplant International* **18**, 727-734 (2005).
330. B. N. Brown *et al.*, Comparison of three methods for the derivation of a biologic scaffold composed of adipose tissue extracellular matrix. *Tissue Eng Part C Methods* **17**, 411-421 (2011).
331. X. Dong *et al.*, RGD-modified acellular bovine pericardium as a bioprosthetic scaffold for tissue engineering. *Journal of materials science. Materials in medicine* **20**, 2327-2336 (2009).
332. R. W. Grauss *et al.*, Histological evaluation of decellularised porcine aortic valves: matrix changes due to different decellularisation methods. *European journal of cardio-thoracic surgery : official journal of the European Association for Cardio-thoracic Surgery* **27**, 566-571 (2005).
333. S. R. Meyer *et al.*, Comparison of aortic valve allograft decellularization techniques in the rat. *Journal of biomedical materials research. Part A* **79**, 254-262 (2006).
334. N. T. Remlinger *et al.*, Hydrated xenogeneic decellularized tracheal matrix as a scaffold for tracheal reconstruction. *Biomaterials* **31**, 3520-3526 (2010).

335. M. M. Stern *et al.*, The influence of extracellular matrix derived from skeletal muscle tissue on the proliferation and differentiation of myogenic progenitor cells *ex vivo*. *Biomaterials* **30**, 2393-2399 (2009).
336. T. W. Gilbert *et al.*, Collagen fiber alignment and biaxial mechanical behavior of porcine urinary bladder derived extracellular matrix. *Biomaterials* **29**, 4775-4782 (2008).
337. J. Hodde *et al.*, Effects of sterilization on an extracellular matrix scaffold: part I. Composition and matrix architecture. *Journal of materials science. Materials in medicine* **18**, 537-543 (2007).
338. J. Hodde, M. Hiles, Virus safety of a porcine-derived medical device: evaluation of a viral inactivation method. *Biotechnol Bioeng* **79**, 211-216 (2002).
339. I. Prasertsung, S. Kanokpanont, T. Bunaprasert, V. Thanakit, S. Damrongsakkul, Development of acellular dermis from porcine skin using periodic pressurized technique. *Journal of biomedical materials research. Part B, Applied biomaterials* **85**, 210-219 (2008).
340. O. Gorschewsky, A. Puetz, K. Riechert, A. Klakow, R. Becker, Quantitative analysis of biochemical characteristics of bone-patellar tendon-bone allografts. *Bio-medical materials and engineering* **15**, 403-411 (2005).
341. B. Cox, A. Emili, Tissue subcellular fractionation and protein extraction for use in mass-spectrometry-based proteomics. *Nature protocols* **1**, 1872-1878 (2006).
342. C. C. Xu, R. W. Chan, N. Tirunagari, A biodegradable, acellular xenogeneic scaffold for regeneration of the vocal fold lamina propria. *Tissue Eng* **13**, 551-566 (2007).
343. M. B. Cole, Jr., Alteration of cartilage matrix morphology with histological processing. *Journal of microscopy* **133**, 129-140 (1984).
344. O. Gorschewsky, A. Klakow, K. Riechert, M. Pitzl, R. Becker, Clinical comparison of the Tutoplast allograft and autologous patellar tendon (bone-patellar tendon-bone) for the reconstruction of the anterior cruciate ligament: 2- and 6-year results. *The American journal of sports medicine* **33**, 1202-1209 (2005).
345. M. C. Jamur, C. Oliver, Cell fixatives for immunostaining. *Methods Mol Biol* **588**, 55-61 (2010).
346. C. V. Montoya, P. S. McFetridge, Preparation of *ex vivo*-based biomaterials using convective flow decellularization. *Tissue Eng Part C Methods* **15**, 191-200 (2009).
347. R. J. Klebe, Isolation of a collagen-dependent cell attachment factor. *Nature* **250**, 248-251 (1974).
348. J. Gailit, E. Ruoslahti, Regulation of the fibronectin receptor affinity by divalent cations. *J Biol Chem* **263**, 12927-12932 (1988).

349. J. Zhou *et al.*, Impact of heart valve decellularization on 3-D ultrastructure, immunogenicity and thrombogenicity. *Biomaterials* **31**, 2549-2554 (2010).
350. L. E. Flynn, The use of decellularized adipose tissue to provide an inductive microenvironment for the adipogenic differentiation of human adipose-derived stem cells. *Biomaterials* **31**, 4715-4724 (2010).
351. A. E. Jakus *et al.*, "Tissue Papers" from Organ-Specific Decellularized Extracellular Matrices. *Adv Funct Mater* **27**, (2017).
352. A. Hassanpour, T. Talaei-Khozani, E. Kargar-Abarghouei, V. Razban, Z. Vojdani, Decellularized human ovarian scaffold based on a sodium lauryl ester sulfate (SLES)-treated protocol, as a natural three-dimensional scaffold for construction of bioengineered ovaries. *Stem cell research & therapy* **9**, 252 (2018).
353. A. B. Alshaikh *et al.*, Decellularization of the mouse ovary: comparison of different scaffold generation protocols for future ovarian bioengineering. *J Ovarian Res* **12**, 58 (2019).
354. F. Eivazkhani *et al.*, Evaluating two ovarian decellularization methods in three species. *Materials science & engineering. C, Materials for biological applications* **102**, 670-682 (2019).
355. S. E. Pors *et al.*, Initial steps in reconstruction of the human ovary: survival of pre-antral stage follicles in a decellularized human ovarian scaffold. *Hum Reprod* **34**, 1523-1535 (2019).
356. G. Pennarossa, M. Ghiringhelli, F. Gandolfi, T. A. L. Brevini, Whole-ovary decellularization generates an effective 3D bioscaffold for ovarian bioengineering. *Journal of assisted reproduction and genetics*, (2020).
357. M. J. Buckenmeyer, T. J. Meder, T. A. Prest, B. N. Brown, Decellularization techniques and their applications for the repair and regeneration of the nervous system. *Methods* **171**, 41-61 (2020).
358. N. Nakamura, T. Kimura, A. Kishida, Overview of the development, applications, and future perspectives of decellularized tissues and organs. *ACS Biomaterials Science & Engineering* **3**, 1236-1244 (2017).
359. M. T. Spang, K. L. Christman, Extracellular matrix hydrogel therapies: In vivo applications and development. *Acta biomaterialia* **68**, 1-14 (2018).
360. E. C. Stahl *et al.*, Evaluation of the host immune response to decellularized lung scaffolds derived from α -Gal knockout pigs in a non-human primate model. *Biomaterials* **187**, 93-104 (2018).

361. A. Kumar, J. K. Placone, A. J. Engler, Understanding the extracellular forces that determine cell fate and maintenance. *Development (Cambridge, England)* **144**, 4261-4270 (2017).
362. B. M. Sicari *et al.*, The promotion of a constructive macrophage phenotype by solubilized extracellular matrix. *Biomaterials* **35**, 8605-8612 (2014).
363. A. D'Amore, J. A. Stella, W. R. Wagner, M. S. Sacks, Characterization of the complete fiber network topology of planar fibrous tissues and scaffolds. *Biomaterials* **31**, 5345-5354 (2010).
364. D. O. Freytes, J. Martin, S. S. Velankar, A. S. Lee, S. F. Badylak, Preparation and rheological characterization of a gel form of the porcine urinary bladder matrix. *Biomaterials* **29**, 1630-1637 (2008).
365. R. A. Gelman, B. R. Williams, K. A. Piez, Collagen fibril formation. Evidence for a multistep process. *J Biol Chem* **254**, 180-186 (1979).
366. D. Meirow, D. Nugent, The effects of radiotherapy and chemotherapy on female reproduction. *Hum Reprod Update* **7**, 535-543 (2001).
367. K. Oktay, M. Sonmezer, Chemotherapy and amenorrhea: risks and treatment options. *Current opinion in obstetrics & gynecology* **20**, 408-415 (2008).
368. H. F. Irving-Rodgers, R. J. Rodgers, Extracellular matrix of the developing ovarian follicle. *Semin Reprod Med* **24**, 195-203 (2006).
369. J. A. MacDonald *et al.*, Extracellular matrix signaling activates differentiation of adult ovary-derived oogonial stem cells in a species-specific manner. *Fertil Steril* **111**, 794-805 (2019).
370. C. B. Berkholtz, B. E. Lai, T. K. Woodruff, L. D. Shea, Distribution of extracellular matrix proteins type I collagen, type IV collagen, fibronectin, and laminin in mouse folliculogenesis. *Histochemistry and cell biology* **126**, 583-592 (2006).
371. J. E. Scott, I. B. Carlsson, B. D. Bavister, O. Hovatta, Human ovarian tissue cultures: extracellular matrix composition, coating density and tissue dimensions. *Reproductive biomedicine online* **9**, 287-293 (2004).
372. B. Brown, K. Lindberg, J. Reing, D. B. Stolz, S. F. Badylak, The basement membrane component of biologic scaffolds derived from extracellular matrix. *Tissue engineering* **12**, 519-526 (2006).
373. A. S. K. Jones, A. Shikanov, Follicle development as an orchestrated signaling network in a 3D organoid. *J Biol Eng* **13**, 2-2 (2019).
374. S. Silber, Ovarian tissue cryopreservation and transplantation: scientific implications. *Journal of assisted reproduction and genetics*, (2016).

375. M. Xu, A. Banc, T. K. Woodruff, L. D. Shea, Secondary follicle growth and oocyte maturation by culture in alginate hydrogel following cryopreservation of the ovary or individual follicles. *Biotechnol Bioeng* **103**, 378-386 (2009).
376. H. Zhang *et al.*, The revascularization and follicular survival of mouse ovarian grafts treated with FSH during cryopreservation by vitrification. *Cryo letters* **37**, 88-102 (2016).
377. C. Y. Andersen *et al.*, Two successful pregnancies following autotransplantation of frozen/thawed ovarian tissue. *Human reproduction (Oxford, England)* **23**, 2266-2272 (2008).
378. J. Oatley, P. A. Hunt, Of mice and (wo)men: purified oogonial stem cells from mouse and human ovaries. *Biology of reproduction* **86**, 196-196 (2012).
379. M. R. Park *et al.*, Intraovarian transplantation of primordial follicles fails to rescue chemotherapy injured ovaries. *Sci Rep* **3**, 1384 (2013).
380. N. F. Henning, R. D. LeDuc, K. A. Even, M. M. Laronda, Proteomic analyses of decellularized porcine ovaries identified new matrisome proteins and spatial differences across and within ovarian compartments. *Scientific reports* **9**, 20001-20001 (2019).
381. E. Ouni, D. Vertommen, M. C. Chiti, M.-M. Dolmans, C. A. Amorim, A Draft Map of the Human Ovarian Proteome for Tissue Engineering and Clinical Applications. *Mol Cell Proteomics* **18**, S159-S173 (2019).
382. S. E. Pors *et al.*, Initial steps in reconstruction of the human ovary: survival of pre-antral stage follicles in a decellularized human ovarian scaffold. *Human reproduction (Oxford, England)* **34**, 1523-1535 (2019).
383. L. J. White *et al.*, The impact of detergents on the tissue decellularization process: A ToF-SIMS study. *Acta biomaterialia* **50**, 207-219 (2017).
384. D. M. Faulk *et al.*, The effect of detergents on the basement membrane complex of a biologic scaffold material. *Acta biomaterialia* **10**, 183-193 (2014).
385. H. Xu *et al.*, Comparison of decellularization protocols for preparing a decellularized porcine annulus fibrosus scaffold. *PloS one* **9**, e86723-e86723 (2014).
386. P. F. Gratzner, R. D. Harrison, T. Woods, Matrix alteration and not residual sodium dodecyl sulfate cytotoxicity affects the cellular repopulation of a decellularized matrix. *Tissue engineering* **12**, 2975-2983 (2006).
387. S. Morgan, R. A. Anderson, C. Gourley, W. H. Wallace, N. Spears, How do chemotherapeutic agents damage the ovary? *Hum Reprod Update* **18**, 525-535 (2012).
388. M. E. Skaznik-Wikiel *et al.*, Granulocyte colony-stimulating factor with or without stem cell factor extends time to premature ovarian insufficiency in female mice treated with alkylating chemotherapy. *Fertility and sterility* **99**, 2045-2054.e2043 (2013).

389. K. L. T. Schmidt, E. Ernst, A. G. Byskov, A. Nyboe Andersen, C. Yding Andersen, Survival of primordial follicles following prolonged transportation of ovarian tissue prior to cryopreservation. *Human reproduction (Oxford, England)* **18**, 2654-2659 (2003).
390. K. L. Schmidt, A. G. Byskov, A. Nyboe Andersen, J. Muller, C. Yding Andersen, Density and distribution of primordial follicles in single pieces of cortex from 21 patients and in individual pieces of cortex from three entire human ovaries. *Hum Reprod* **18**, 1158-1164 (2003).
391. M. D. Hornstein, State of the ART: Assisted Reproductive Technologies in the United States. *Reproductive sciences (Thousand Oaks, Calif.)* **23**, 1630-1633 (2016).
392. J. Y. J. Huang, Z. Rosenwaks, Assisted reproductive techniques. *Methods Mol Biol* **1154**, 171-231 (2014).
393. S. Y. Kim, S. K. Kim, J. R. Lee, T. K. Woodruff, Toward precision medicine for preserving fertility in cancer patients: existing and emerging fertility preservation options for women. *J Gynecol Oncol* **27**, e22 (2016).
394. J. Smitz *et al.*, Current achievements and future research directions in ovarian tissue culture, in vitro follicle development and transplantation: implications for fertility preservation. *Hum Reprod Update* **16**, 395-414 (2010).
395. B. A. Malizia, M. R. Hacker, A. S. Penzias, Cumulative live-birth rates after in vitro fertilization. *The New England journal of medicine* **360**, 236-243 (2009).
396. E. E. Telfer, Future developments: In vitro growth (IVG) of human ovarian follicles. *Acta obstetricia et gynecologica Scandinavica*, (2019).
397. I. S. Batchvarov *et al.*, A grafted ovarian fragment rescues host fertility after chemotherapy. *Molecular human reproduction*, (2016).
398. V. Luyckx *et al.*, A new step toward the artificial ovary: survival and proliferation of isolated murine follicles after autologous transplantation in a fibrin scaffold. *Fertil Steril* **101**, 1149-1156 (2014).
399. C. A. Amorim, A. Van Langendonck, A. David, M. M. Dolmans, J. Donnez, Survival of human pre-antral follicles after cryopreservation of ovarian tissue, follicular isolation and in vitro culture in a calcium alginate matrix. *Hum Reprod* **24**, 92-99 (2009).
400. M. M. Laronda *et al.*, Alginate encapsulation supports the growth and differentiation of human primordial follicles within ovarian cortical tissue. *Journal of assisted reproduction and genetics* **31**, 1013-1028 (2014).
401. D. Tagler, Y. Makanji, N. R. Anderson, T. K. Woodruff, L. D. Shea, Supplemented alphaMEM/F12-based medium enables the survival and growth of primary ovarian follicles encapsulated in alginate hydrogels. *Biotechnol Bioeng* **110**, 3258-3268 (2013).

402. D. Tagler *et al.*, Promoting extracellular matrix remodeling via ascorbic acid enhances the survival of primary ovarian follicles encapsulated in alginate hydrogels. *Biotechnol Bioeng* **111**, 1417-1429 (2014).
403. M. Xu *et al.*, In vitro grown human ovarian follicles from cancer patients support oocyte growth. *Hum Reprod* **24**, 2531-2540 (2009).
404. J. I. Ahn *et al.*, Culture of preantral follicles in poly(ethylene) glycol-based, three-dimensional hydrogel: a relationship between swelling ratio and follicular developments. *J Tissue Eng Regen Med* **9**, 319-323 (2015).
405. M. McLaughlin, D. F. Albertini, W. H. B. Wallace, R. A. Anderson, E. E. Telfer, Metaphase II oocytes from human unilaminar follicles grown in a multi-step culture system. *Molecular human reproduction* **24**, 135-142 (2018).
406. E. Mouloungui, T. Zver, C. Roux, C. Amiot, A protocol to isolate and qualify purified human preantral follicles in cases of acute leukemia, for future clinical applications. *Journal of ovarian research* **11**, 4-4 (2018).